Vibration and Stability of Vertical Tubes Conveying Fluid Subjected to Planar Excitation

R.L. Engelstad

May 1988

UWFDM-785

Ph.D. thesis.

FUSION TECHNOLOGY INSTITUTE

UNIVERSITY OF WISCONSIN

MADISON WISCONSIN

Vibration and Stability of Vertical Tubes Conveying Fluid Subjected to Planar Excitation

R.L. Engelstad

Fusion Technology Institute
University of Wisconsin
1500 Engineering Drive
Madison, WI 53706

http://fti.neep.wisc.edu

May 1988

UWFDM-785

Ph.D. thesis.

VIBRATION AND STABILITY
OF VERTICAL TUBES CONVEYING FLUID
SUBJECTED TO PLANAR EXCITATION

by

ROXANN LOUISE ENGELSTAD

A thesis submitted in partial fulfillment of the
requirements for the degree of

Doctor of Philosophy

(Engineering Mechanics)

at the

UNIVERSITY OF WISCONSIN-MADISON

1988

VIBRATION AND STABILITY OF VERTICAL TUBES CONVEYING FLUID SUBJECTED TO PLANAR EXCITATION

Roxann Louise Engelstad

Under the Supervision of Professor Edward George Lovell

Inertial confinement fusion reactor conceptual designs have been proposed in which flexible silicon carbide tubes conveying liquid lithium-lead are subjected to repetitive impulsive pressures. Exact mode shapes and natural frequencies have been determined for the tubes which include an internal tension variation as a result of gravity in addition to axial preloading. The dynamic response of these tubular components to such mechanical impulses has been numerically simulated. Amplitude-frequency relationships including nonlinear jump phenomena have been determined. The conditions under which whirling motion will develop have also been identified. Further results show that if the flow has a pulsating characteristic, large amplitude displacements are likely to develop over a wide range of system parameters. Regions of instabilities are determined for various flow velocities and pulsating amplification factors using Bolotin's stability criterion.

Approved:

Edward G. Lovell

Professor Edward George Lovell
Engineering Mechanics

ACKNOWLEDGEMENT

Support for this work was provided by Kernforschungszentrum Karlsruhe, Sandia National Laboratories, Fusion Power Associates, Department of Energy - Office of Inertial Confinement Fusion, Oak Ridge National Laboratories, Livermore National Laboratories, the Wisconsin Electric Utilities Research Foundation and Shell Oil Foundation.

TABLE OF CONTENTS

LIST OF FIGURES

LIST OF TABLES

LIST OF SYMBOLS

A_f	cross-sectional flow area
A_t	cross-sectional area of the tube
c	flow velocity
c_o	mean velocity
E	elastic modulus
F	forcing function
g	gravitational constant
I	moment of inertia of tube section
I_p	impulsive pressure
K	kinetic energy
ℓ	tube length
m_f	mass/length of fluid
m_t	mass/length of tube
M	total mass/length of tube and fluid
p	internal mean pressure
R	tube radius
t	time
$\bar{t}$	dimensionless time
T	absolute tension
T_e	effective tension defined by Eq. (4.3-3)
T_o	static pretension

$\bar{T}$	dimensionless tension defined by Eq. (4.1-10)
T^*	effective tension defined by Eq. (3.2-14)
T^{**}	constant tension defined by Eq. (5.1-4)
u	x displacement
U	potential energy
v	y displacement
$\bar{v}$	dimensionless y displacement (v/l)
$V_n(x)$	eigenfunctions
w	z displacement
$\bar{w}$	dimensionless z displacement (w/l)
W	total weight of tube and fluid
W_{nc}	work done by nonconservative forces
x	axial coordinate
y	transverse coordinate
z	transverse coordinate
α_k	series coefficient
β_k	series coefficient
δ	perturbation parameter
ε	perturbation parameter
κ	dimensionless damping coefficient
κ_o	equivalent damping coefficient
λ_n	complex constant defined by Eq. (4.1-8)
μ	amplification factor on fluid forcing frequency

ν	Poisson's ratio
ξ	dimensionless variable in x defined by Eq. (4.1-2)
τ	dimensionless time ($\sqrt{g/l}\ t$)
ϕ_n, Φ_n	eigenfunctions
ψ	precessional angle
ω_n	natural frequencies
$\bar{\omega}_n$	dimensionless natural frequencies
Ω	fluid forcing frequency
$\bar{\Omega}$	dimensionless fluid forcing frequency (Ω/ω_1)
$\bar{a},\bar{b},\bar{c},\bar{d},\bar{e}$	dimensionless constants defined by Eq. (5.3-5)
k,m,n,r	indices
A_n, B_n	complex constants
α_n, X_n, $\bar{X}_n$	complex constants

CHAPTER 1

INTRODUCTION

Over the past thirty-five years, a considerable amount of work has been devoted to the mechanical analysis of tubes conveying fluids. The early investigations were primarily concerned with the problems encountered with the transport of oil in pipelines. A review of the literature revealed that the majority of research was concerned with the study of the transverse vibrations and stability of simply supported, cantilevered or articulated pipes. In most cases, the internal flow and/or variation in flow was the system excitation. More recently, various nuclear fission reactor components, such as heat-exchanger tubes, control rods and fuel pins, have been studied for both axial flow and cross-flow vibratory problems.

However, in the study of inertial confinement fusion, reactor chamber designs call for another application of tubes conveying fluid. Here the first wall protection scheme involves an annular bank of vertical tubes carrying liquid lithium-lead. Individual tubes are braided from silicon carbide fibers producing a very long, flexible component. The primary external loading on these tubes is a planar impulsive pressure distribution applied at the repetition rate of the driver. The investigation presented in this dissertation examines the vibration and stability of these tubes to aid in the development of the proposed reactor designs.

Three major issues of the design are separately addressed. The first pertains to the fact that with the tubes in a vertical configuration, the effect of gravity will result in an internal tension variation. In order to avoid resonance problems due to synchronization with the repetition rate of the impulsive loadings, it is necessary to determine accurate values for the natural frequencies.

Secondly, the dynamic response of the tubes to an externally applied impulsive pressure is needed to guide in the tube placement within the bank. The nonplanar response of strings, and more recently beams, subjected to a strictly planar harmonic excitation is a well-known phenomenon. Conditions under which the tube will begin to whirl need to be outlined, along with amplitude-frequency relationships for planar motion.

Finally, considering the fluid being pumped through the tubes, the flow velocity may have a pulsating characteristic. Consequently, this could result in parametric excitation of the tube. Regions of instability for various flow velocities and pulsating amplification factors need to be identified.

CHAPTER 2

LITERATURE SURVEY

2.1 AXIAL FLOW-INDUCED OSCILLATIONS

The vibration and stability of tubes conveying fluids has been extensively studied for the last thirty-five years. However, the first investigator of self-excited oscillations was Brillouin in 1885. His work remained unpublished until 1939 when one of his students, Bourrières [2.1], examined analytically and experimentally, the flutter-type of instability associated with cantilevered pipes.

In the early 1950's, the bending vibrations observed on the Trans-Arabian pipeline renewed interest in the subject. Ashley and Haviland [2.2] derived the transverse equation of motion for a simply supported pipe containing a flowing fluid. This was corrected by Feodos'yev [2.3] and Housner [2.4] who independently predicted the same critical flow velocity for which the pipe would buckle. Niordson [2.5] derived the equation of motion of a simply supported pipe from shell theory and determined the relationship between natural frequency and fluid velocity. This work was followed by Long [2.6] who considered various support conditions in his experimental and analytical work. His experimental results were inconclusive, however, since the stiffness of the pipeline was too large for the maximum fluid velocity available. Handelman [2.7] determined the character of the frequencies for various end conditions from the

structure of the differential equation of motion without determining specific solutions.

Other investigations of the problem in the late 1950's were done by Heinrich [2.8], Bolotin [2.9] and Hu and Tsoon [2.10]. Heinrich was the first to include the effects of internal pressure on the transverse vibrations of a pipe with zero stiffness. However, Hu and Tsoon independently included hydrostatic pressure in their study of the natural frequencies of simply supported, clamped and infinitely long pipes.

In the next decade, work continued on describing the planar vibrations of simply supported pipes. Movchan [2.11] determined the critical velocity using Liapunov's method and proved Feodos'yev's result was exact. Dodds and Runyan [2.12] experimentally verified Housner's predictions on the effects of flow velocity on vibration frequency. In addition, Li and DiMaggio [2.13] numerically calculated the eigenvalues of the problem, substantiating the results of Niordson.

The effect of internal pressure on the equation of motion received additional attention also. Stein and Tobriner [2.14] considered the special case of an elastically supported pipe of infinite length conveying an ideal pressurized fluid. Naguleswaran and Williams [2.15] investigated the combined effect of axial tension and internal pressure on the natural frequency of pipes with both ends supported. In a more recent study, Plaut and Huseyin [2.16] allowed the axial load to be either tensile or compressive.

A general derivation of the equations of motion for pipe flow including both lateral and longitudinal motion was completed by Roth [2.17]. His analysis also included damping and restoring forces, variable pipe cross section, compressibility of the fluid and time-dependent internal pressure. Later, Thurman and Mote [2.18] presented the first nonlinear equations describing two-dimensional motion. Using perturbation methods, they determined the fundamental and second periods of transverse vibration for a simply supported tube, emphasizing the effects of longitudinal inertia and nonlinear tension. Although their analysis involved flow velocities below the critical, they did observe that as the fluid velocity increased so did the importance of the nonlinear terms.

Before the 1960's, buckling (divergence) had been the only flow-induced instability studied, with the exception of Bourrières. It was Benjamin [2.19,2.20] in 1961, who investigated a system of articulated cantilevered pipes and found that both buckling and flutter (oscillations with increasing amplitude) could occur in pipe segments constrained to planar motion. He was also the first to observe that fluid friction did not affect the motion of the pipe. In 1966, Gregory and Paidoussis [2.21,2.22] considered the case of a continuous cantilevered pipe subjected to relatively high flow velocities. They showed both theoretically and experimentally that for horizontal tubular cantilevers the system is subject to flexural instability only. Later, Paidoussis [2.23] found the same to be true for vertical cantilevers. Previously, it had been assumed by Benjamin that

the dynamic behavior of a continuously flexible tube could be modeled as an articulated system with an infinite number of degrees of freedom. Instead, it was found that the articulated system may exhibit an entirely different oscillatory motion and therefore cannot serve as a lumped-parameter model of a continuous system. This was further verified by Paidoussis and Deksnis [2.24].

Additional studies were done on the stability of continuous cantilevers to determine the effect of lumped masses [2.25,2.26], forced vibrations [2.27] and velocity-dependent forces. Nemat-Nasser, Prasad and Herrmann [2.28] found that internal and external damping, as well as Coriolis forces, may have a destabilizing effect in nonconservative continuous systems. The analogy between a cantilever conveying fluid and a cantilever subjected to a follower force was used by Herrmann and Nemat-Nasser [2.29] to show the same results. Related work can be found in Refs. [2.30] and [2.31].

In the mid-1960's, other industrial applications of pipes conveying fluid produced papers that were of considerable interest. The lateral motion of a deep-water drill string was analyzed by Graham, Frost and Wilhoit [2.32]. Here the effect of the Coriolis acceleration of the enclosed fluid was neglected when compared with the drag forces involved. Greenwald and Dugundji [2.33] investigated the instabilities of cantilevered propellant lines both experimentally and theoretically. Also, the effects of initial tube curvature on the motion of a completely flexible fuel line with a catenary geometry were studied by Svetlitskii [2.34].

After 1970, flow-induced instabilities took on an even greater importance with the applications to fuel rods and piping systems in nuclear reactors. Work on improving the analytical solutions of existing problems could be found [2.35-2.39], however most of the research was extended to include more sophisticated structural models and fluid flow patterns.

Paidoussis and Denise [2.40,2.41] were the first to observe that shell-type oscillatory instabilities were possible in sufficiently thin tubes. They found that both clamped and cantilevered pipes were subject to instability by flutter in their second circumferential mode. Weaver and Unny [2.42] independently determined similar results for simply supported cylinders. Further analytical investigations were presented by Paidoussis [2.43-2.45].

The dynamic behavior of curved pipe-fluid systems received considerable attention also. For this case, a dominant effect in the tube response is the centrifugal force resulting from the fluid following a curved path. Unny, Martin and Dubey [2.46] and Chen [2.47-2.50] derived the in-plane and out-of-plane equations of motions and computed the critical flow velocities for various end conditions. The effect of initial forces was analyzed by Hill and Davis [2.51], and in a more extensive study, Doll and Mote [2.52] formulated the longitudinal, torsional and both transverse equations of motion, utilizing isoparametric finite elements in their natural frequency calculations.

The influence of unsteady flow was found to be particularly important since periodic variations of the fluid velocity could cause parametric resonance of the tube. Chen [2.53] was the first to investigate the stability of a simply supported pipe conveying a pulsating fluid whose flow velocity had a harmonic fluctuation about a mean value. He determined the boundaries of the parametric instability regions and showed that combination resonances were also possible. Further results were obtained by Chen and Rosenberg [2.54] and Ginsberg [2.55]. Paidoussis and Issid [2.56] extended the study to include stability maps for pinned, clamped and cantilevered pipes. They reported that Chen [2.53] had previously neglected the axial acceleration of the fluid induced by velocity perturbations which could result in underestimating instability zones. Later, they attempted to verify their conclusions experimentally [2.57] and found them to be in good qualitative agreement. In a more recent study, Paidoussis and Sundararajan [2.58] examined both parametric and combination resonances for clamped and cantilevered tubes by using Bolotin's method and a numerical Floquet analysis. A check on their work was provided by Ariaratnam and Sri Namachchivaya [2.59] by using the method of averaging. A comparable analysis for articulated pipes was presented by Bohn and Herrmann [2.60].

Numerous nonlinear investigations were done to further predict oscillatory behavior near critical velocities. Holmes [2.61,2.62] considered first-order structural nonlinearities in his computations to prove that simply supported pipes cannot sustain flutter insta-

bilities. Ch'ng and Dowell [2.63] used Hamilton's principle to derive the differential equation of motion that included nonlinear tension and curvature effects. They calculated the amplitude of limit cycle oscillations of cantilevered tubes and the divergence characteristics of simply supported tubes for the case of steady flow. Other nonlinear, planar motions with periodic flow were studied for continuous cantilevers [2.64-2.66] and two-segmented articulated tube systems [2.67,2.68].

In the past decade various experimental studies were conducted to establish the correlation between theoretical models and physical systems and to indicate areas for further considerations [2.69-2.73]. Another effort focused on verifying the transitions between the instability modes of articulated tubes both experimentally and analytically. Bohn and Herrmann [2.74] examined a system of pipes that was allowed to oscillate in two different planes with the level of "out-of-planeness" being one of the controlled parameters. They found that for various steady flow rates, instability, either by buckling or by flutter, depended upon that spatial parameter. In a more recent study Edelstein and Chen [2.75] investigated the stability transitions from the case of a cantilevered tube to that of a tube supported at both ends.

Subsequent research on the three-dimensional nonlinear motion of articulated tubes was presented by Bajaj and Sethna [2.76,2.77]. They analyzed the equations of motion for bifurcating periodic solutions near critical flow velocities. Lundgren, Sethna and Bajaj

[2.78] considered the nonplanar, nonlinear motion of a vertical continuous cantilevered tube having a nozzle at the free end. This study was motivated by the engineering problems encountered when a pipe ruptures (pipe whip). They determined the critical flow rates at which instability occurred and obtained the stability boundaries for both in-plane and out-of-plane motion. Their analysis did not, however, include the effects of gravity, damping or pulsating flow. In addition, the nonplanar, nonlinear studies of the motion of a simply supported tube is absent in the literature.

2.2 NONPLANAR STRING OSCILLATIONS

Carrier [2.79,2.80] was recognized as the first to derive the nonlinear equations of motion for large-amplitude planar oscillations of an undamped string. He indicated how his analysis could be extended to nonplanar motion, but his primary interest was in determining the period of free vibrations. In 1948, Harrison [2.81] reported the out-of-plane response of a wire to a strictly planar excitation. In subsequent experiments, Lee [2.82] and Oplinger [2.83] considered the planar forced vibrations of a string near resonance and observed the phenomenon of mode jumping. They both noted discrepancies when comparing their results with theory, which could be attributed to the presence of nonplanar motion.

By the 1960's, it was a well-known fact that large-amplitude oscillations of a forced string could become unstable and display a component of vibration in a direction normal to the plane of the

force. The general equations of motion that describe this "whirling" or tubular response were derived by Murthy and Ramakrishna [2.84]. Miles [2.85] considered the stability of forced vibrations near resonance while Anand [2.86] included the effect of viscous damping.

In all of the above studies, the longitudinal displacement of the string had been neglected. Narasimha [2.87] investigated this basic assumption and concluded that there definitely was a coupling between the longitudinal and transverse modes of vibration. Anand [2.88] rederived the equations of motion and considered the large-amplitude free vibration of a damped string. Later, he outlined the planar and nonplanar stability regions for forced vibrations [2.89]. Eller [2.90] found the theoretical results to be in good qualitative agreement with experimental observations. Further analytical studies were presented by Lee and Ames [2.91] and Anand [2.92].

More recently, Gough [2.93] returned to the nonlinear free vibrations of a damped string. He described the precession of the orbital motion of the string and confirmed his results with experimental measurements. Additional work on the nonplanar forced response of a stretched string was completed by Miles [2.94]. His analysis included a description of the bifurcation points as a function of the damping parameter.

2.3 NONPLANAR BEAM OSCILLATIONS

A review of the literature revealed that only a limited amount of research has been done on the whirling response of rods or beams.

In 1971, Haight and King [2.95] studied the nonlinear oscillations of a circular cantilevered rod. They observed analytically and experimentally the elliptical path of the free end of the rod when the base was subjected to a planar harmonic excitation. Hyer [2.96,2.97] extended the study by investigating amplitude-frequency relationships and stability characteristics. Ho, Scott and Eisley [2.98,2.99] examined the free and forced nonlinear vibrations of a simply supported, axially restrained beam. They presented amplitude-frequency plots and outlined stability regions for both in-plane and out-of-plane motions. Finally, the effect of flexural-torsional coupling on the nonplanar vibrations of beams with various support conditions was considered by Crespo da Silva and Glynn [2.100,2.101].

2.4 REFERENCES

[2.1] Bourrières, F.J., "Sur un Phenomène D'Oscillation Auto-entretenue en Mécanique des Fluides Réels," *Publications Scientifiques et Techniques du Ministere de l'Air*, No. 147, 1939.

[2.2] Ashley, H. and Haviland, G., "Bending Vibrations of a Pipeline Containing Flowing Fluid," *Journal of Applied Mechanics*, Trans. ASME, Vol. 17, 1950, pp. 229-232.

[2.3] Feodos'yev, V.P., "Vibrations and Stability of a Pipe When a Liquid Flows Through It," *Inzhenernyi Sbornik*, Vol. 10, 1951, pp. 169-170.

[2.4] Housner, G.W., "Bending Vibrations of a Pipe Line Containing Flowing Fluid," *Journal of Applied Mechanics*, Trans. ASME, Vol. 19, 1952, pp. 205-208.

[2.5] Niordson, F.I.N., "Vibrations of a Cylindrical Tube Containing Flowing Fluid," *Transactions of the Royal Institute of Technology (Stockholm)*, No. 73, 1953.

[2.6] Long, R.H., Jr., "Experimental and Theoretical Study of Transverse Vibration of a Tube Containing Flowing Fluid," *Journal of Applied Mechanics*, Trans. ASME, Vol. 22, 1955, pp. 65-68.

[2.7] Handelman, G.H., "A Note on the Transverse Vibration of a Tube Containing Flowing Fluid," *Quarterly of Applied Mathematics*, Vol. 13, No. 3, 1955, pp. 326-330.

[2.8] Heinrich, G., "Vibrations of Tubes With Flow," *Zeitschrift für angewandte Mathematik und Mechanik*, Vol. 36, No. 11/12, 1956, pp. 417-427.

[2.9] Bolotin, V.V., "End Deformations of Flexible Pipelines," *Trudy Moskovskogo Energeticheskogo Instituta*, No. 19, 1956, pp. 272-291.

[2.10] Hu, H.-C. and Tsoon, W.-S., "On the Flexural Vibrations of a Pipe Line Containing Flowing Fluid," *Proceedings of Theoretical and Applied Mechanics (India)*, 1957, pp. 203-216.

[2.11] Movchan, A.A., "On One Problem of Stability of a Pipe With a Fluid Flowing Through It," *Journal of Applied Mathematics and Mechanics (Prikladnaya Matematika i Mekhanika)*, Vol. 29, No. 4, 1965, pp. 760-762.

[2.12] Dodds, H.L., Jr. and Runyan, H.L., "Effect of High-Velocity Fluid Flow on the Bending Vibrations and Static Divergence of a Simply Supported Pipe," NASA Technical Note D-2870, 1965.

[2.13] Li, T. and DiMaggio, O.D., "Vibration of a Propellant Line Containing Flowing Fluid," AIAA Fifth Annual Structures and Materials Conference, AIAA Publication No. CP-8, April 1964, pp. 194-199.

[2.14] Stein, R.A. and Tobriner, M.W., "Vibration of Pipes Containing Flowing Fluid," *Journal of Applied Mechanics*, Trans. ASME, Vol. 37, 1970, pp. 906-916.

[2.15] Naguleswaran, S. and Williams, C.J.H., "Lateral Vibration of a Pipe Conveying Fluid," *Journal of Mechanical Engineering Science*, Vol. 10, No. 3, 1968, pp. 228-238.

[2.16] Plaut, R.H. and Huseyin, K., "Instability of Fluid-Conveying Pipes Under Axial Load," *Journal of Applied Mechanics*, Trans. ASME, Vol. 42, 1975, pp. 889-890.

[2.17] Roth, V.W., "Instabilität durchströmter Rohre," *Ingenieur-Archiv*, Vol. 33, No. 4, 1964, pp. 236-263.

[2.18] Thurman, A.L. and Mote, C.D., Jr., "Nonlinear Oscillation of a Cylinder Containing a Flowing Fluid," *Journal of Engineering for Industry*, Trans. ASME, Vol. 91, 1969, pp. 1147-1155.

[2.19] Benjamin, T.B., "Dynamics of a System of Articulated Pipes Conveying Fluid - I. Theory," *Proceedings of the Royal Society (London)*, Series A, Vol. 261, 1961, pp. 457-486.

[2.20] Benjamin, T.B., "Dynamics of a System of Articulated Pipes Conveying Fluid - II. Experiments," *Proceedings of the Royal Society (London)*, Series A, Vol. 261, 1961, pp. 487-499.

[2.21] Gregory, R.W. and Paidoussis, M.P., "Unstable Oscillation of Tubular Cantilevers Conveying Fluid - I. Theory," *Proceedings of the Royal Society (London)*, Series A, Vol. 293, 1966, pp. 512-527.

[2.22] Gregory, R.W. and Paidoussis, M.P., "Unstable Oscillation of Tubular Cantilevers Conveying Fluid - II. Experiments," *Proceedings of the Royal Society (London)*, Series A, Vol. 293, 1966, pp. 528-542.

[2.23] Paidoussis, M.P., "Dynamics of Tubular Cantilevers Conveying Fluid," *Journal of Mechanical Engineering Science*, Vol. 12, 1970, pp. 85-103.

[2.24] Paidoussis, M.P. and Deksnis, E.B., "Articulated Models of Cantilevers Conveying Fluid: The Study of a Paradox," *Journal of Mechanical Engineering Science*, Vol. 12, 1970, pp. 288-300.

[2.25] Hill, J.L. and Swanson, C.P., "Effects of Lumped Masses on the Stability of Fluid Conveying Tubes," *Journal of Applied Mechanics*, Trans. ASME, Vol. 37, 1970, pp. 494-497.

[2.26] Sugiyama, Y., Kumagai, Y., Kishi, T. and Kawagoe, H., "Studies on Stability of Pipes Conveying Fluid (The Effect of a Lumped Mass and Damping)," *Bulletin of the Japan Society of Mechanical Engineers*, Vol. 29, No. 249, 1986, pp. 929-934.

[2.27] Chen, S.-S., "Forced Vibration of a Cantilevered Tube Conveying Fluid," *The Journal of the Acoustical Society of America*, Vol. 48, No. 3, Pt. 2, 1970, pp. 773-775.

[2.28] Nemat-Nasser, S., Prasad, S.N. and Herrmann, G., "Destabilizing Effect of Velocity-Dependent Forces in Nonconservative Continuous Systems," *American Institute of Aeronautics and Astronautics Journal*, Vol. 4, No. 7, 1966, pp. 1276-1280.

[2.29] Herrmann, G. and Nemat-Nasser, S., "Instability Modes of Cantilevered Bars Induced by Fluid Flow Through Attached Pipes," *International Journal of Solids and Structures*, Vol. 3, 1967, pp. 39-52.

[2.30] Mote, C.D., Jr., "Nonconservative Stability by Finite Element," *Journal of the Engineering Mechanics Division, Proceedings of the American Society of Civil Engineers*, Vol. 97, 1971, pp. 645-656.

[2.31] Wiley, J.C. and Furkert, R.E., "Beams Subjected to Follower Force Within the Span," *Journal of the Engineering Mechanics Division, Proceedings of the American Society of Civil Engineers*, Vol. 98, 1972, pp. 1353-1364.

[2.32] Graham, R.D., Frost, M.A., III and Wilhoit, J.C., Jr., "Analysis of the Motion of Deep-Water Drill Strings -- Part 1: Forced Lateral Motion," *Journal of Engineering for Industry*, Trans. ASME, Series B, Vol. 87, 1965, pp. 137-144.

[2.33] Greenwald, A.S. and Dugundji, J., "Static and Dynamic Instabilities of a Propellant Line," AFOSR 67-1395, U.S. Air Force, May 1967.

[2.34] Svetlitskii, V.A., "Vibrations of Flexible Hoses Filled With a Moving Fluid (Fuel)," *Izvestiia Vysshikh Uchebnykh Zavedenii - Mashinostroenie*, Vol. 3, 1966, pp. 22-30.

[2.35] Srinvasan, P. and Lakshminarayanan, V., "Vibration of Pipe Carrying Flowing Fluid," *Transportation Engineering Journal, Proceedings of the American Society of Civil Engineers*, Vol. 96, 1970, pp. 165-174.

[2.36] Jones, L.H. and Goodwin, B.E., "The Transverse Vibrations of a Pipe Containing Flowing Fluid: Methods of Integral Equations," *Quarterly of Applied Mathematics*, Vol. 29, No. 3, 1971, pp. 363-374.

[2.37] Bishop, R.E.D. and Fawzy, I., "Free and Forced Oscillation of a Vertical Tube Containing a Flowing Fluid," *Philosophical Transactions of the Royal Society of London, Mathematical and Physical Sciences*, Vol. 284, 1976, pp. 1-47.

[2.38] Becker, M., Hauger, W. and Winzen, W., "Exact Stability Analysis of Uniform Cantilevered Pipes Conveying Fluid or Gas," *Archives of Mechanics*, Vol. 30, No. 6, 1978, pp. 757-768.

[2.39] Ting, E.C. and Kanning, J.L., "Dynamics of Flow-Conveying Structures," *The Third National Congress on Pressure Vessel and Piping Technology: Flow Induced Vibrations*, ed. Chen, S.-S., 1979, pp. 57-61.

[2.40] Paidoussis, M.P. and Denise, J.-P., "Flutter of Cylindrical Shells Conveying Fluid," *Journal of Sound and Vibration*, Vol. 16, No. 3, 1971, pp. 459-461.

[2.41] Paidoussis, M.P. and Denise, J.-P., "Flutter of Thin Cylindrical Shells Conveying Fluid," *Journal of Sound and Vibration*, Vol. 20, No. 1, 1972, pp. 9-26.

[2.42] Weaver, D.S. and Unny, T.E., "On the Dynamic Stability of Fluid-Conveying Pipes," *Journal of Applied Mechanics*, Trans. ASME, Vol. 40, 1973, pp. 48-52.

[2.43] Paidoussis, M.P., "Stability of Tubular Cylinders Conveying Fluid," *Proceedings of IUTAM/IAHR Symposium on Flow-Induced Structural Vibrations (Karlsruhe, FRG)*, 1972, pp. 676-683.

[2.44] Paidoussis, M.P., "Flutter of Conservative Systems of Pipes Conveying Incompressible Fluid," *Journal of Mechanical Engineering Science*, Vol. 17, 1975, pp. 19-25.

[2.45] Paidoussis, M.P., Luu, T.P. and Laithier, B.E., "Dynamics of Finite-Length Tubular Beams Conveying Fluid," *Journal of Sound and Vibration*, Vol. 106, No. 2, 1986, pp. 311-331.

[2.46] Unny, T.E., Martin, E.L. and Dubey, R.N., "Hydroelastic Instability of Uniformly Curved Pipe-Fluid Systems," *Journal of Applied Mechanics*, Trans. ASME, Vol. 37, 1970, pp. 817-822.

[2.47] Chen, S.-S., "Instability of a Uniformly Curved Tube Conveying Fluid," *Journal of Applied Mechanics*, Trans. ASME, Vol. 38, 1971, p. 1087.

[2.48] Chen, S.-S., "Vibration and Stability of a Uniformly Curved Tube Conveying Fluid," *The Journal of the Acoustical Society of America*, Vol. 51, 1972, pp. 223-232.

[2.49] Chen, S.-S., "Flow-Induced In-Plane Instabilities of Curved Pipes," *Nuclear Engineering and Design*, Vol. 23, 1972, pp. 29-38.

[2.50] Chen, S.-S., "Out-of-Plane Vibration and Stability of Curved Tubes Conveying Fluid," *Journal of Applied Mechanics*, Trans. ASME, Vol. 40, 1973, pp. 362-368.

[2.51] Hill, J.L. and Davis, C.G., "The Effect of Initial Forces on the Hydroelastic Vibration and Stability of Planar Curved Tubes," *Journal of Applied Mechanics*, Trans. ASME, Vol. 41, 1974, pp. 355-359.

[2.52] Doll, R.W. and Mote, C.D., Jr., "On the Dynamic Analysis of Curved and Twisted Cylinders Transporting Fluids," *Journal of Pressure Vessel Technology*, Trans. ASME, Vol. 98, 1976, pp. 143-150.

[2.53] Chen, S.-S., "Dynamic Stability of Tube[sic] Conveying Fluid," *Journal of the Engineering Mechanics Division, Proceedings of the American Society of Civil Engineers*, Vol. 97, 1971, pp. 1469-1485.

[2.54] Chen, S.-S. and Rosenberg, G.S., "Vibrations and Stability of a Tube Conveying Fluid," USAEC Report ANL-7762, Argonne National Laboratory, March 1971.

[2.55] Ginsberg, J.H., "The Dynamic Stability of a Pipe Conveying a Pulsatile Flow," *International Journal of Engineering Science*, Vol. 11, 1973, pp. 1013-1024.

[2.56] Paidoussis, M.P. and Issid, N.T., "Dynamic Stability of Pipes Conveying Fluid," *Journal of Sound and Vibration*, Vol. 33, No. 3, 1974, pp. 267-294.

[2.57] Paidoussis, M.P. and Issid, N.T., "Experiments on Parametric Resonance of Pipes Containing Pulsatile Flow," *Journal of Applied Mechanics*, Trans. ASME, Vol. 43, 1976, pp. 198-202.

[2.58] Paidoussis, M.P. and Sundararajan, C., "Parametric and Combination Resonances of a Pipe Conveying Pulsating Fluid," *Journal of Applied Mechanics*, Trans. ASME, Vol. 42, 1975, pp. 780-784.

[2.59] Ariaratnam, S.T. and Sri Namachchivaya, N., "Dynamic Stability of Pipes Conveying Pulsating Fluid," *Journal of Sound and Vibration*, Vol. 107, No. 2, 1986, pp. 215-230.

[2.60] Bohn, M.P. and Herrmann, G., "The Dynamic Behavior of Articulated Pipes Conveying Fluid With Periodic Flow Rate," *Journal of Applied Mechanics*, Trans. ASME, Vol. 41, 1974, pp. 55-62.

[2.61] Holmes, P.J., "Bifurcations to Divergence and Flutter in Flow-Induced Oscillations: A Finite Dimensional Analysis," *Journal of Sound and Vibration*, Vol. 53, No. 4, 1977, pp. 471-503.

[2.62] Holmes, P.J., "Pipes Supported at Both Ends Cannot Flutter," *Journal of Applied Mechanics*, Trans. ASME, Vol. 45, 1978, pp. 619-622.

[2.63] Ch'ng, E. and Dowell, E.H., "A Theoretical Analysis of Nonlinear Effects on the Flutter and Divergence of a Tube Conveying Fluid," *The Third National Congress on Pressure Vessel and Piping Technology: Flow Induced Vibrations*, ed. Chen, S.-S., 1979, pp. 65-81.

[2.64] Rousselet, J. and Herrmann, G., "Dynamic Behavior of Continuous Cantilevered Pipes Conveying Fluid Near Critical Velocities," *Journal of Applied Mechanics*, Trans. ASME, Vol. 48, 1981, pp. 943-947.

[2.65] Bajaj, A.K., Sethna, P.R. and Lundgren, T.S., "Hopf Bifurcation Phenomena in Tubes Carrying a Fluid," *SIAM Journal of Applied Mathematics*, Vol. 39, No. 2, 1980, pp. 213-230.

[2.66] Edelstein, W.S., Chen, S.S. and Jendrzejczyk, J.A., "A Finite Element Computation of the Flow-Induced Oscillations in a Cantilevered Tube," *Journal of Sound and Vibration*, Vol. 107, No. 1, 1986, pp. 121-129.

[2.67] Rousselet, J. and Herrmann, G., "Flutter of Articulated Pipes at Finite Amplitude," *Journal of Applied Mechanics*, Trans. ASME, Vol. 44, 1977, pp. 154-158.

[2.68] Bajaj, A.K., "Interactions Between Self and Parametrically Excited Motions in Articulated Tubes," *Journal of Applied Mechanics*, Trans. ASME, Paper No. 84-APM-30, 1984.

[2.69] Liu, H.-S. and Mote, C.D., Jr., "Dynamic Response of Pipes Transporting Fluids," *Journal of Engineering for Industry*, Trans. ASME, Vol. 96, 1974, pp. 591-596.

[2.70] Shilling, R., III and Lou, Y.K., "An Experimental Study on the Dynamic Response of a Vertical Cantilever Pipe Conveying Fluid," *Journal of Energy Resources Technology*, Trans. ASME, Vol. 102, 1980, pp. 129-135.

[2.71] Jendrzejczyk, J.A. and Chen, S.S., "Experiments on Tubes Conveying Fluid," *Thin-Walled Structures*, Vol. 3, No. 2, 1985, pp. 109-134.

[2.72] Chen, S.S. and Jendrzejczyk, J.A., "General Characteristics, Transition, and Control of Instability of Tubes Conveying Fluid," *The Journal of the Acoustical Society of America*, Vol. 77, No. 3, 1985, pp. 887-895.

[2.73] Yoshizawa, M., Moritani, E., Hasegawa, E. and Tsujioka, Y., "Lateral Vibration of a Flexible Pipe Conveying Fluid," *Nihon Kikaigakkai Rombunshu, Transactions of the Japan Society of Mechanical Engineers*, Vol. 52, No. 474, 1986, pp. 710-717.

[2.74] Bohn, M.P. and Herrmann, G., "Instabilities of a Spatial System of Articulated Pipes Conveying Fluid," *Journal of Fluids Engineering*, Trans. ASME, Vol. 96, Series 1, No. 3, 1974, pp. 289-296.

[2.75] Edelstein, W.S. and Chen, S.S., "Flow-Induced Instability of an Elastic Tube with a Variable Support," *Nuclear Engineering and Design*, Vol. 84, No. 1, 1985, pp. 1-11.

[2.76] Bajaj, A.K. and Sethna, P.R., "Bifurcations in Three-Dimensional Motions of Articulated Tubes, Part 1: Linear Systems and Symmetry," *Journal of Applied Mechanics*, Trans. ASME, Vol. 49, 1982, pp. 606-611.

[2.77] Bajaj, A.K. and Sethna, P.R., "Bifurcations in Three-Dimensional Motions of Articulated Tubes, Part 2: Nonlinear Analysis," *Journal of Applied Mechanics*, Trans. ASME, Vol. 49, 1982, pp. 612-618.

[2.78] Lundgren, T.S., Sethna, P.R. and Bajaj, A.K., "Stability Boundaries for Flow Induced Motions of Tubes With an Inclined Terminal Nozzle," *Journal of Sound and Vibration*, Vol. 64, No. 4, 1979, pp. 553-571.

[2.79] Carrier, G.F., "On the Non-linear Vibration Problem of the Elastic String," *Quarterly of Applied Mathematics*, Vol. 3, No. 2, 1945, pp. 157-165.

[2.80] Carrier, G.F., "A Note on the Vibrating String," *Quarterly of Applied Mathematics*, Vol. 7, No. 1, 1949, pp. 97-101.

[2.81] Harrison, H., "Plane and Circular Motion of a String," *The Journal of the Acoustical Society of America*, Vol. 20, No. 6, 1948, pp. 874-875.

[2.82] Lee, E.W., "Non-linear Forced Vibration of a Stretched String," *British Journal of Applied Physics*, Vol. 8, 1957, pp. 411-413.

[2.83] Oplinger, D.W., "Frequency Response of a Nonlinear Stretched String," *The Journal of the Acoustical Society of America*, Vol. 32, No. 12, 1960, pp. 1529-1538.

[2.84] Murthy, G.S.S. and Ramakrishna, B.S., "Nonlinear Character of Resonance in Stretched Strings," *The Journal of the Acoustical Society of America*, Vol. 38, No. 3, 1965, pp. 461-471.

[2.85] Miles, J.W., "Stability of Forced Oscillations of a Vibrating String," *The Journal of the Acoustical Society of America*, Vol. 38, No. 5, 1965, pp. 855-861.

[2.86] Anand, G.V., "Nonlinear Resonance in Stretched Strings with Viscous Damping," *The Journal of the Acoustical Society of America*, Vol. 40, No. 6, 1966, pp. 1517-1528.

[2.87] Narasimha, R., "Non-linear Vibration of an Elastic String," *Journal of Sound and Vibration*, Vol. 8, No. 1, 1968, pp. 134-146.

[2.88] Anand, G.V., "Large-Amplitude Damped Free Vibration of a Stretched String," *The Journal of the Acoustical Society of America*, Vol. 45, No. 5, 1969, pp. 1089-1096.

[2.89] Anand, G.V., "Stability of Nonlinear Oscillations of Stretched Strings," *The Journal of the Acoustical Society of America*, Vol. 46, No. 3, 1969, pp. 667-677.

[2.90] Eller, A.I., "Driven Nonlinear Oscillations of a String," *The Journal of the Acoustical Society of America*, Vol. 51, No. 3, 1972, pp. 960-966.

[2.91] Lee, S.-Y. and Ames, W.F., "A Class of General Solutions to the Nonlinear Dynamic Equations of Elastic Strings," *Journal of Applied Mechanics*, Trans. ASME, Vol. 40, 1973, pp. 1035-1039.

[2.92] Anand, G.V., "Negative Resistance Mode of Forced Oscillations of a String," *The Journal of the Acoustical Society of America*, Vol. 54, No. 3, 1973, pp. 692-698.

[2.93] Gough, C., "The Nonlinear Free Vibration of a Damped Elastic String," *The Journal of the Acoustical Society of America*, Vol. 75, No. 6, 1984, pp. 1770-1776.

[2.94] Miles, J., "Resonant, Nonplanar Motion of a Stretched String," *The Journal of the Acoustical Society of America*, Vol. 75, No. 5, 1984, pp. 1505-1510.

[2.95] Haight, E.C. and King, W.W., "Stability of Nonlinear Oscillations of an Elastic Rod," *The Journal of the Acoustical Society of America*, Vol. 52, No. 3, 1971, pp. 899-911.

[2.96] Hyer, M.W., "Whirling of a Base-Excited Cantilever Beam," *The Journal of the Acoustical Society of America*, Vol. 65, No. 4, 1979, pp. 931-939.

[2.97] Hyer, M.W., "Nonplanar Motions of a Base-Excited Cantilever," *Recent Advances in Structural Dynamics*, ed. Petyt, M., University of Southampton, Institute of Sound and Vibration Research, 1980, pp. 621-630.

[2.98] Ho, C.-H., Scott, R.A. and Eisley, J.G., "Non-planar, Nonlinear Oscillations of a Beam - I. Forced Motion," *International Journal of Non-Linear Mechanics*, Vol. 10, 1975, pp. 113-127.

[2.99] Ho, C.-H., Scott, R.A. and Eisley, J.G., "Non-planar, Nonlinear Oscillations of a Beam - II. Free Motions," *Journal of Sound and Vibration*, Vol. 47, No. 3, 1976, pp. 333-339.

[2.100] Crespo da Silva, M.R.M. and Glynn, C.C., "Non-linear Nonplanar Resonant Oscillations in Fixed-Free Beams With Support Asymmetry," *International Journal of Solids and Structures*, Vol. 15, 1979, pp. 209-219.

[2.101] Crespo da Silva, M.R.M. and Glynn, C.C., "Out-of-Plane Vibrations of a Beam Including Non-linear Inertia and Nonlinear Curvature Effects," *International Journal of Non-Linear Mechanics*, Vol. 13, 1979, pp. 261-271.

CHAPTER 3

PROBLEM FORMULATION

3.1 MODEL DESCRIPTION

The general configuration to be studied in this investigation is shown in Fig. 3.1-1. It consists of a uniform tube of length ℓ supported at each end. It has a cross-sectional area A_t, mass per unit length m_t and flexural rigidity EI. The internal fluid flows axially with velocity c, cross-sectional flow area A_f and mass per unit length m_f. The mean pressure within the tube is p, measured above atmospheric.

In its undeformed (equilibrium) position the longitudinal axis of the tube coincides with the x axis. With this vertical configuration, gravity effects will be assessed. Free and forced response of the tube is allowed in both the x-y and x-z planes along with longitudinal deformations.

In the problem formulation, various assumptions have been made concerning both the tube and the fluid. They include:

1. The effects of rotary inertia and shear deformation of the tube are neglected.
2. Nominal dimensions of the tube do not change significantly with internal pressure or displacements.
3. External drag forces are neglected.
4. The fluid is viscous and incompressible.

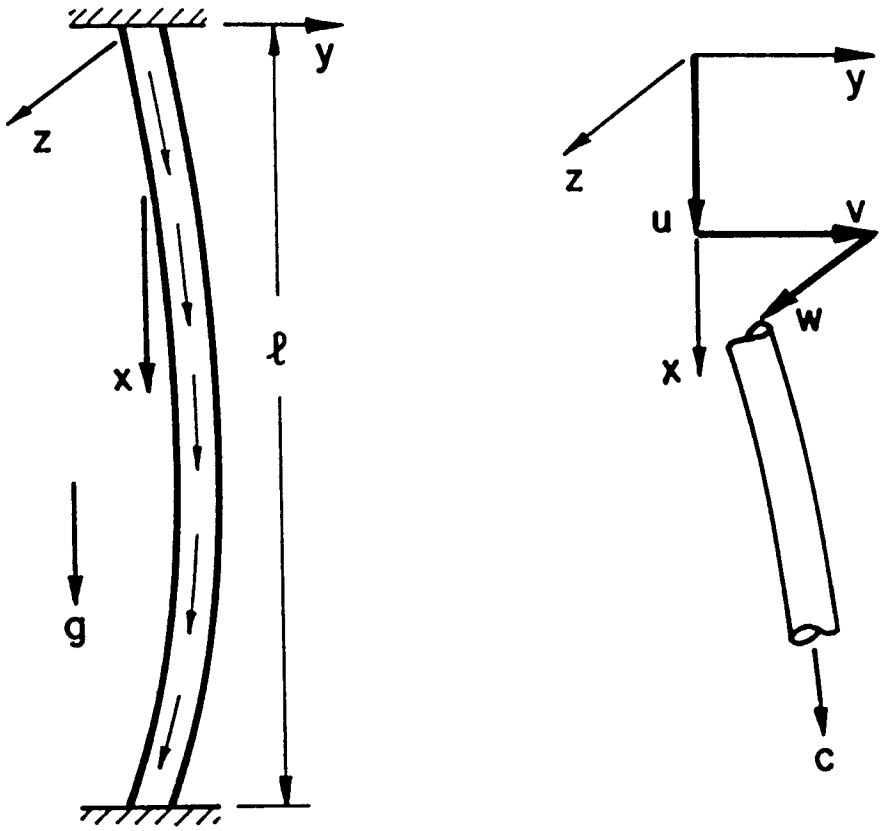

Fig. 3.1-1. Tube Geometry and Coordinate System.

5. Secondary flow effects and radial variations in the flow velocity are neglected.
6. Only the mechanical response of the tube is considered; thermal effects are not assessed.

3.2 DERIVATION OF THE EQUATIONS OF MOTION

An energy approach has been used to derive the equations of motion for the system. Hamilton's principle can be expressed in the form

$$\delta \int_{t_1}^{t_2} (K - U)\, dt + \int_{t_1}^{t_2} \delta W_{nc}\, dt = 0 \qquad (3.2\text{-}1)$$

where K and U represent the kinetic and potential energies, and W_{nc} accounts for the work done by nonconservative forces.

The kinetic energy associated with the motion of the tube is given by

$$K_{tube} = \frac{1}{2} m_t \int_0^{\ell} \left[\left(\frac{\partial u}{\partial t}\right)^2 + \left(\frac{\partial v}{\partial t}\right)^2 + \left(\frac{\partial w}{\partial t}\right)^2 \right] dx \qquad (3.2\text{-}2)$$

where u, v and w are the displacement components in the x, y and z directions, respectively.

For the fluid, the magnitude of the flow velocity c may have a harmonic component to include the possibility of pulsating flow, i.e.,

$$c = c_0(1 + \mu \cos \Omega t) \qquad (3.2\text{-}3)$$

where c_o is the mean velocity, μ is the amplification factor and Ω is the forcing frequency. The velocity components of the fluid flow can be described using Fig. 3.1-1, which shows the direction of c tangent to the deformed tube centerline. Thus, the kinetic energy due to the flowing fluid can be expressed as

$$K_{fluid} = \frac{1}{2} m_f \int_0^{\ell} \left[\left(\frac{\partial u}{\partial t} + c\right)^2 + \left(\frac{\partial v}{\partial t} + c \frac{\partial v}{\partial x}\right)^2 + \left(\frac{\partial w}{\partial t} + c \frac{\partial w}{\partial x}\right)^2\right] dx \ . \tag{3.2-4}$$

It should be noted that nonlinear inertia effects from the fluid have not been included.

The potential energy of the system consists of the elastic energy stored in tension and the elastic strain energy due to bending. The contribution from the axial load is

$$U_{tension} = \frac{1}{2A_t E} \int_0^{\ell} T^2 \, dx \tag{3.2-5}$$

where T is the absolute tension in the tube. In general, this tension is comprised of a number of components including a static pretensile load T_o and the weight of the tube and fluid which results in a linear axial variation. Also, since the lower end of the tube is not free and the fluid is allowed to discharge into a pool, there will be an additional tensile term equal to $pA_t(2\nu - 1)$ for a thin tube. In order to take into account the possibility of large

amplitude motion, nonlinear tension effects can be included by considering higher order terms in the expression for the tube extension. Thus, the tension can be written as

$$T = T_o - pA_f(1 - 2\nu) + (m_f + m_t)g(\ell - x) + EA_t \left(\frac{ds - dx}{dx}\right) \qquad (3.2\text{-}6)$$

where

$$\frac{ds}{dx} = \left[\left(1 + \frac{\partial u}{\partial x}\right)^2 + \left(\frac{\partial v}{\partial x}\right)^2 + \left(\frac{\partial w}{\partial x}\right)^2\right]^{1/2} \qquad (3.2\text{-}7)$$

$$\cong 1 + \frac{\partial u}{\partial x} + \frac{1}{2}\left(\frac{\partial v}{\partial x}\right)^2 + \frac{1}{2}\left(\frac{\partial w}{\partial x}\right)^2 - \frac{1}{2}\frac{\partial u}{\partial x}\left(\frac{\partial v}{\partial x}\right)^2 - \frac{1}{2}\left(\frac{\partial u}{\partial x}\right)\left(\frac{\partial w}{\partial x}\right)^2$$

$$+ \frac{1}{2}\left(\frac{\partial u}{\partial x}\right)^2\left(\frac{\partial v}{\partial x}\right)^2 + \frac{1}{2}\left(\frac{\partial u}{\partial x}\right)^2\left(\frac{\partial w}{\partial x}\right)^2 - \frac{1}{8}\left(\frac{\partial v}{\partial x}\right)^4 - \frac{1}{4}\left(\frac{\partial v}{\partial x}\right)^2\left(\frac{\partial w}{\partial x}\right)^2$$

$$- \frac{1}{8}\left(\frac{\partial w}{\partial x}\right)^4 + \ldots .$$

The strain energy due to bending is given by

$$U_{bending} = \frac{1}{2EI}\int_0^{\ell}\left[\left(\frac{EI\,\frac{\partial^2 v}{\partial x^2}}{\left[1 + \left(\frac{\partial v}{\partial x}\right)^2\right]^{3/2}}\right)^2 + \left(\frac{EI\,\frac{\partial^2 w}{\partial x^2}}{\left[1 + \left(\frac{\partial w}{\partial x}\right)^2\right]^{3/2}}\right)^2\right] dx \; . \qquad (3.2\text{-}8)$$

Using a binomial expansion, Eq. (3.2-8) becomes

$$U_{bending} = \frac{1}{2}\int_0^{\ell} \{EI\,(\frac{\partial^2 v}{\partial x^2})^2[1 - 3\,(\frac{\partial v}{\partial x})^2 + 6\,(\frac{\partial v}{\partial x})^4 - \ldots] + EI\,(\frac{\partial^2 w}{\partial x^2})^2[1 - 3\,(\frac{\partial w}{\partial x})^2 + 6\,(\frac{\partial w}{\partial x})^4 - \ldots]\}\,dx\,. \tag{3.2-9}$$

The work done by nonconservative damping forces can be expressed as

$$\int_{t_1}^{t_2} \delta W_{nc}\,dt = \int_{t_1}^{t_2}\int_0^{\ell} \kappa_o\,[\frac{\partial u}{\partial t}\,\delta u\,dx + \frac{\partial v}{\partial t}\,\delta v\,dx + \frac{\partial w}{\partial t}\,\delta w\,dx]\,dt \tag{3.2-10}$$

where κ_o is considered to be an equivalent damping coefficient that includes both internal structural damping and viscous damping due to the friction of the tube with the surrounding medium. It should be noted that κ_o can be adjusted to comply with the conditions of the problem.

Finally, substituting into Eq. (3.2-1) and employing variational calculus, the three-dimensional equations of motion are

$$(m_f + m_t)\frac{\partial^2 u}{\partial t^2} + m_f\frac{\partial c}{\partial t} + \kappa_o\frac{\partial u}{\partial t} - \frac{T^*(m_f + m_t)g}{A_t E} + (m_f + m_t)g[1 - \frac{\partial u}{\partial x} - \frac{1}{2}(\frac{\partial v}{\partial x})^2 - \frac{1}{2}(\frac{\partial w}{\partial x})^2 + \frac{1}{2}(\frac{\partial u}{\partial x})(\frac{\partial v}{\partial x})^2 + \frac{1}{2}(\frac{\partial u}{\partial x})(\frac{\partial w}{\partial x})^2] - EA_t\frac{\partial^2 u}{\partial x^2} - \frac{\partial}{\partial x}\{(EA_t - T^*)[\frac{1}{2}(\frac{\partial v}{\partial x})^2 + \frac{1}{2}(\frac{\partial w}{\partial x})^2 - (\frac{\partial u}{\partial x})(\frac{\partial v}{\partial x})^2 - (\frac{\partial u}{\partial x})(\frac{\partial w}{\partial x})^2]\} = 0 \tag{3.2-11}$$

$$(m_f + m_t)\frac{\partial^2 v}{\partial t^2} + 2m_f c\frac{\partial^2 v}{\partial x \partial t} + m_f c^2\frac{\partial^2 v}{\partial x^2} + m_f\frac{\partial c}{\partial t}\frac{\partial v}{\partial x} + \kappa_o\frac{\partial v}{\partial t} - \frac{\partial}{\partial x}\{T^*\frac{\partial v}{\partial x}$$

$$+ (EA_t - T^*)[\frac{\partial u}{\partial x} - (\frac{\partial u}{\partial x})^2 + \frac{1}{2}(\frac{\partial v}{\partial x})^2 + \frac{1}{2}(\frac{\partial w}{\partial x})^2]\frac{\partial v}{\partial x}\} + EI\frac{\partial^4 v}{\partial x^4}$$

$$- 3EI(\frac{\partial v}{\partial x})^2\frac{\partial^4 v}{\partial x^4} - 12EI(\frac{\partial v}{\partial x})(\frac{\partial^2 v}{\partial x^2})(\frac{\partial^3 v}{\partial x^3}) - 3EI(\frac{\partial^2 v}{\partial x^2})^3 = 0 \qquad (3.2\text{-}12)$$

$$(m_f + m_t)\frac{\partial^2 w}{\partial t^2} + 2m_f c\frac{\partial^2 w}{\partial x \partial t} + m_f c^2\frac{\partial^2 w}{\partial x^2} + m_f\frac{\partial c}{\partial t}\frac{\partial w}{\partial x} + \kappa_o\frac{\partial w}{\partial t} - \frac{\partial}{\partial x}\{T^*\frac{\partial w}{\partial x}$$

$$+ (EA_t - T^*)[\frac{\partial u}{\partial x} - (\frac{\partial u}{\partial x})^2 + \frac{1}{2}(\frac{\partial v}{\partial x})^2 + \frac{1}{2}(\frac{\partial w}{\partial x})^2]\frac{\partial w}{\partial x}\} + EI\frac{\partial^4 w}{\partial x^4}$$

$$- 3EI(\frac{\partial w}{\partial x})^2\frac{\partial^4 w}{\partial x^4} - 12EI(\frac{\partial w}{\partial x})(\frac{\partial^2 w}{\partial x^2})(\frac{\partial^3 w}{\partial x^3}) - 3EI(\frac{\partial^2 w}{\partial x^2})^3 = 0 \qquad (3.2\text{-}13)$$

where $$T^* = T_o - pA_f(1 - 2\nu) + (m_f + m_t)g(\ell - x) \; . \qquad (3.2\text{-}14)$$

These equations are presented in general form with the order of the nonlinear terms high enough to cover a wider range of potential problems. When different categories of problems are analyzed, simplifications will reduce the complexity of the equations, e.g., negligible flexural stiffness, axial displacements which are much smaller than lateral and transverse components, etc.

For planar analysis, Eq. (3.2-12) can be linearized to decouple the lateral and longitudinal displacements

$$(m_f + m_t)\frac{\partial^2 v}{\partial t^2} + 2m_f c\frac{\partial^2 v}{\partial x \partial t} + m_f\frac{\partial c}{\partial t}\frac{\partial v}{\partial x} + \kappa_o\frac{\partial v}{\partial t} - \frac{\partial}{\partial x}\{[T_o$$

$$- pA_f(1 - 2\nu) + (m_f + m_t)g(\ell - x) - m_f c^2]\frac{\partial v}{\partial x}\} + EI\frac{\partial^4 v}{\partial x^4} = 0 \ . \tag{3.2-15}$$

Such reductions will be further developed for particular free and forced response cases.

3.3 FORCING FUNCTION

The primary external loading to be considered is a dynamic pressure pulse applied to one side of the tube. Chapter 6 deals with the response of a tube to an impulse applied uniformly over the length. However, Chapter 7 examines the results of pulsating flow which produces a parametric excitation of the tube.

CHAPTER 4

TENSION GRADIENT EFFECTS

4.1 GOVERNING EQUATION

In order to determine the basic modal characteristics of a completely flexible tube, the planar equation of motion is considered. In the work which follows, the tension gradient is assessed in the development of an exact solution for the natural frequencies and mode shapes of a flexible tube with steady fluid flow.

Equation (3.2-15) can be reduced to

$$\frac{\partial}{\partial x}\left\{\left[T_o - pA_f(1 - 2\nu) + (m_f + m_t)g(\ell - x) - m_f c^2 \right] \frac{\partial v}{\partial x}\right\} - \kappa_o \frac{\partial v}{\partial t} - (m_f + m_t) \frac{\partial^2 v}{\partial t^2} = 0 \; . \tag{4.1-1}$$

where the Coriolis acceleration of the fluid is also neglected. The equation of motion may be expressed in dimensionless terms by defining the following dimensionless quantities:

$$\bar{v} = \frac{v}{\ell}$$

$$\xi = \frac{T_o - pA_f(1 - 2\nu) + (m_f + m_t)g(\ell - x) - m_f c^2}{(m_f + m_t)g\ell} \tag{4.1-2}$$

$$\tau = \sqrt{\frac{g}{\ell}}\, t \; .$$

Substitution into Eq. (4.1-1) yields

$$\frac{\partial}{\partial \xi}\left\{\xi \frac{\partial \bar{v}}{\partial \xi}\right\} - \kappa \frac{\partial \bar{v}}{\partial \tau} - \frac{\partial^2 \bar{v}}{\partial \tau^2} = 0 \qquad (4.1\text{-}3)$$

where the damping parameter κ is given by

$$\kappa = \frac{\kappa_o}{(m_f + m_t)} \sqrt{\frac{\ell}{g}} \quad . \qquad (4.1\text{-}4)$$

Equation (4.1-3) can be reduced to an ordinary differential equation by assuming a harmonic solution of the form

$$\bar{v}(\xi,\tau) = \mathrm{Re}\{\phi(\xi)\bar{X}e^{i\bar{\omega}\tau}\} \qquad (4.1\text{-}5)$$

where $\phi(\xi)$ is a complex function and $\bar{\omega}$ is the dimensionless frequency. Substitution of Eq. (4.1-5) into (4.1-3) gives

$$\frac{d}{d\xi}\left(\xi \frac{d\phi(\xi)}{d\xi}\right) + (\bar{\omega}^2 - i\kappa\bar{\omega})\,\phi(\xi) = 0 \; . \qquad (4.1\text{-}6)$$

The solution to Eq. (4.1-6) involves Bessel functions of the first and second kind of zero order [4.1], namely

$$\phi(\xi) = AJ_o(\lambda\sqrt{\xi}) + BY_o(\lambda\sqrt{\xi}) \qquad (4.1\text{-}7)$$

where

$$\lambda = \{4(\bar{\omega}^2 - i\kappa\bar{\omega})\}^{1/2} \; . \qquad (4.1\text{-}8)$$

For a general solution, A and B must be complex constants.

A closer look at the argument of J_0 and Y_0 indicates

$$\lambda\sqrt{\xi} = \{4\bar{\omega}^2(\bar{T} - \frac{x}{\ell}) - 4i\kappa\bar{\omega}(\bar{T} - \frac{x}{\ell})\}^{1/2} \qquad (4.1\text{-}9)$$

where the dimensionless tension and frequency are given by

$$\bar{T} = \frac{T_o - pA_f(1 - 2\nu) + (m_f + m_t)g\ell - m_f c^2}{(m_f + m_t)g\ell} \qquad (4.1\text{-}10)$$

$$\bar{\omega} = \sqrt{\frac{\ell}{g}}\,\omega \ . \qquad (4.1\text{-}11)$$

Finally, the complete solution to Eq. (4.1-3) can be expressed as a superposition of an infinite set of the normal modes of the tube, i.e.,

$$\bar{v}(\xi,\tau) = \mathrm{Re}\{\sum_{n=1}^{\infty} \phi_n(\xi)\bar{X}_n e^{i\bar{\omega}_n\tau}\} \qquad (4.1\text{-}12)$$

which also includes the complex constant

$$\bar{X}_n = X_n e^{i\alpha_n} \qquad (4.1\text{-}13)$$

where X_n and α_n are determined by initial conditions. Here $\phi_n(\xi)$ represents the eigenfunctions of the tube which must satisfy the boundary conditions of the problem. For this case

$$\bar{v}(\xi,\tau) = \phi_n(\xi) = 0 \qquad \text{at } x = 0 \text{ and } x = \ell \ . \qquad (4.1\text{-}14)$$

Equation (4.1-14) can then be used to determine the dimensionless frequencies $\bar{\omega}_n$ and complex constants A_n and B_n of Eq. (4.1-7).

For convenience, Eq. (4.1-12) has been rewritten so it contains only the real part. Complex terms can be broken up into their real and imaginary parts by letting

$$\begin{aligned} A_n &= A_{Rn} + iA_{In} \\ B_n &= B_{Rn} + iB_{In} \\ J_o(\lambda_n\sqrt{\xi}) &= J_{oR}(\lambda_n\sqrt{\xi}) + iJ_{oI}(\lambda_n\sqrt{\xi}) \\ Y_o(\lambda_n\sqrt{\xi}) &= Y_{oR}(\lambda_n\sqrt{\xi}) + iY_{oI}(\lambda_n\sqrt{\xi}) \end{aligned} \qquad (4.1\text{-}15)$$

where R and I represent the real and imaginary parts, respectively. Also, let

$$\bar{X}_n e^{i\bar{\omega}_n\tau} = X_n e^{i(\bar{\omega}_n\tau - \alpha_n)} \ . \qquad (4.1\text{-}16)$$

Equations (4.1-15) and (4.1-16) are substituted into (4.1-7) and (4.1-12). After simplifying and retaining the real part only

$$\bar{v}(\xi,\tau) = \sum_{n=1}^{\infty} X_n[A_{Rn}J_{oR}(\lambda_n\sqrt{\xi}) - A_{In}J_{oI}(\lambda_n\sqrt{\xi}) + B_{Rn}Y_{oR}(\lambda_n\sqrt{\xi})$$

$$- B_{In}Y_{oI}(\lambda_n\sqrt{\xi})] \cos(\bar{\omega}_n\tau - \alpha_n) - X_n[A_{Rn}J_{oI}(\lambda_n\sqrt{\xi})$$

$$+ A_{In}J_{oR}(\lambda_n\sqrt{\xi}) + B_{Rn}Y_{oI}(\lambda_n\sqrt{\xi}) + B_{In}Y_{oR}(\lambda_n\sqrt{\xi})]$$

$$\times \sin(\bar{\omega}_n\tau - \alpha_n) \qquad (4.1\text{-}17)$$

which is the general solution to Eq. (4.1-3).

To determine natural frequencies and mode shapes, the eigenfunctions $\phi_n(\xi)$ are required to satisfy the boundary conditions given in Eq. (4.1-14). This results in the following set of equations

$$A_{Rn}J_{oR}(\lambda_n\sqrt{\xi_1}) - A_{In}J_{oI}(\lambda_n\sqrt{\xi_1}) + B_{Rn}Y_{oR}(\lambda_n\sqrt{\xi_1})$$
$$- B_{In}Y_{oI}(\lambda_n\sqrt{\xi_1}) = 0$$

$$A_{Rn}J_{oI}(\lambda_n\sqrt{\xi_1}) + A_{In}J_{oR}(\lambda_n\sqrt{\xi_1}) + B_{Rn}Y_{oI}(\lambda_n\sqrt{\xi_1})$$
$$+ B_{In}Y_{oR}(\lambda_n\sqrt{\xi_1}) = 0$$

(4.1-18)

$$A_{Rn}J_{oR}(\lambda_n\sqrt{\xi_2}) - A_{In}J_{oI}(\lambda_n\sqrt{\xi_2}) + B_{Rn}Y_{oR}(\lambda_n\sqrt{\xi_2})$$
$$- B_{In}Y_{oI}(\lambda_n\sqrt{\xi_2}) = 0$$

$$A_{Rn}J_{oI}(\lambda_n\sqrt{\xi_2}) + A_{In}J_{oR}(\lambda_n\sqrt{\xi_2}) + B_{Rn}Y_{oI}(\lambda_n\sqrt{\xi_2})$$
$$+ B_{In}Y_{oR}(\lambda_n\sqrt{\xi_2}) = 0$$

where ξ_1 and ξ_2 have been used to represent ξ evaluated at $x = 0$ and $x = \ell$, respectively. For a nontrivial solution to (4.1-18) the n determinants of the terms multiplying the A's and B's must equal zero, i.e.,

$$\begin{vmatrix} J_{oR}(\lambda_n\sqrt{\xi_1}) & -J_{oI}(\lambda_n\sqrt{\xi_1}) & Y_{oR}(\lambda_n\sqrt{\xi_1}) & -Y_{oI}(\lambda_n\sqrt{\xi_1}) \\ J_{oI}(\lambda_n\sqrt{\xi_1}) & J_{oR}(\lambda_n\sqrt{\xi_1}) & Y_{oI}(\lambda_n\sqrt{\xi_1}) & Y_{oR}(\lambda_n\sqrt{\xi_1}) \\ J_{oR}(\lambda_n\sqrt{\xi_2}) & -J_{oI}(\lambda_n\sqrt{\xi_2}) & Y_{oR}(\lambda_n\sqrt{\xi_2}) & -Y_{oI}(\lambda_n\sqrt{\xi_2}) \\ J_{oI}(\lambda_n\sqrt{\xi_2}) & J_{oR}(\lambda_n\sqrt{\xi_2}) & Y_{oI}(\lambda_n\sqrt{\xi_2}) & Y_{oR}(\lambda_n\sqrt{\xi_2}) \end{vmatrix} = 0 \qquad (4.1\text{-}19)$$

where $n = 1, 2, 3, \ldots, \infty$. The solution procedure, then, involves choosing a value of $\bar{\omega}$, calculating the argument given by Eq. (4.1-9) and corresponding Bessel function, and finally checking the value of the determinant. After $\bar{\omega}$ is found, the relative values of the complex constants A and B can be determined from (4.1-18). This procedure is repeated until the number of modes identified is sufficient to completely describe the tube motion.

4.2 NUMERICAL RESULTS

An analysis was performed to determine natural frequencies and mode shapes for the special case of zero damping. Setting the damping parameter, κ, to zero in Eq. (4.1-9), eliminates the imaginary term of the argument. With the restriction $\bar{T} > 1.0$, J_o and Y_o are assured to be real. Consequently, the equations in (4.1-18) will uncouple giving the following two sets of equations

$$
\begin{aligned}
A_{Rn}J_{oR}(\lambda_n\sqrt{\xi_1}) + B_{Rn}Y_{oR}(\lambda_n\sqrt{\xi_1}) &= 0 \\
A_{Rn}J_{oR}(\lambda_n\sqrt{\xi_2}) + B_{Rn}Y_{oR}(\lambda_n\sqrt{\xi_2}) &= 0 \\
A_{In}J_{oR}(\lambda_n\sqrt{\xi_1}) + B_{In}Y_{oR}(\lambda_n\sqrt{\xi_1}) &= 0 \\
A_{In}J_{oR}(\lambda_n\sqrt{\xi_2}) + B_{In}Y_{oR}(\lambda_n\sqrt{\xi_2}) &= 0 \ .
\end{aligned}
\tag{4.2-1}
$$

From the above, it is obvious that

$$
\begin{aligned}
A_{Rn} &= A_{In} \\
B_{Rn} &= B_{In}
\end{aligned}
\tag{4.2-2}
$$

and the necessary condition for a nontrivial solution is

$$
J_{oR}(\lambda_n\sqrt{\xi_1})Y_{oR}(\lambda_n\sqrt{\xi_2}) - Y_{oR}(\lambda_n\sqrt{\xi_1})J_{oR}(\lambda_n\sqrt{\xi_2}) = 0 \ . \tag{4.2-3}
$$

Therefore, Eq. (4.2-3) is used to define the natural frequencies of the system.

Along the same lines, the eigenfunctions describing the mode shapes can be simplified to:

$$
\phi_n(\xi) = C_n\left[J_o(\lambda_n\sqrt{\xi}) - \frac{J_o(\lambda_n\sqrt{\xi_1})}{Y_o(\lambda_n\sqrt{\xi_1})}\,Y_o(\lambda_n\sqrt{\xi})\right] \tag{4.2-4}
$$

where C_n is an arbitrary constant and can be incorporated into X_n in (4.1-16).

Equations (4.2-3) and (4.2-4) have been programmed to cover a range of tensions, $\overline{T}$. Accuracy problems arise when solving these equations since the arguments of the Bessel functions given in (4.1-9) can become "relatively" large. Therefore, to eliminate the possibility of round-off errors, calculations were done on a Cray computer. Function subroutines from IMSL were used to calculate J_0's and Y_0's. These allowed arguments in the following ranges

Function	Range of Argument
J_0	$<< 1.3 \times 10^8$
Y_0	2.9×10^{-39} to 1.3×10^8

where both single and double precision are supported. Also, the method of bisection, based on the use of sign changes to detect a zero, was used to determine the roots of (4.2-3).

The first ten natural frequencies computed are shown in Fig. 4.2-1. Tabular values to three decimal places corresponding to these curves are given in Table 4.2-1. Calculations were performed letting $\overline{T}$ approach 1 since $Y_0(0)$ is negatively infinite. Figures 4.2-2 through 4.2-11 show the first ten mode shapes for dimensionless tensions of 1.1, 2.0 and 3.0. Again, Tables 4.2-2 through 4.2-4 show the tabulated values of these mode shapes. For convenience, each has been individually normalized. As shown by the graphs, asymmetry is significant with the lower tensions. Figure 4.2-12 shows the shifts of the maximum amplitude and zero crossing for modes 1 and 2 due to

the nonlinear effects of the tension. Consequently, as $\overline{T}$ becomes much greater than the weight, the natural frequencies and mode shapes will approach that of a classic string.

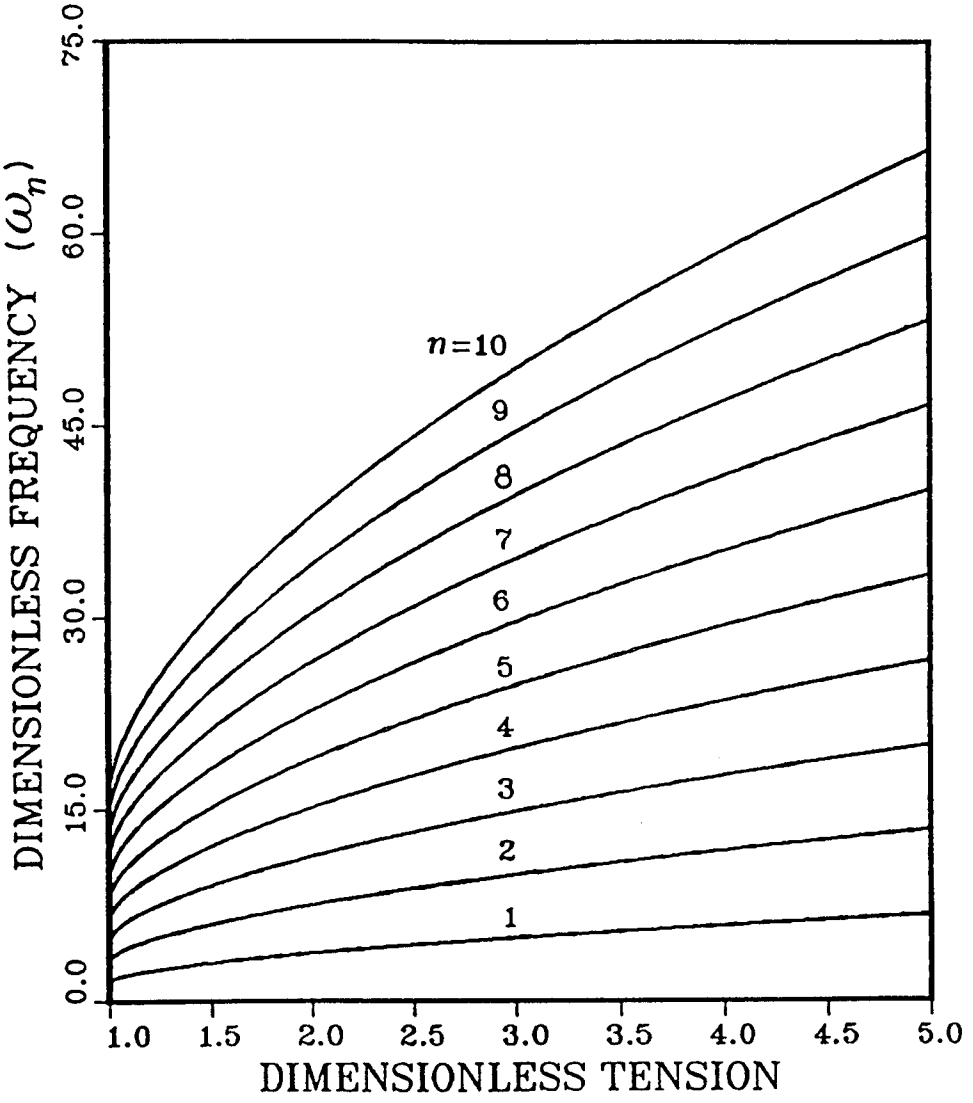

Fig. 4.2-1. Natural Frequencies of Heavy Tubes.

Table 4.2-1. Natural Frequencies of Heavy Tubes
($\bar{\omega}_n$ n = 1,2,3,...,10.)

T	1	2	3	4	5
1.1ØØ	2.1Ø8	4.268	6.419	8.566	1Ø.712
1.2ØØ	2.4ØØ	4.834	7.261	9.686	12.111
1.3ØØ	2.634	5.294	7.948	1Ø.6Ø1	13.253
1.4ØØ	2.838	5.697	8.551	11.4Ø5	14.257
1.5ØØ	3.Ø23	6.Ø63	9.1ØØ	12.135	15.17Ø
1.6ØØ	3.194	6.4Ø2	9.6Ø8	12.812	16.Ø16
1.7ØØ	3.354	6.72Ø	1Ø.Ø84	13.447	16.81Ø
1.8ØØ	3.5Ø5	7.Ø21	1Ø.535	14.Ø48	17.561
1.9ØØ	3.649	7.3Ø8	1Ø.964	14.62Ø	18.276
2.ØØØ	3.786	7.582	11.375	15.167	18.96Ø
2.1ØØ	3.919	7.845	11.77Ø	15.694	19.618
2.2ØØ	4.Ø46	8.Ø99	12.15Ø	16.2Ø1	2Ø.252
2.3ØØ	4.169	8.344	12.518	16.692	2Ø.865
2.4ØØ	4.288	8.582	12.875	17.167	21.459
2.5ØØ	4.4Ø4	8.813	13.221	17.629	22.Ø37
2.6ØØ	4.516	9.Ø38	13.558	18.Ø78	22.598
2.7ØØ	4.626	9.257	13.886	18.516	23.145
2.8ØØ	4.733	9.47Ø	14.2Ø7	18.943	23.679
2.9ØØ	4.837	9.679	14.52Ø	19.36Ø	24.2ØØ
3.ØØØ	4.94Ø	9.883	14.826	19.768	24.71Ø
3.1ØØ	5.Ø4Ø	1Ø.Ø83	15.125	2Ø.167	25.2Ø9
3.2ØØ	5.138	1Ø.279	15.419	2Ø.559	25.699
3.3ØØ	5.234	1Ø.47Ø	15.7Ø6	2Ø.942	26.178
3.4ØØ	5.328	1Ø.659	15.989	21.319	26.649
3.5ØØ	5.42Ø	1Ø.844	16.266	21.689	27.111
3.6ØØ	5.511	11.Ø26	16.539	22.Ø52	27.566
3.7ØØ	5.6Ø1	11.2Ø4	16.8Ø7	22.41Ø	28.Ø12
3.8ØØ	5.689	11.38Ø	17.Ø71	22.761	28.452
3.9ØØ	5.775	11.553	17.331	23.1Ø8	28.885
4.ØØØ	5.861	11.724	17.586	23.449	29.311
4.1ØØ	5.945	11.892	17.838	23.785	29.731
4.2ØØ	6.Ø28	12.Ø57	18.Ø87	24.116	3Ø.145
4.3ØØ	6.1Ø9	12.221	18.332	24.443	3Ø.554
4.4ØØ	6.19Ø	12.382	18.574	24.765	3Ø.956
4.5ØØ	6.27Ø	12.541	18.812	25.Ø83	31.354
4.6ØØ	6.348	12.698	19.Ø48	25.397	31.746
4.7ØØ	6.426	12.853	19.28Ø	25.7Ø7	32.134
4.8ØØ	6.5Ø2	13.ØØ6	19.51Ø	26.Ø14	32.517
4.9ØØ	6.578	13.158	19.737	26.316	32.896
5.ØØØ	6.653	13.3Ø7	19.962	26.616	33.27Ø

Table 4.2-1. Continued.

T	6	7	8	9	10
1.100	12.858	15.003	17.148	19.293	21.438
1.200	14.535	16.959	19.382	21.806	24.229
1.300	15.905	18.557	21.208	23.860	26.511
1.400	17.110	19.962	22.815	25.667	28.519
1.500	18.205	21.240	24.275	27.310	30.344
1.600	19.220	22.424	25.628	28.832	32.036
1.700	20.172	23.535	26.897	30.260	33.622
1.800	21.073	24.586	28.098	31.611	35.123
1.900	21.931	25.587	29.242	32.898	36.553
2.000	22.752	26.545	30.337	34.129	37.922
2.100	23.542	27.466	31.389	35.313	39.237
2.200	24.303	28.354	32.404	36.455	40.505
2.300	25.039	29.212	33.385	37.559	41.732
2.400	25.752	30.044	34.336	38.628	42.920
2.500	26.444	30.852	35.259	39.667	44.074
2.600	27.118	31.638	36.158	40.677	45.197
2.700	27.774	32.404	37.033	41.662	46.291
2.800	28.415	33.151	37.887	42.623	47.359
2.900	29.041	33.881	38.721	43.561	48.401
3.000	29.652	34.595	39.537	44.479	49.421
3.100	30.251	35.294	40.336	45.377	50.419
3.200	30.838	35.978	41.118	46.258	51.398
3.300	31.414	36.650	41.886	47.121	52.357
3.400	31.979	37.309	42.639	47.969	53.299
3.500	32.534	37.956	43.379	48.801	54.223
3.600	33.079	38.592	44.105	49.619	55.132
3.700	33.615	39.218	44.820	50.423	56.026
3.800	34.143	39.833	45.524	51.214	56.905
3.900	34.662	40.439	46.216	51.993	57.770
4.000	35.174	41.036	46.898	52.760	58.623
4.100	35.678	41.624	47.570	53.516	59.463
4.200	36.174	42.204	48.233	54.262	60.291
4.300	36.664	42.775	48.886	54.997	61.108
4.400	37.148	43.339	49.531	55.722	61.913
4.500	37.625	43.896	50.167	56.438	62.708
4.600	38.096	44.445	50.795	57.144	63.494
4.700	38.561	44.988	51.415	57.842	64.269
4.800	39.021	45.524	52.028	58.531	65.035
4.900	39.475	46.054	52.633	59.213	65.792
5.000	39.924	46.578	53.232	59.886	66.540

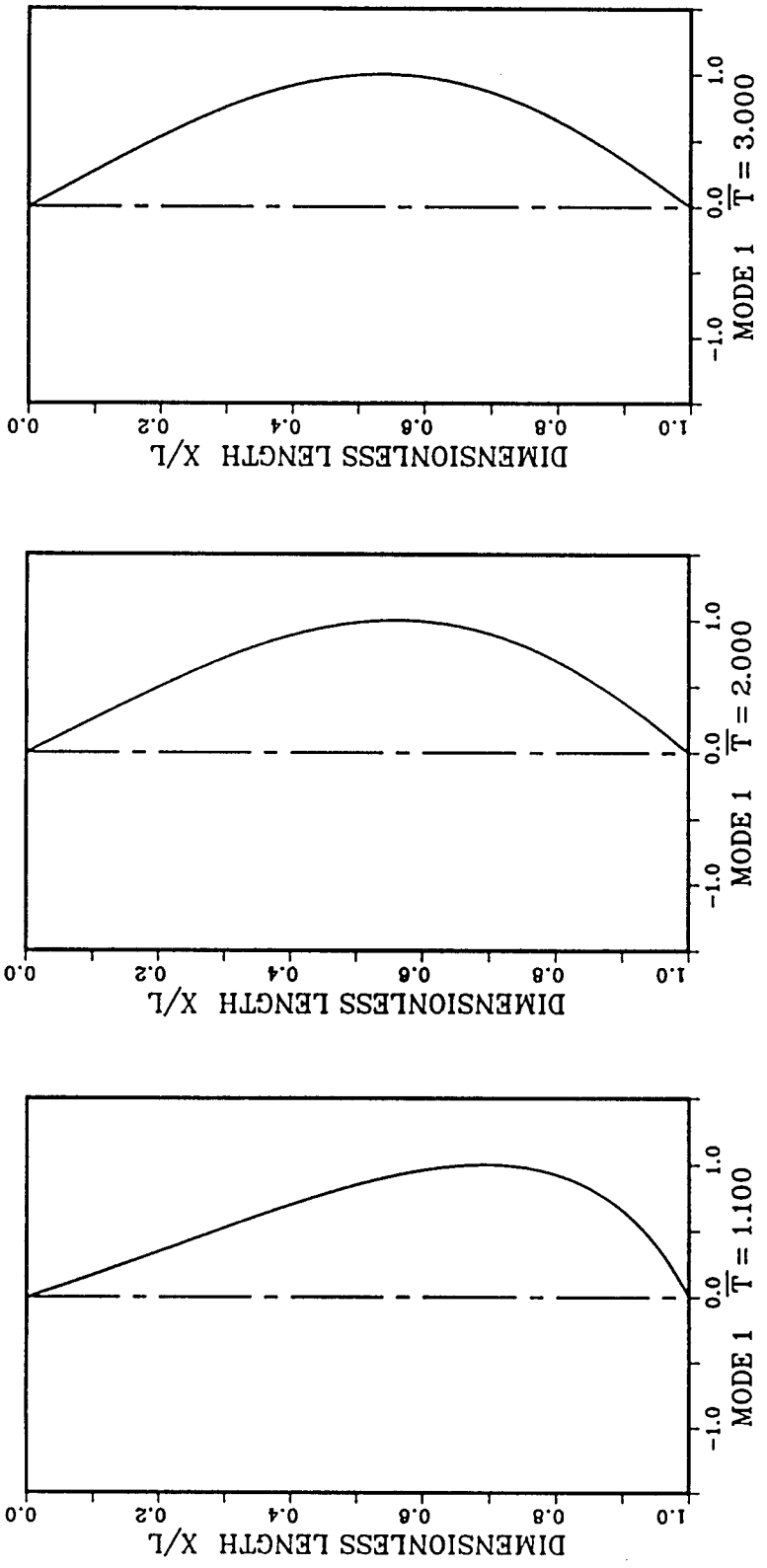

Fig. 4.2-2. Mode Shape 1 for Dimensionless Tensions of 1.1, 2.0 and 3.0.

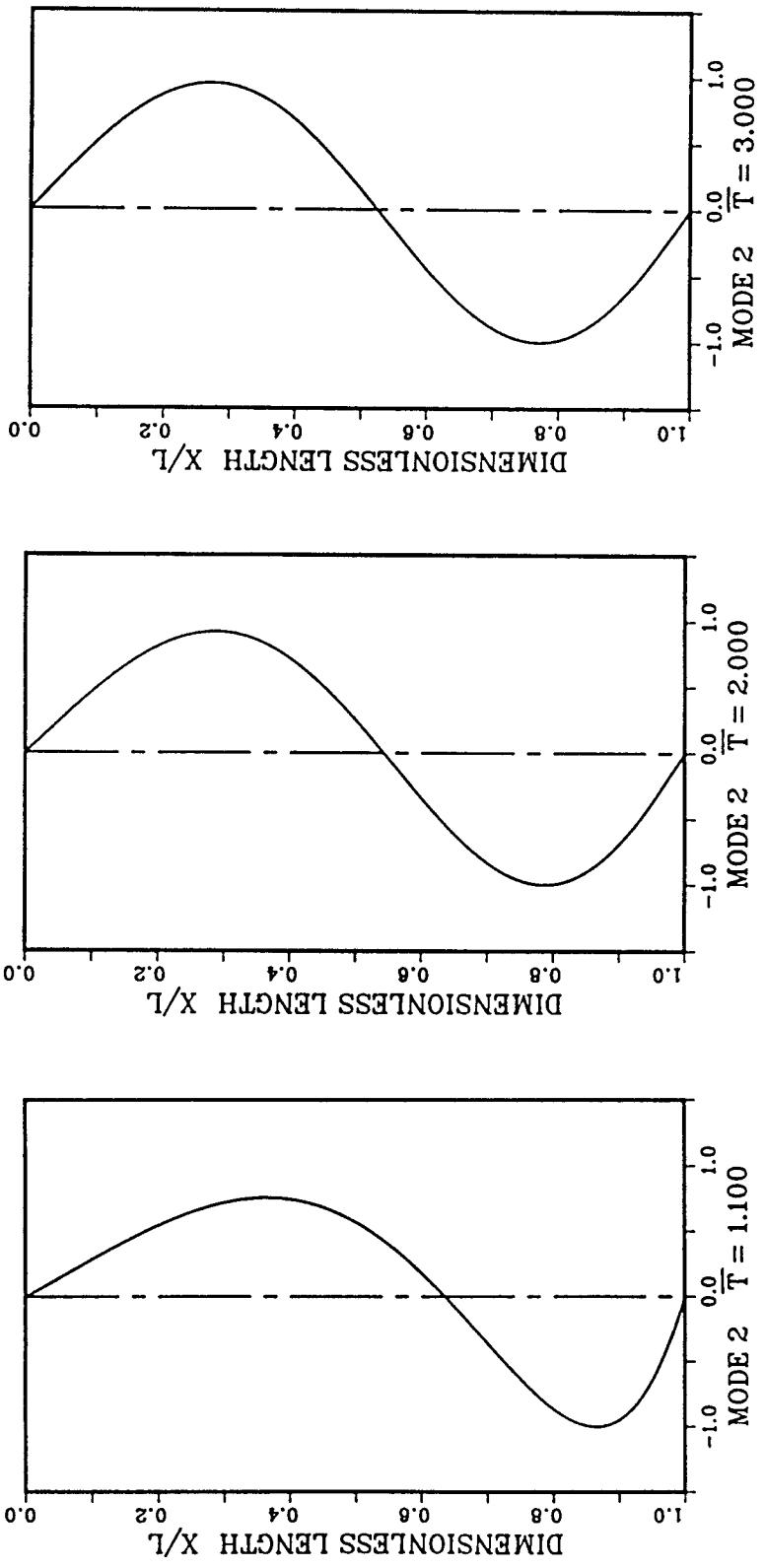

Fig. 4.2-3. Mode Shape 2 for Dimensionless Tensions of 1.1, 2.0 and 3.0.

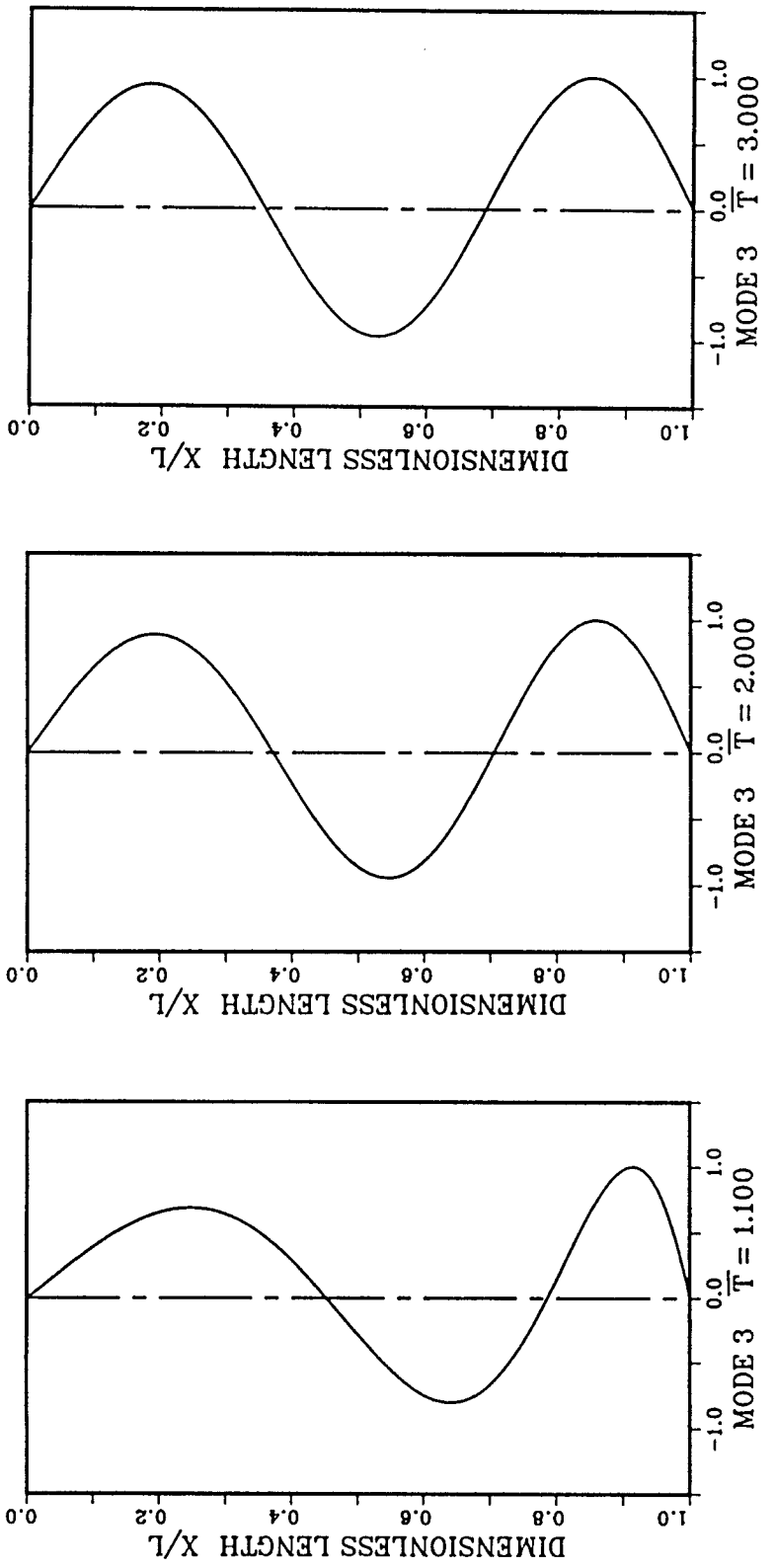

Fig. 4.2-4. Mode Shape 3 for Dimensionless Tensions of 1.1, 2.0 and 3.0.

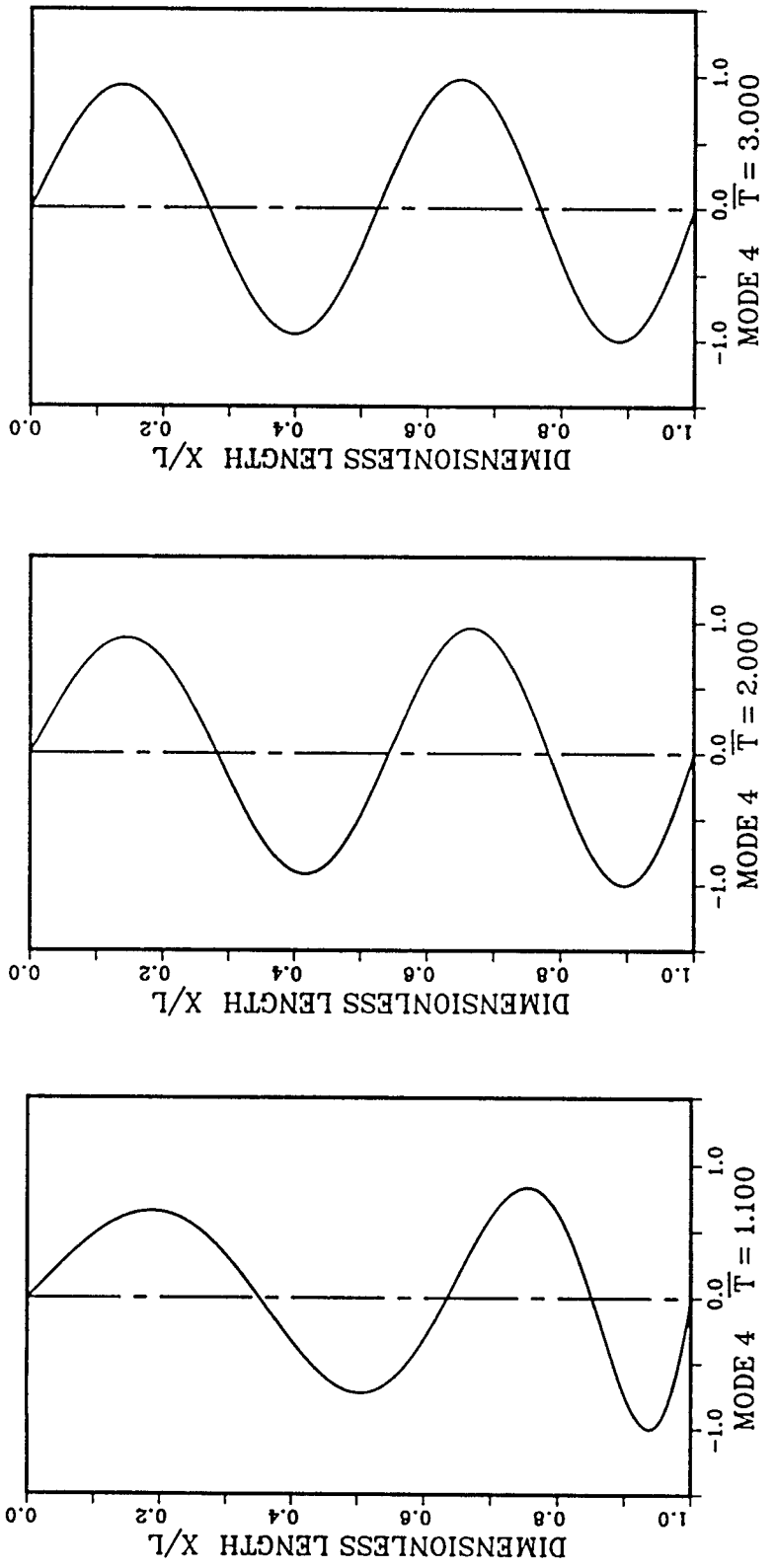

Fig. 4.2-5. Mode Shape 4 for Dimensionless Tensions of 1.1, 2.0 and 3.0.

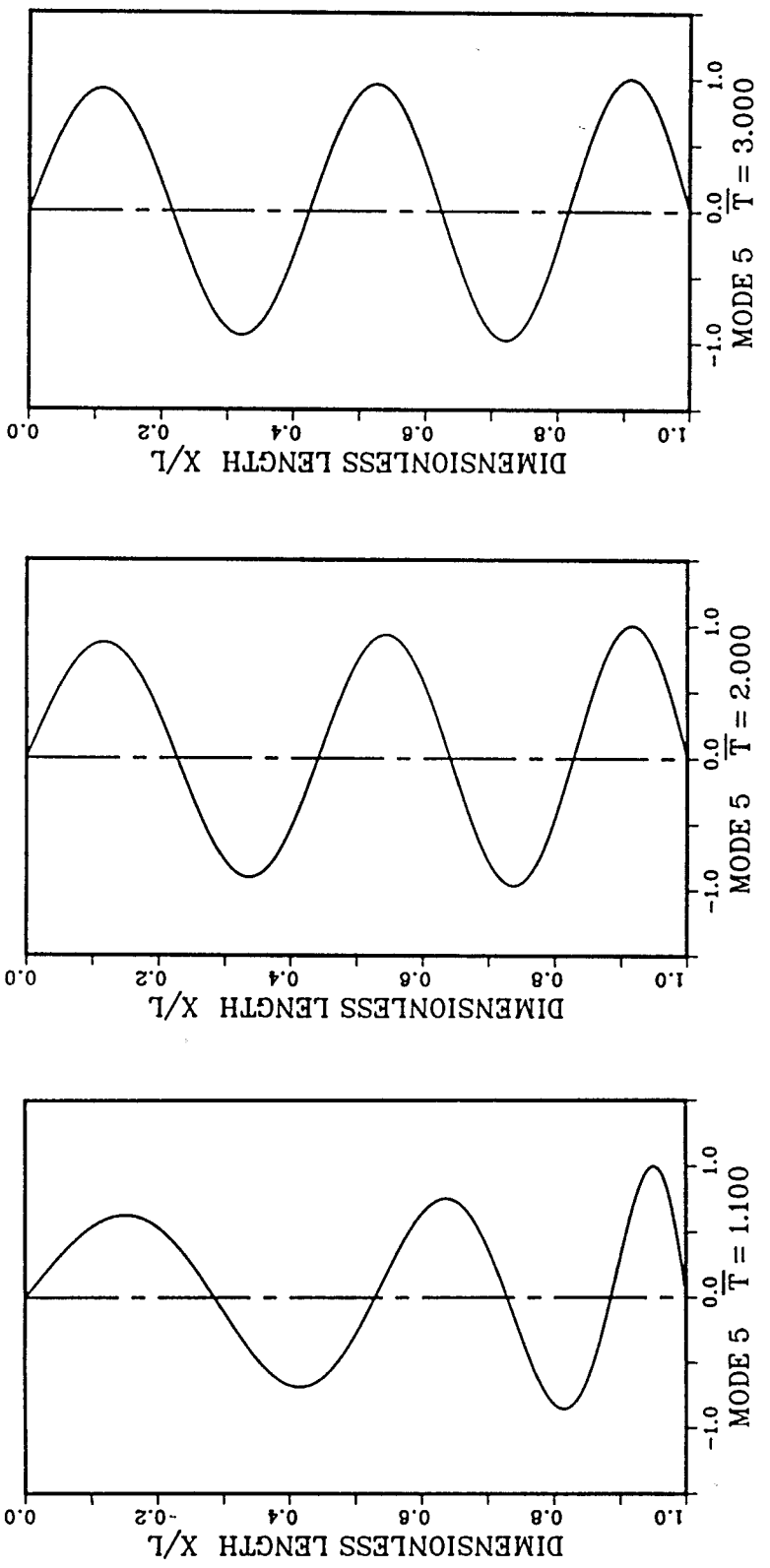

Fig. 4.2-6. Mode Shape 5 for Dimensionless Tensions of 1.1, 2.0 and 3.0.

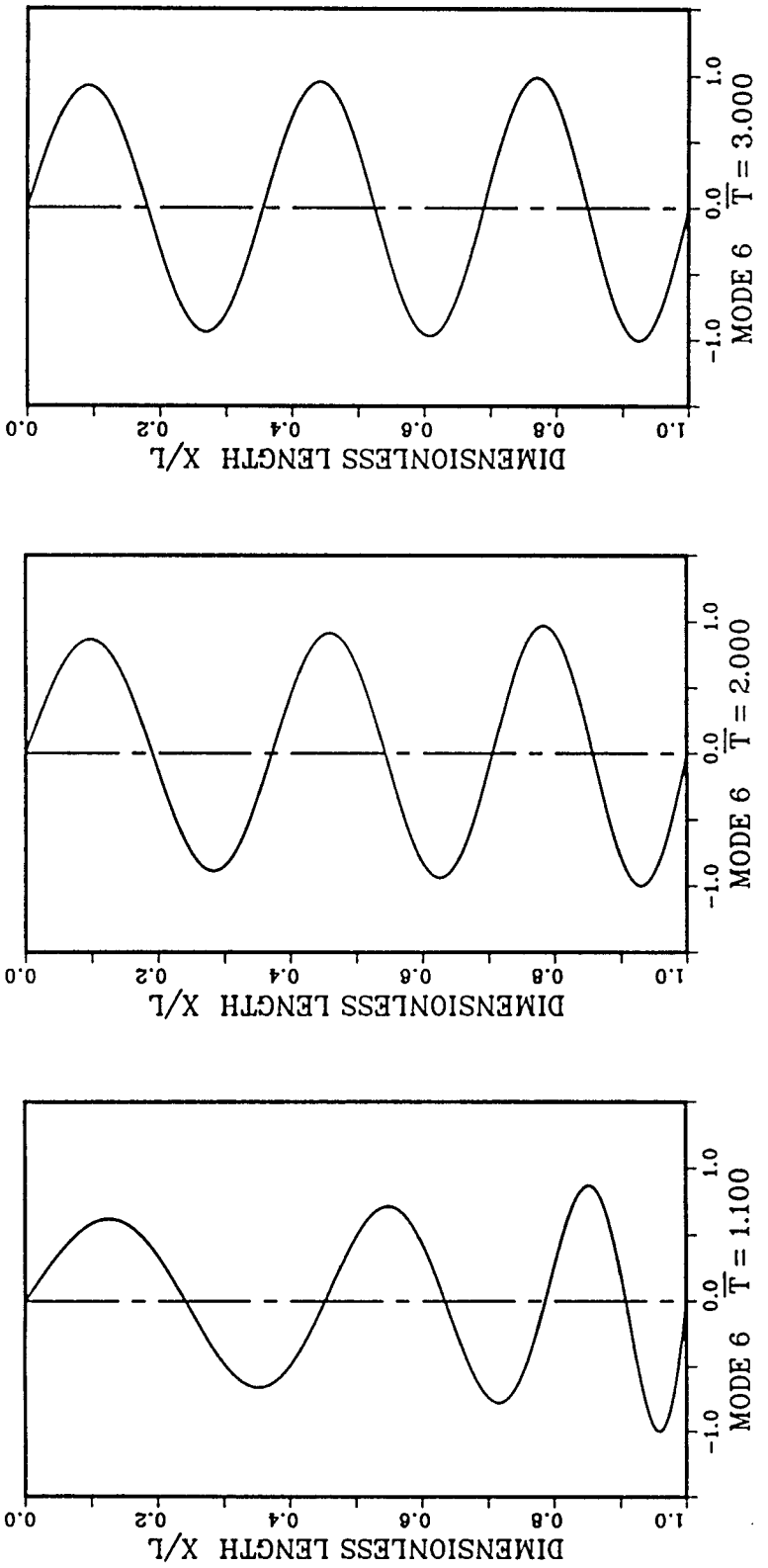

Fig. 4.2-7. Mode Shape 6 for Dimensionless Tensions of 1.1, 2.0 and 3.0.

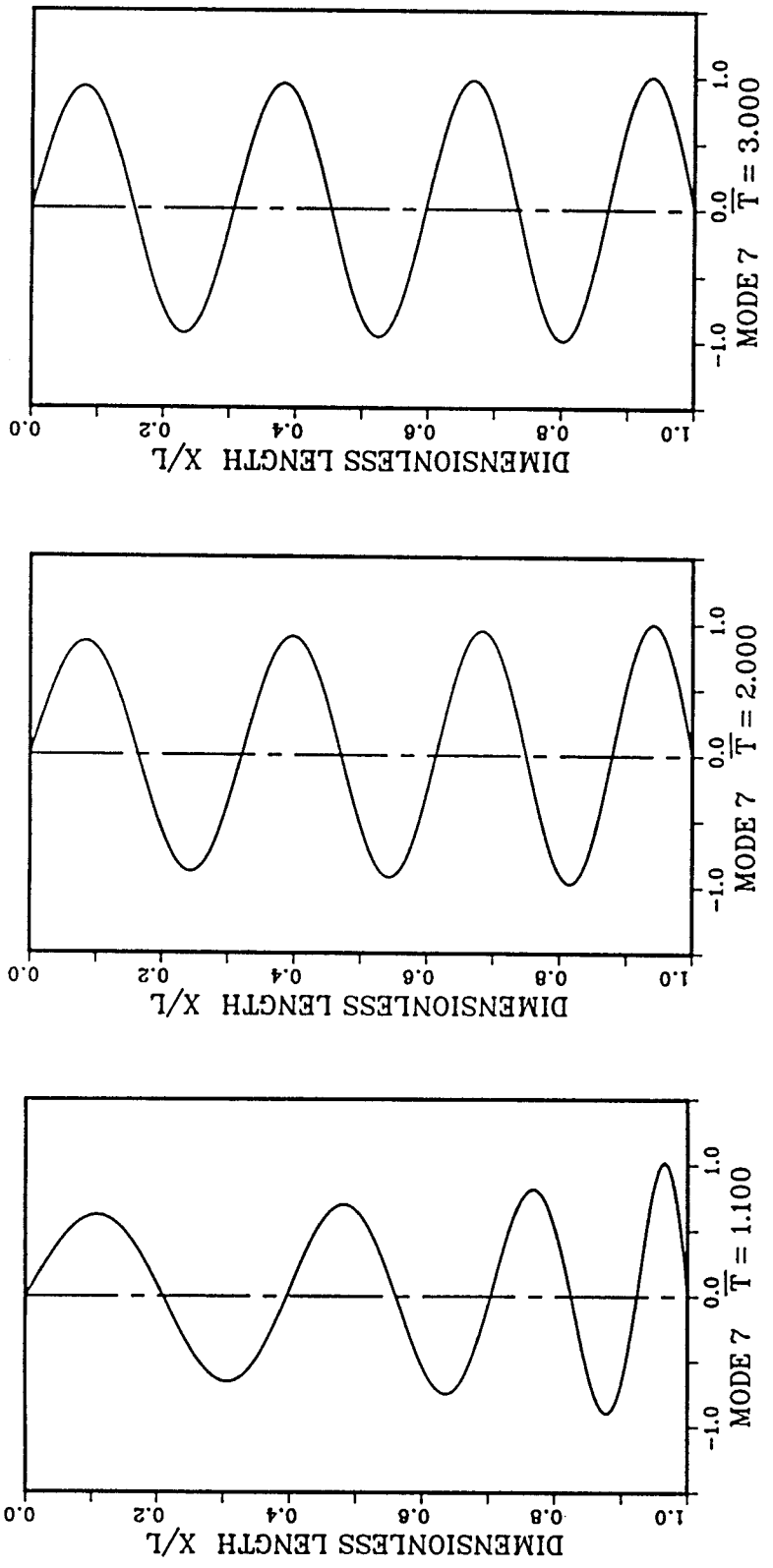

Fig. 4.2-8. Mode Shape 7 for Dimensionless Tensions of 1.1, 2.0 and 3.0.

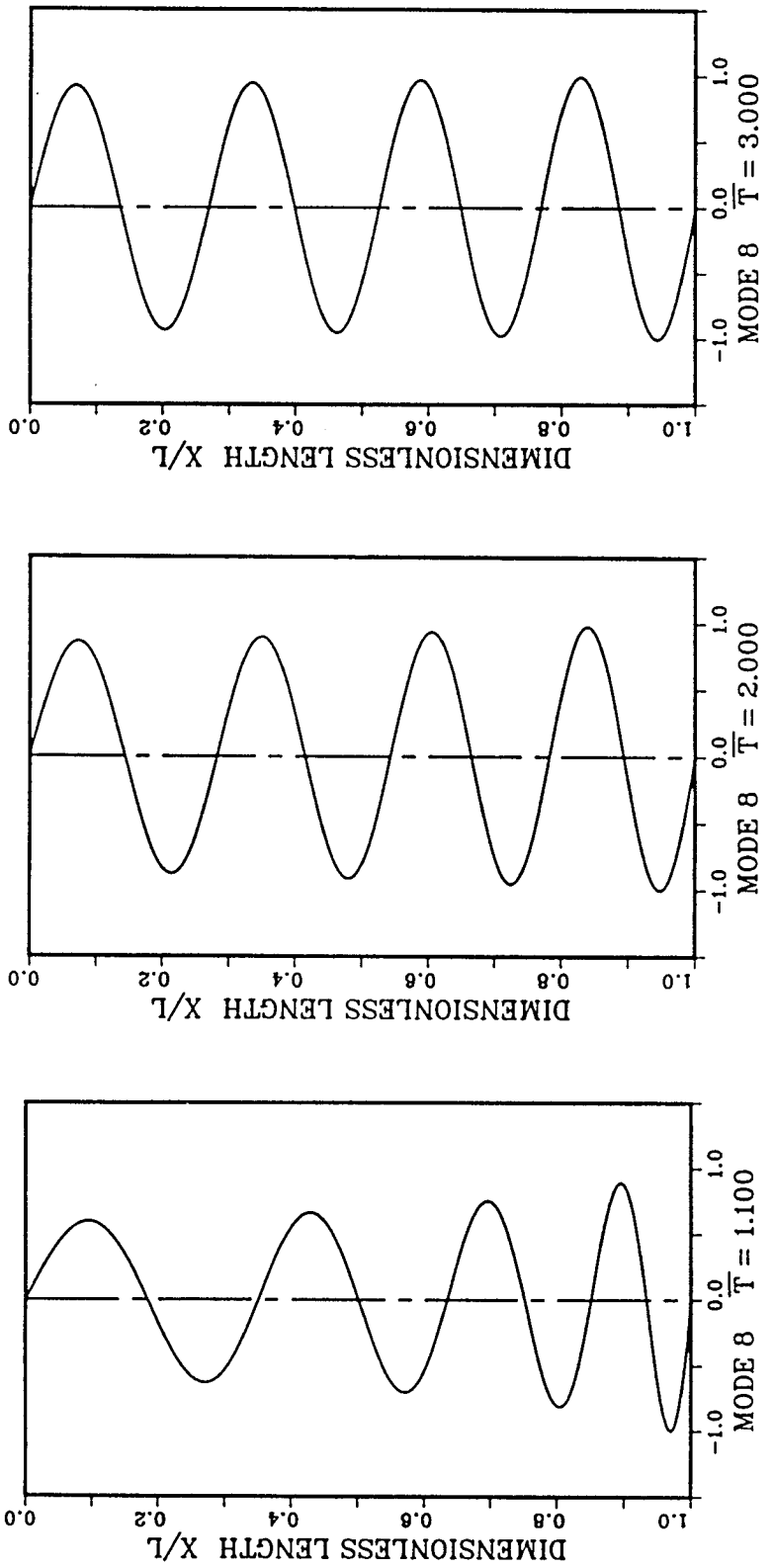

Fig. 4.2-9. Mode Shape 8 for Dimensionless Tensions of 1.1, 2.0 and 3.0.

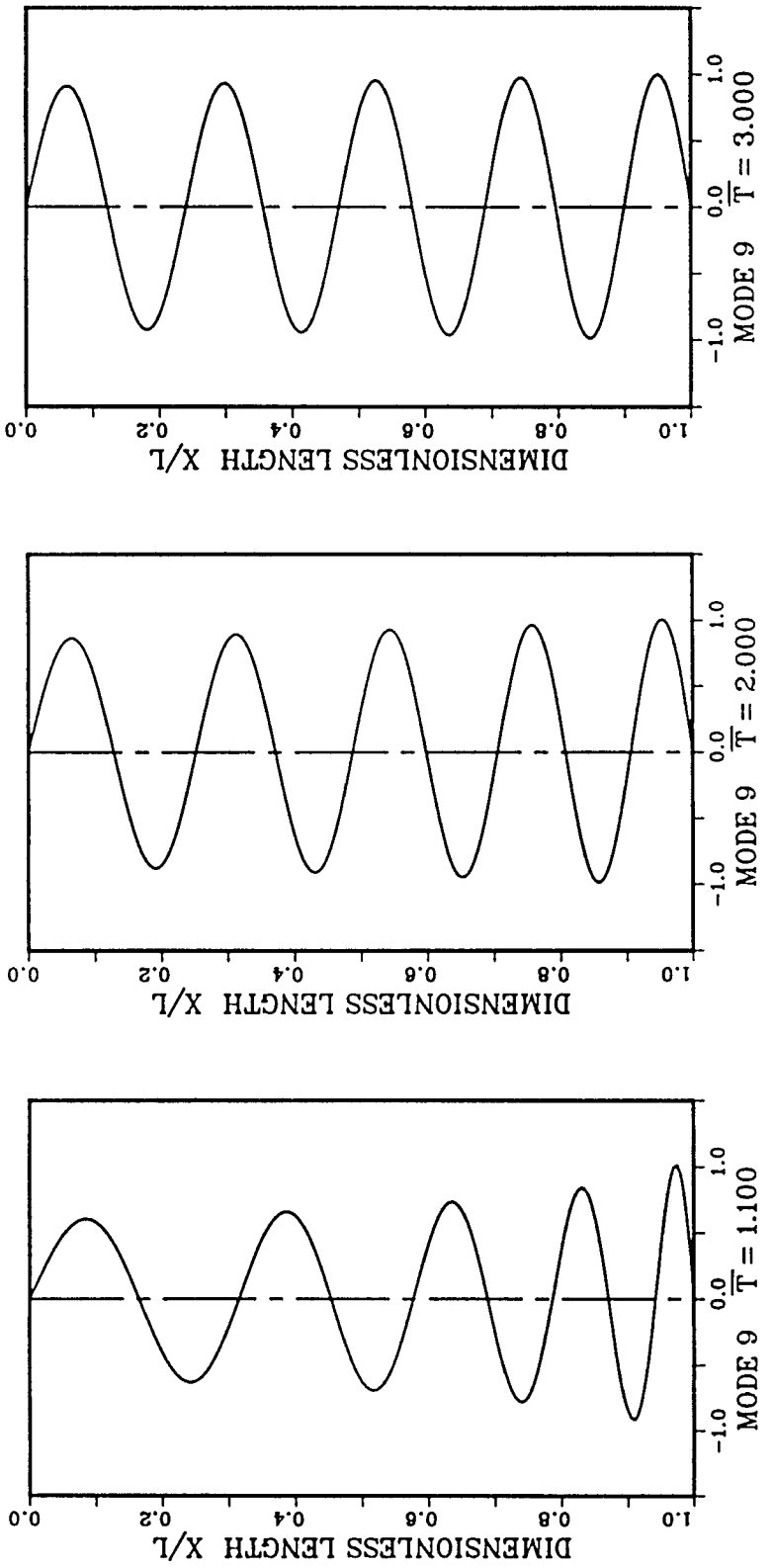

Fig. 4.2-10. Mode Shape 9 for Dimensionless Tensions of 1.1, 2.0 and 3.0.

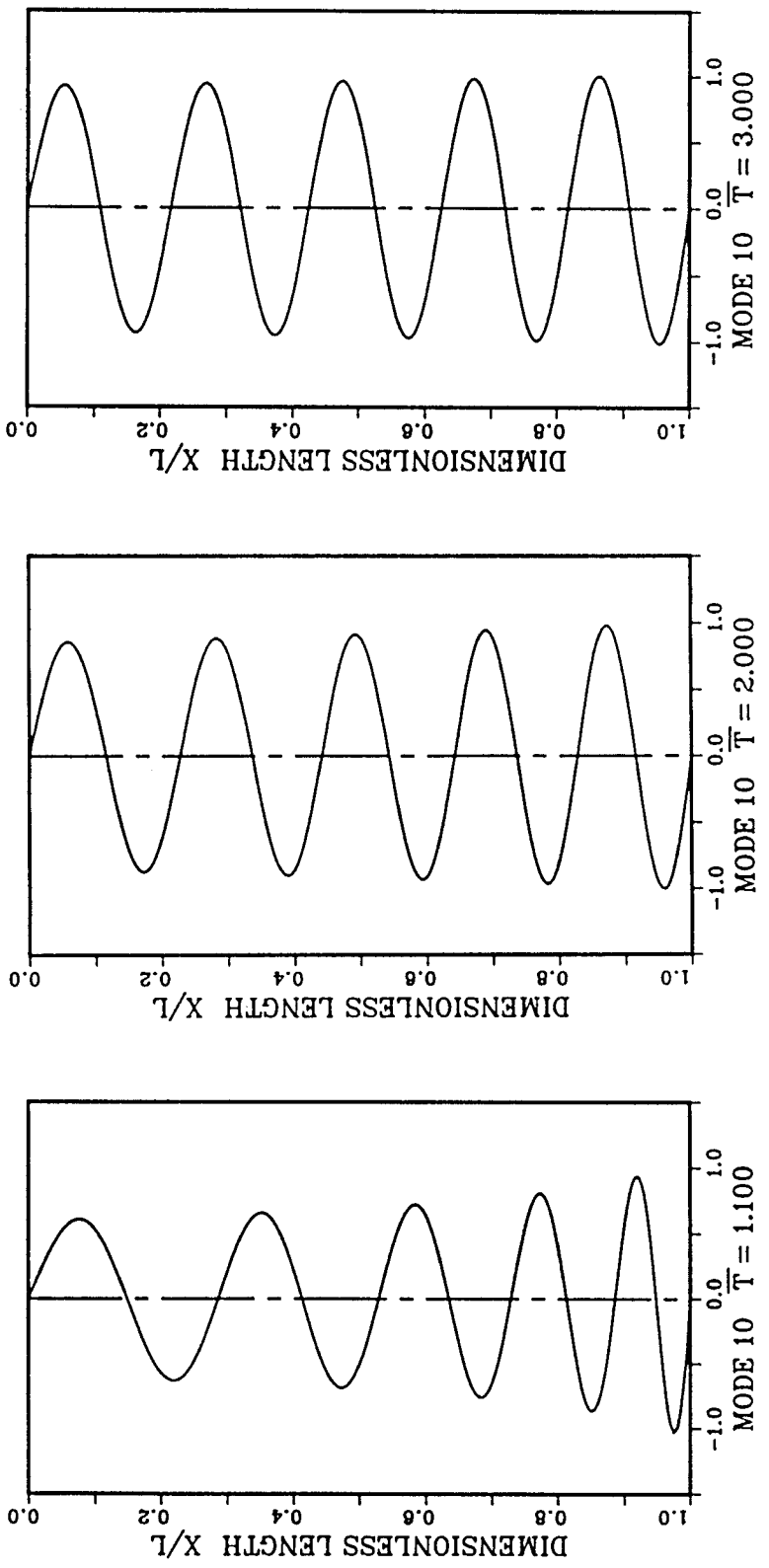

Fig. 4.2-11. Mode Shape 10 for Dimensionless Tensions of 1.1, 2.0 and 3.0.

Table 4.2-2. Normalized Mode Shapes
$\bar{T}$ = 1.100

x/l	1	2	3	4	5
Ø.ØØØ	Ø.ØØØ	Ø.ØØØ	Ø.ØØØ	Ø.ØØØ	Ø.ØØØ
Ø.Ø25	Ø.Ø41	Ø.Ø71	Ø.1Ø1	Ø.132	Ø.156
Ø.Ø5Ø	Ø.Ø82	Ø.143	Ø.2Ø2	Ø.261	Ø.3Ø4
Ø.Ø75	Ø.125	Ø.215	Ø.3ØØ	Ø.382	Ø.436
Ø.1ØØ	Ø.168	Ø.286	Ø.393	Ø.489	Ø.54Ø
Ø.125	Ø.211	Ø.356	Ø.478	Ø.576	Ø.6Ø7
Ø.15Ø	Ø.255	Ø.423	Ø.552	Ø.637	Ø.631
Ø.175	Ø.3ØØ	Ø.487	Ø.614	Ø.669	Ø.6Ø8
Ø.2ØØ	Ø.345	Ø.547	Ø.659	Ø.669	Ø.537
Ø.225	Ø.39Ø	Ø.6Ø2	Ø.687	Ø.634	Ø.421
Ø.25Ø	Ø.435	Ø.65Ø	Ø.696	Ø.565	Ø.267
Ø.275	Ø.48Ø	Ø.69Ø	Ø.683	Ø.462	Ø.Ø85
Ø.3ØØ	Ø.525	Ø.723	Ø.648	Ø.331	-Ø.11Ø
Ø.325	Ø.569	Ø.746	Ø.591	Ø.176	-Ø.3ØØ
Ø.35Ø	Ø.613	Ø.758	Ø.512	Ø.ØØ6	-Ø.469
Ø.375	Ø.656	Ø.759	Ø.413	-Ø.17Ø	-Ø.598
Ø.4ØØ	Ø.698	Ø.748	Ø.296	-Ø.342	-Ø.672
Ø.425	Ø.738	Ø.725	Ø.163	-Ø.497	-Ø.679
Ø.45Ø	Ø.777	Ø.688	Ø.Ø18	-Ø.623	-Ø.614
Ø.475	Ø.815	Ø.637	-Ø.132	-Ø.71Ø	-Ø.477
Ø.5ØØ	Ø.849	Ø.573	-Ø.283	-Ø.748	-Ø.28Ø
Ø.525	Ø.882	Ø.494	-Ø.428	-Ø.729	-Ø.Ø41
Ø.55Ø	Ø.911	Ø.4Ø3	-Ø.56Ø	-Ø.65Ø	Ø.214
Ø.575	Ø.938	Ø.298	-Ø.672	-Ø.513	Ø.452
Ø.6ØØ	Ø.96Ø	Ø.182	-Ø.755	-Ø.323	Ø.639
Ø.625	Ø.978	Ø.Ø55	-Ø.8Ø2	-Ø.Ø94	Ø.743
Ø.65Ø	Ø.991	-Ø.Ø79	-Ø.8Ø8	Ø.157	Ø.738
Ø.675	Ø.999	-Ø.22Ø	-Ø.767	Ø.4Ø6	Ø.613
Ø.7ØØ	1.ØØØ	-Ø.362	-Ø.675	Ø.624	Ø.376
Ø.725	Ø.994	-Ø.5Ø4	-Ø.533	Ø.784	Ø.Ø56
Ø.75Ø	Ø.98Ø	-Ø.639	-Ø.344	Ø.856	-Ø.297
Ø.775	Ø.958	-Ø.762	-Ø.115	Ø.818	-Ø.613
Ø.8ØØ	Ø.924	-Ø.868	Ø.142	Ø.659	-Ø.815
Ø.825	Ø.879	-Ø.948	Ø.4Ø8	Ø.382	-Ø.835
Ø.85Ø	Ø.821	-Ø.996	Ø.659	Ø.Ø14	-Ø.634
Ø.875	Ø.746	-1.ØØØ	Ø.866	-Ø.394	-Ø.226
Ø.9ØØ	Ø.653	-Ø.952	Ø.992	-Ø.765	Ø.3Ø2
Ø.925	Ø.538	-Ø.839	1.ØØØ	-1.ØØØ	Ø.783
Ø.95Ø	Ø.396	-Ø.651	Ø.852	-Ø.993	1.ØØØ
Ø.975	Ø.221	-Ø.375	Ø.521	-Ø.662	Ø.753
1.ØØØ	Ø.ØØØ	Ø.ØØØ	Ø.ØØØ	Ø.ØØØ	Ø.ØØØ

Table 4.2-2. Continued.

x/l	6	7	8	9	10
0.000	0.000	0.000	0.000	0.000	0.000
0.025	0.192	0.228	0.244	0.263	0.287
0.050	0.370	0.432	0.451	0.475	0.505
0.075	0.516	0.583	0.585	0.588	0.591
0.100	0.612	0.657	0.617	0.571	0.516
0.125	0.648	0.640	0.537	0.421	0.292
0.150	0.616	0.531	0.354	0.168	-0.022
0.175	0.516	0.340	0.098	-0.132	-0.338
0.200	0.355	0.092	-0.184	-0.407	-0.558
0.225	0.149	-0.177	-0.436	-0.585	-0.608
0.250	-0.081	-0.425	-0.605	-0.614	-0.463
0.275	-0.308	-0.610	-0.647	-0.477	-0.159
0.300	-0.502	-0.696	-0.548	-0.203	0.208
0.325	-0.638	-0.663	-0.320	0.138	0.512
0.350	-0.692	-0.508	-0.009	0.449	0.639
0.375	-0.653	-0.253	0.314	0.632	0.529
0.400	-0.518	0.060	0.569	0.620	0.210
0.425	-0.302	0.372	0.683	0.404	-0.205
0.450	-0.031	0.618	0.617	0.042	-0.549
0.475	0.255	0.739	0.375	-0.347	-0.667
0.500	0.510	0.698	0.013	-0.624	-0.489
0.525	0.687	0.492	-0.367	-0.673	-0.074
0.550	0.747	0.156	-0.646	-0.455	0.393
0.575	0.669	-0.234	-0.723	-0.038	0.680
0.600	0.455	-0.580	-0.552	0.414	0.616
0.625	0.135	-0.779	-0.171	0.698	0.204
0.650	-0.231	-0.758	0.294	0.660	-0.348
0.675	-0.564	-0.498	0.666	0.284	-0.712
0.700	-0.777	-0.058	0.772	-0.265	-0.628
0.725	-0.801	0.428	0.533	-0.695	-0.103
0.750	-0.604	0.786	0.020	-0.728	0.530
0.775	-0.213	0.851	-0.538	-0.291	0.783
0.800	0.277	0.553	-0.835	0.380	0.389
0.825	0.710	-0.029	-0.650	0.814	-0.391
0.850	0.911	-0.646	-0.021	0.615	-0.841
0.875	0.749	-0.958	0.681	-0.155	-0.413
0.900	0.221	-0.703	0.906	-0.844	0.549
0.925	-0.488	0.076	0.341	-0.665	0.869
0.950	-1.000	0.897	-0.644	0.373	-0.089
0.975	-0.888	1.000	-1.000	1.000	-1.000
1.000	0.000	0.000	0.000	0.000	0.000

Table 4.2-3. Normalized Mode Shapes
$\overline{T}$ = 2.000

x/l	1	2	3	4	5
0.000	0.000	0.000	0.000	0.000	0.000
0.025	0.062	0.119	0.176	0.231	0.288
0.050	0.125	0.238	0.346	0.447	0.546
0.075	0.188	0.353	0.504	0.634	0.746
0.100	0.251	0.464	0.644	0.775	0.861
0.125	0.313	0.567	0.757	0.860	0.876
0.150	0.375	0.660	0.839	0.880	0.787
0.175	0.436	0.742	0.886	0.831	0.601
0.200	0.496	0.811	0.894	0.717	0.339
0.225	0.553	0.864	0.861	0.544	0.031
0.250	0.609	0.900	0.789	0.324	-0.285
0.275	0.663	0.918	0.679	0.074	-0.569
0.300	0.714	0.918	0.536	-0.185	-0.783
0.325	0.762	0.897	0.365	-0.432	-0.897
0.350	0.806	0.857	0.174	-0.646	-0.893
0.375	0.847	0.798	-0.029	-0.807	-0.768
0.400	0.884	0.720	-0.233	-0.899	-0.535
0.425	0.916	0.625	-0.429	-0.912	-0.224
0.450	0.943	0.513	-0.606	-0.841	0.124
0.475	0.966	0.388	-0.754	-0.691	0.459
0.500	0.983	0.252	-0.864	-0.474	0.733
0.525	0.994	0.107	-0.929	-0.208	0.902
0.550	1.000	-0.043	-0.944	0.084	0.936
0.575	0.999	-0.194	-0.907	0.371	0.827
0.600	0.993	-0.343	-0.817	0.627	0.586
0.625	0.979	-0.486	-0.679	0.822	0.248
0.650	0.959	-0.619	-0.497	0.935	-0.137
0.675	0.932	-0.737	-0.283	0.951	-0.507
0.700	0.898	-0.838	-0.047	0.863	-0.797
0.725	0.858	-0.917	0.197	0.678	-0.956
0.750	0.810	-0.972	0.432	0.414	-0.951
0.775	0.756	-1.000	0.645	0.096	-0.775
0.800	0.695	-0.999	0.818	-0.239	-0.454
0.825	0.627	-0.967	0.940	-0.553	-0.043
0.850	0.553	-0.906	1.000	-0.805	0.386
0.875	0.473	-0.814	0.990	-0.962	0.748
0.900	0.388	-0.694	0.909	-1.000	0.970
0.925	0.297	-0.548	0.758	-0.908	1.000
0.950	0.202	-0.381	0.547	-0.692	0.823
0.975	0.103	-0.196	0.288	-0.376	0.466
1.000	0.000	0.000	0.000	0.000	0.000

Table 4.2-3. Continued.

x/l	6	7	8	9	10
0.000	0.000	0.000	0.000	0.000	0.000
0.025	0.339	0.401	0.439	0.489	0.545
0.050	0.627	0.718	0.757	0.808	0.856
0.075	0.816	0.879	0.860	0.837	0.789
0.100	0.871	0.844	0.713	0.557	0.365
0.125	0.779	0.615	0.351	0.066	-0.231
0.150	0.553	0.241	-0.120	-0.456	-0.727
0.175	0.228	-0.195	-0.561	-0.810	-0.888
0.200	-0.142	-0.590	-0.835	-0.854	-0.629
0.225	-0.491	-0.848	-0.850	-0.563	-0.063
0.250	-0.756	-0.902	-0.596	-0.043	0.541
0.275	-0.887	-0.733	-0.146	0.501	0.885
0.300	-0.854	-0.377	0.357	0.847	0.789
0.325	-0.660	0.080	0.750	0.845	0.290
0.350	-0.336	0.523	0.895	0.487	-0.366
0.375	0.057	0.835	0.738	-0.085	-0.839
0.400	0.445	0.929	0.323	-0.629	-0.872
0.425	0.750	0.772	-0.212	-0.902	-0.435
0.450	0.907	0.400	-0.679	-0.776	0.246
0.475	0.879	-0.089	-0.907	-0.295	0.801
0.500	0.665	-0.561	-0.805	0.330	0.911
0.525	0.307	-0.878	-0.399	0.809	0.500
0.550	-0.125	-0.943	0.164	0.910	-0.209
0.575	-0.536	-0.727	0.674	0.570	-0.805
0.600	-0.833	-0.287	0.926	-0.056	-0.925
0.625	-0.946	0.250	0.812	-0.665	-0.479
0.650	-0.840	0.717	0.365	-0.944	0.273
0.675	-0.533	0.963	-0.241	-0.737	0.864
0.700	-0.092	0.899	-0.756	-0.137	0.907
0.725	0.380	0.535	-0.955	0.548	0.354
0.750	0.766	-0.016	-0.739	0.944	-0.446
0.775	0.963	-0.573	-0.189	0.819	-0.955
0.800	0.912	-0.938	0.458	0.224	-0.809
0.825	0.618	-0.974	0.904	-0.512	-0.085
0.850	0.150	-0.653	0.930	-0.958	0.713
0.875	-0.370	-0.080	0.506	-0.832	1.000
0.900	-0.796	0.535	-0.177	-0.188	0.538
0.925	-1.000	0.954	-0.785	0.588	-0.348
0.950	-0.912	1.000	-1.000	1.000	-0.977
0.975	-0.545	0.638	-0.690	0.760	-0.833
1.000	0.000	0.000	0.000	0.000	0.000

Table 4.2-4. Normalized Mode Shapes
$\bar{T}$ = 3.000

x/l	1	2	3	4	5
0.000	0.000	0.000	0.000	0.000	0.000
0.025	0.068	0.133	0.196	0.262	0.325
0.050	0.137	0.264	0.385	0.505	0.610
0.075	0.205	0.390	0.558	0.708	0.820
0.100	0.273	0.510	0.705	0.854	0.926
0.125	0.340	0.620	0.821	0.930	0.911
0.150	0.405	0.717	0.898	0.927	0.776
0.175	0.470	0.800	0.933	0.845	0.536
0.200	0.532	0.867	0.923	0.690	0.223
0.225	0.592	0.915	0.867	0.473	-0.123
0.250	0.649	0.943	0.768	0.213	-0.456
0.275	0.703	0.951	0.629	-0.069	-0.729
0.300	0.753	0.937	0.458	-0.347	-0.902
0.325	0.800	0.902	0.262	-0.596	-0.951
0.350	0.843	0.846	0.050	-0.793	-0.866
0.375	0.881	0.770	-0.166	-0.919	-0.656
0.400	0.914	0.675	-0.376	-0.961	-0.349
0.425	0.942	0.564	-0.567	-0.914	0.011
0.450	0.965	0.437	-0.731	-0.780	0.373
0.475	0.983	0.300	-0.856	-0.569	0.683
0.500	0.994	0.153	-0.936	-0.302	0.894
0.525	1.000	0.002	-0.966	-0.003	0.971
0.550	1.000	-0.152	-0.942	0.299	0.901
0.575	0.993	-0.303	-0.865	0.575	0.690
0.600	0.980	-0.448	-0.738	0.796	0.370
0.625	0.960	-0.583	-0.568	0.938	-0.012
0.650	0.934	-0.704	-0.363	0.986	-0.396
0.675	0.902	-0.808	-0.134	0.932	-0.720
0.700	0.863	-0.893	0.104	0.780	-0.931
0.725	0.819	-0.954	0.339	0.544	-0.998
0.750	0.768	-0.990	0.557	0.247	-0.886
0.775	0.711	-1.000	0.742	-0.080	-0.631
0.800	0.649	-0.982	0.884	-0.402	-0.267
0.825	0.582	-0.937	0.972	-0.683	0.148
0.850	0.510	-0.865	1.000	-0.891	0.541
0.875	0.433	-0.767	0.964	-1.000	0.844
0.900	0.353	-0.647	0.866	-0.996	1.000
0.925	0.268	-0.505	0.709	-0.877	0.978
0.950	0.181	-0.348	0.504	-0.653	0.777
0.975	0.091	-0.178	0.262	-0.349	0.431
1.000	0.000	0.000	0.000	0.000	0.000

Table 4.2-4. Continued.

x/l	6	7	8	9	10
0.000	0.000	0.000	0.000	0.000	0.000
0.025	0.380	0.446	0.501	0.547	0.606
0.050	0.694	0.785	0.846	0.877	0.917
0.075	0.882	0.931	0.920	0.854	0.775
0.100	0.909	0.845	0.694	0.481	0.243
0.125	0.765	0.543	0.238	-0.094	-0.416
0.150	0.475	0.100	-0.300	-0.634	-0.868
0.175	0.093	-0.372	-0.743	-0.913	-0.877
0.200	-0.311	-0.752	-0.938	-0.806	-0.431
0.225	-0.658	-0.937	-0.816	-0.355	0.243
0.250	-0.879	-0.877	-0.413	0.254	0.795
0.275	-0.929	-0.581	0.137	0.757	0.929
0.300	-0.794	-0.127	0.644	0.932	0.565
0.325	-0.498	0.366	0.928	0.696	-0.108
0.350	-0.099	0.763	0.884	0.148	-0.728
0.375	0.324	0.953	0.523	-0.473	-0.951
0.400	0.684	0.877	-0.031	-0.883	-0.648
0.425	0.905	0.553	-0.579	-0.892	0.022
0.450	0.937	0.069	-0.918	-0.488	0.685
0.475	0.770	-0.439	-0.918	0.148	0.962
0.500	0.436	-0.825	-0.572	0.720	0.686
0.525	0.005	-0.973	-0.006	0.954	0.008
0.550	-0.432	-0.834	0.568	0.731	-0.682
0.575	-0.778	-0.444	0.927	0.150	-0.972
0.600	-0.953	0.084	0.927	-0.510	-0.682
0.625	-0.915	0.591	0.561	-0.923	0.024
0.650	-0.668	0.921	-0.034	-0.878	0.722
0.675	-0.264	0.968	-0.620	-0.388	0.980
0.700	0.206	0.710	-0.960	0.305	0.629
0.725	0.632	0.224	-0.907	0.847	-0.122
0.750	0.912	-0.339	-0.477	0.953	-0.803
0.775	0.976	-0.798	0.159	0.557	-0.973
0.800	0.803	-1.000	0.734	-0.140	-0.512
0.825	0.431	-0.871	0.999	-0.769	0.291
0.850	-0.053	-0.449	0.832	-0.985	0.909
0.875	-0.528	0.131	0.298	-0.661	0.921
0.900	-0.875	0.672	-0.375	0.035	0.308
0.925	-1.000	0.986	-0.886	0.718	-0.524
0.950	-0.866	0.956	-1.000	1.000	-1.000
0.975	-0.502	0.586	-0.654	0.708	-0.778
1.000	0.000	0.000	0.000	0.000	0.000

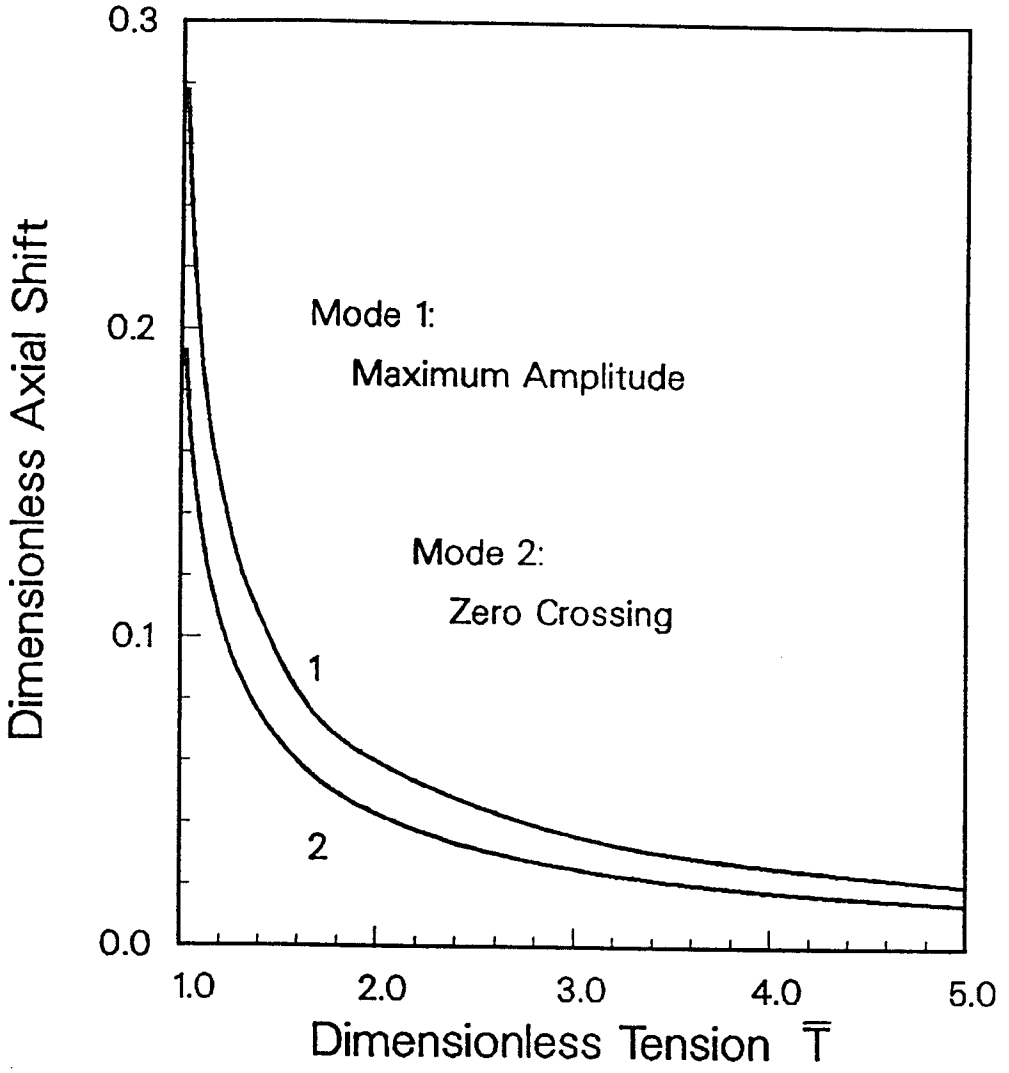

Fig. 4.2-12. Shifts in Locations of Maximum Amplitude and Zero Crossings.

4.3 COMPARISON OF RESULTS

The results from the exact solution can be verified to a limited degree by a perturbation analysis developed for the response of flexible tubes with small linear variations in the axial tension. Details of the derivation can be found in Appendix B.

The equations for natural frequencies and mode shapes are given by

$$\omega_n^2 = \left(T_e + \frac{W}{2}\right) n^2\pi^2/M\ell^2 \ . \tag{4.3-1}$$

$$\Phi_n(x) = \sin\frac{n\pi x}{\ell} - \frac{2W}{\pi^2 T_e}\sum_{m\neq n}\frac{mn}{(m^2 - n^2)}\left[\frac{1}{(n-m)^2} + \frac{1}{(n+m)^2}\right]\sin\frac{m\pi x}{\ell} \tag{4.3-2}$$

where M and W represent the total mass and weight, respectively. The effective tension has been expressed as

$$T_e = (T_o - pA_f(1 - 2\nu) - m_f c^2) \ . \tag{4.3-3}$$

For the mode shapes, the shifts in positions of maximum amplitude and crossing points are in good agreement. The differences between numerical values for frequencies from the two solutions are small, particularly for small tension variations. This is shown, for example, in Fig. 4.3-1 where a comparison is made for the fundamental frequency. The results for higher modes are similar. Thus, for cases characterized by significant tension variations, the exact solution is of greater importance.

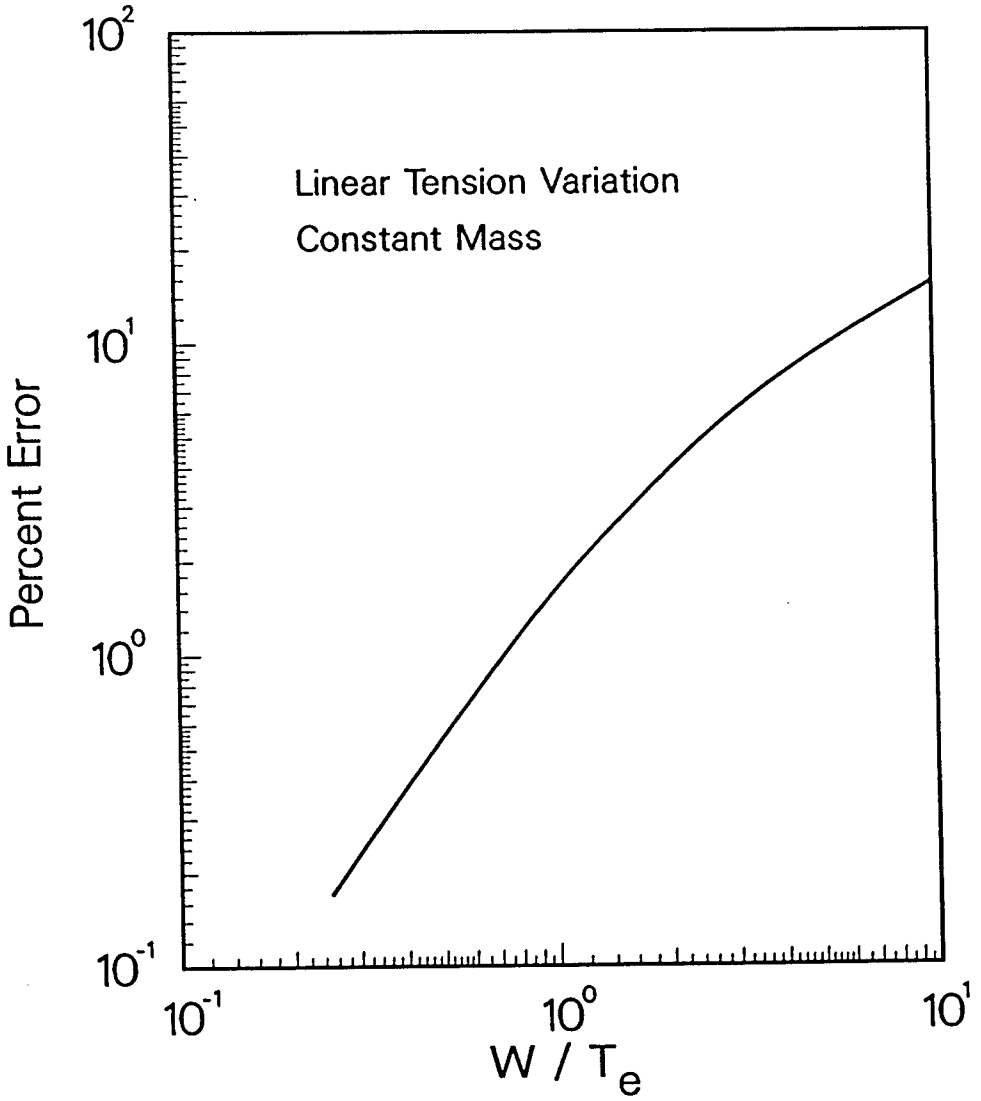

Fig. 4.3-1. Error in the Fundamental Frequency from the Perturbation Solution.

4.4 REFERENCES

[4.1] McLachlan, N.W., *Bessel Functions for Engineers,* Oxford University Press, London, 1955.

CHAPTER 5

REDUCTION OF THE EQUATIONS OF MOTION

5.1 FLEXIBLE TUBE WITH CONSTANT TENSION

It was shown in Chapter 4 that the tension gradient due to gravity can become insignificant if the tension is relatively large compared with the weight. It was also determined that the error in neglecting gravity could be further reduced if the effective tension would include half of the weight. With this in mind, the equations of motion (3.2-11) - (3.2-13) for a flexible tube can be reduced to the following

$$(m_f + m_t)\frac{\partial^2 u}{\partial t^2} + m_f \frac{\partial c}{\partial t} + \kappa_o \frac{\partial u}{\partial t} - EA_t \frac{\partial^2 u}{\partial x^2} - \frac{\partial}{\partial x}\{(EA_t - T^{**})[\frac{1}{2}(\frac{\partial v}{\partial x})^2 + \frac{1}{2}(\frac{\partial w}{\partial x})^2 - (\frac{\partial u}{\partial x})(\frac{\partial v}{\partial x})^2 - (\frac{\partial u}{\partial x})(\frac{\partial w}{\partial x})^2]\} = 0 \tag{5.1-1}$$

$$(m_f + m_t)\frac{\partial^2 v}{\partial t^2} + 2m_f c \frac{\partial^2 v}{\partial x \partial t} + m_f c^2 \frac{\partial^2 v}{\partial x^2} + m_f \frac{\partial c}{\partial t}\frac{\partial v}{\partial x} + \kappa_o \frac{\partial v}{\partial t} - \frac{\partial}{\partial x}\{T^{**}\frac{\partial v}{\partial x} + (EA_t - T^{**})[\frac{\partial u}{\partial x} - (\frac{\partial u}{\partial x})^2 + \frac{1}{2}(\frac{\partial v}{\partial x})^2 + \frac{1}{2}(\frac{\partial w}{\partial x})^2]\frac{\partial v}{\partial x}\} = 0 \tag{5.1-2}$$

$$(m_f + m_t)\frac{\partial^2 w}{\partial t^2} + 2m_f c\frac{\partial^2 w}{\partial x \partial t} + m_f c^2\frac{\partial^2 w}{\partial x^2} + m_f\frac{\partial c}{\partial t}\frac{\partial w}{\partial x} + \kappa_o\frac{\partial w}{\partial t}$$

$$- \frac{\partial}{\partial x}\{T^{**}\frac{\partial w}{\partial x} + (EA_t - T^{**})[\frac{\partial u}{\partial x} - (\frac{\partial u}{\partial x})^2 + \frac{1}{2}(\frac{\partial v}{\partial x})^2 + \frac{1}{2}(\frac{\partial w}{\partial x})^2]\frac{\partial w}{\partial x} = 0$$

(5.1-3)

where the constant tension, T^{**}, is given by

$$T^{**} = T_o - pA_f(1 - 2\nu) + (m_f + m_t)g\,\ell/2\ . \qquad (5.1\text{-}4)$$

These equations can be rewritten as

$$\frac{\partial^2 u}{\partial t^2} + \frac{m_f}{(m_f + m_t)}\frac{\partial c}{\partial t} + \frac{\kappa_o}{(m_f + m_t)}\frac{\partial u}{\partial t} - \frac{EA_t}{(m_f + m_t)}\frac{\partial^2 u}{\partial x^2}$$

$$- \frac{(EA_t - T^{**})}{(m_f + m_t)}\frac{\partial}{\partial x}[\frac{1}{2}(\frac{\partial v}{\partial x})^2 + \frac{1}{2}(\frac{\partial w}{\partial x})^2 - (\frac{\partial u}{\partial x})(\frac{\partial v}{\partial x})^2 - (\frac{\partial u}{\partial x})(\frac{\partial w}{\partial x})^2] = 0$$

(5.1-5)

$$\frac{\partial^2 v}{\partial t^2} + \frac{2m_f c}{(m_f + m_t)}\frac{\partial^2 v}{\partial x \partial t} + \frac{m_f}{(m_f + m_t)}\frac{\partial c}{\partial t}\frac{\partial v}{\partial x} + \frac{\kappa_o}{(m_f + m_t)}\frac{\partial v}{\partial t}$$

$$- \frac{(T^{**} - m_f c^2)}{(m_f + m_t)}\frac{\partial^2 v}{\partial x} - \frac{(EA_t - T^{**})}{(m_f + m_t)}\frac{\partial}{\partial x}\{[\frac{\partial u}{\partial x} - (\frac{\partial u}{\partial x})^2 + \frac{1}{2}(\frac{\partial v}{\partial x})^2$$

$$+ \frac{1}{2}(\frac{\partial w}{\partial x})^2]\frac{\partial v}{\partial x}\} = 0\ .$$

(5.1-6)

$$\frac{\partial^2 w}{\partial t^2} + \frac{2m_f c}{(m_f + m_t)} \frac{\partial^2 w}{\partial x \partial t} + \frac{m_f}{(m_f + m_t)} \frac{\partial c}{\partial t} \frac{\partial w}{\partial x} + \frac{\kappa_o}{(m_f + m_t)} \frac{\partial w}{\partial t}$$

$$- \frac{(T^{**} - m_f c^2)}{(m_f + m_t)} \frac{\partial^2 w}{\partial x} - \frac{(EA_t - T^{**})}{(m_f + m_t)} \frac{\partial}{\partial x} \{[\frac{\partial u}{\partial x} - (\frac{\partial u}{\partial x})^2 + \frac{1}{2} (\frac{\partial v}{\partial x})^2$$

$$+ \frac{1}{2} (\frac{\partial w}{\partial x})^2] \frac{\partial w}{\partial x}\} = 0 \ . \qquad (5.1\text{-}7)$$

5.2 LONGITUDINAL INERTIA NEGLECTED

If the wave speed of the longitudinal equation of motion is compared with the wave speed of the transverse equations it can be seen that for most practical applications

$$\frac{EA_t}{(m_f + m_t)} >> \frac{(T^{**} - m_f c^2)}{(m_f + m_t)} \qquad (5.2\text{-}1)$$

or

$$EA_t >> (T^{**} - m_f c^2) \ . \qquad (5.2\text{-}2)$$

Therefore, the interaction between longitudinal and transverse modes should be insignificant and longitudinal inertia can be neglected. Equation (5.1-5) then becomes

$$m_f \frac{\partial c}{\partial t} - EA_t \frac{\partial^2 u}{\partial x^2} - (EA_t - T^{**}) \frac{\partial}{\partial x} \left[\frac{1}{2} \left(\frac{\partial v}{\partial x}\right)^2\right.$$

$$\left. + \frac{1}{2} \left(\frac{\partial w}{\partial x}\right)^2 - \left(\frac{\partial u}{\partial x}\right)\left(\frac{\partial v}{\partial x}\right)^2 - \left(\frac{\partial u}{\partial x}\right)\left(\frac{\partial w}{\partial x}\right)^2\right] = 0 \ . \qquad (5.2\text{-}3)$$

However, from (5.2-1) it can also be concluded that $EA_t >> T^{**}$ so $(EA_t - T^{**}) \cong EA_t$. Consequently, Eq. (5.2-3) can be written as

$$\frac{\partial^2 u}{\partial x^2} + \frac{\partial}{\partial x} \left[\frac{1}{2} \left(\frac{\partial v}{\partial x}\right)^2 + \frac{1}{2} \left(\frac{\partial w}{\partial x}\right)^2\right] = \frac{m_f}{EA_t} \frac{\partial c}{\partial t} \qquad (5.2\text{-}4)$$

where only terms up to the second order have been retained.

Integrating Eq. (5.2-4) and using the boundary conditions on $u(x,t)$ as

$$u(0,t) = u(\ell,t) = 0 \qquad (5.2\text{-}5)$$

it follows that

$$\frac{\partial u}{\partial x} + \frac{1}{2} \left(\frac{\partial v}{\partial x}\right)^2 + \frac{1}{2} \left(\frac{\partial w}{\partial x}\right)^2 =$$

$$\frac{1}{2\ell} \int_0^{\ell} \left[\left(\frac{\partial v}{\partial x}\right)^2 + \left(\frac{\partial w}{\partial x}\right)^2\right] dx + \frac{m_f (x - \frac{\ell}{2})}{EA_t} \frac{\partial c}{\partial t} \ . \qquad (5.2\text{-}6)$$

Substituting (5.2-6) into the two transverse equations of motion, (5.1-6) and 5.1-7), one obtains

$$\frac{\partial^2 v}{\partial t^2} + \frac{2m_f c}{(m_f + m_t)} \frac{\partial^2 v}{\partial x \partial t} + \frac{\kappa_o}{(m_f + m_t)} \frac{\partial v}{\partial t} - \frac{(T^{**} - m_f c^2)}{(m_f + m_t)} \frac{\partial^2 v}{\partial x^2}$$

$$- \frac{EA_t}{2\ell(m_f + m_t)} \left(\frac{\partial^2 v}{\partial x^2}\right) \int_o^\ell \left[\left(\frac{\partial v}{\partial x}\right)^2 + \left(\frac{\partial w}{\partial x}\right)^2\right] dx$$

$$+ \frac{m_f}{(m_f + m_t)} \left(\frac{\ell}{2} - x\right)\left(\frac{\partial c}{\partial t}\right)\left(\frac{\partial^2 v}{\partial x^2}\right) = 0 \qquad (5.2\text{-}7)$$

$$\frac{\partial^2 w}{\partial t^2} + \frac{2m_f c}{(m_f + m_t)} \frac{\partial^2 w}{\partial x \partial t} + \frac{\kappa_o}{(m_f + m_t)} \frac{\partial w}{\partial t} - \frac{(T^{**} - m_f c^2)}{(m_f + m_t)} \frac{\partial^2 w}{\partial x^2}$$

$$- \frac{EA_t}{2\ell(m_f + m_t)} \left(\frac{\partial^2 w}{\partial x^2}\right) \int_o^\ell \left[\left(\frac{\partial v}{\partial x}\right)^2 + \left(\frac{\partial w}{\partial x}\right)^2\right] dx$$

$$+ \frac{m_f}{(m_f + m_t)} \left(\frac{\ell}{2} - x\right)\left(\frac{\partial c}{\partial t}\right)\left(\frac{\partial^2 w}{\partial x^2}\right) = 0 \qquad (5.2\text{-}8)$$

where cubic terms in v and w are kept.

5.3 GALERKIN'S PROCEDURE

To reduce the partial differential equations of motion to a system of coupled ordinary differential equations, Galerkin's method is used. Assuming a solution in the form of a summation of linear modes, i.e.,

$$v(x,t) = \sum_{n=1}^{\infty} v_n(t)\, \phi_n(x) = \sum_{n=1}^{\infty} v_n(t) \sin \frac{n\pi x}{\ell} \qquad (5.3\text{-}1)$$

$$w(x,t) = \sum_{n=1}^{\infty} w_n(t)\, \phi_n(x) = \sum_{n=1}^{\infty} w_n(t) \sin \frac{n\pi x}{\ell} \qquad (5.3\text{-}2)$$

and using the orthogonality condition of the eigenfunctions $\phi_n(x)$, Eqs. (5.2-7) and (5.2-8) become

$$\ddot{v}_r + \frac{8m_f c}{\ell(m_f + m_t)} \sum_{n=1}^{\infty} \frac{rn}{(r^2 - n^2)} \dot{v}_n + \frac{\kappa_o r}{(m_f + m_t)} \dot{v}_r$$

$$+ \frac{(T^{**} - m_f c^2)\, \pi^2 r^2}{\ell^2(m_f + m_t)} v_r + \frac{EA_t\, \pi^4 r^2}{4\ell^4(m_f + m_t)} v_r \sum_{m=1}^{\infty} m^2 (v_m^2 + w_m^2)$$

$$- \frac{8m_f \dot{c}}{\ell(m_f + m_t)} \sum_{n=1}^{\infty} \frac{rn^3}{(n^2 - r^2)} v_n = 0 \qquad r = 1,2,3 \ldots$$

(5.3-3)

$$\ddot{w}_r + \frac{8m_f c}{\ell(m_f + m_t)} \sum_{n=1}^{\infty} \frac{rn}{(r^2 - n^2)} \dot{w}_n + \frac{\kappa_o r}{(m_f + m_t)} \dot{w}_r$$

$$+ \frac{(T^{**} - m_f c^2)\, \pi^2 r^2}{\ell^2(m_f + m_t)} w_r + \frac{EA_t\, \pi^4 r^2}{4\ell^4(m_f + m_t)} w_r \sum_{m=1}^{\infty} m^2 (v_m^2 + w_m^2)$$

$$- \frac{8m_f \dot{c}}{\ell(m_f + m_t)} \sum_{n=1}^{\infty} \frac{rn^3}{(n^2 - r^2)} w_n = 0 \qquad r = 1,2,3 \ldots$$

(5.3-4)

where $(\dot{})$ = d/dt and $(r \pm n)$ = odd.

The problem may be expressed in dimensionless terms by introducing the following quantities:

$$\bar{v} = \frac{v}{\ell} \qquad \bar{w} = \frac{w}{\ell} \qquad \bar{t} = \omega_1 t \qquad \bar{\Omega} = \frac{\Omega}{\omega_1}$$

$$\bar{a} = \frac{8m_f c_o}{\ell(m_f + m_t)\omega_1} \qquad \bar{b} = \frac{\kappa_o}{(m_f + m_t)\omega_1} \qquad \bar{c} = \frac{EA_t\,\pi^4}{4\ell^2(m_f + m_t)\omega_1^2}$$

$$\bar{d} = \frac{m_f\,\pi^2 c_o}{2\ell(m_f + m_t)\omega_1} \qquad \bar{e} = \frac{m_f\,\pi^2\,c_o^2}{\ell^2(m_f + m_t)\omega_1^2} \tag{5.3-5}$$

where the natural frequencies of the system can be written in the form

$$\omega_r^2 = \frac{(T^{**} - m_f c_o^2)\,\pi^2 r^2}{\ell^2(m_f + m_t)} \,. \tag{5.3-6}$$

Also, the flow velocity c has been represented as $c = c_o(1 + \mu \cos \Omega t)$ as first given in Eq. (3.2-3). Substituting Eqs. (5.3-5) and (3.2-3) into (5.3-3) and (5.3-4), one obtains the dimensionless equations of motion

$$\bar{v}_r'' + \bar{a}\,(1 - \mu \cos \bar{\Omega}\,\bar{t}) \sum_{n=1}^{\infty} \frac{rn}{(r^2 - n^2)}\,\bar{v}_n' + \bar{b}\,r\,\bar{v}_r'$$

$$+ r^2\,\bar{v}_r + \bar{c}\,r^2\,\bar{v}_r \sum_{m=1}^{\infty} m^2\,(\bar{v}_m^{\,2} + \bar{w}_m^{\,2})$$

$$+ \bar{d}\,\mu\,\bar{\Omega}\,(\sin \bar{\Omega}\,\bar{t}) \sum_{n=1}^{\infty} \frac{(rn)^3}{(n^2 - r^2)}\,\bar{v}_n$$

$$- \bar{e}\,r^2\,(2\,\mu \cos \bar{\Omega}\,\bar{t} + \mu^2 \cos^2 \bar{\Omega}\,\bar{t})\,\bar{v}_r = 0 \qquad \begin{array}{l} r = 1,2,3 \ldots \\ (r \pm n) = \text{odd} \end{array}$$

(5.3-7)

$$\bar{w}_r'' + \bar{a}\,(1 - \mu \cos \bar{\Omega}\,\bar{t}) \sum_{n=1}^{\infty} \frac{rn}{(r^2 - n^2)}\,\bar{w}_n' + \bar{b}\,r\,\bar{w}_r'$$

$$+ r^2\,\bar{w}_r + \bar{c}\,r^2\,\bar{w}_r \sum_{m=1}^{\infty} m^2\,(\bar{v}_m^{\,2} + \bar{w}_m^{\,2})$$

$$+ \bar{d}\,\mu\,\bar{\Omega}\,(\sin \bar{\Omega}\,\bar{t}) \sum_{n=1}^{\infty} \frac{(rn)^3}{(n^2 - r^2)}\,\bar{w}_n$$

$$- \bar{e}\,r^2\,(2\,\mu \cos \bar{\Omega}\,\bar{t} + \mu^2 \cos^2 \bar{\Omega}\,\bar{t})\,\bar{w}_r = 0 \qquad \begin{array}{l} r = 1,2,3 \ldots \\ (r \pm n) = \text{odd} \end{array}$$

(5.3-8)

with the prime denoting differentiation with respect to dimensionless time $\bar{t}$. It should be noted that for a symmetric loading condition on the tube, usually only odd modes would be excited. However, because of the presence of fluid, the series involving sums on n contain even

modes. Therefore, the various modes of v (or w) are coupled through the Coriolis acceleration term with coefficient $\bar{a}$ and the parametric excitation term with coefficient $\bar{d}$. Coupling between the two transverse motions (v and w) is found only in the cubic nonlinear terms in the summation on m.

CHAPTER 6

ICF APPLICATIONS

6.1 FIRST WALL PROTECTION SCHEME

A major problem in inertial confinement fusion (ICF) reactor design is the protection of the first wall from x-rays, neutrons, target debris and mechanical shock all resulting from target ignition [6.1]. A new concept has been proposed for two types of conceptual reactors, HIBALL and HIBALL-II (Heavy Ion Beams and Lithium/Lead) [6.2,6.3] and LIBRA (Light Ion Beam Reactor Analysis) [6.4]. These ICF reactors have been developed jointly by the University of Wisconsin Fusion Technology Institute and the Kernforschungszentrum Karlsruhe, FRG. Recently, Sandia National Laboratories has joined in the LIBRA effort. Cross-sectional views of the reaction chambers are shown in Figs. 6.1-1 and 6.1-2. In each, the cylindrical cavity is protected by an annular bank of vertical tubes conveying liquid lithium/lead ($Li_{17}Pb_{83}$). Individual tubes, referred to as INPORTs (Inhibited Flow/Porous Tube) [6.5] are braided from silicon carbide fibers to produce a flexible porous component. The liquid metal flows through the walls of the tube and forms a 1 mm thick film on the exterior surface (Fig. 6.1-3). This external layer is sufficient to absorb x-rays and debris from the target, whereas the internal flow is used as a coolant and breeding material.

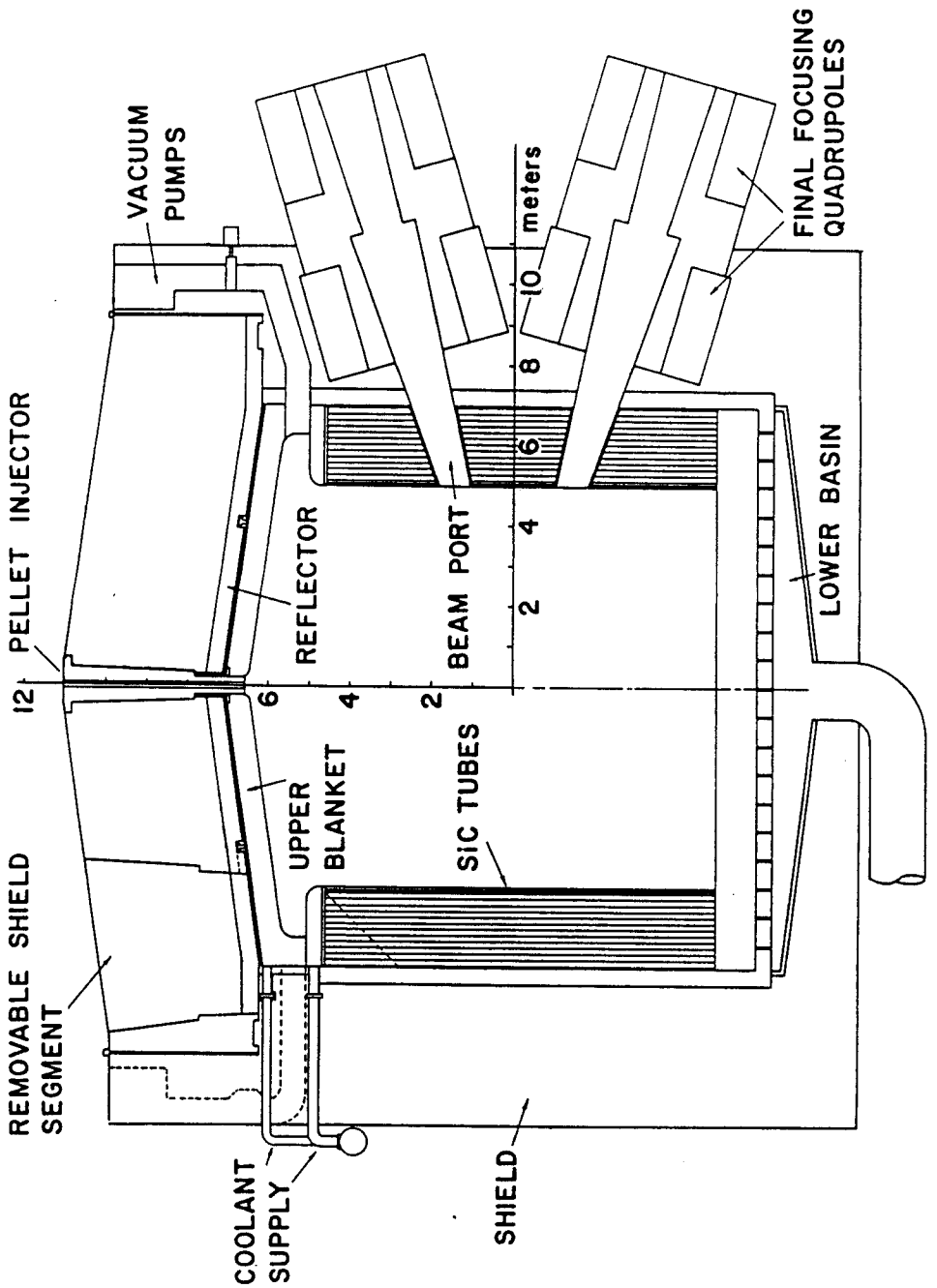

Fig. 6.1-1. Schematic of HIBALL Reactor Chamber [6.2].

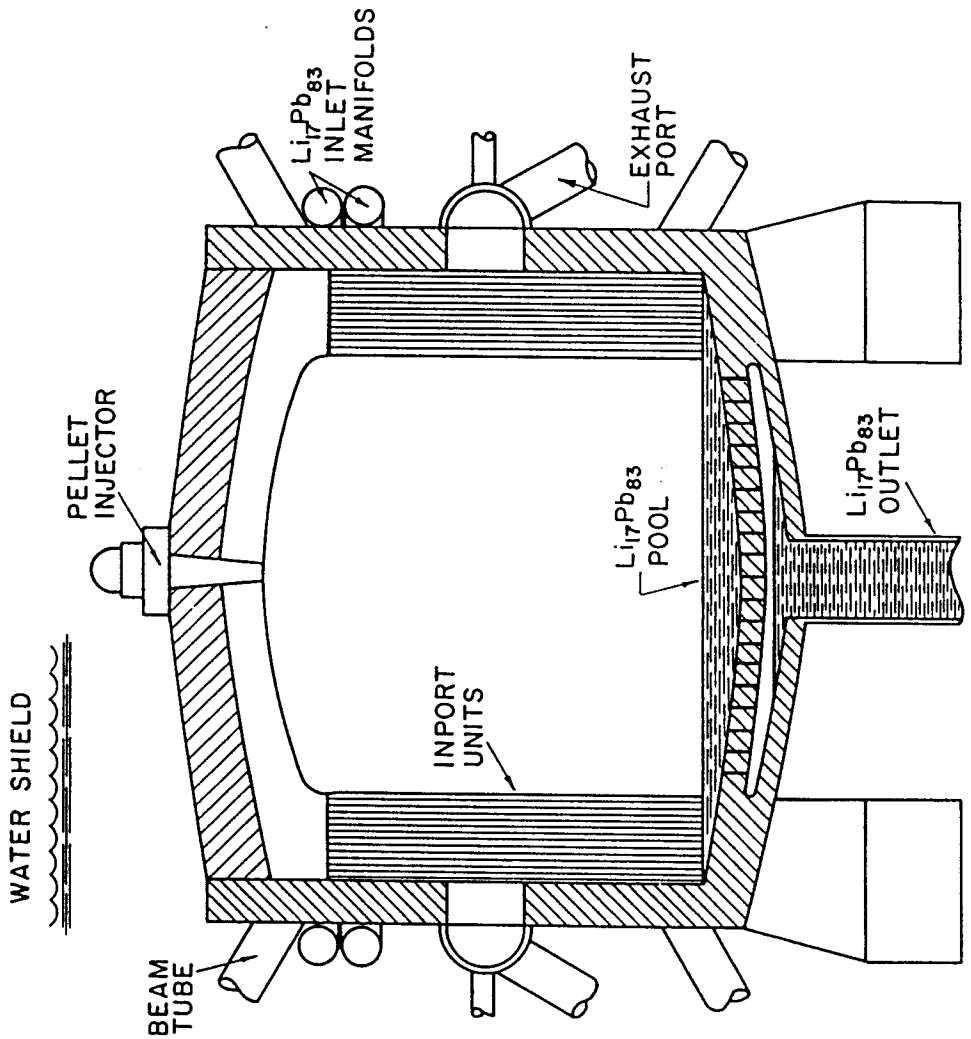

Fig. 6.1-2. Schematic of LIBRA Reactor Chamber [6.6].

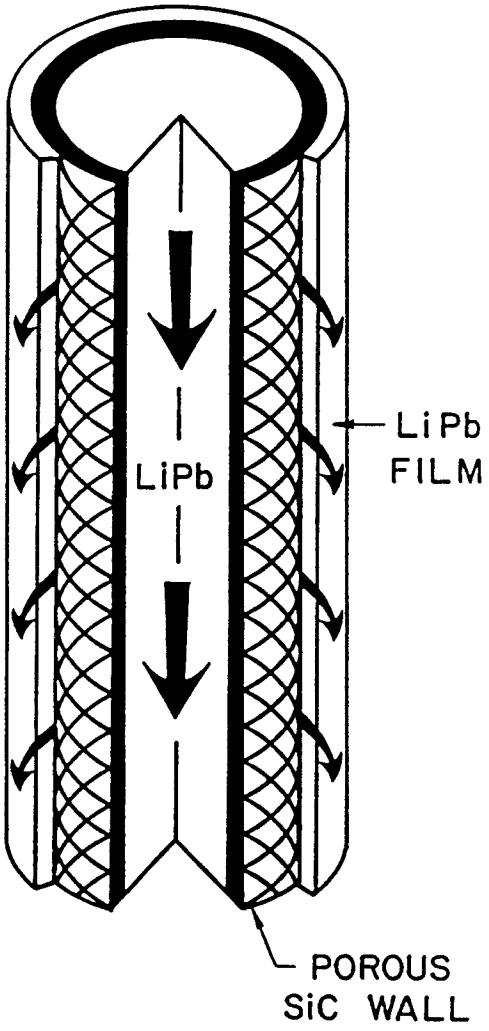

Fig. 6.1-3. Sectioned INPORT Unit.

The SiC fibers used in the INPORTs are manufactured by Nippon Carbon Co., Japan and are currently being distributed by Dow Corning Co. Individual fibers are composed of approximately 500 filaments, each approximately 13 μm in diameter. Actual INPORT tubes have been braided and tested by McDonnell-Douglas Corp. It was found that the tubes could be rigidized and strengthened by using a chemical vapor deposition (CVD) treatment. Additional tests to determine the tension and fatigue characteristics of the fibers were completed at the University of Wisconsin. The results of all tests can be found in Appendix A.

The INPORTs are elastically supported at the top and bottom as shown by the preliminary design of Fig. 6.1-4. The compression spring system allows tensile preloading of the tubes. In addition, a modification of this support mechanism will be used which permits end rotation, essentially as a ball-and-socket joint.

The first two rows of tubes are subjected to repetitive mechanical shock loading during operation (Fig. 6.1-5). For the HIBALL and HIBALL-II reactors, a radial pressure impulse is imparted to the INPORTs when the LiPb is vaporized by the target-generated x-rays. This impulsive pressure has been estimated at 60 Pa-s. In the case of LIBRA, the dynamic loading of the tubes is from the target blast wave transmitted through the cavity gas. The overpressure, shown in Fig. 6.1-6, is obtained from the University of Wisconsin simulation code "CONRAD" [6.7]. Since the pulse width is small compared to the

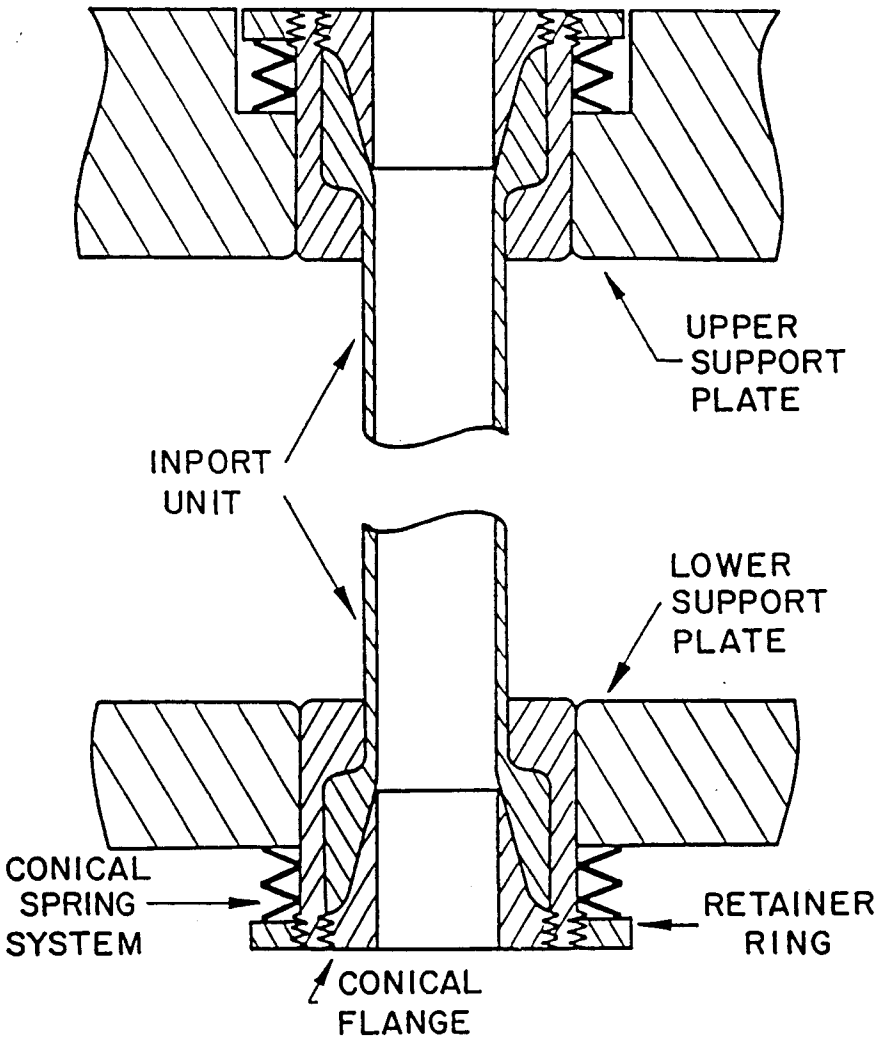

Fig. 6.1-4. Support Mechanisms for INPORTs.

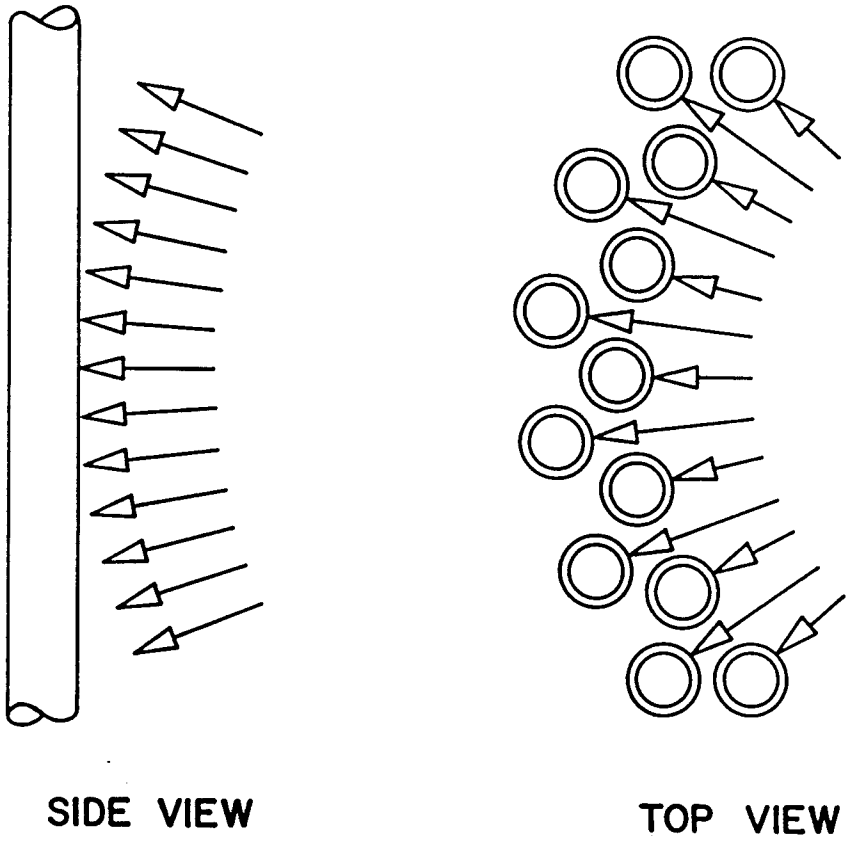

Fig. 6.1-5. Dynamic Pressure Loading on the Tube.

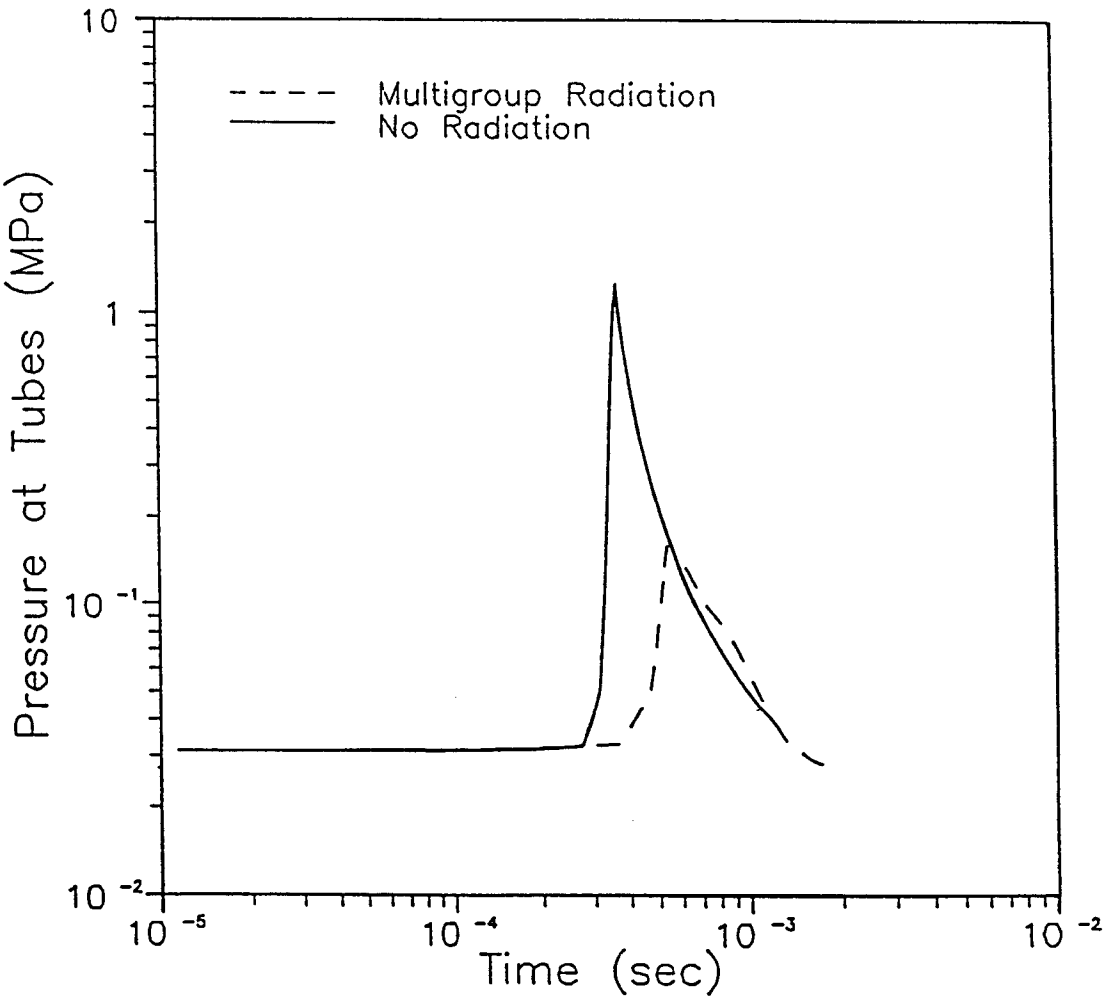

Fig. 6.1-6. Dynamic Overpressure at Tube Wall [6.8].

fundamental period of the tubes, the response of the INPORTs is virtually the same as applying an impulse.

To avoid resonance problems due to synchronization with the driver repetition rate, it is important to determine accurate values for the natural frequencies of the INPORTs. It is also necessary to examine the dynamic response of the tubes since they are relatively close-packed and mechanical interference must be avoided.

6.2 INPORT MECHANICAL MODELING

The INPORTs are modeled as completely flexible tubes, neglecting any shear or bending resistance. The spring support mechanism allows for the control of axial tension in each unit. It is assumed that the preloading will be substantial compared with the weight, consequently a constant tension is used.

Viscous damping is included in the model and expressed as a percent of critical damping. It is expected that the INPORTs will naturally display a higher level of damping than metallic components. Therefore, a level up to 20% has been used which complies with experimental values found for electrical conductors and transmission lines [6.8].

The flow velocity of the LiPb is considered constant, and in addition, internal pressure and secondary effects of flow through the tube wall are not considered at this time.

The shock transmission to the INPORT unit is taken as uniform over the entire length without any time variation in the axial direction. It is also assumed that the tube reacts as a rigid surface

component receiving the full intensity of the impulsive pressure. A less conservative response would result if surface movement was assessed.

6.3 PLANAR EQUATION OF MOTION

The planar response of the INPORTs has been considered first in order to observe the Coriolis effects of the fluid and the effects of the cubic nonlinear terms. For steady flow the corresponding dimensionless equation of motion is given by

$$\bar{v}_r'' + \bar{a} \sum_{n=1}^{\infty} \frac{rn}{(r^2 - n^2)} \bar{v}_n' + \bar{b}\, r\, \bar{v}_r' + r^2 \bar{v}_r + \bar{c}\, r^2 \bar{v}_r \sum_{m=1}^{\infty} m^2 v_m^2 = 0 \,. \qquad \begin{matrix} r = 1,2,3... \\ (r \pm n) = \text{odd} \end{matrix} \tag{6.3-1}$$

where $\bar{a}$, $\bar{b}$ and $\bar{c}$ are given in (5.3-5). Consequently, the effect of the Coriolis acceleration of the fluid can be seen by varying $\bar{a}$, and the nonlinear effects can be seen through $\bar{c}$.

A computer code has been developed to numerically integrate Eq. (6.3-1). A Runge-Kutta method was used with a 15 mode solution. This yields 30 first order differential equations coupled through the Coriolis and nonlinear terms.

As was previously stated, the primary driving force here is the mechanical shock imparted to the tube after the ignition of the

target (Fig. 6.1-5). This dynamic pressure pulse is applied sequentially, and in a radial direction, at the repetition rate (Rep Rate) of the reactor. Schematically, this is shown in Fig. 6.3-1.

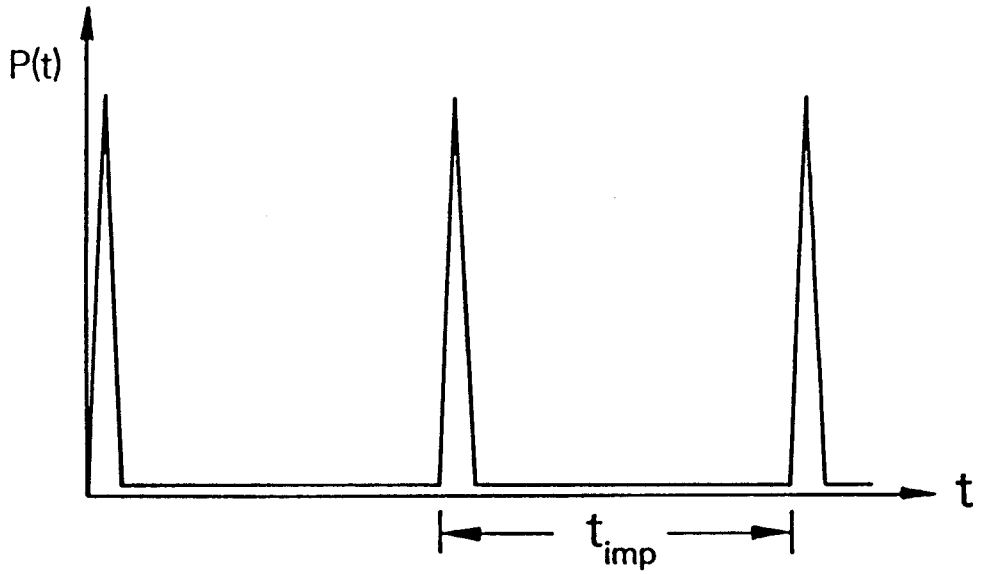

Fig. 6.3-1. Sequential Impulse Loading on the Tube.

If the positive v displacement direction is allowed to directly correspond to the radial direction of the pulse, it follows that the initial velocity given to the INPORT can be expressed as

$$\dot{v}\ (0) = \frac{I_p\ (2R)}{(m_f + m_t)} \qquad (6.3\text{-}2)$$

where I_p is the area under an individual pressure pulse and R is the radius of the tube. In dimensionless quantities Eq. (6.3-2) can be written as

$$\bar{v}'(0) = \frac{I_p\ (2R)}{\ell(m_f + m_t)\omega_1} \ . \qquad (6.3\text{-}3)$$

Since the impulse is considered to be uniformly applied over the length of the tube, the initial velocity can be represented in terms of the Fourier series

$$\frac{\partial\ \bar{v}_n\ (x,0)}{\partial \bar{t}} = \sum_{n=1}^{\infty} \bar{v}_n'(0)\ \sin\frac{n\pi x}{\ell} = \sum_{n=1}^{\infty} \frac{4\ \bar{v}'(0)}{n\pi}\ \sin\frac{n\pi x}{\ell} \ . \qquad (6.3\text{-}4)$$

It is the coefficients of this series that are used as the initial conditions for $\bar{v}_1$, $\bar{v}_3$, $\bar{v}_5$, ... in the Runge-Kutta integration program. At the end of the first shot ($\bar{t} = \bar{t}_{imp}$) the modal displacements and velocities are used as the initial conditions just prior to the application of the next pulse. Similarly, this is repeated for each pulse sequentially.

6.4 PLANAR DISPLACEMENT HISTORIES - LINEAR

Specifically, a number of calculations were done for the LIBRA design using the range of parameters given in Table 6.4-1. Modal frequencies as dimensional quantities were determined for a tube length of 6 m and are shown in Fig. 6.4-1. It can be seen that the natural frequencies are moderately increased by higher mean tensions and reduced as the fluid velocity increases. Repetition rates anticipated in the LIBRA design are checked with graphs such as Fig. 6.4-1 to avoid any potential resonance problems.

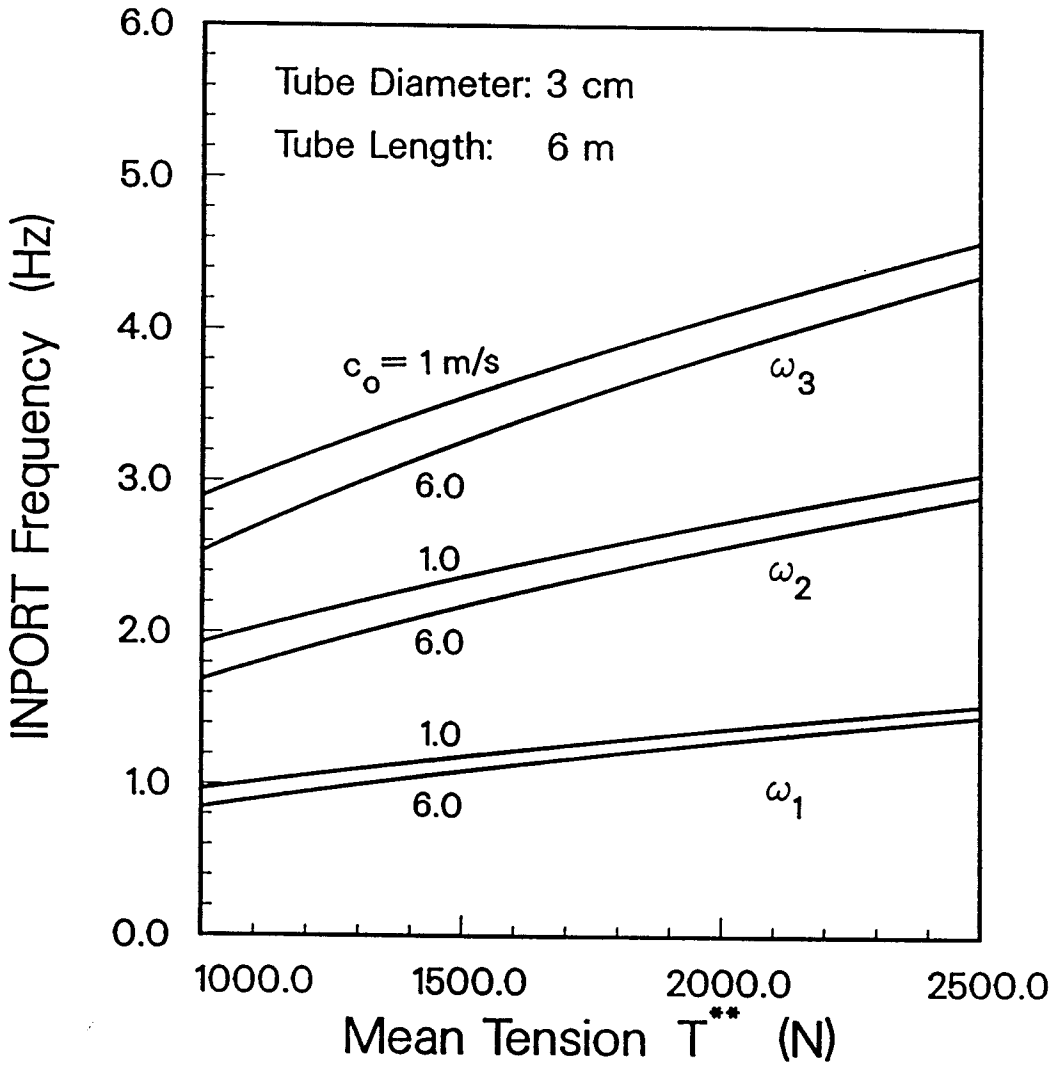

Fig. 6.4-1. INPORT Natural Frequencies.

Table 6.4-1

LIBRA INPORT Parameters

Tube Diameter (cm)	3.0
Tube Length, ℓ (m)	6.0 - 10.0
Tube Thickness (mm)	3.0
Mean Tension, T** (N)	1500 - 2500
LiPb Density (g/cm^3)	9.44
SiC Density (g/cm^3)	2.60
Flow Velocity, c_o (m/s)	1.0 - 6.0
Damping (%)	$\leq$ 20
Rep Rate (Hz)	1.0 - 5.0
Impulse, I_p (Pa-s)	77.0

Midpoint displacement histories were calculated for a number of different parameter sets. The numerical integration program executes over 2000 time steps per cycle. Figures 6.4-2 through 6.4-4 show the effect of the Rep Rate for the linear case ($\overline{c}$ = 0.0) when the following parameters were chosen as constant:

Tube Diameter = 3.0 cm

Tube Length = 6.0 m

Mean Tension = 1500 N

Flow Velocity = 1 m/s

Damping = 20%

Impulse = 77 Pa-s

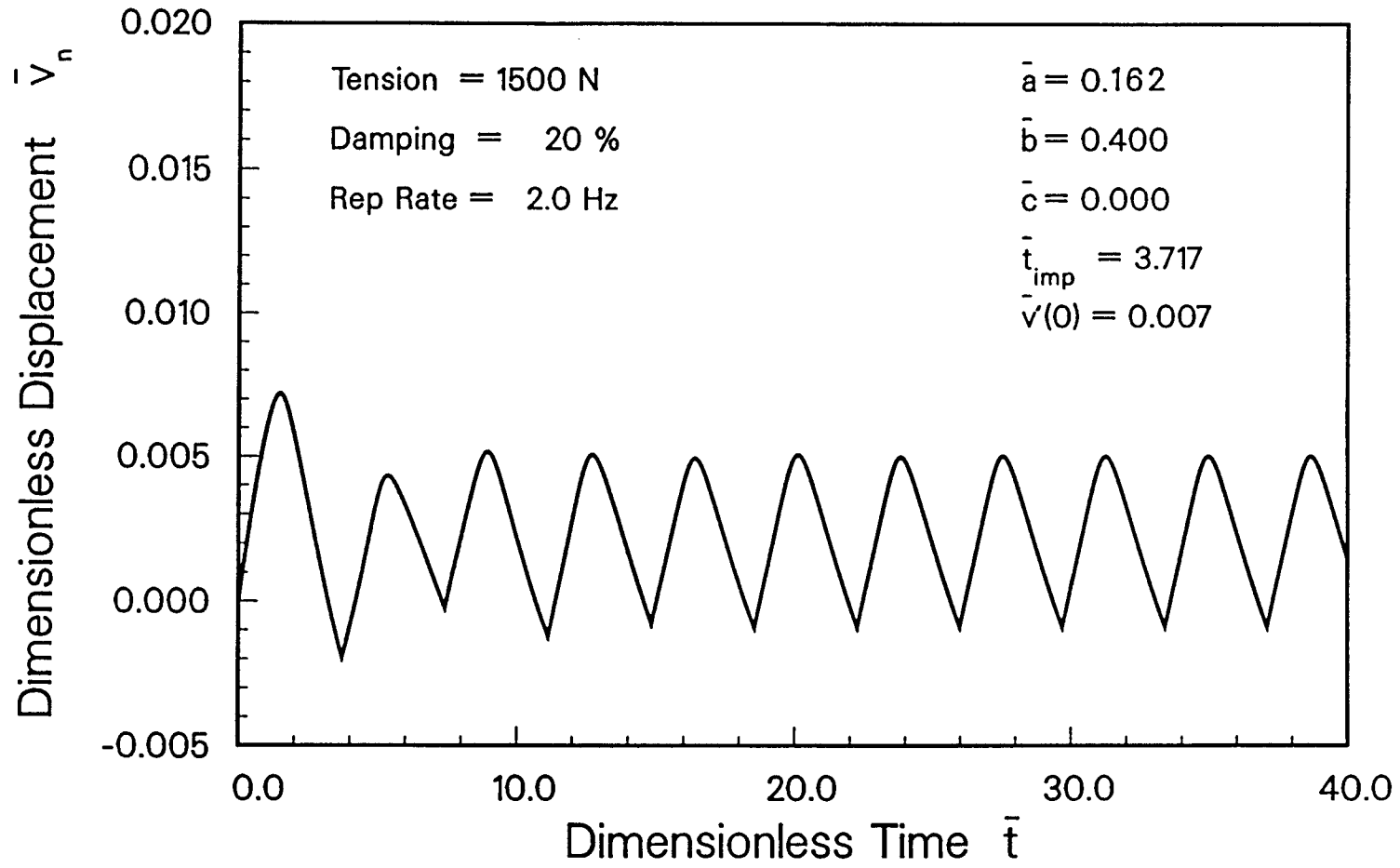

Fig. 6.4-2. INPORT Midspan Displacement History.
(Damping = 20%, Rep Rate = 2.0 Hz)

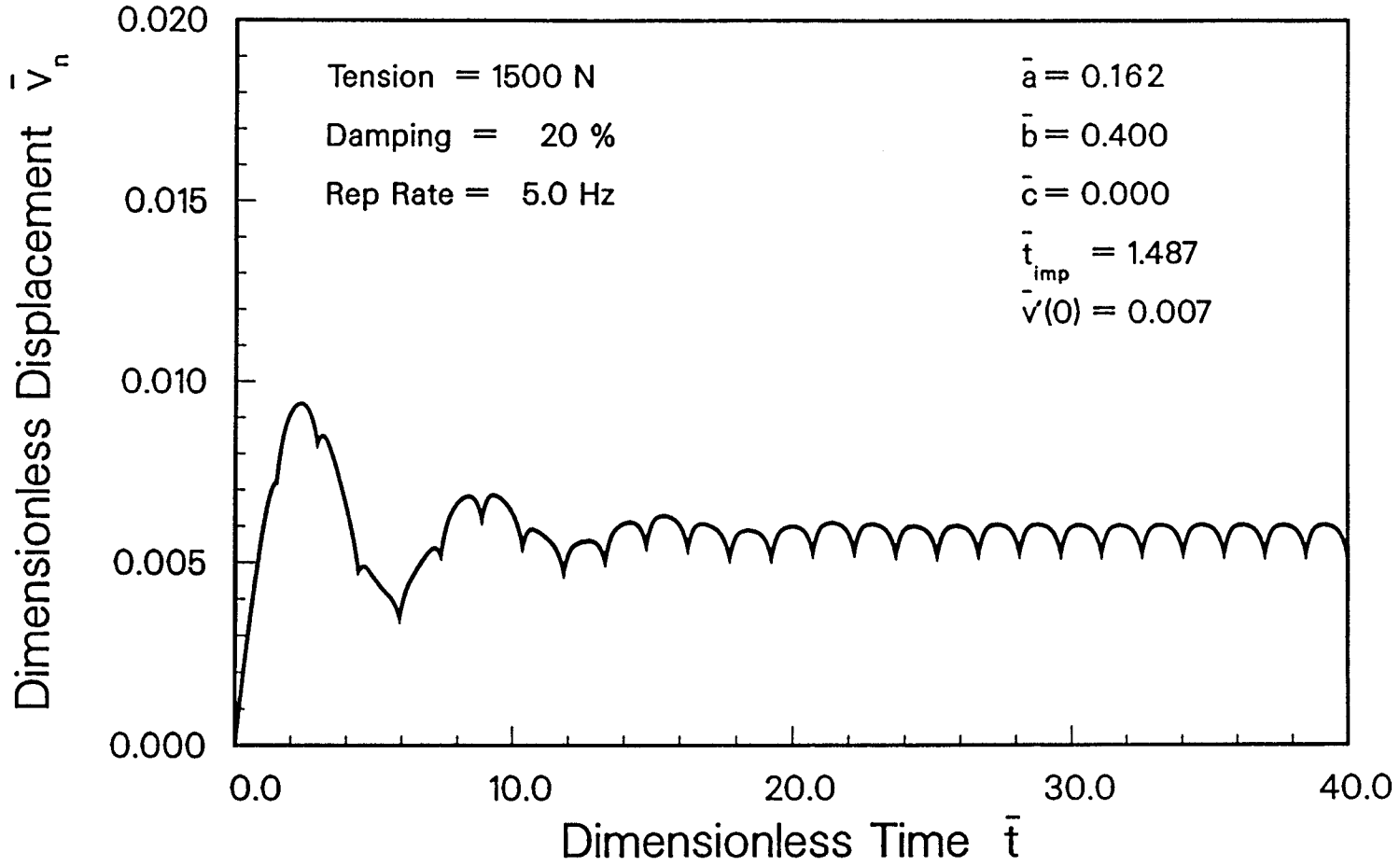

Fig. 6.4-3. INPORT Midspan Displacement History.
(Damping = 20%, Rep Rate = 5.0 Hz)

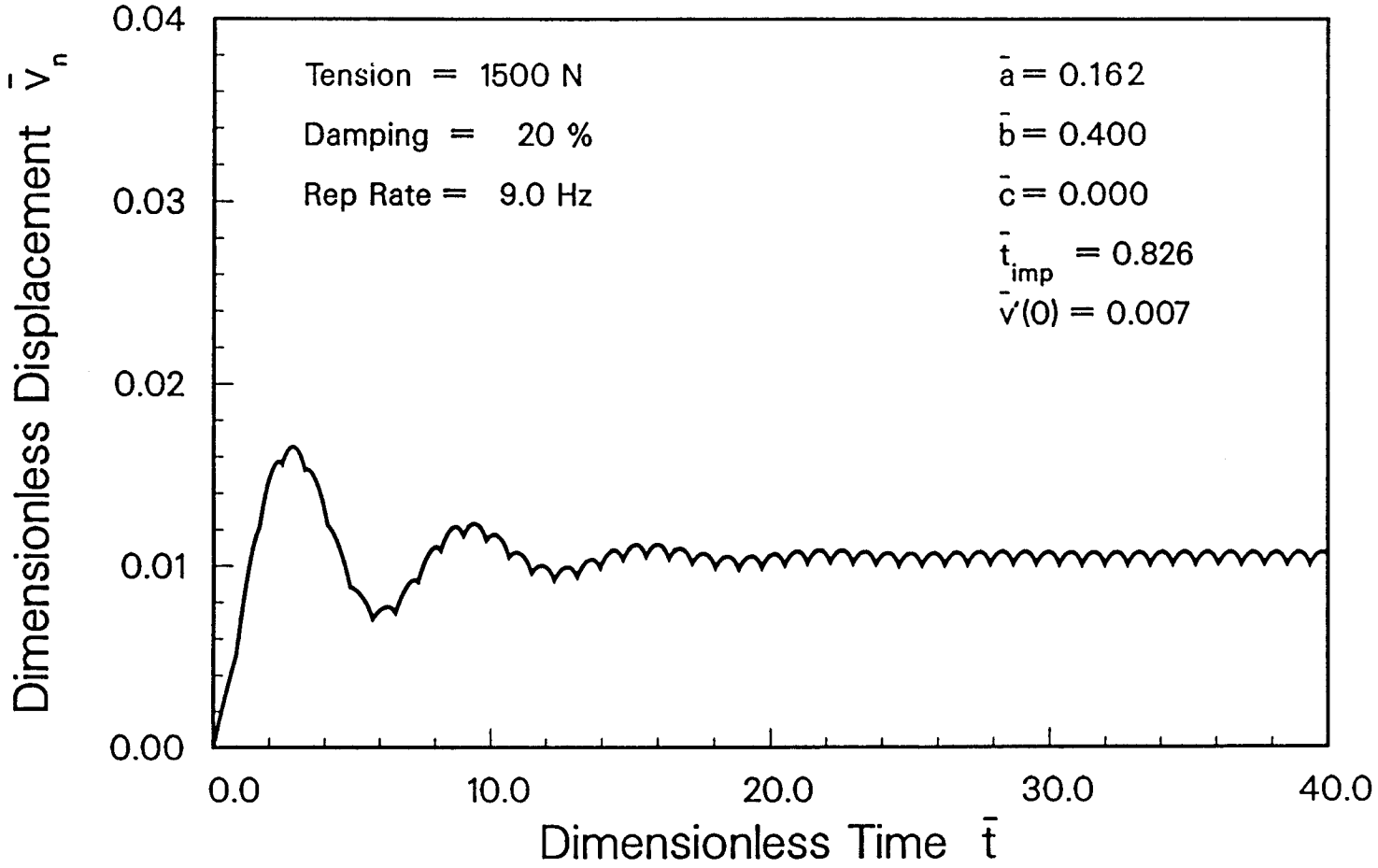

Fig. 6.4-4. INPORT Midspan Displacement History.
(Damping = 20%, Rep Rate = 9.0 Hz)

With such a low flow velocity the coefficient $\bar{a}$ is very small ($\bar{a}$ = 0.162) and the Coriolis acceleration of the fluid will be insignificant. In each plot there is an initial transient response followed by the steady state response. This first maximum peak can be controlled in an actual "start-up" situation by gradually increasing the yield of each consecutive target, thus giving a gradual rise in the magnitude of the impulses. Consequently, it is the maximum steady state displacement that is the most significant.

The effect of damping can also be seen in the response graphs. For 20% critical damping the fundamental mode is dominant. In contrast to Fig. 6.4-2, Fig. 6.4-5 shows the results of 2% damping at a Rep Rate of 2.0 Hz. There is a steady state repetitive displacement pattern as shown by brackets A and B on the figure. Table 6.4-2 summarizes the mode contributions for two extreme damping levels.

Table 6.4-2

Modal Displacement Contributions

Damping = 0%	Damping = 20%
v_1: 83.3%	v_1: 93.3%
v_3: 9.2%	v_3: 5.4%
v_5: 3.3%	v_5: 0.9%
v_7: 1.7%	v_7: 0.2%
v_9-v_{15}: < 2.5%	v_9-v_{15}: < 0.2%

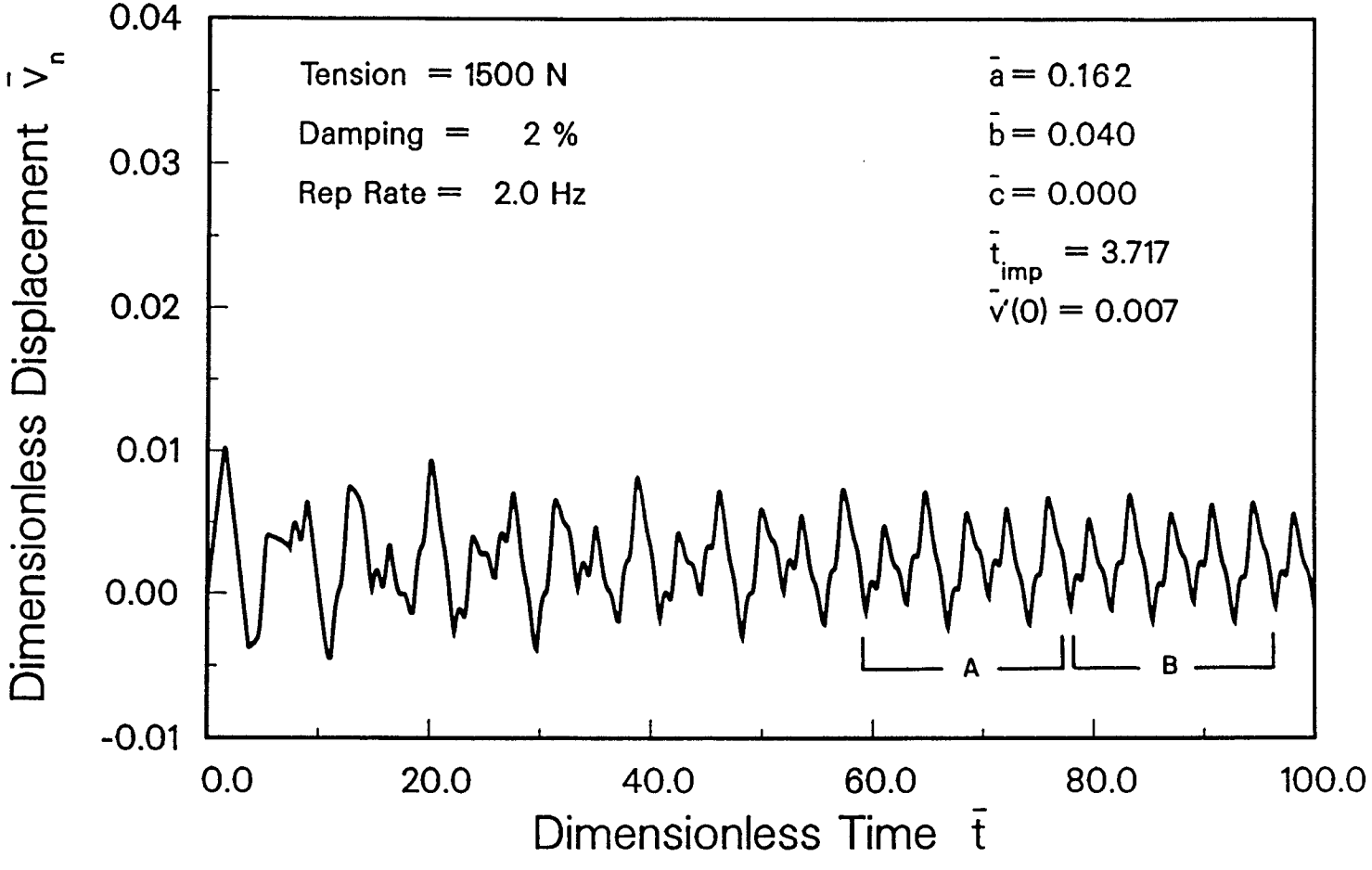

Fig. 6.4-5. INPORT Midspan Displacement History.
(Damping = 2%, Rep Rate = 2.0 Hz)

As previously noted, it is the maximum steady state displacement that is needed for determining tube placement within the reactor cavity. Consequently, amplitude-frequency plots have been developed for the linear case with the magnitude of the excitation remaining fixed. Since the initial velocity (impulsive pressure) will scale proportionally with the displacement, $\bar{v}'(0)$ was set at 0.10 for convenience. Figure 6.4-6 shows the "base" case ($\bar{a} = \bar{c} = 0.0$) with various levels of damping. Over 100 data points per curve are needed to accurately display the features of the response. Each data point is obtained by starting the system from rest, then applying sequential impulses at a particular frequency until a steady state oscillation occurs. Finally, the maximum displacement during steady state motion is recorded. This may take up to 1000 shots as $\bar{t}_{imp}$ approaches zero. From Figure 6.4-6 it can be seen that the fundamental period is verified as 2π. Note that ω_3 also shows peaks at intervals of $\bar{t}_{imp} = 2.09$ since $\omega_3 = 2\pi/3$. Besides reducing the amplitudes, damping shifts the peaks to the right of the vertical through 2π. Overall, the amplitude-frequency results resemble the response to forced harmonic excitation.

It should be noted here that conventional means of analytically determining the displacement characteristics of a forced system are inappropriate for this situation. Perturbation methods and the method of harmonic balance, for example, are not amenable to the application of sequential impulses. In addition, generally a number

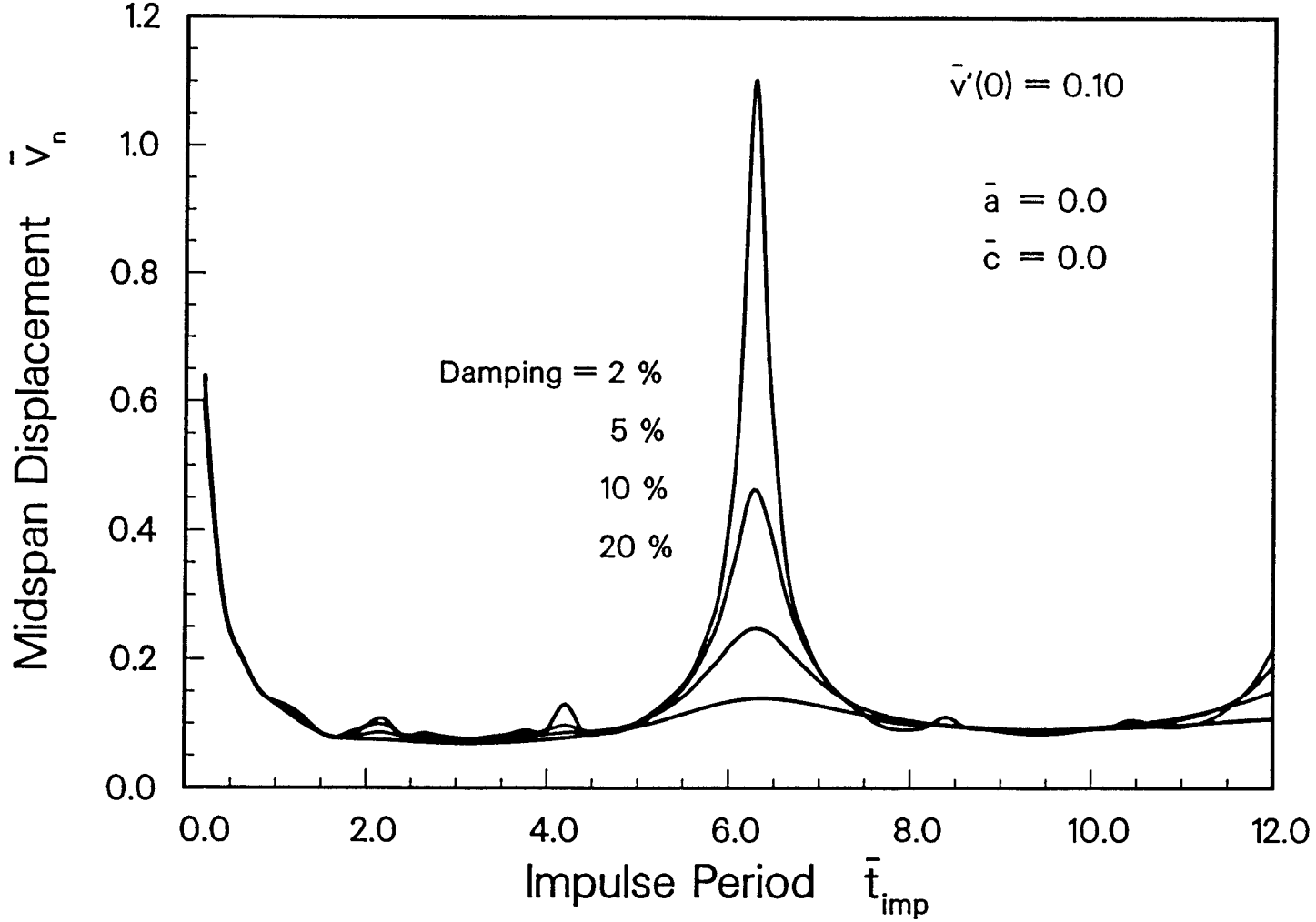

Fig. 6.4-6. Planar Midspan Amplitude-Frequency Response.
($\bar{a}$ = 0.0, $\bar{c}$ = 0.0)

of modes are needed in the solution of the problem especially with the presence of the Coriolis acceleration term. To show the effect that the even modes have on the solution, the coefficient $\bar{a}$ was increased in small increments and the corresponding amplitude-frequency curves were plotted (Figs. 6.4-7 through 6.4-9). Specifically, as $\bar{a}$ increases, the resonant peak shifts to the right and decreases in amplitude. This can clearly be seen in Fig. 6.4-10 where only the case of 2% critical damping is considered.

In summary, maximum steady state amplitudes for a very wide range of excitation frequencies have been determined for the linear problem. Additional results can be predicted by interpolating from the response curves which are presented.

6.5 PLANAR DISPLACEMENT HISTORIES - NONLINEAR

If the Coriolis acceleration term in Eq. (6.3-1) is neglected, any of the r equations are similar in form to the classic Duffing equation (without a harmonic driving force). It is therefore expected that the nonlinear amplitude-frequency response will display discontinuous jumps near resonant frequencies. (A detailed description of the jump phenomenon can be found in Appendix C).

Calculations were performed with $\bar{a} = 0$ to determine maximum response amplitudes as the impulse period was scanned and various magnitudes of $\bar{c}$ were examined. With the original program, the system was started from rest and sequential impulses were applied at a particular frequency until steady state oscillations appeared. The

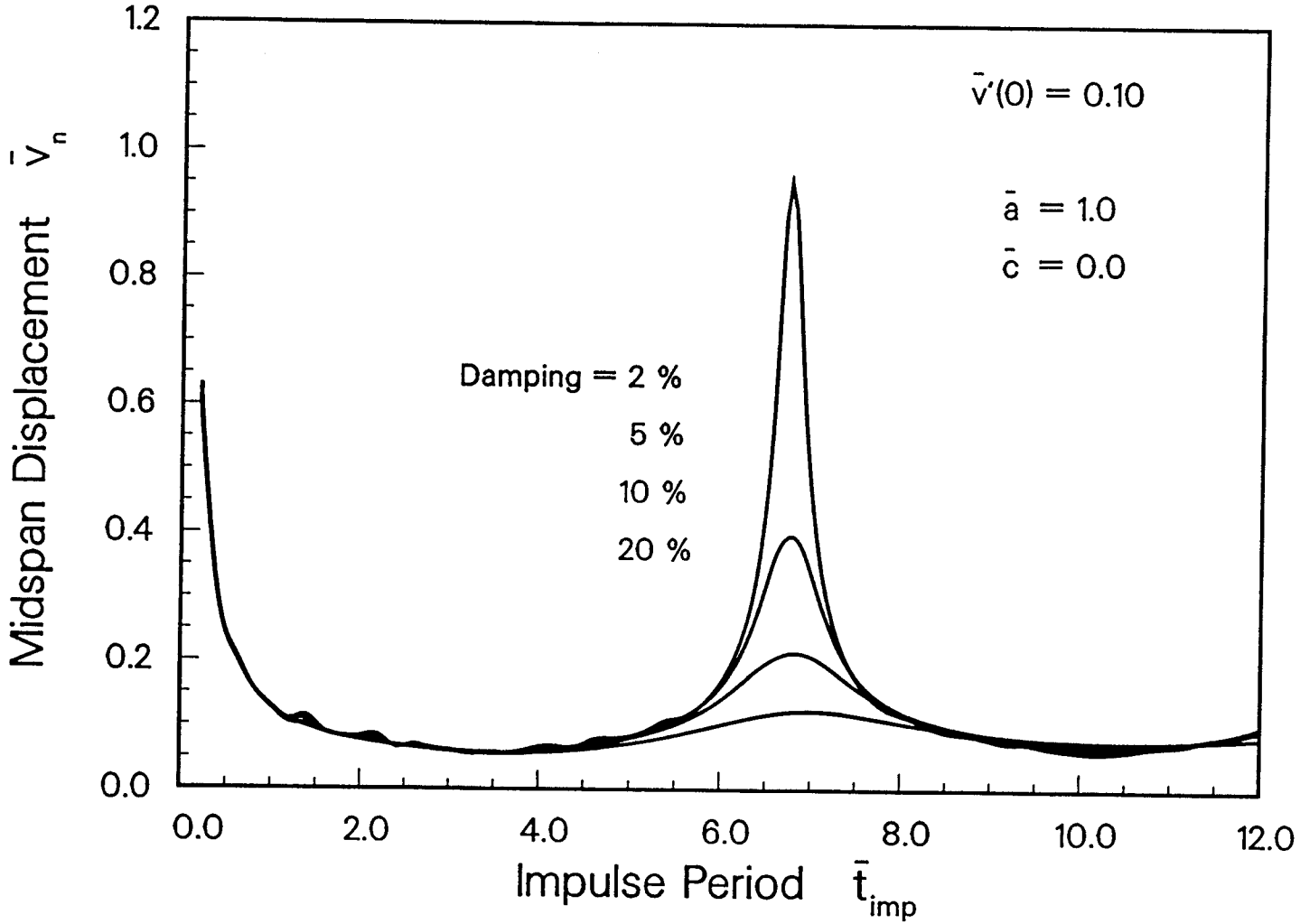

Fig. 6.4-7. Planar Midspan Amplitude-Frequency Response.
($\bar{a}$ = 1.0, $\bar{c}$ = 0.0)

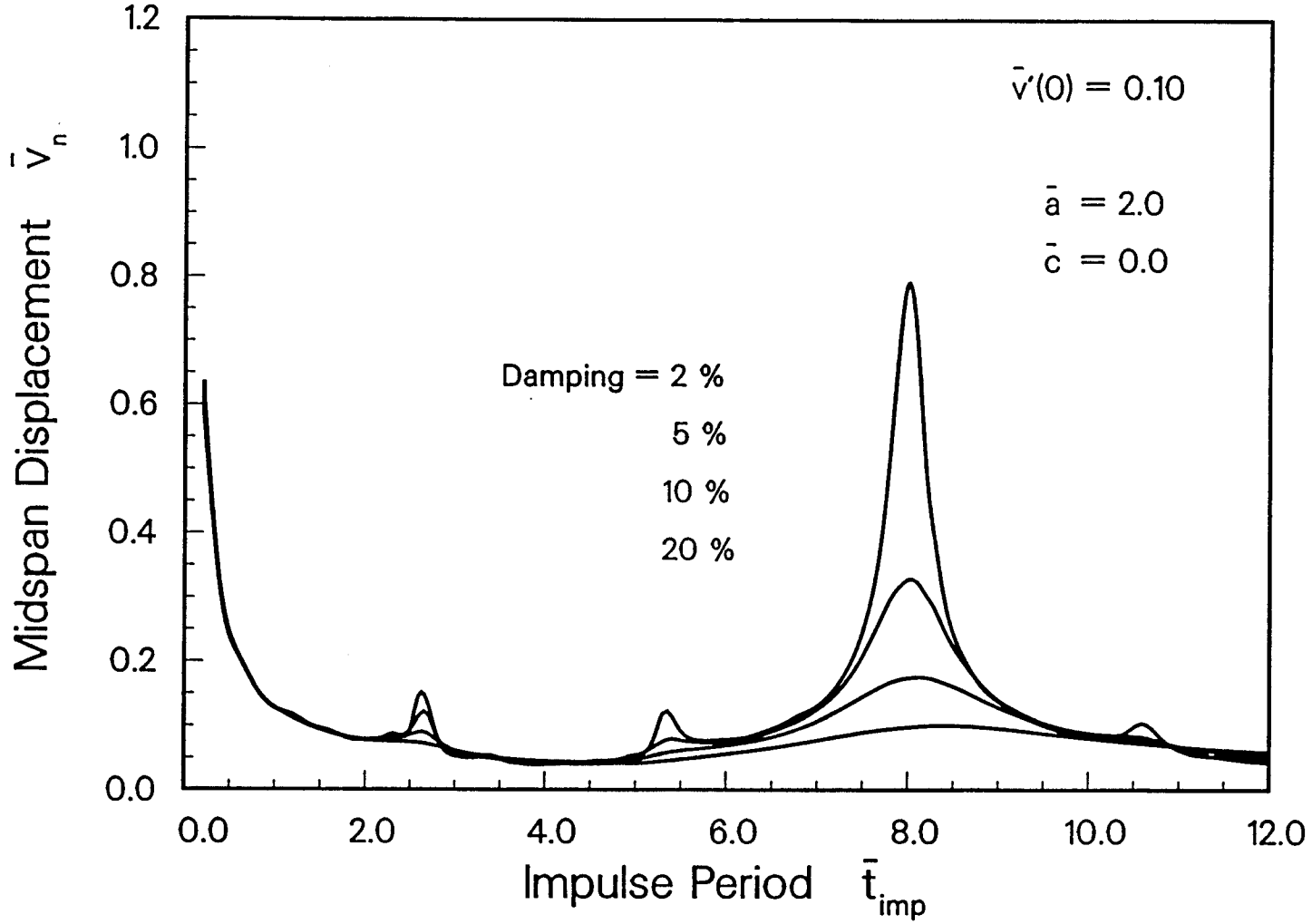

Fig. 6.4-8. Planar Midspan Amplitude-Frequency Response.
($\bar{a}$ = 2.0, $\bar{c}$ = 0.0)

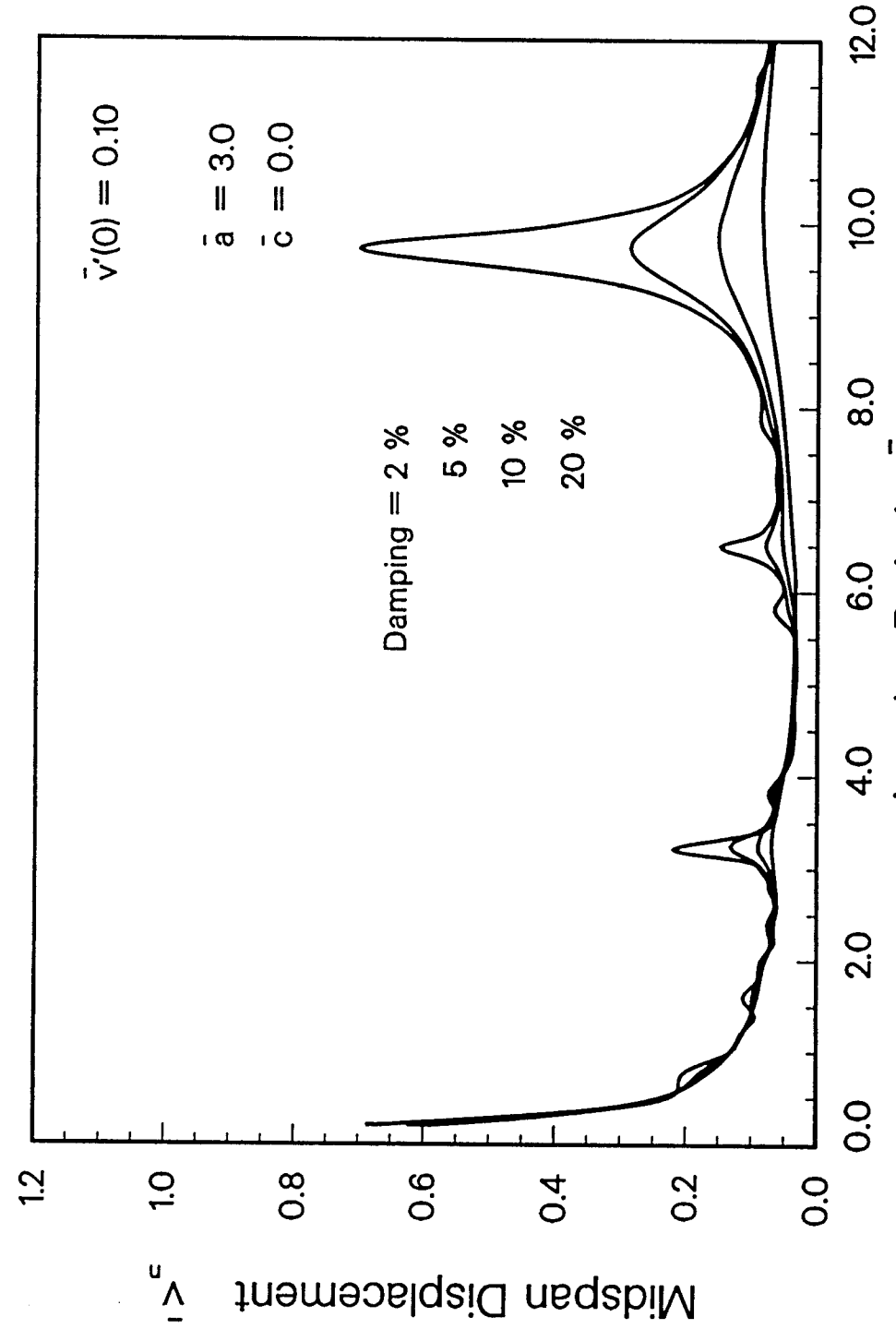

Fig. 6.4-9. Planar Midspan Amplitude-Frequency Response. ($\bar{a} = 3.0$, $\bar{c} = 0.0$)

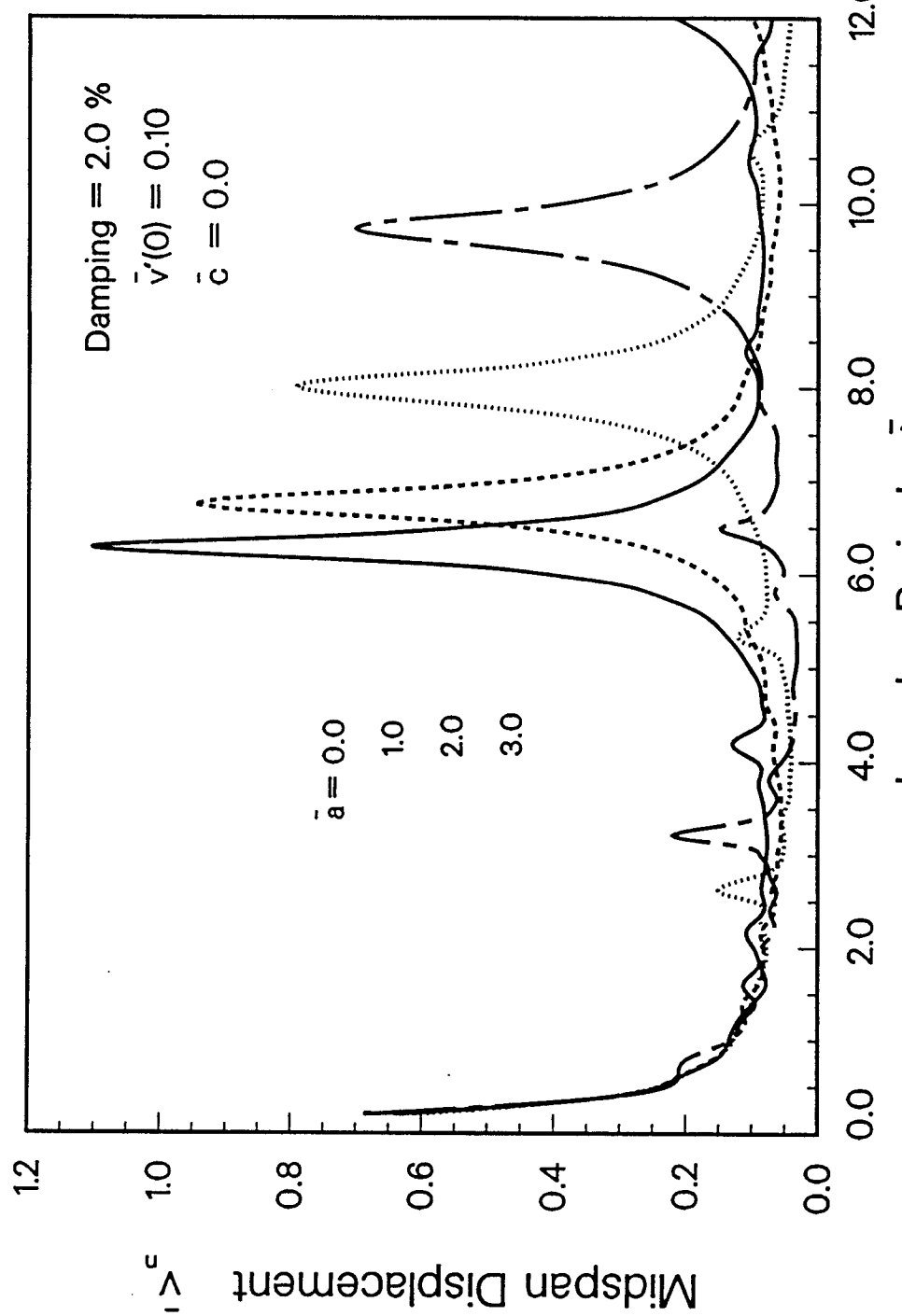

Fig. 6.4-10. Planar Midspan Amplitude-Frequency Response.
(Damping = 2%, $\bar{c}$ = 0.0)

maximum peak was recorded and the process was repeated at another frequency. Here it was necessary to develop a program that would simulate an actual experimental procedure. In order to observe the jump phenomenon the frequency of the excitation force must be gradually increased or decreased (see Appendix C). This was accomplished by gradually varying $\bar{t}_{imp}$ and keeping the magnitude of the impulsive pressure fixed.

Figure 6.5-1 shows the results for a modest value of $\bar{c}$. It can be seen that for damping levels of 5, 10 and 20% the magnitude of the impulse is not large enough to pass the critical point for which jumping occurs. However, at 2% damping there is a sizeable jump associated with the fundamental frequency. The curves have a tendency to bend to the left, with $\bar{c}$ greater than zero, because the period $\bar{t}_{imp}$ is plotted instead of its reciprocal (frequency). The value of $\bar{c}$ was then increased to 10 and 50. Figures 6.5-2 and 6.5-3 show the results again at 2% damping. On Fig. 6.5-3, data points have been marked to show the response of the system if $\bar{t}_{imp}$ is not allowed to slowly increase or decrease - as was done for the linear case.

To show how the nonlinear terms affect the general characteristics of the displacement histories, Figs. 6.5-4 and 6.5-5 give the results for $\bar{c} = 0.0$ and $\bar{c} = 50.0$, respectively. The magnitude of the impulse and the Rep Rate are the same, but the Coriolis acceleration has been neglected ($\bar{a} = 0.0$). The maximum steady state amplitude for

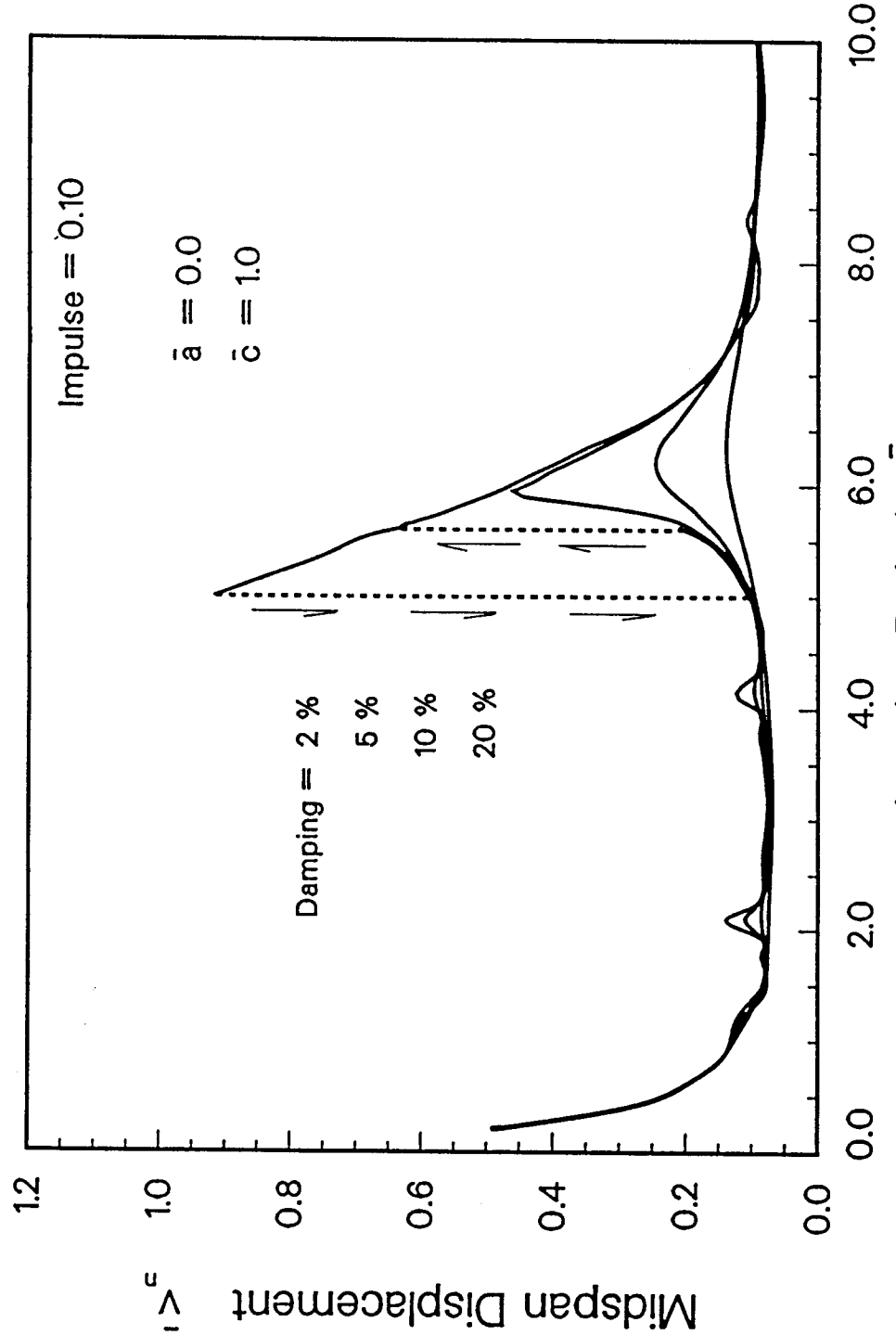

Fig. 6.5-1. Planar Midspan Amplitude-Frequency Response.
($\bar{a}$ = 0.0, $\bar{c}$ = 1.0)

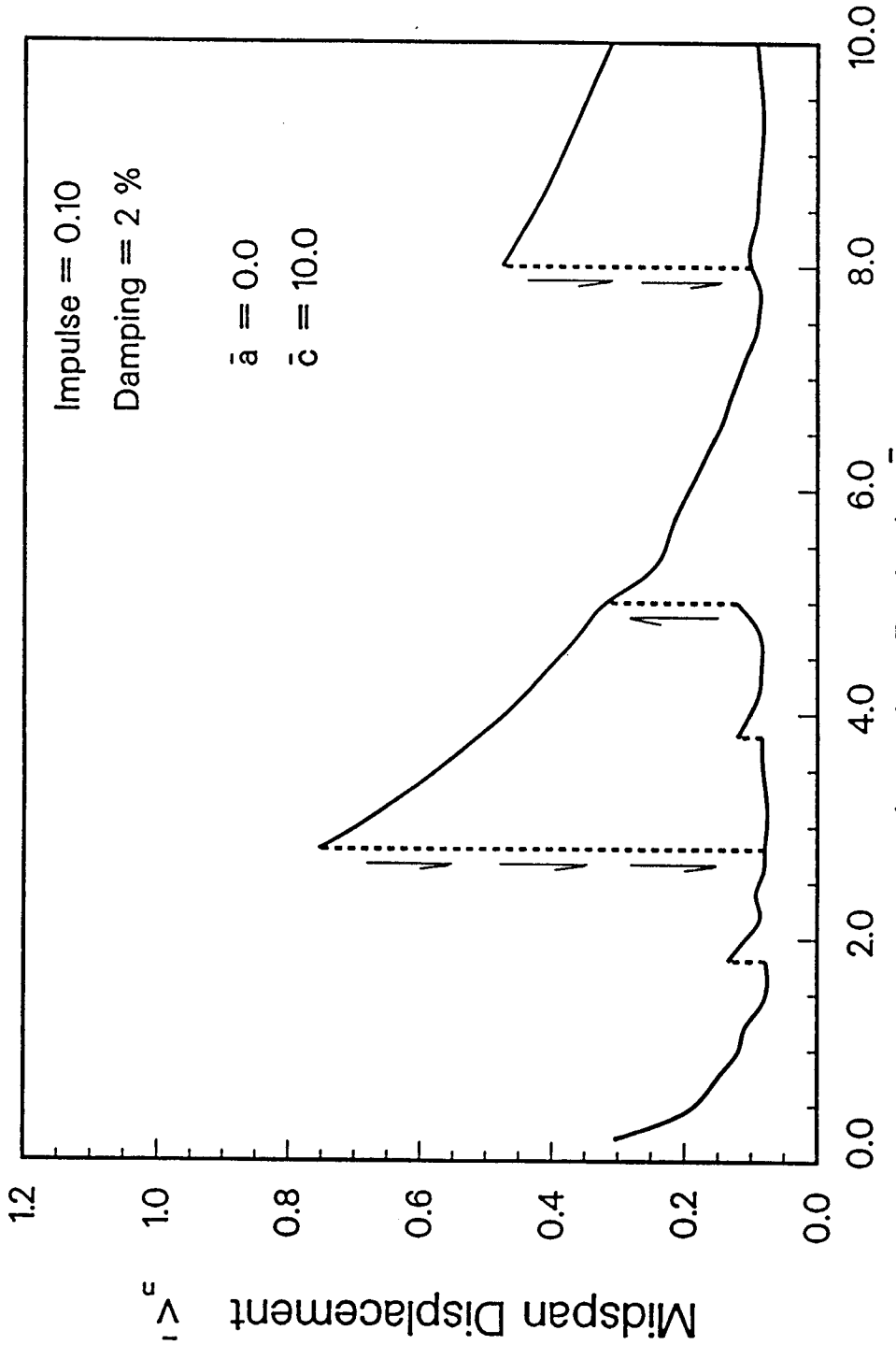

Fig. 6.5-2. Planar Midspan Amplitude-Frequency Response.
($\bar{a}$ = 0.0, $\bar{c}$ = 10.0)

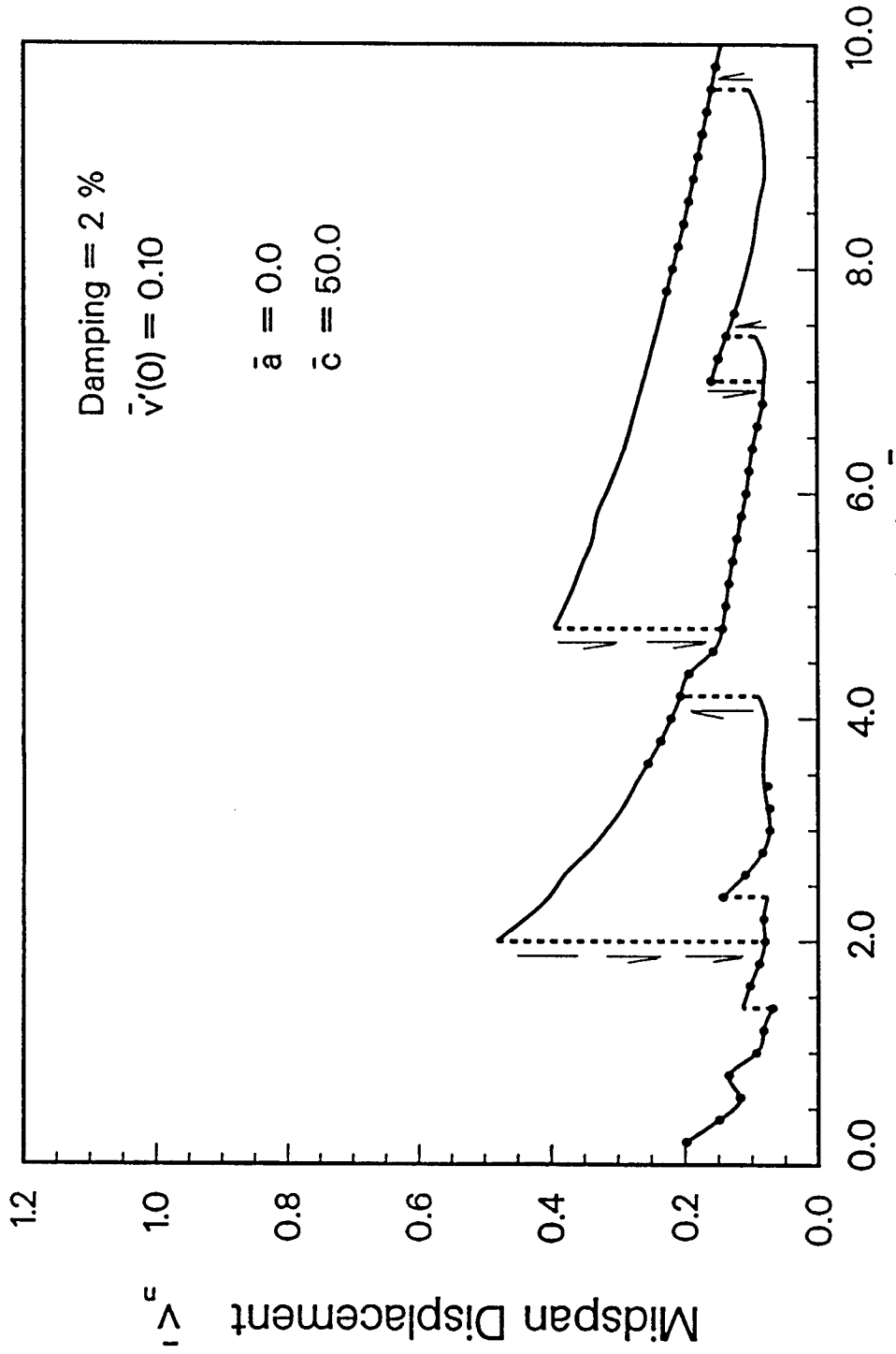

Fig. 6.5-3. Planar Midspan Amplitude-Frequency Response.
($\bar{a} = 0.0$, $\bar{c} = 50.0$)

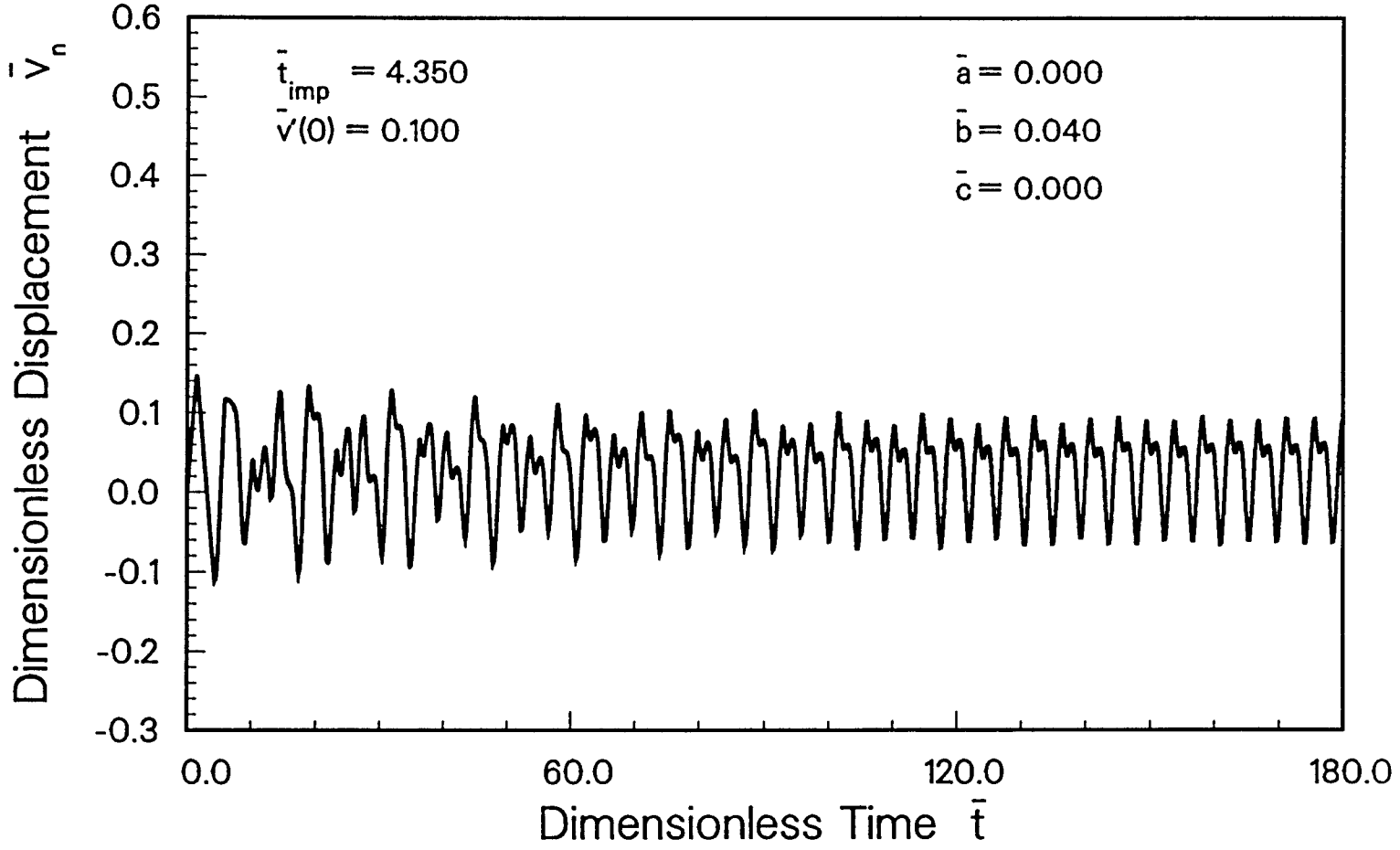

Fig. 6.5-4. Midspan Displacement History.
($\bar{a}$ = 0.0, $\bar{c}$ = 0.0)

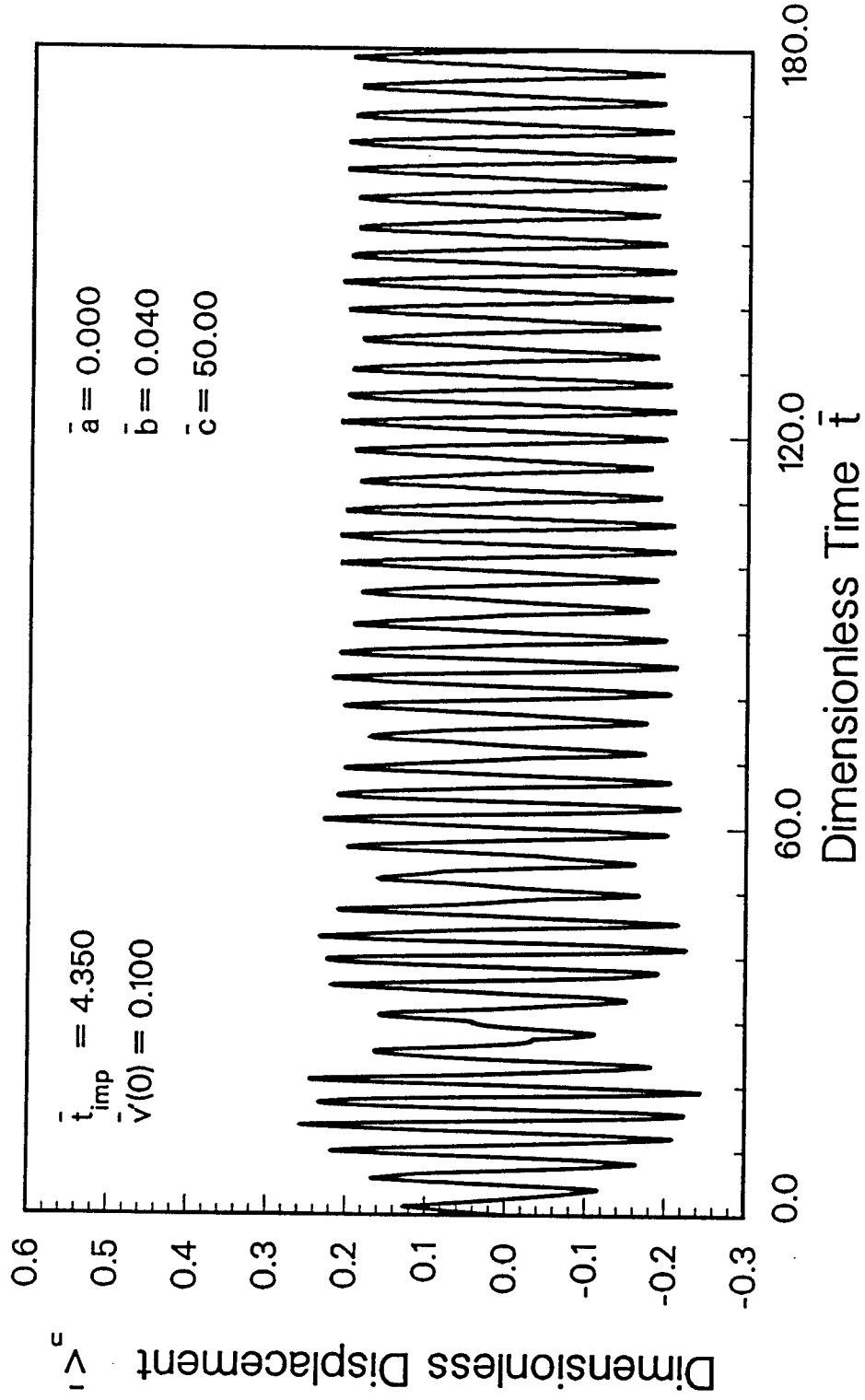

Fig. 6.5-5. Midspan Displacement History.
($\bar{a}$ = 0.0, $\bar{c}$ = 50.0)

both the linear and nonlinear curves could have been predicted from Figs. 6.4-6 and 6.5-3. It can be seen from the nonlinear amplitude-frequency curve that for the pulse frequency used ($\bar{t}_{imp} = 4.35$) the response is on the upper branch of the fundamental frequency jump. Therefore, as shown by the displacement histories, the steady state amplitudes are much larger for $\bar{c} = 50.0$.

Finally, the effect of the Coriolis acceleration terms can be seen by including a value of $\bar{a}$. Figure 6.5-6 shows an example of $\bar{a} = 3.0$ with all other values remaining the same as for the nonlinear case. All three displacement histories are the result of approximately 40 sequential impulses with thousands of data points plotted for each. For the linear case, a steady state response is actually reached in less than 40 shots. But for the nonlinear case with Coriolis acceleration present (Fig. 6.5-6), it takes nearly 250 shots before the response stabilizes. (For example, the actual steady state peaks for $\bar{v}_n$ are 0.05012, 0.02422 and 0.04347 consecutively.)

With the large number of variables involved in the planar case alone, it is impossible to generate parametric amplitude-frequency curves to cover the range of values for each variable. This is especially true with the nonlinear work, since the displacements will not necessarily scale directly with the magnitude of the applied impulse. In addition, with INPORT units being one of the major applications of the research work, the nonlinear coefficient $\bar{c}$ could get relatively large. It contains the value EA_t as given by Eq. (5.3-5).

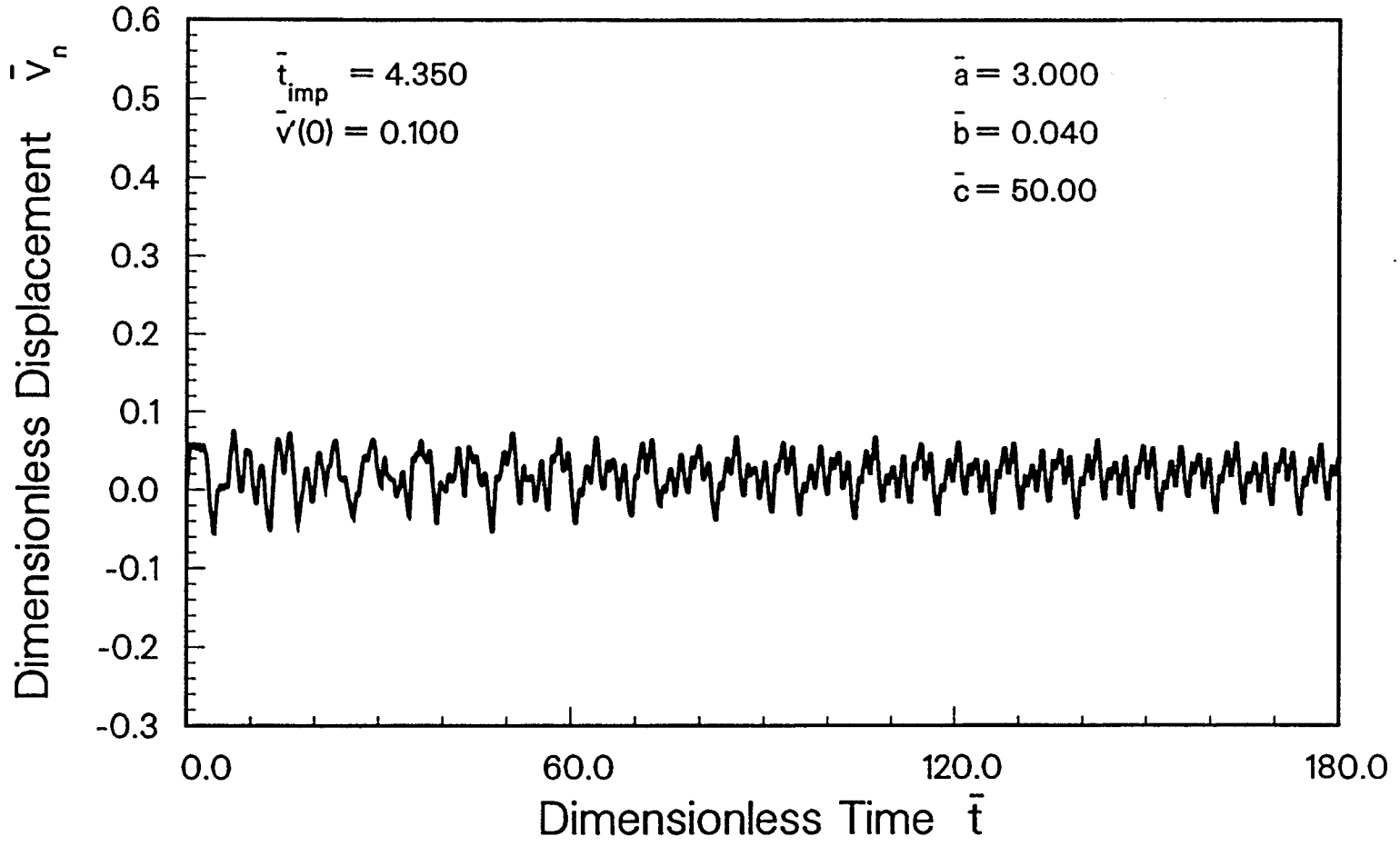

Fig. 6.5-6. Midspan Displacement History.
($\bar{a}$ = 3.0, $\bar{c}$ = 50.0)

Depending upon future experimental data (see Appendix A), $\bar{c}$ could get much larger than 50. Therefore, for any ICF design application it may be necessary to pinpoint a number of variables and consider specific cases separately.

6.6 NONPLANAR DISPLACEMENT HISTORIES

The three dimensional motion of the tube with steady flow can be addressed by considering Eqs. (5.3-7) and (5.3-8) with the pulsating component set to zero.

$$\bar{v}_r'' + \bar{a} \sum_{n=1}^{\infty} \frac{rn}{(r^2 - n^2)} \bar{v}_n' + \bar{b}\, r\, \bar{v}_r' \qquad (6.6\text{-}1)$$

$$+ r^2 \bar{v}_r + \bar{c}\, r^2 \bar{v}_r \sum_{m=1}^{\infty} m^2 (\bar{v}_m^2 + \bar{w}_m^2) = 0 \qquad \begin{array}{l} r = 1,2,3 \ldots \\ (r \pm n) = \text{odd} \end{array}$$

$$\bar{w}_r'' + \bar{a} \sum_{n=1}^{\infty} \frac{rn}{(r^2 - n^2)} \bar{w}_n' + \bar{b}\, r\, \bar{w}_r' \qquad (6.6\text{-}2)$$

$$+ r^2 \bar{w}_r + \bar{c}\, r^2 \bar{w}_r \sum_{m=1}^{\infty} m^2 (\bar{v}_m^2 + \bar{w}_m^2) = 0 \qquad \begin{array}{l} r = 1,2,3 \ldots \\ (r \pm n) = \text{odd} \end{array}$$

As was previously noted, coupling between the two transverse motions (v and w) is found only in the cubic nonlinear terms in the summation on m. The Coriolis acceleration term with coefficient $\bar{a}$ couples the various modes of each equation independently.

With this in mind a preliminary analysis of Eqs. (6.6-1) and (6.6-2) is considered to determine characteristics of the coupling. Since the Coriolis terms are independent for each equation they have been omitted. If Eq. (6.6-1) is then multiplied by $\bar{w}_r$ and (6.6-2) by $\bar{v}_r$ and the two equations are subtracted, the following is obtained

$$\bar{v}_r'' \bar{w}_r - \bar{v}_r \bar{w}_r'' + \bar{b}\, r(\bar{v}_r' \bar{w}_r - \bar{v}_r \bar{w}_r') = 0 . \qquad (6.6\text{-}3)$$

However, this can be rewritten as

$$[\bar{v}_r' \bar{w}_r - \bar{v}_r \bar{w}_r']' = - \bar{b}r\, [\bar{v}_r' \bar{w}_r - \bar{v}_r \bar{w}_r'] . \qquad (6.6\text{-}4)$$

Integrating Eq. (6.6-4) yields

$$\bar{v}_r' \bar{w}_r - \bar{v}_r \bar{w}_r' = Ce^{-\bar{b}r\bar{t}} \qquad (6.6\text{-}5)$$

where the constant C can be determined from initial conditions.

If the initial conditions are such that C is zero then

$$\frac{\bar{v}_r'}{\bar{w}_r'} = \frac{\bar{v}_r}{\bar{w}_r} \qquad (6.6\text{-}6)$$

and the result is coplanar motion of the tube. In other words, the tube can have v and w displacement components but the magnitude of the displacements will remain in the same ratio relative to each

other and there would be no exchange of energy between the components. Therefore, the following sets of initial conditions would result in coplanar motion:

Case I	Case II	Case III	Case IV
$\bar{w}_r(0) = 0$	$\bar{v}_r(0) = 0$	$\bar{v}_r'(0) = 0$	$\bar{v}_r(0) = 0$
and	and	and	and
$\bar{w}_r'(0) = 0$	$\bar{v}_r'(0) = 0$	$\bar{w}_r'(0) = 0$	$\bar{w}_r(0) = 0$

The previous calculations on the planar response of the INPORT units due to sequential impulses assumed an impulse $\bar{v}'(0)$ only. According to Eq. (6.6-5), this would still constitute coplanar (planar) motion even with coupling terms present. Therefore, with ICF reactor applications in mind, an obvious case to consider is an initial displacement in the out-of-plane direction ($\bar{w}(0)$) with the impulsive loading remaining in-plane ($\bar{v}'(0)$).

To develop a better understanding of the characteristics of three-dimensional motion a single shot analysis is investigated first. Consequently, the problem is virtually one of free vibration with a specific set of initial conditions. Equations (6.6-1) and (6.6-2) were programmed again using the Runge-Kutta method. With the inclusion of the out-of-plane displacements, the solutions were limited to 5 modes in both $\bar{v}$ and $\bar{w}$, yielding 20 coupled first order

differential equations. (Five modes would be sufficient according to the modal displacement contributions given in Table 6.4-2.)

To illustrate the effect of the coupling coefficient $\bar{c}$, the Coriolis acceleration is neglected and damping is set to zero. Figure 6.6-1 shows the midspan displacement histories for both transverse displacements with an initial velocity $\bar{v}'(0) = 0.10$ and an initial displacement $\bar{w}(0) = 0.05$. For the small value of $\bar{c} = 1.0$ there is very little energy exchanged between $\bar{v}$ and $\bar{w}$ even with $\bar{t}$ carried out for an extended length of time. On the contrary, Fig. 6.6-2 shows the interchange of energy between the two motions when $\bar{c}$ is increased to 10.0. To illustrate the whirling motion associated with this system, Fig. 6.6-3 shows $\bar{v}$ versus $\bar{w}$ for a time span of approximately $0 \leq \bar{t} \leq 450$. This is the amount of time for the orbital axis to precess a full 360°. Denoting this precessional angle by ψ, Fig. 6.6-3 then corresponds to $0° \leq \psi \leq 360°$. The oval-like shape of the orbital path can be seen more clearly in Figs. 6.6-4 and 6.6-5 where the precessional angle has been limited to a quarter of a revolution, consecutively. It should be noted that the direction of the precession is the opposite sense to the orbital motion.

Traditionally, the study of the nonplanar oscillatory response of strings would include a single mode analysis only. If the present system were analyzed with the fundamental mode, the envelopes of the orbital path would be circular as shown in Fig. 6.6-6. The corresponding orbital path can be seen as elliptical in Figs. 6.6-7 and 6.6-8. The characteristics of this response for a single mode are

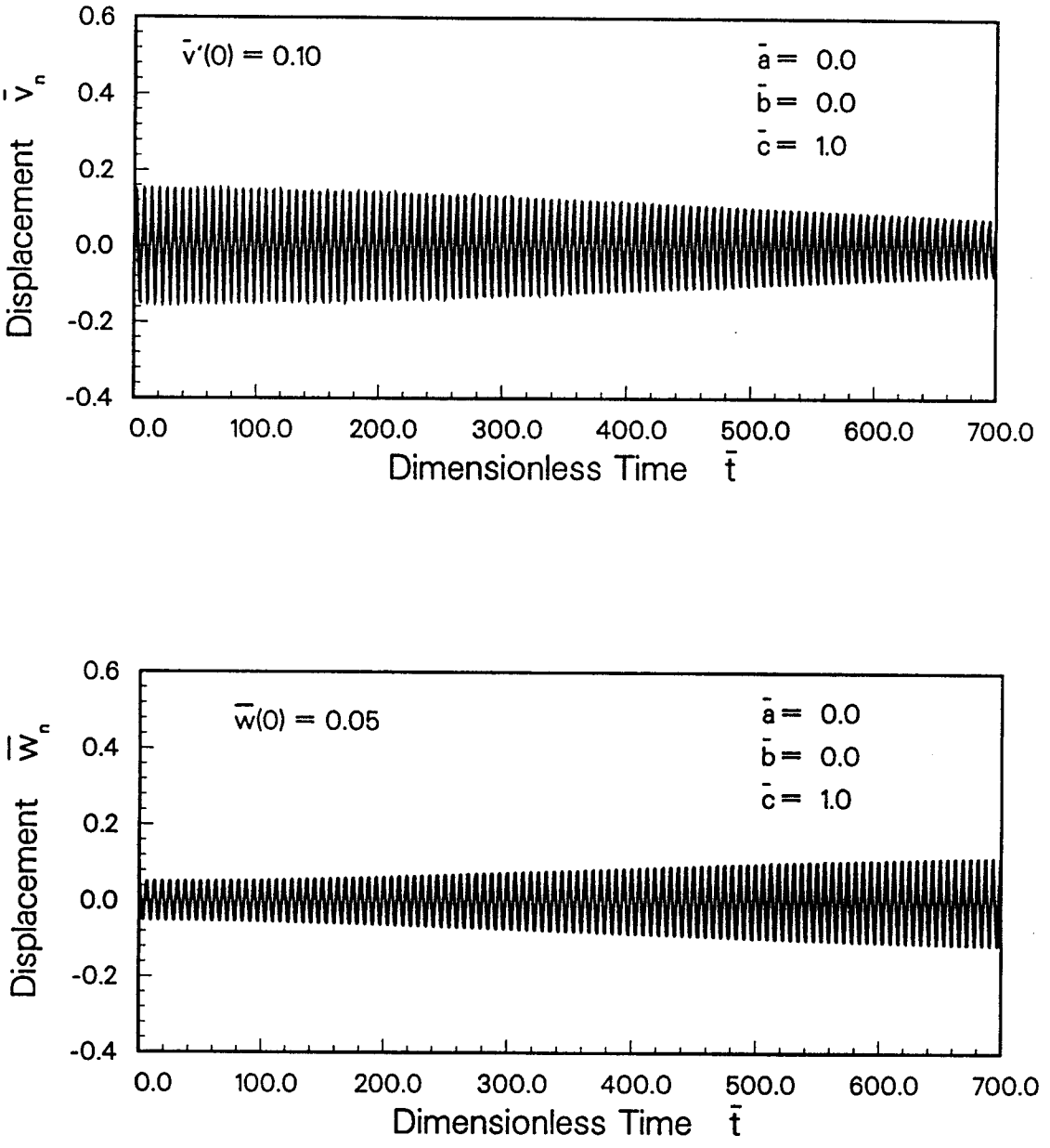

Fig. 6.6-1. Nonplanar Midspan Displacement Histories for Single Shot Analysis. ($\bar{a}$ = 0.0, $\bar{c}$ = 1.0, Damping = 0%)

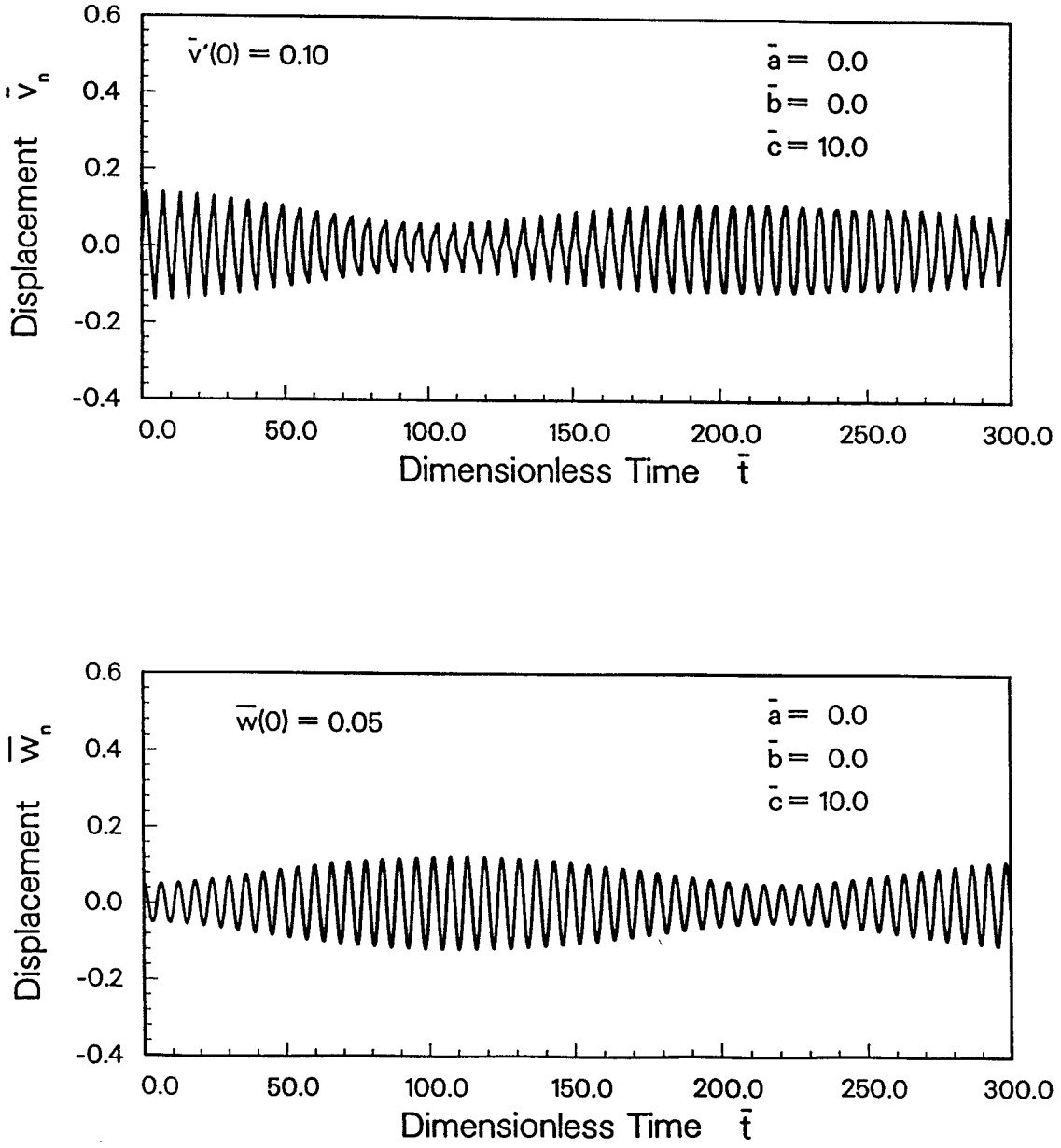

Fig. 6.6-2. Nonplanar Midspan Displacement Histories for Single Shot Analysis. ($\bar{a}$ = 0.0, $\bar{c}$ = 10.0, Damping = 0%)

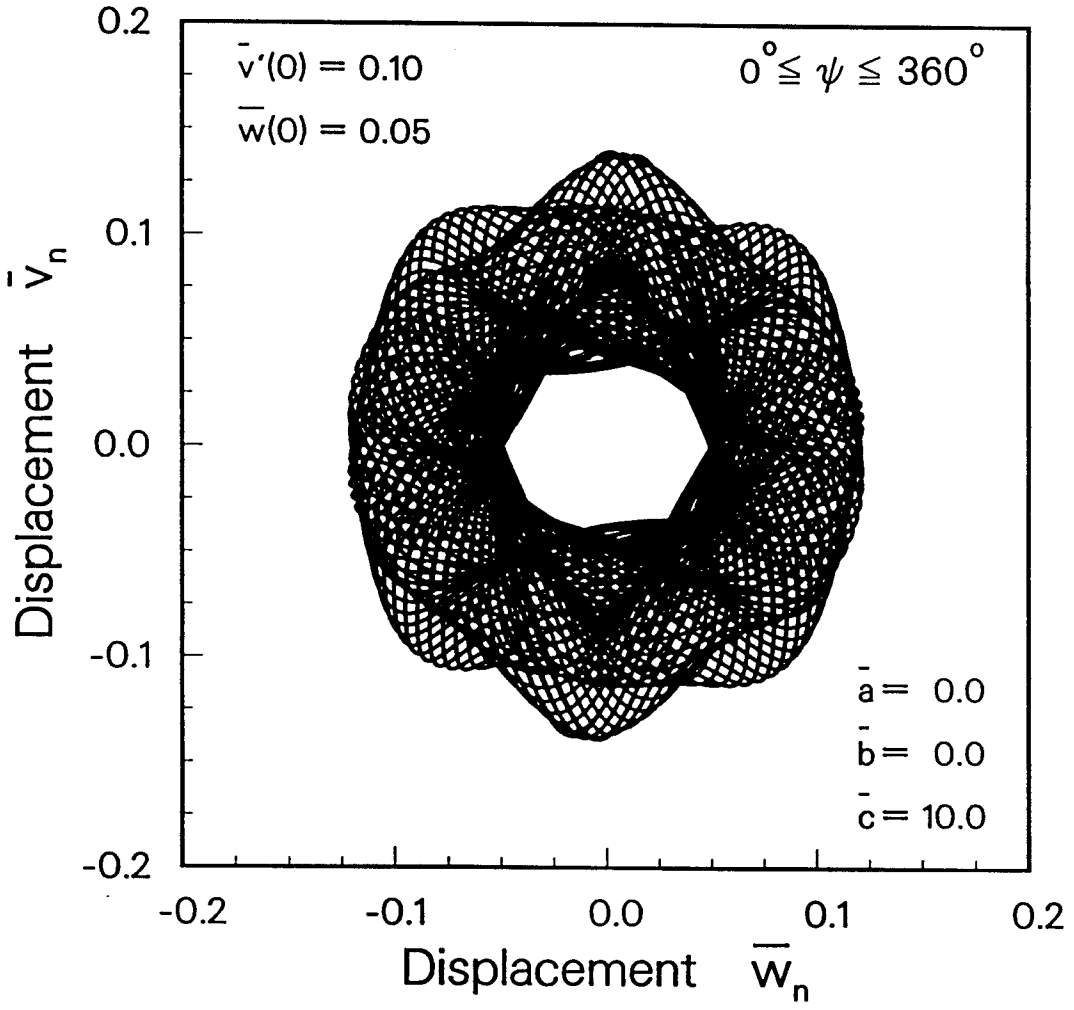

Fig. 6.6-3. Nonplanar Midspan Orbital Path for Single Shot Analysis for $0° \leq \psi \leq 360°$. ($\bar{a}$ = 0.0, $\bar{c}$ = 10.0, Damping = 0%)

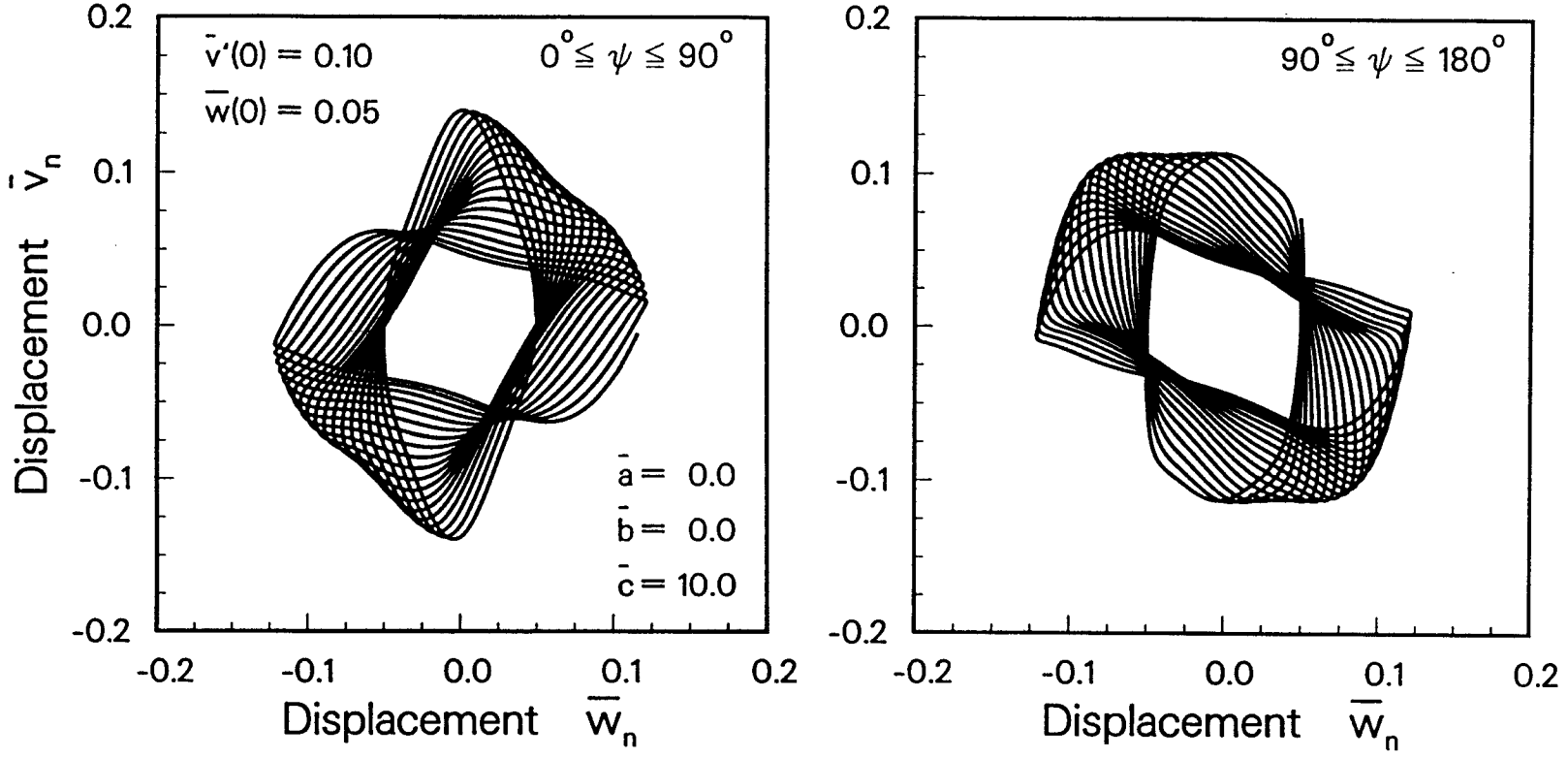

Fig. 6.6-4. Nonplanar Midspan Orbital Path for Single Shot Analysis for $0° \leq \psi \leq 90°$ and $90° \leq \psi \leq 180°$. ($\bar{a}$ = 0.0, $\bar{c}$ = 10.0, Damping = 0%)

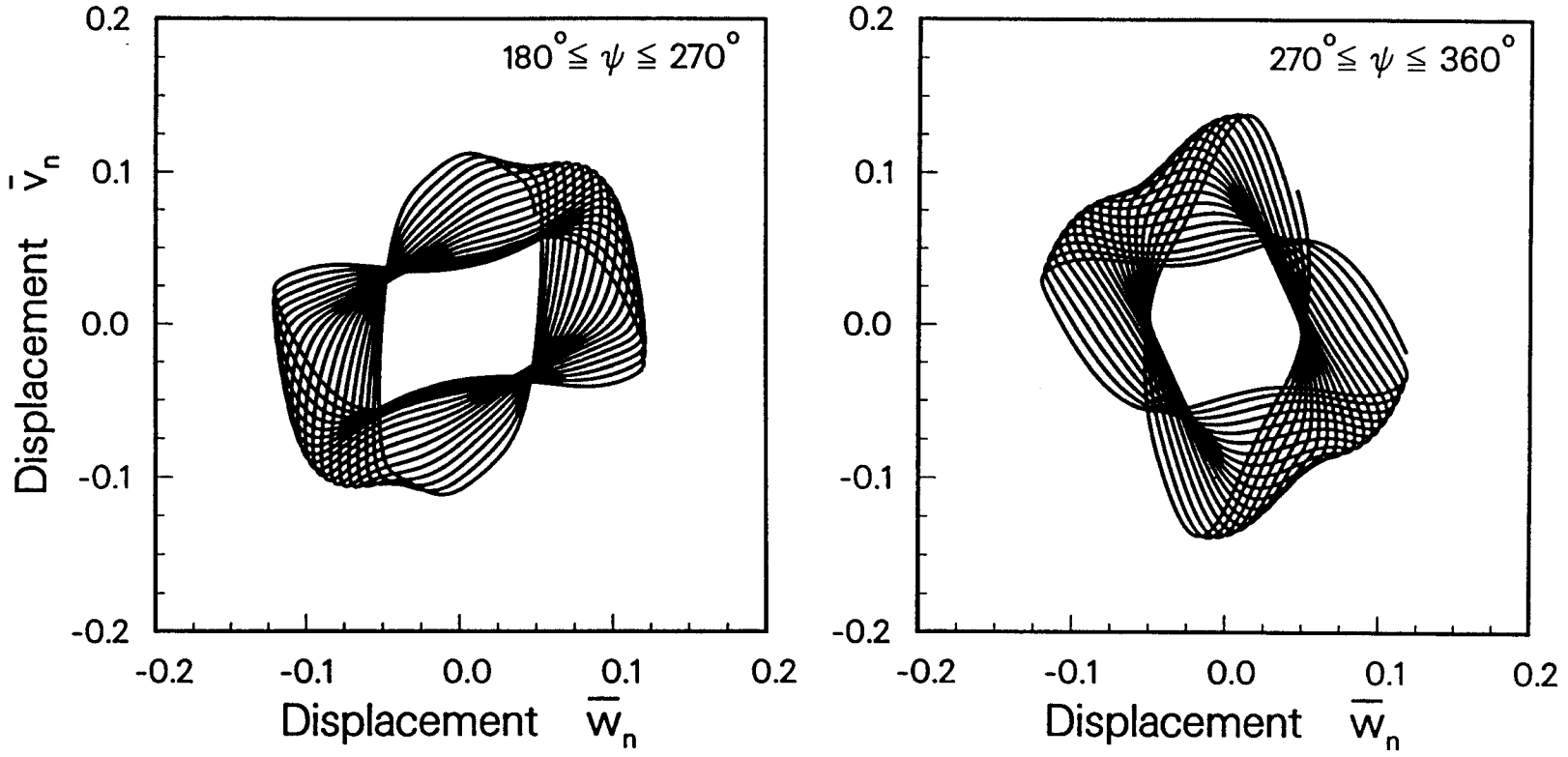

Fig. 6.6-5. Nonplanar Midspan Orbital Path for Single Shot Analysis for 180° ≤ ψ ≤ 270° and 270° ≤ ψ ≤ 360°. ($\bar{a}$ = 0.0, $\bar{c}$ = 10.00, Damping = 0%)

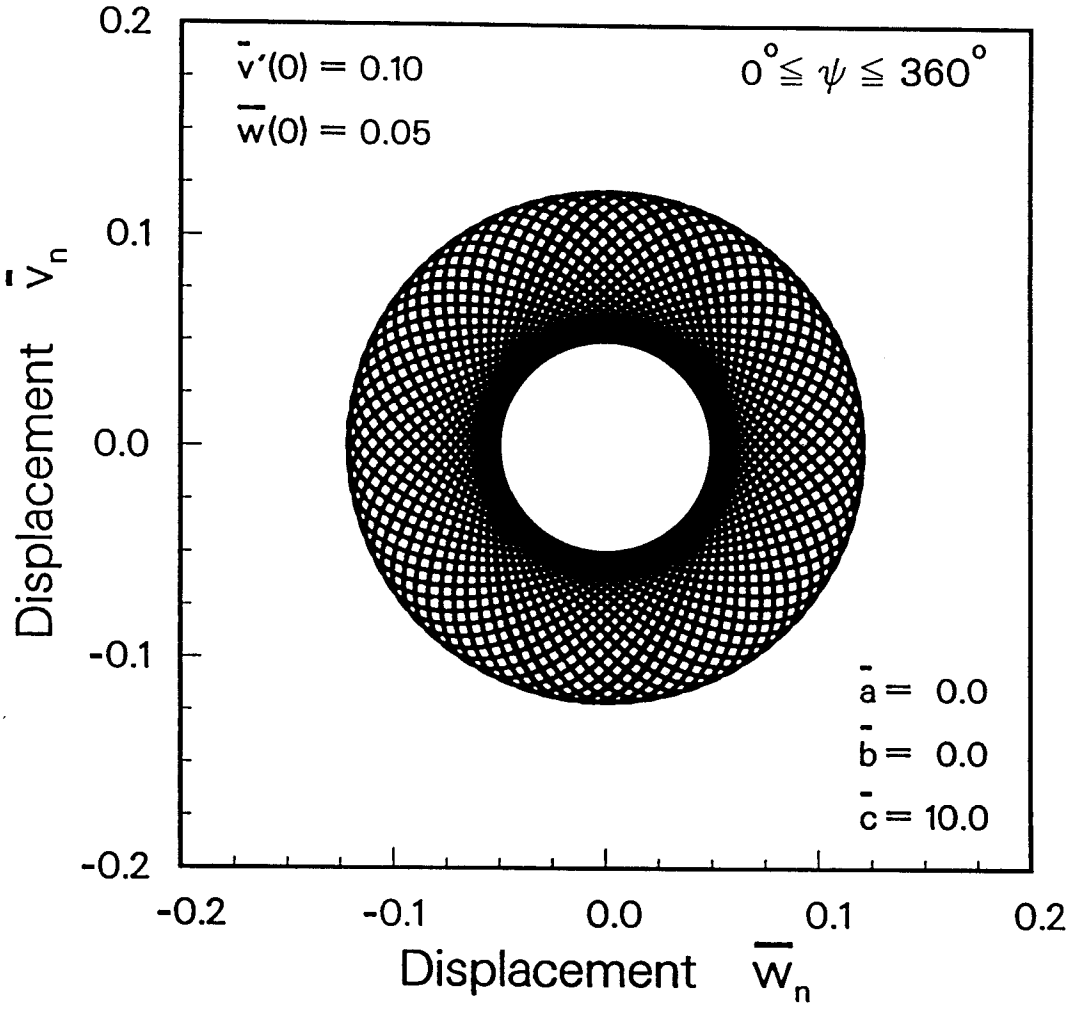

Fig. 6.6-6. Nonplanar Midspan Orbital Path for Single Shot Analysis with Fundamental Mode for $0° \leq \psi \leq 360°$. ($\bar{a} = 0.0$, $\bar{c} = 10.0$, Damping = 0%)

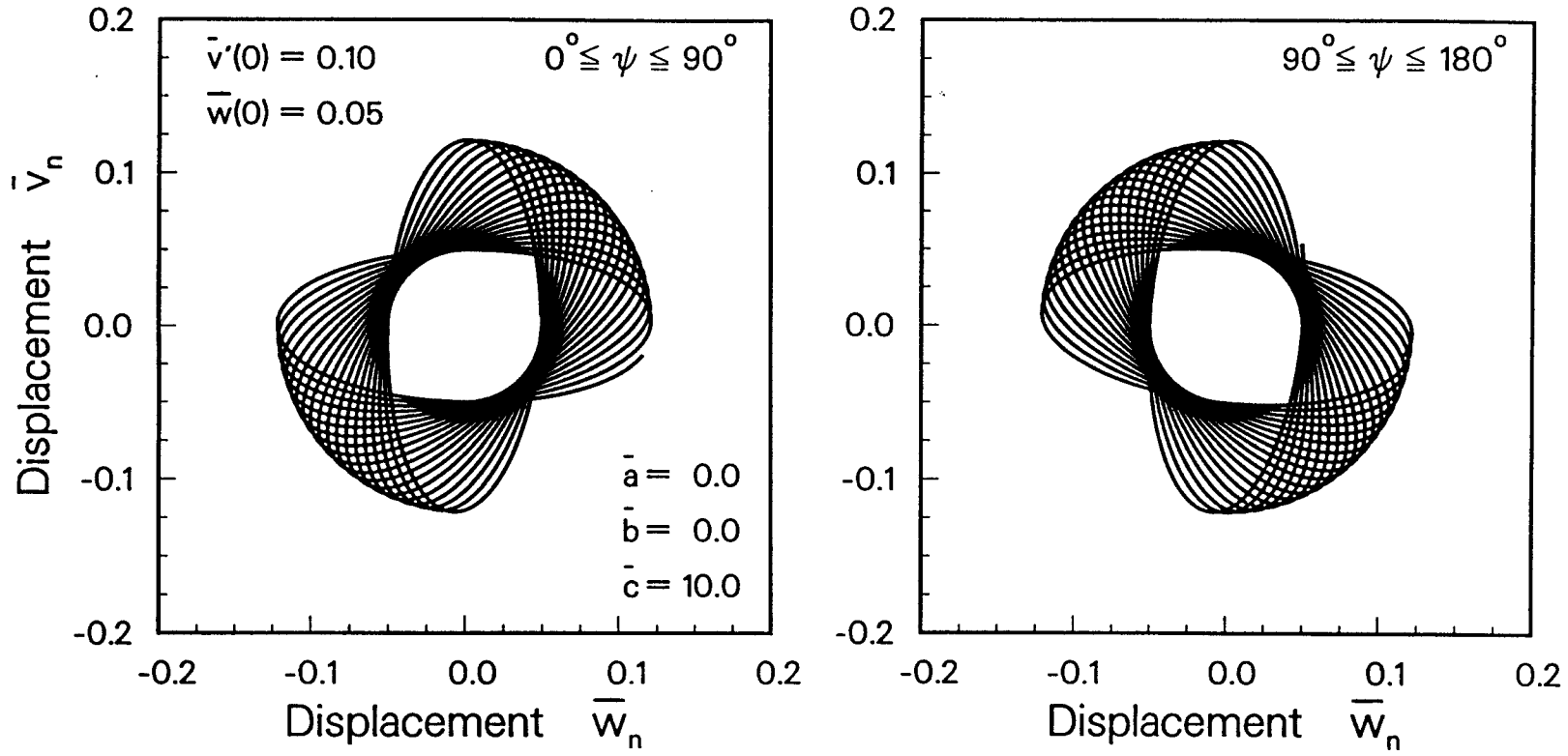

Fig. 6.6-7. Nonplanar Midspan Orbital Path for Single Shot Analysis with Fundamental Mode for $0° \leq \psi \leq 90°$ and $90° \leq \psi \leq 180°$. ($\bar{a} = 0.0$, $\bar{c} = 10.0$, Damping = 0%)

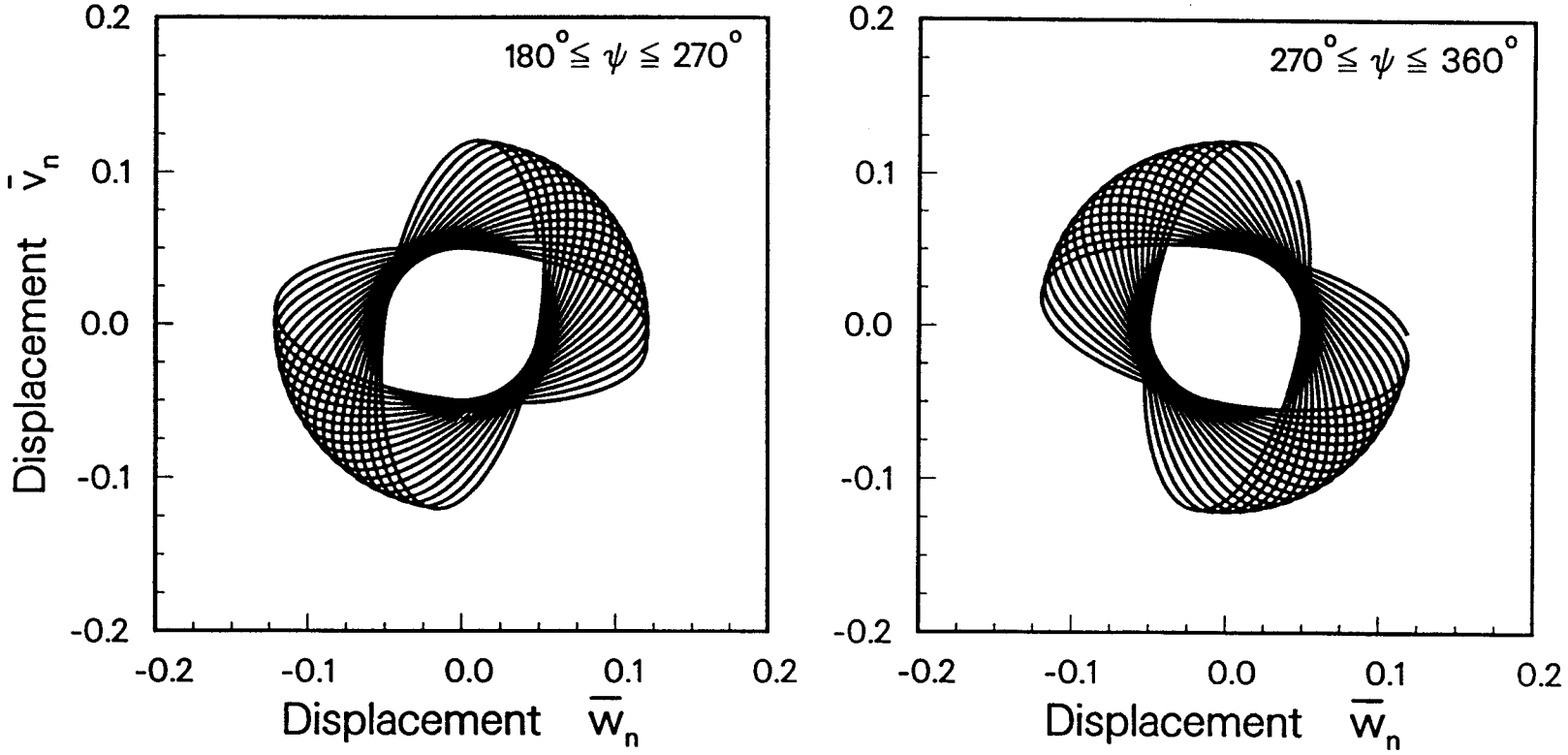

Fig. 6.6-8. Nonplanar Midspan Orbital Path for Single Shot Analysis with Fundamental Mode for $180° \leq \psi \leq 270°$ and $270° \leq \psi \leq 360°$. ($\bar{a}$ = 0.0, $\bar{c}$ = 10.0, Damping = 0%)

in agreement with investigations of the nonlinear, nonplanar free vibration of strings (Refs. [2.88] and [2.93]).

As a third example of the effect of the coupling coefficient $\bar{c}$, Fig. 6.6-9 shows the midspan displacement histories with $\bar{c}$ = 50.0. In this case, energy is readily exchanged between the $\bar{v}$ and $\bar{w}$ components and the precessional rate has been substantially increased. The corresponding orbital path is shown in Figs. 6.6-10 through 6.6-12. Overall, amplitudes are slightly less than for $\bar{c}$ = 10.0 but the envelopes of the orbital path are basically the same.

The nonplanar free vibration cases described thus far have not included damping. With the planar analysis in Sections 6.4 and 6.5, four damping levels were considered, i.e., 2, 5, 10, and 20%. In Figs. 6.6-13 and 6.6-14 the nonplanar orbital response is shown for these four damping values. With 2% damping it is evident that the orbital motion begins to precess before it damps out. For the other cases the precessional motion is not as evident because of the higher damping.

Finally, the effect of the Coriolis acceleration of the fluid is addressed considering the case where $\bar{c}$ = 50.0. The Coriolis coefficient $\bar{a}$ is increased in small increments (1.0, 2.0, 3.0) and the midspan displacement histories and orbital paths are shown for each in Figs. 6.6-15 through 6.6-20. In general, for the examples shown, it can be seen that as $\bar{a}$ increases, the displacement amplitudes tend to decrease and the rate at which the orbital motion precesses

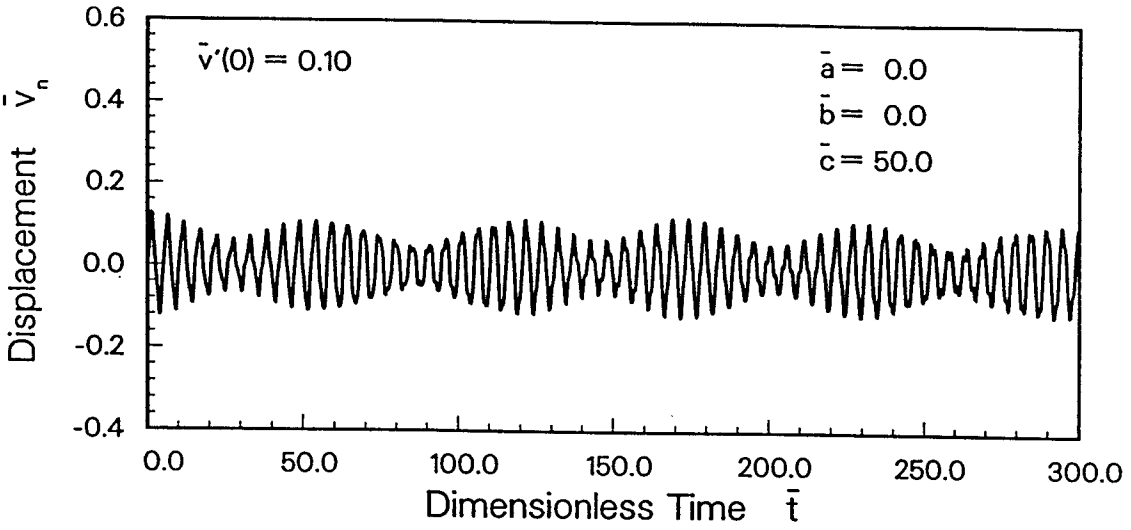

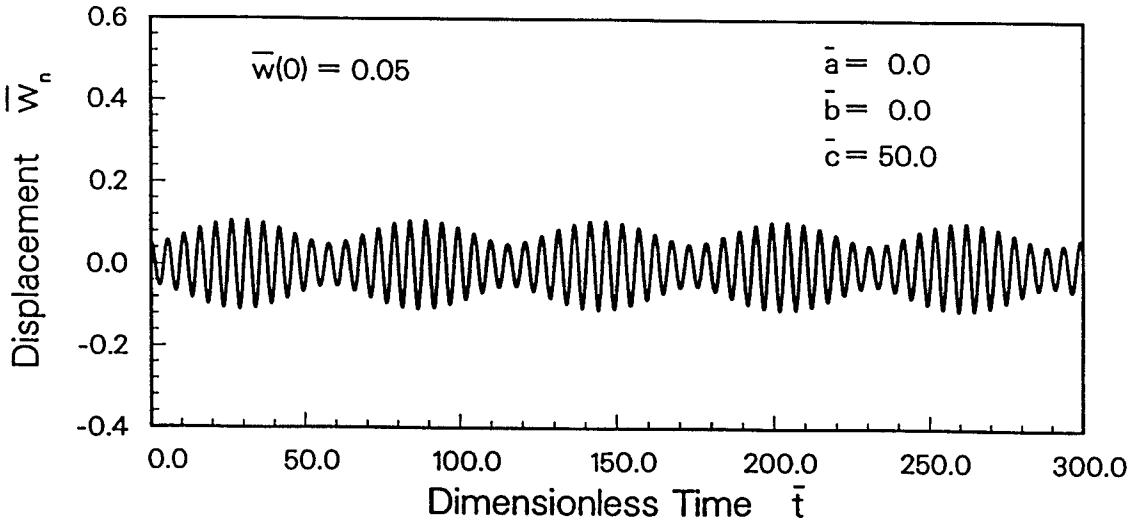

Fig. 6.6-9 Nonplanar Midspan Displacement Histories for Single Shot Analysis. ($\bar{a}$ = 0.0, $\bar{c}$ = 50.0, Damping = 0%)

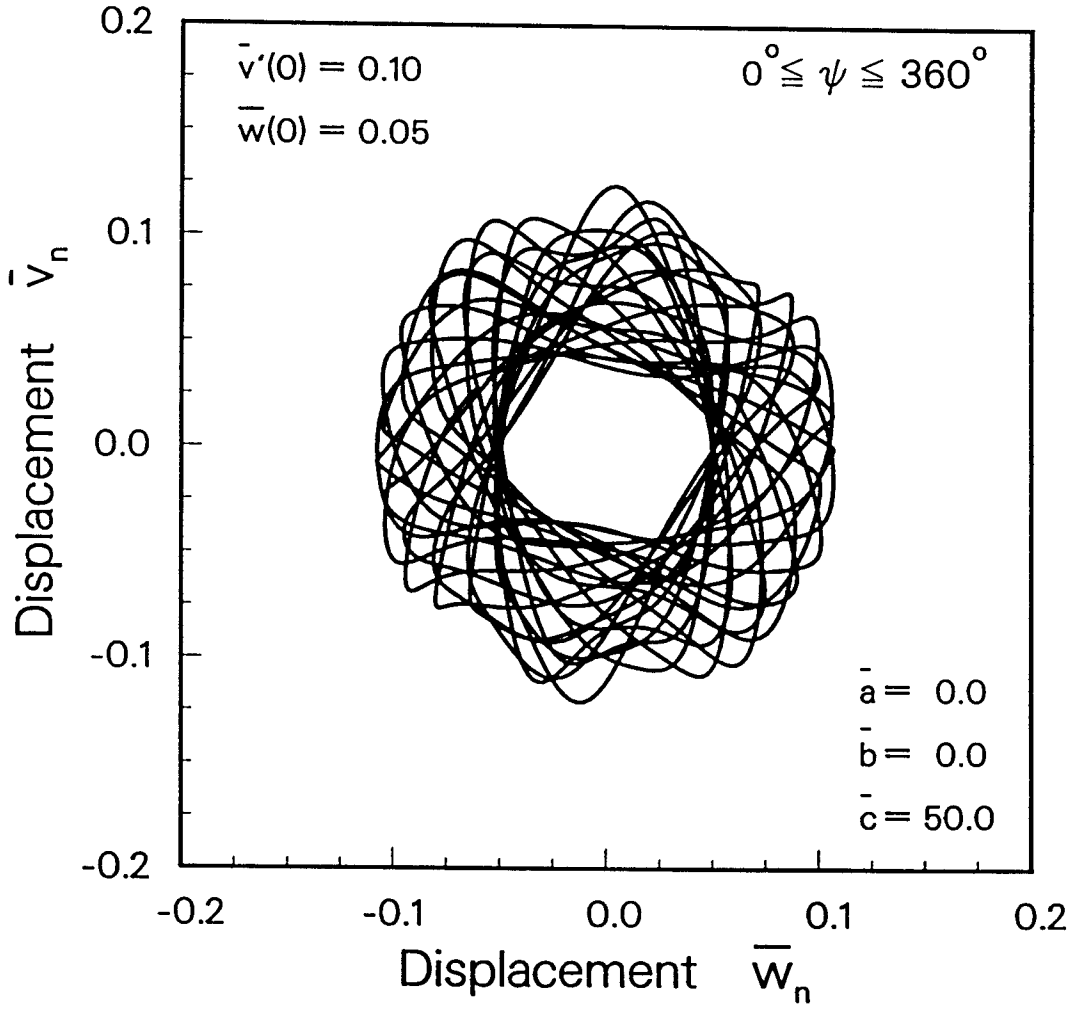

Fig. 6.6-10. Nonplanar Midspan Orbital Path for Single Shot Analysis for $0° \leq \psi \leq 360°$. ($\bar{a} = 0.0$, $\bar{c} = 50.0$, Damping = 0%)

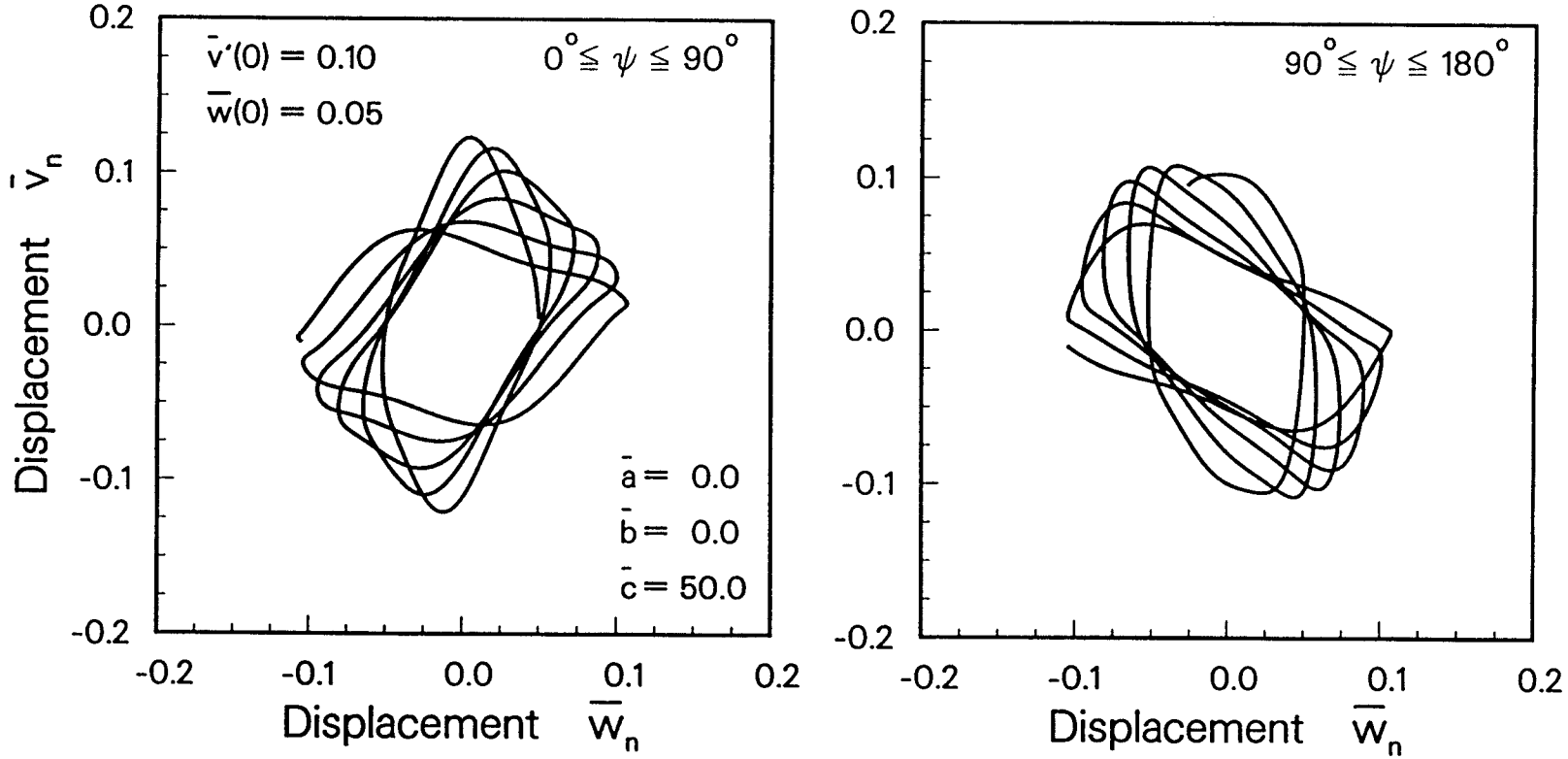

Fig. 6.6-11. Nonplanar Midspan Orbital Path for Single Shot Analysis for $0° \leq \psi \leq 90°$ and $90° \leq \psi \leq 180°$. ($\bar{a} = 0.0$, $\bar{c} = 50.0$, Damping = 0%)

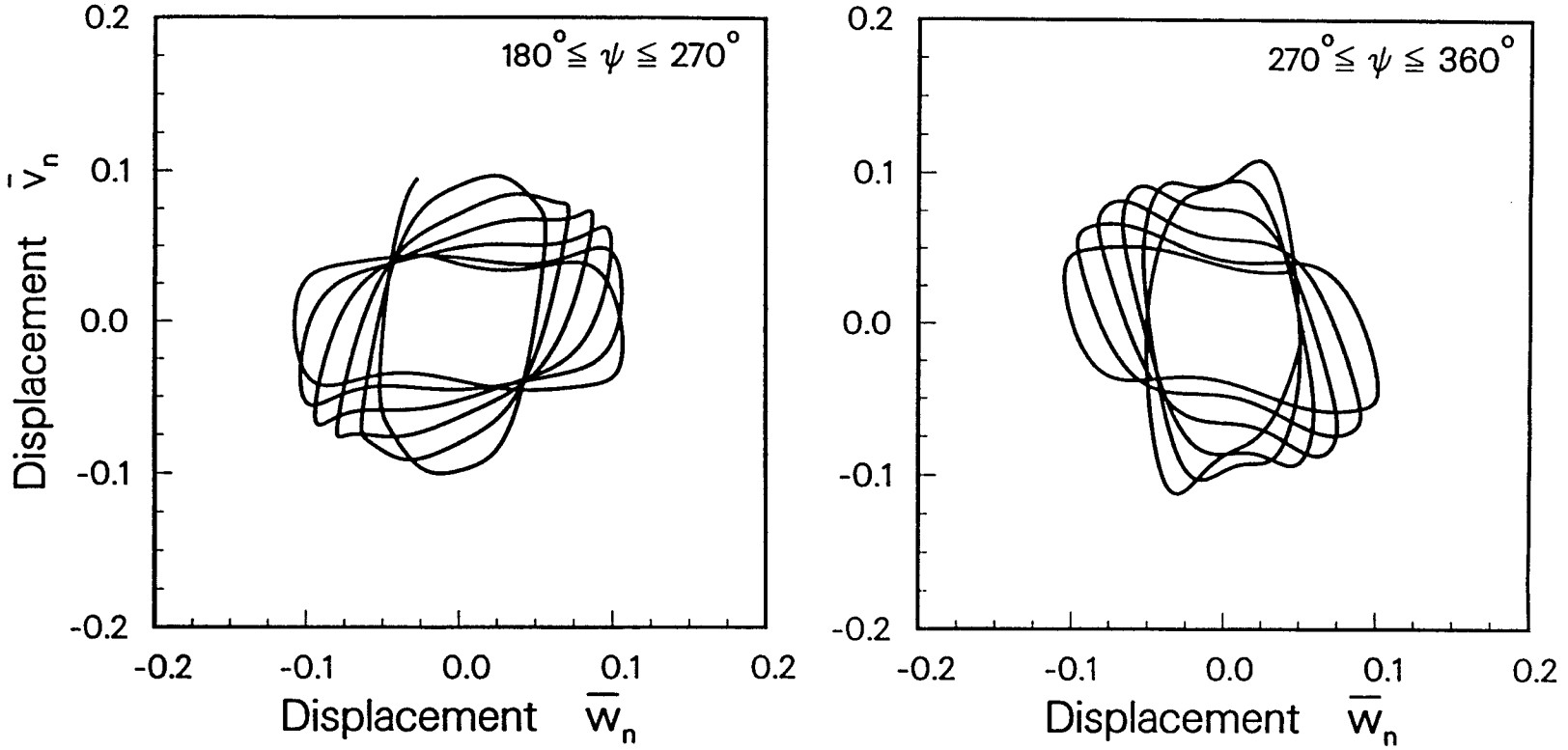

Fig. 6.6-12. Nonplanar Midspan Orbital Path for Single Shot Analysis for 180° ≤ ψ ≤ 270° and 270° ≤ ψ ≤ 360°. ($\bar{a}$ = 0.0, $\bar{c}$ = 50.0, Damping = 0%)

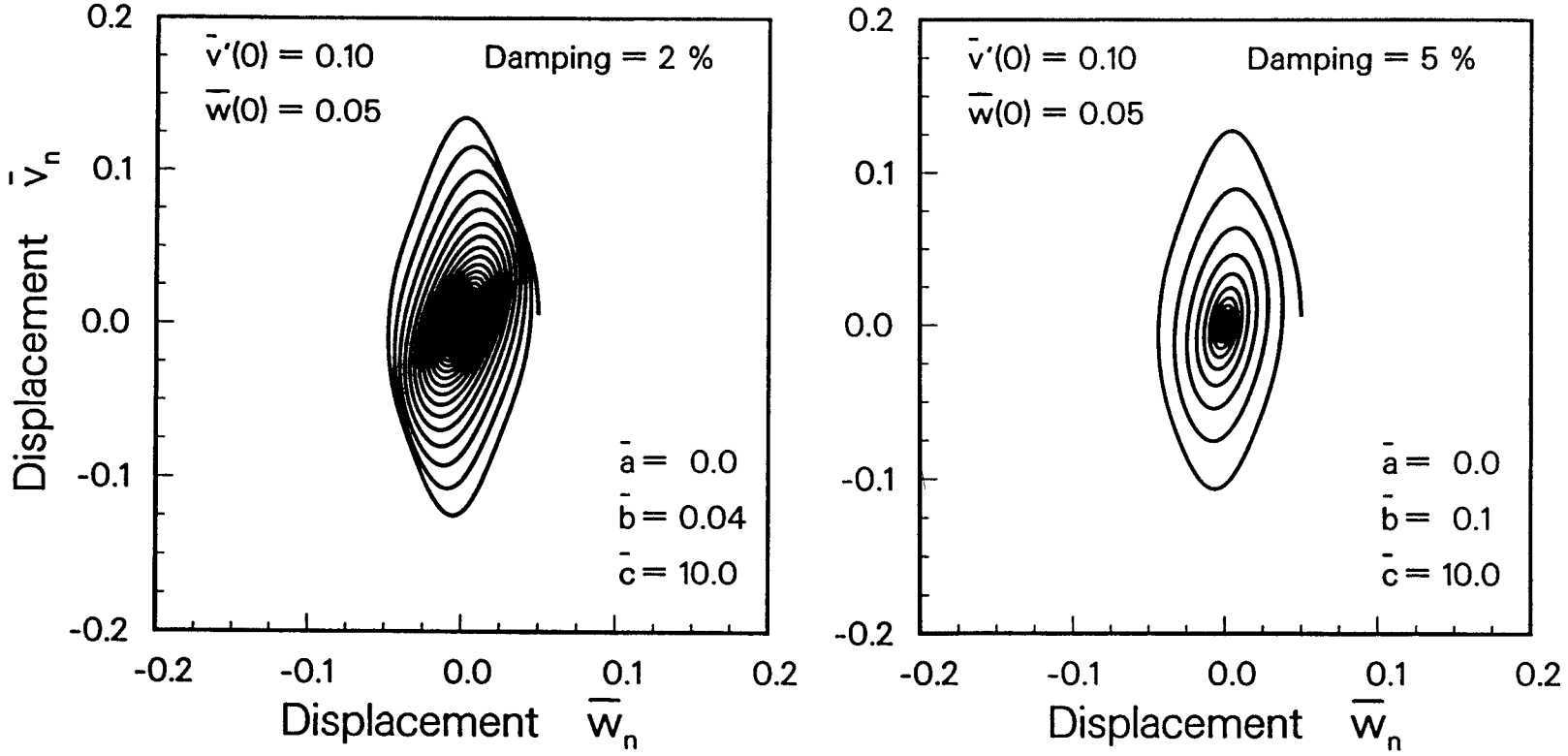

Fig. 6.6-13. Nonplanar Midspan Orbital Path for Single Shot Analysis for 2% and 5% Damping. ($\bar{a}$ = 0.0, $\bar{c}$ = 10.0)

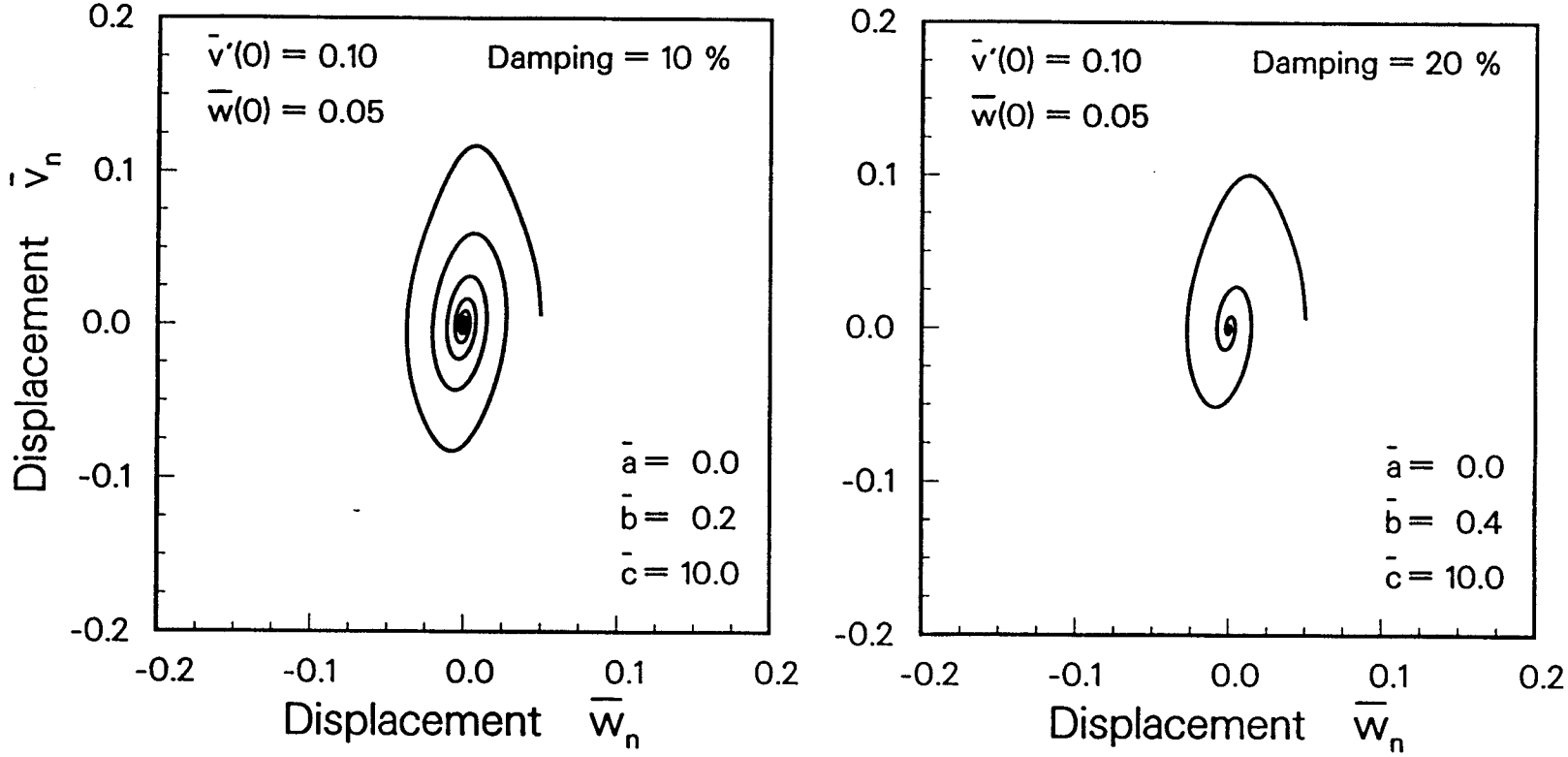

Fig. 6.6-14. Nonplanar Midspan Orbital Path for Single Shot Analysis for 10% and 20% Damping. ($\bar{a}$ = 0.0, $\bar{c}$ = 10.0)

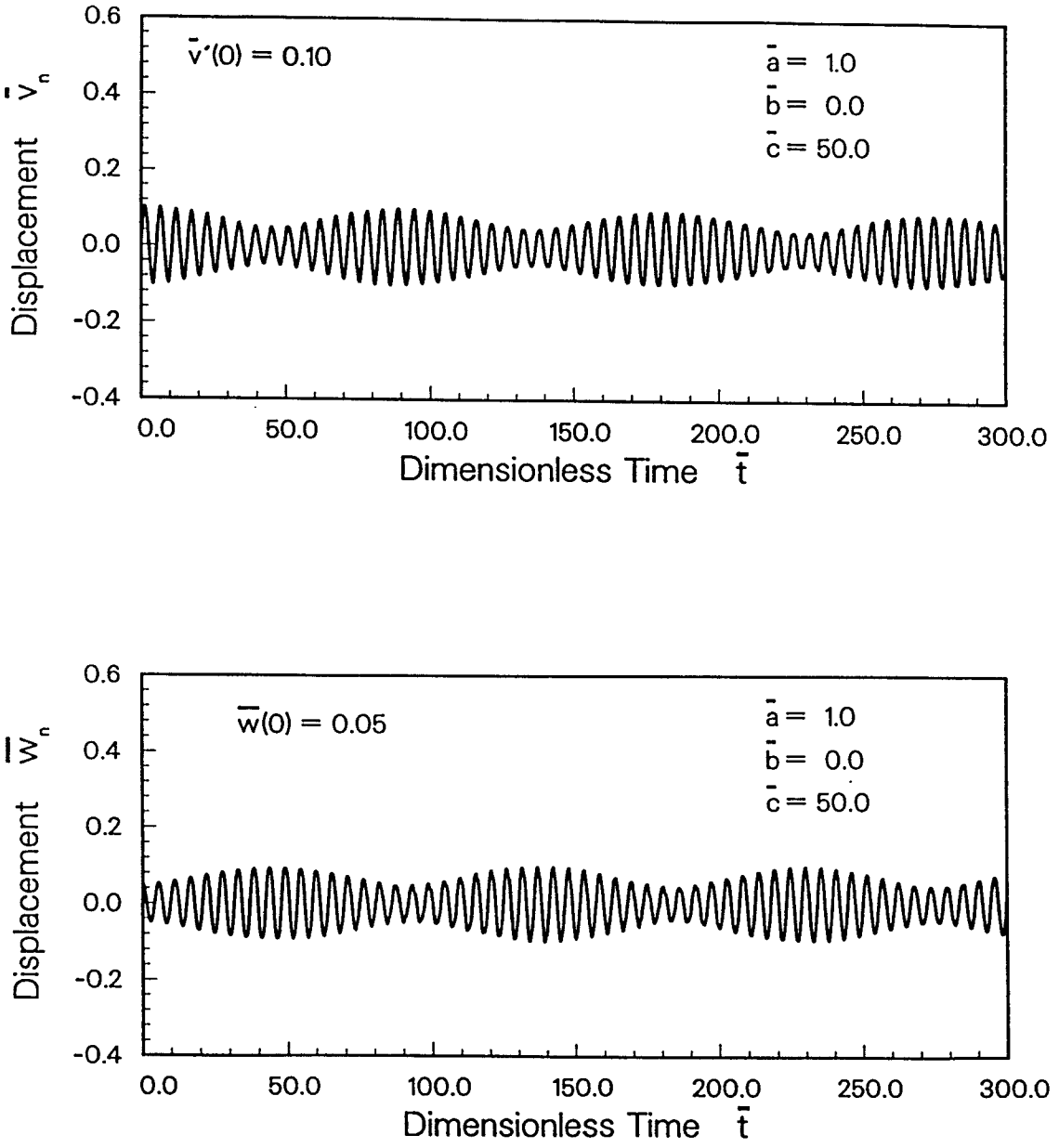

Fig. 6.6-15. Nonplanar Midspan Displacement Histories for Single Shot Analysis. ($\bar{a}$ = 1.0, $\bar{c}$ = 50.0, Damping = 0%)

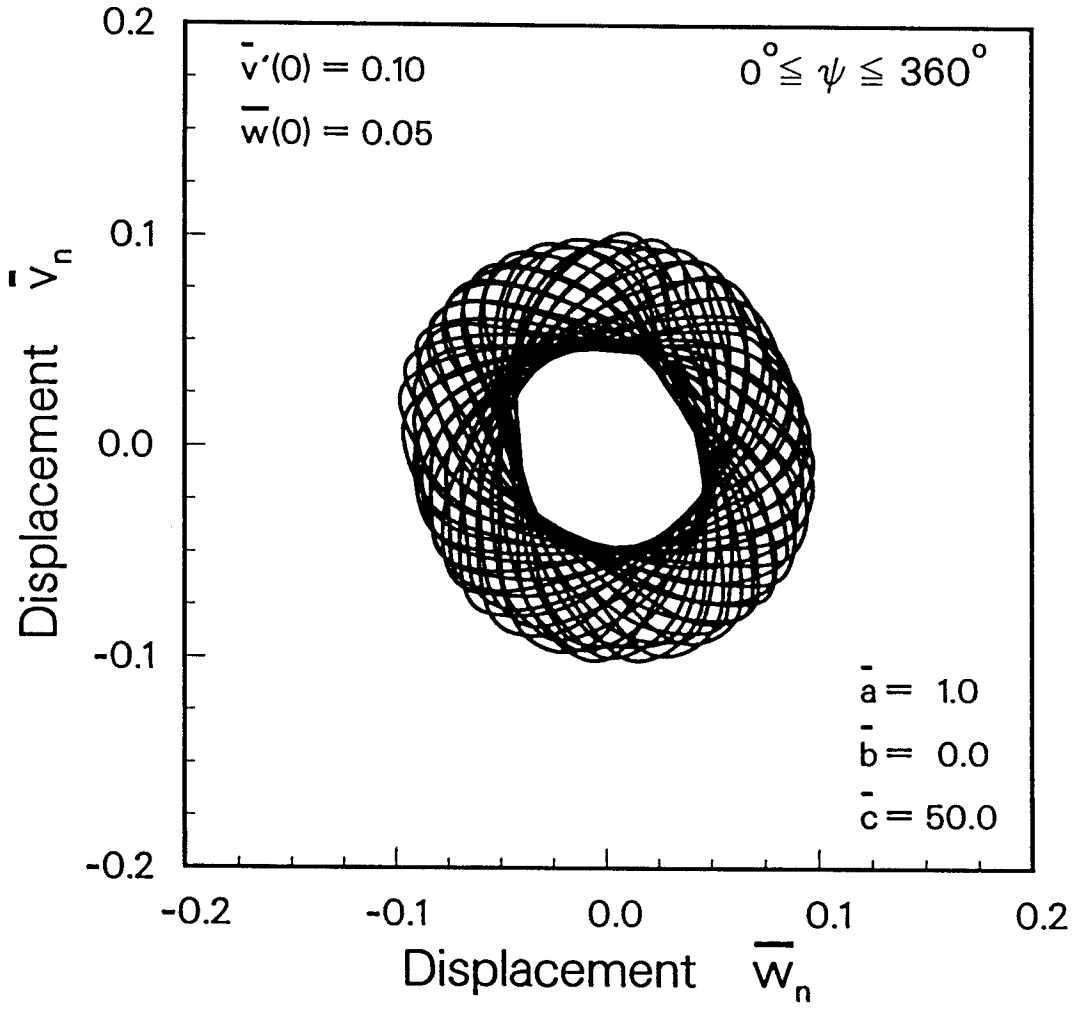

Fig. 6.6-16. Nonplanar Midspan Orbital Path for Single Shot Analysis for $0° \leq \psi \leq 360°$. ($\bar{a}$ = 1.0, $\bar{c}$ = 50.0, Damping = 0%)

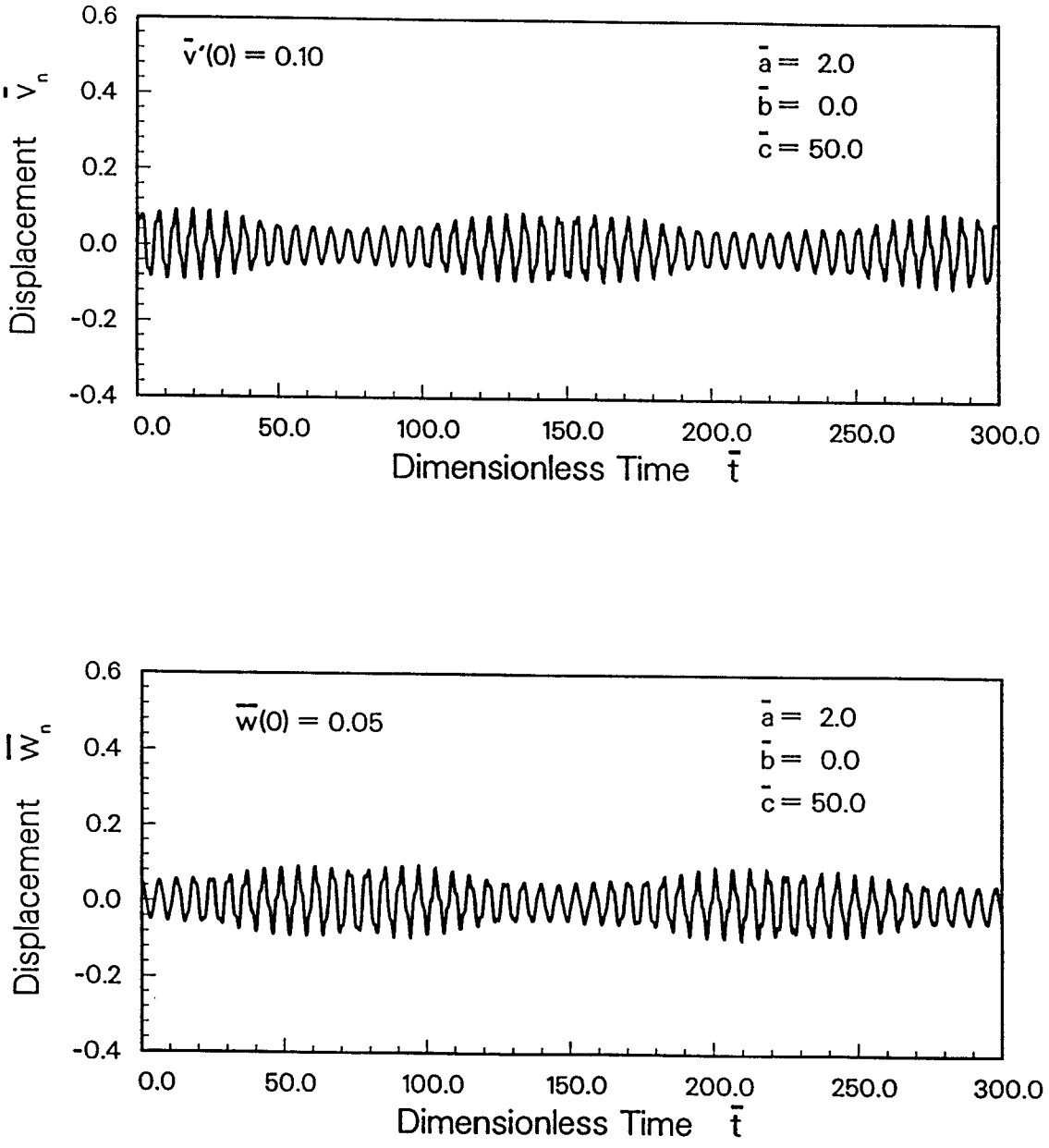

Fig. 6.6-17. Nonplanar Midspan Displacement Histories for Single Shot Analysis. ($\bar{a}$ = 2.0, $\bar{c}$ = 50.0, Damping = 0%)

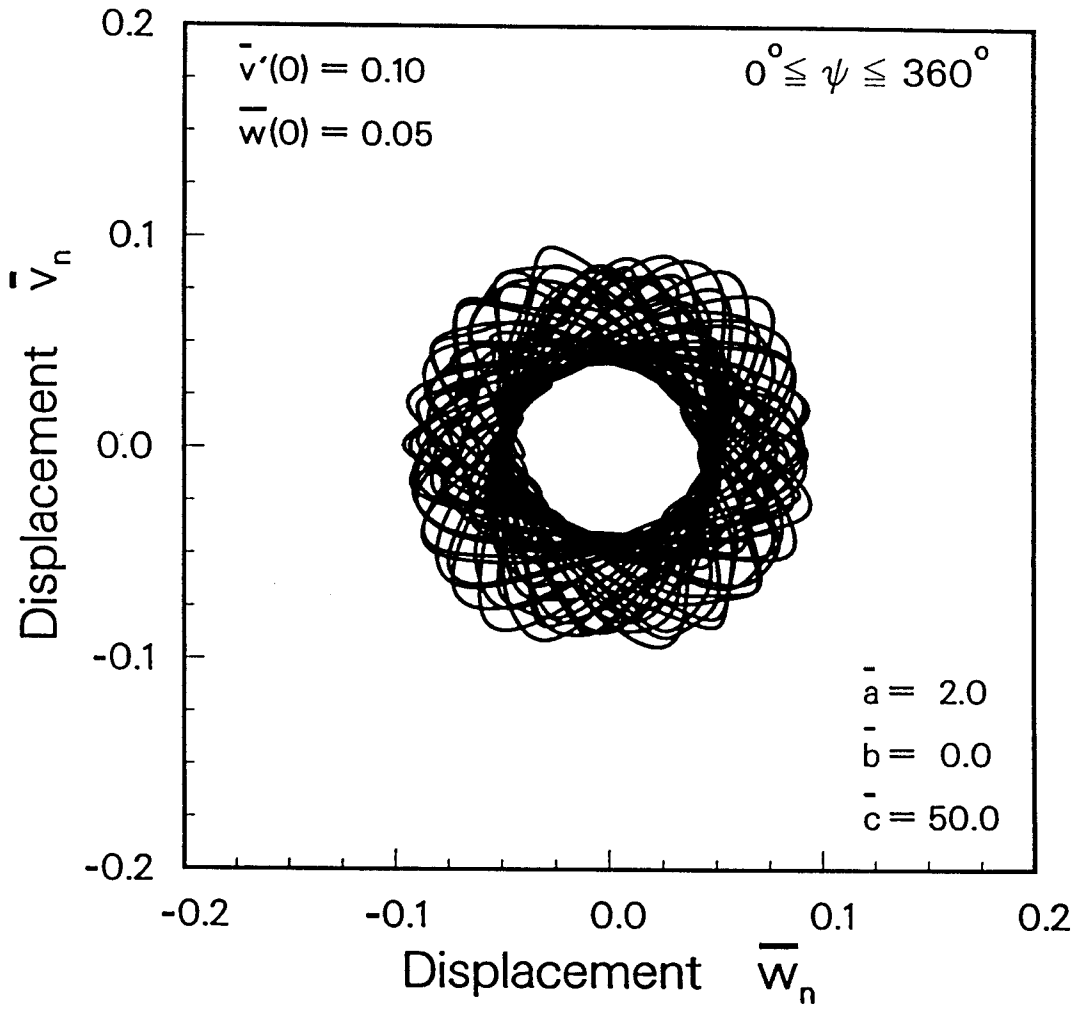

Fig. 6.6-18. Nonplanar Midspan Orbital Path for Single Shot Analysis for $0° \leq \psi \leq 360°$. ($\bar{a} = 2.0$, $\bar{c} = 50.0$, Damping = 0%)

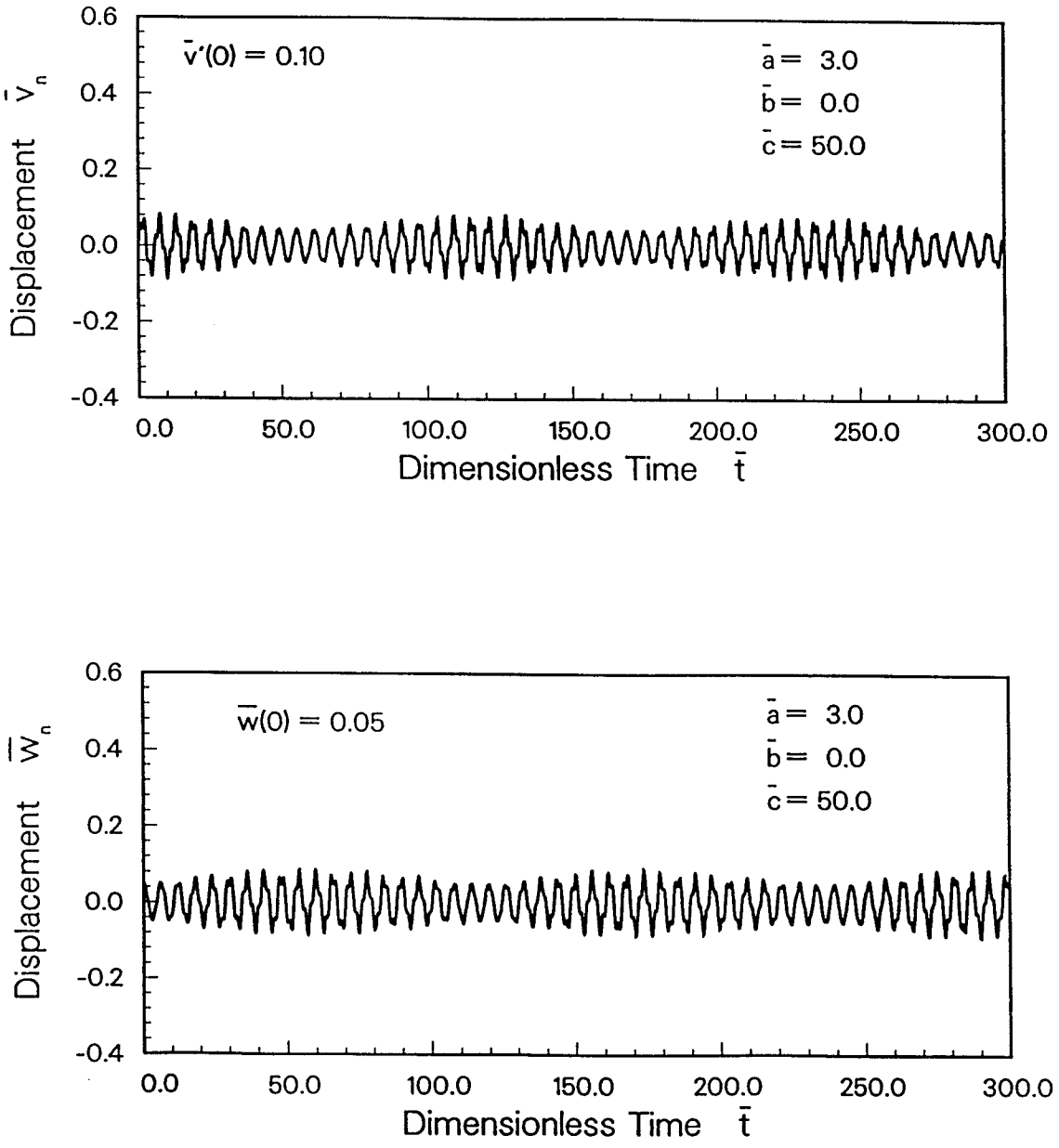

Fig. 6.6-19. Nonplanar Midspan Displacement Histories for Single Shot Analysis. ($\bar{a}$ = 3.0, $\bar{c}$ = 50.0, Damping = 0%)

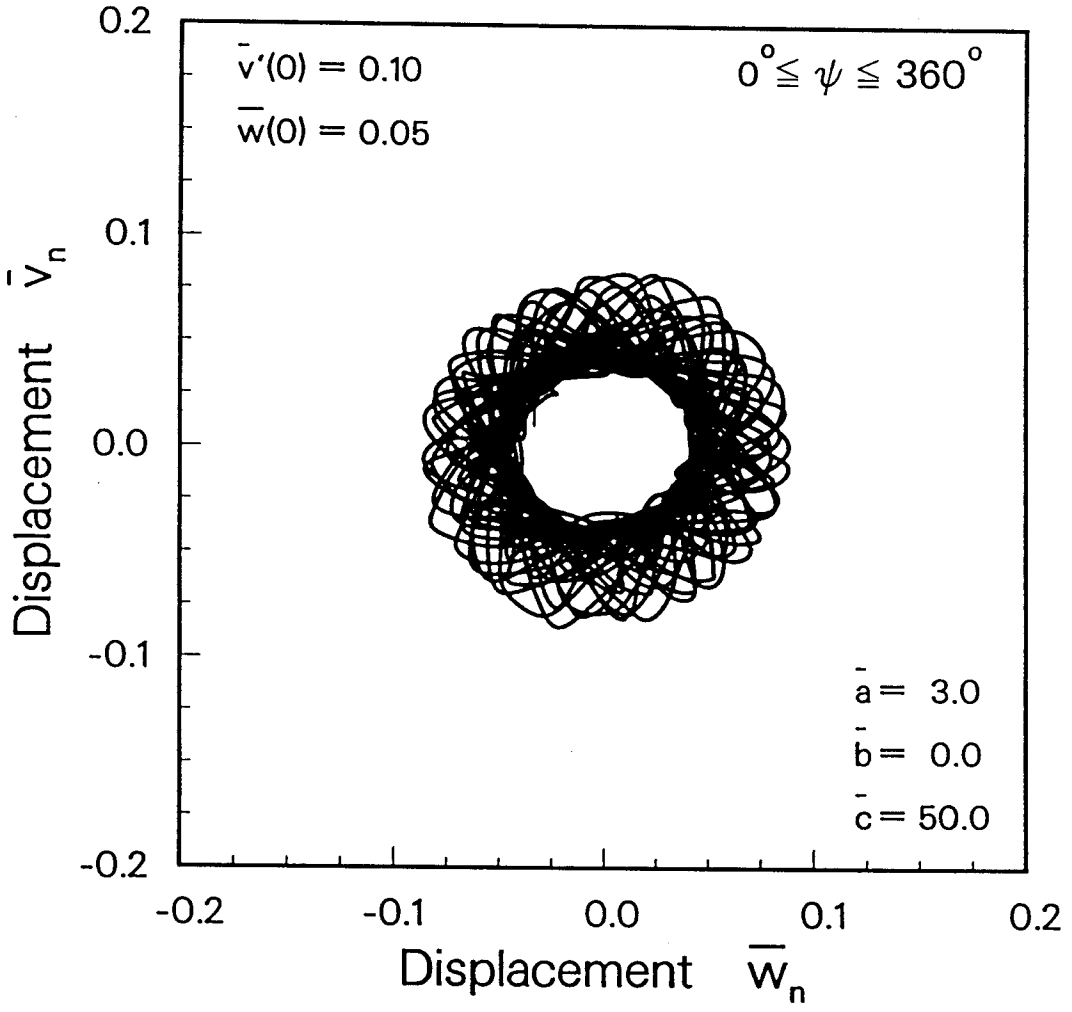

Fig. 6.6-20. Nonplanar Midspan Orbital Path for Single Shot Analysis for $0° \leq \psi \leq 360°$. ($\bar{a} = 3.0$, $\bar{c} = 50.0$, Damping = 0%)

decreases. Also, when $\bar{a}$ is present both even and odd modes contribute to the response, resulting in a more irregular orbital path. This is more obvious in Fig. 6.6-20 where $\bar{c}$ = 3.0.

To simulate the actual loading conditions from an ICF reactor, the nonplanar response code was expanded to include sequential impulses, or multiple shots. All calculations were done assuming damping was present. In order to compare with the calculations done in the planar analysis, a damping level of 2% was used along with $\bar{c}$ = 10.0 and $\bar{v}'(0) = 0.10$.

Three specific Rep Rates or impulse periods, $\bar{t}_{imp}$, were considered. With $\bar{t}_{imp}$ = 3.0 and the Coriolis acceleration coefficient set to zero, the midspan displacement histories have been plotted for approximately 80 shots (Fig. 6.6-21). As was done for the free vibration analysis, an initial displacement of $\bar{w}(0) = 0.05$ was applied to initiate the nonplanar motion. However, from Fig. 6.6-21 it can be seen that the out-of-plane displacement eventually damps out and the steady-state displacement consists of the in-plane component ($\bar{v}$) only. Figure 6.6-22 shows the corresponding "start-up" and steady state orbital motions. It should be noted that the maximum amplitude of $\bar{v}$ during steady state motion agrees with the planar analysis (Fig. 6.5-2). For a larger value of $\bar{t}_{imp}$, however, the response of the tube is no longer planar. Figures 6.6-23 and 6.6-24 show the whirling motion associated with an impulsive pressure applied every 5 units of dimensionless time. Finally, at $\bar{t}_{imp}$ = 7.0 the response

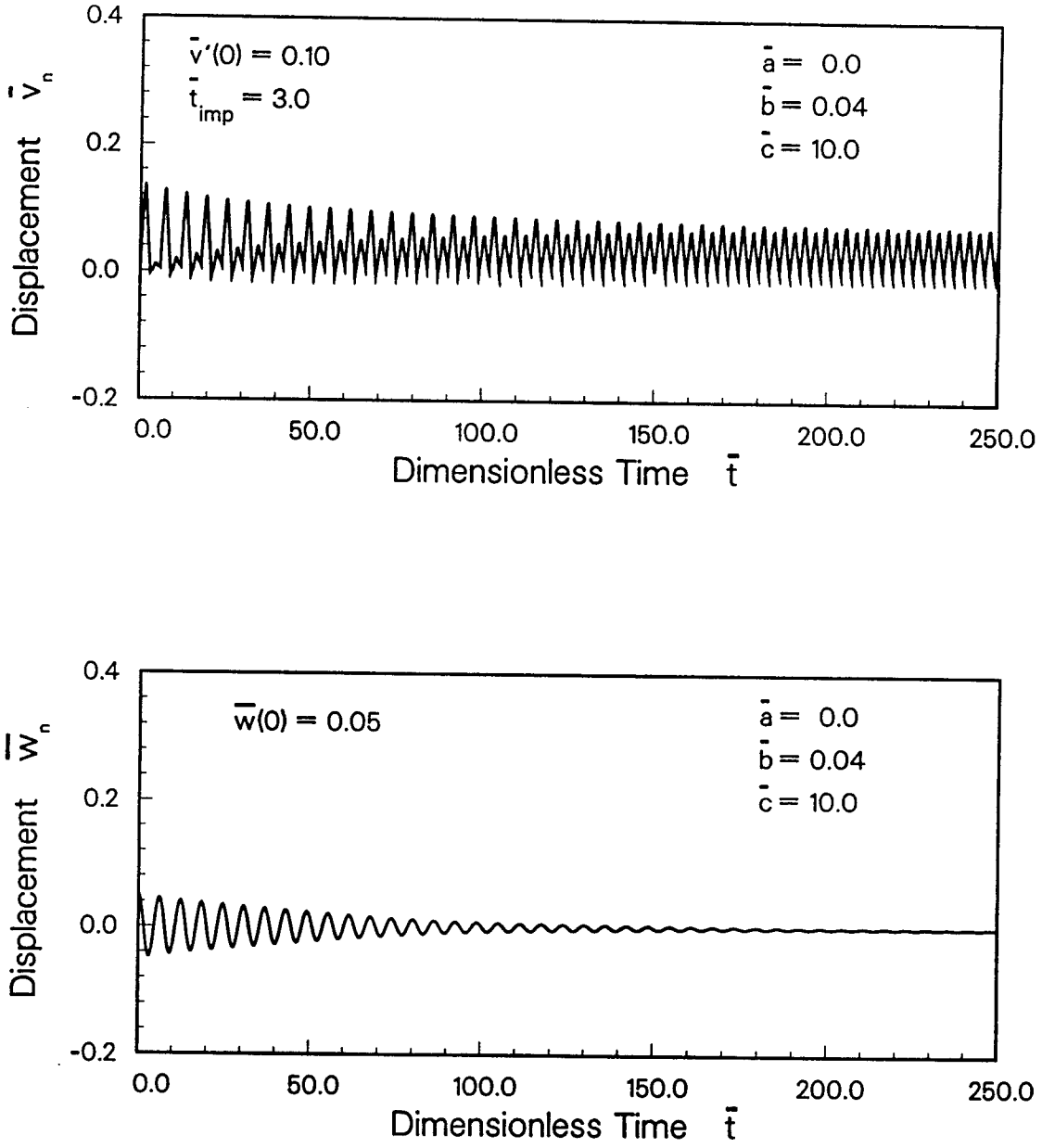

Fig. 6.6-21. Nonplanar Midspan Displacement Histories for Multiple Shot Analysis. ($\bar{a}$ = 0.0, $\bar{c}$ = 10.0, $\bar{t}_{imp}$ = 3.0, Damping = 2%)

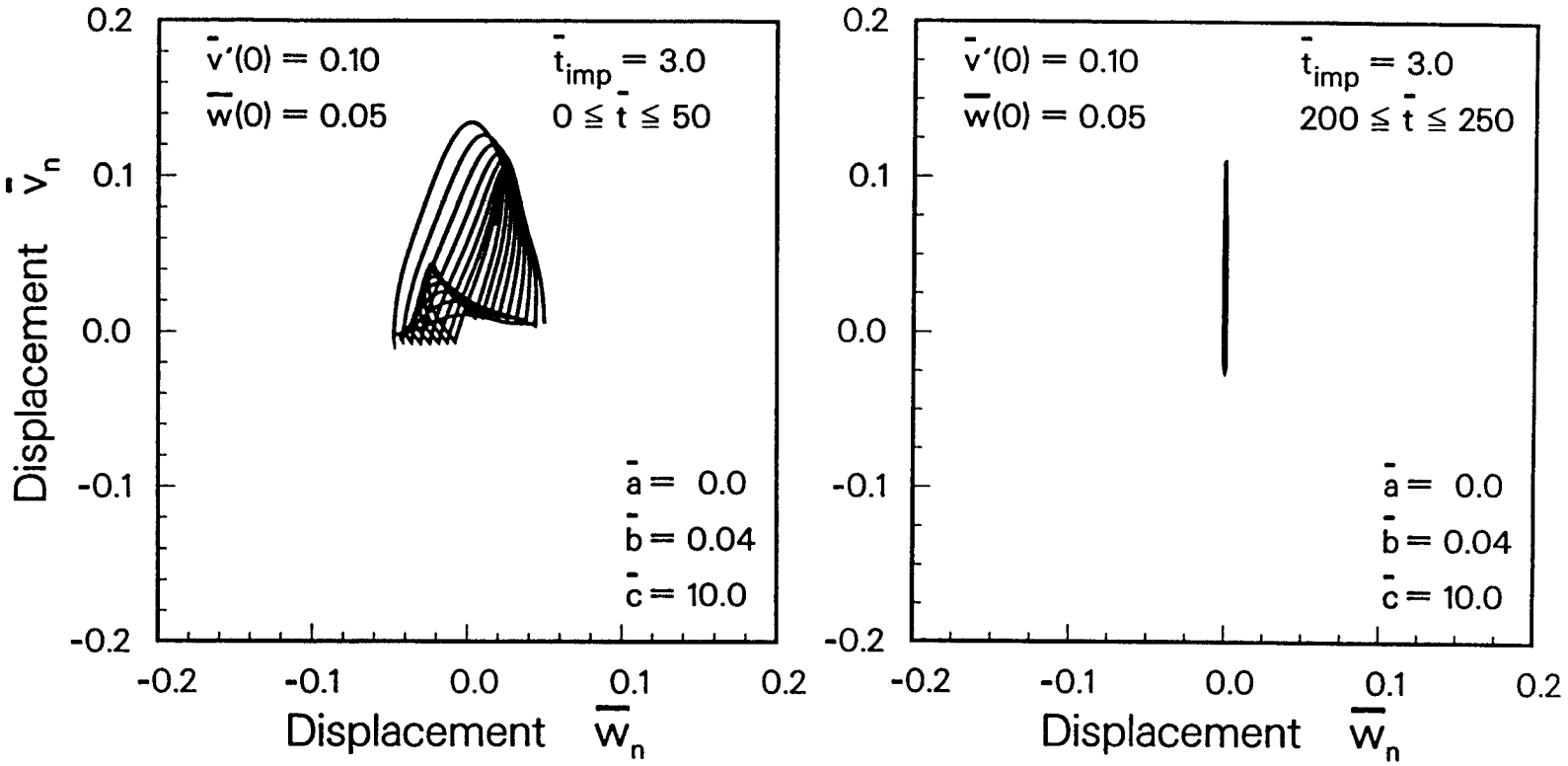

Fig. 6.6-22. Nonplanar Midspan Orbital Path for Multiple Shot Analysis. ($\bar{a}$ = 0.0, $\bar{c}$ = 10.0, $\bar{t}_{imp}$ = 3.0, Damping = 2%)

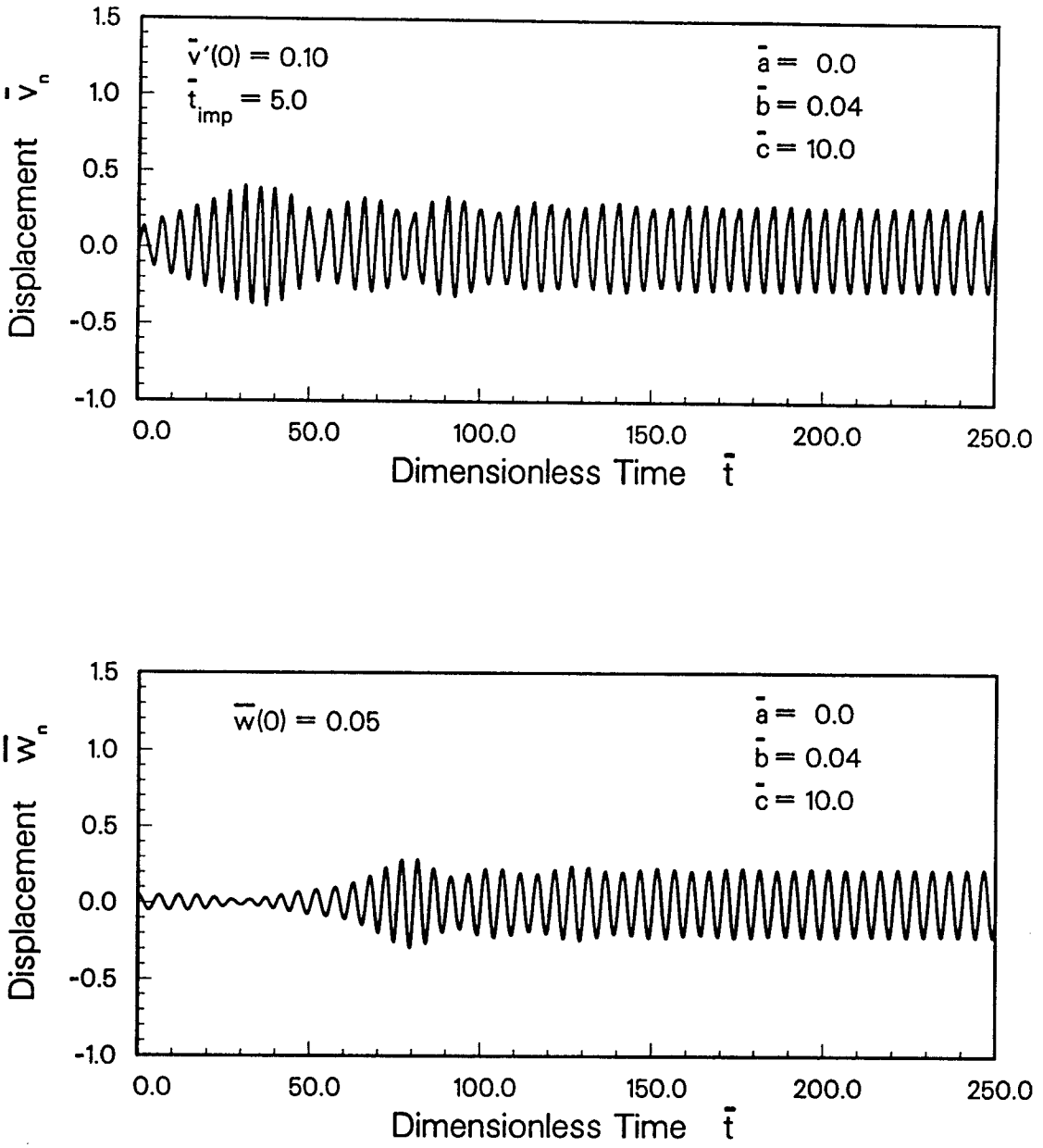

Fig. 6.6-23. Nonplanar Midspan Displacement Histories for Multiple Shot Analysis. ($\bar{a}$ = 0.0, $\bar{c}$ = 10.0, $\bar{t}_{imp}$ = 5.0, Damping = 2%)

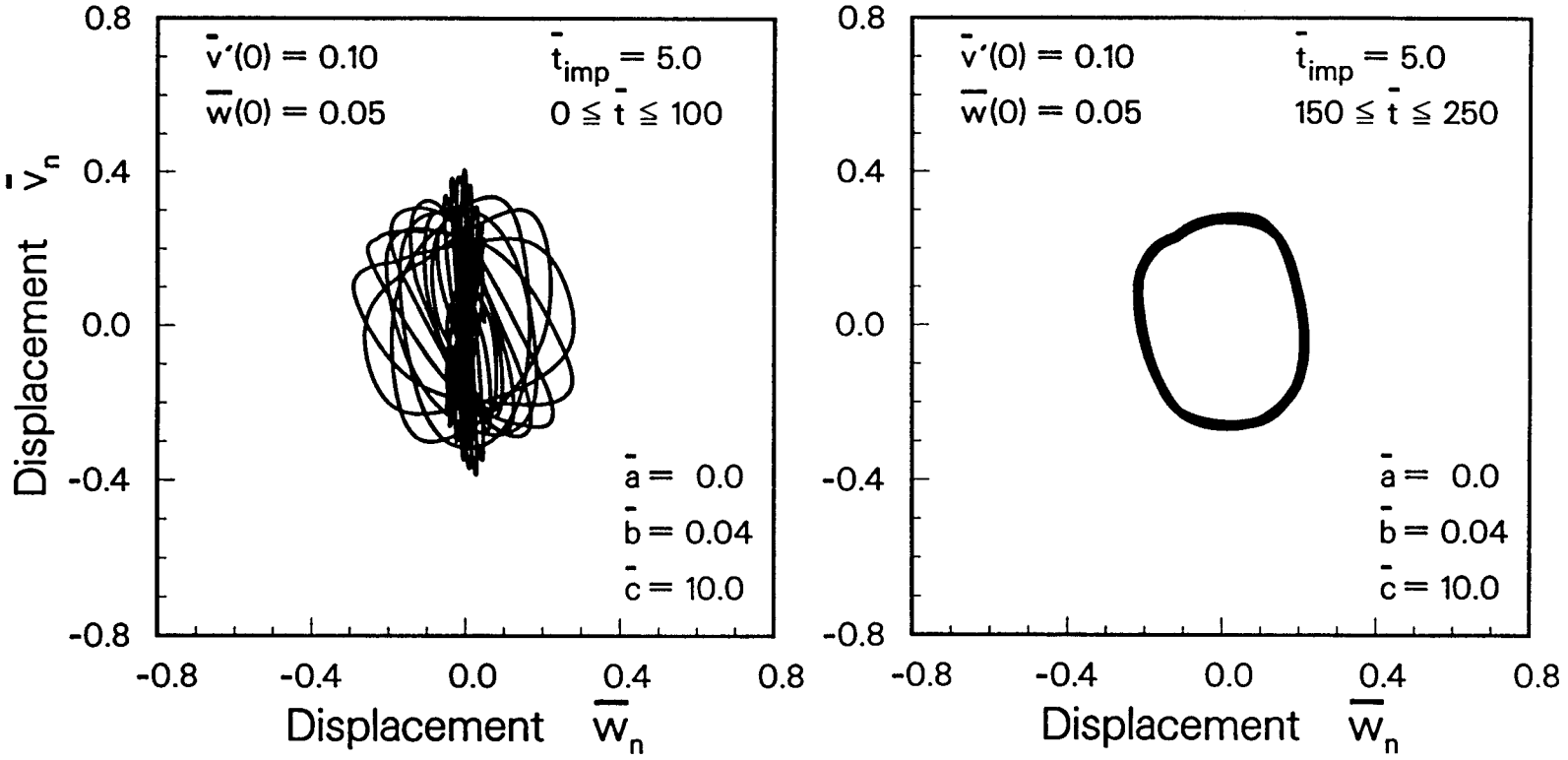

Fig. 6.6-24. Nonplanar Midspan Orbital Path for Multiple Shot Analysis. ($\bar{a}$ = 0.0, $\bar{c}$ = 10.0, $\bar{t}_{imp}$ = 5.0, Damping = 2%)

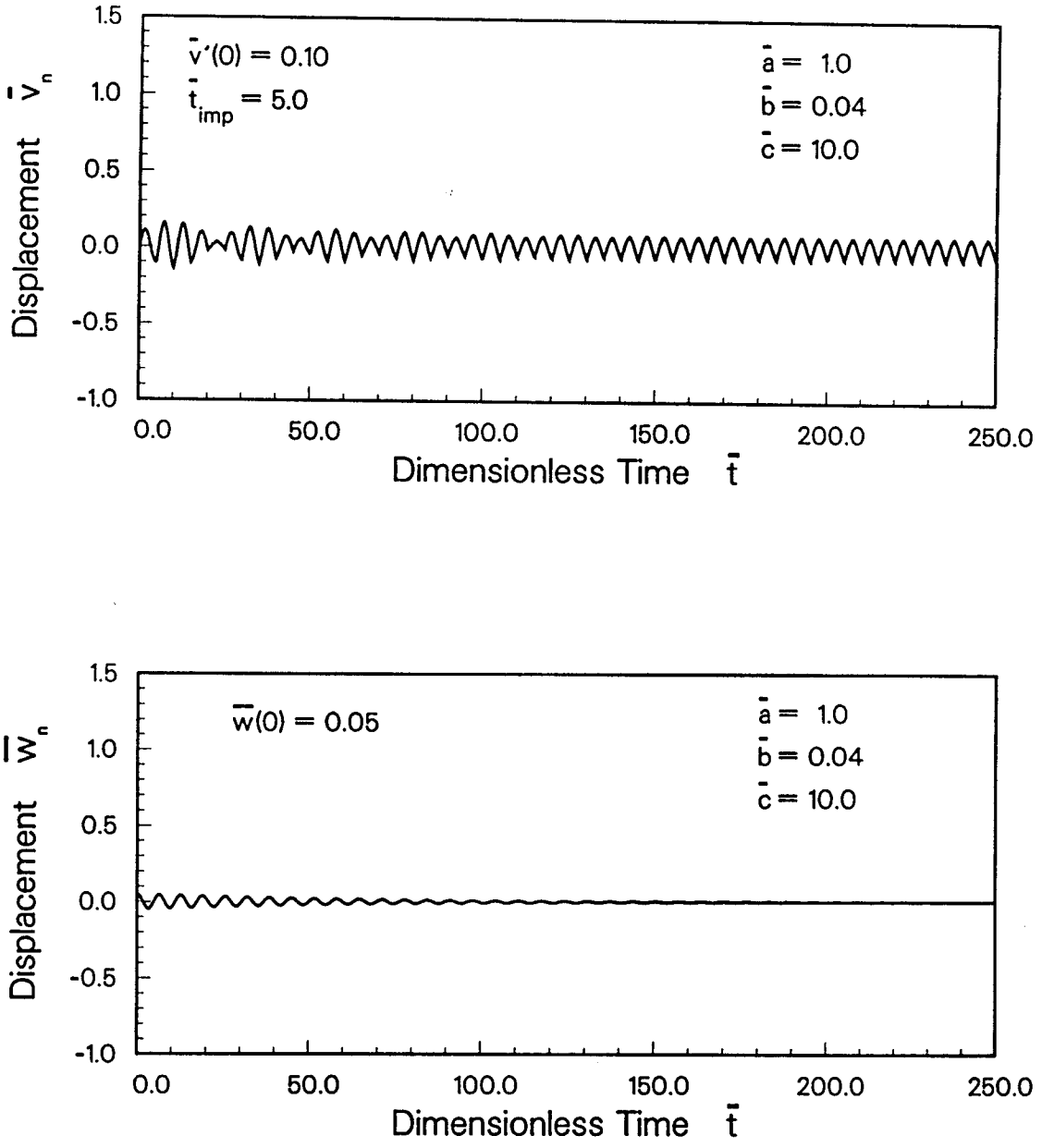

Fig. 6.6-25. Nonplanar Midspan Displacement Histories for Multiple Shot Analysis. ($\bar{a}$ = 0.0, $\bar{c}$ = 10.0, $\bar{t}_{imp}$ = 7.0, Damping = 2%)

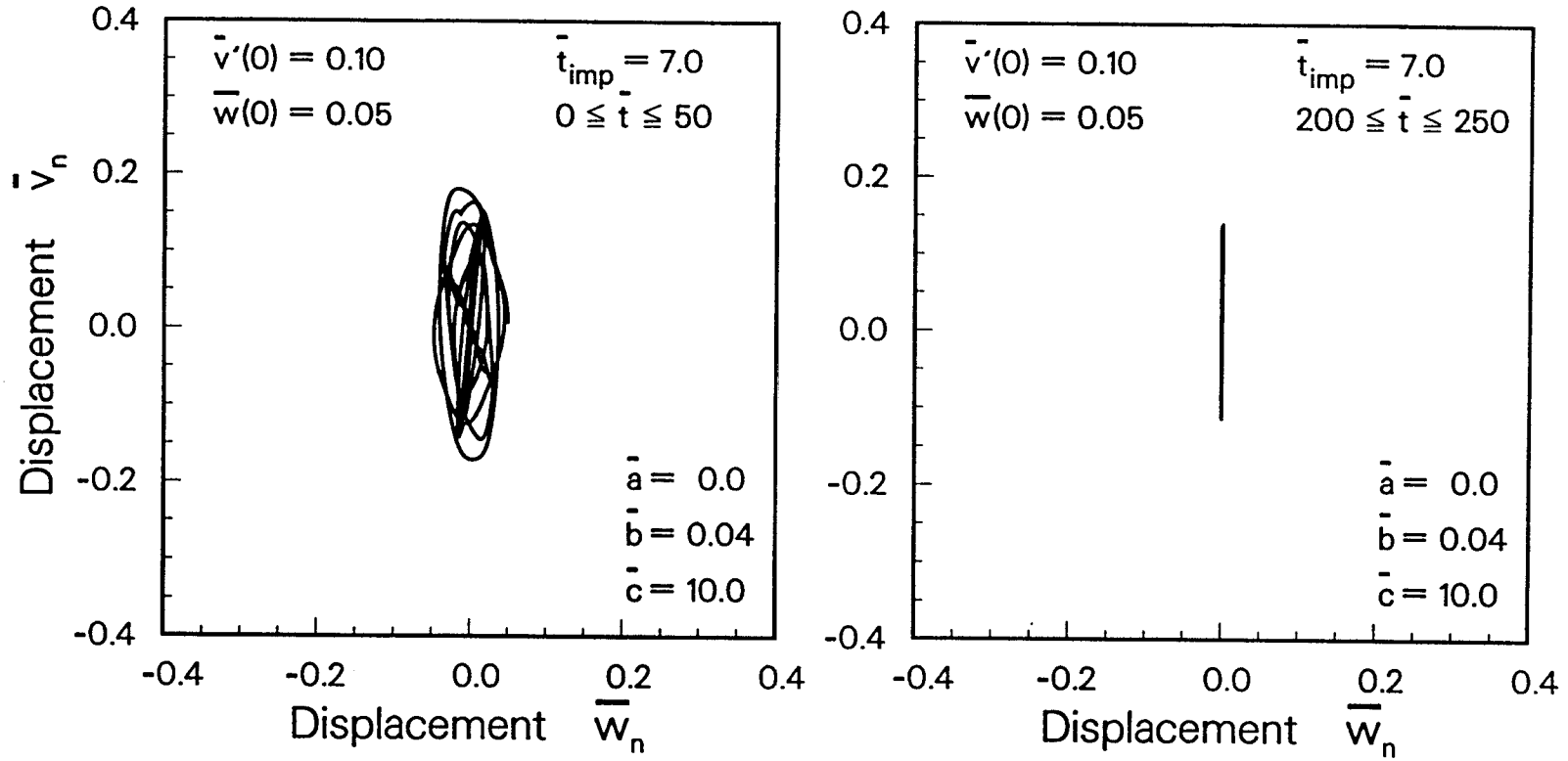

Fig. 6.6-26. Nonplanar Midspan Orbital Path for Multiple Shot Analysis. ($\bar{a}$ = 0.0, $\bar{c}$ = 10.0, $\bar{t}_{imp}$ = 7.0, Damping = 2%)

returns to a planar motion (Figs. 6.6-25 and 6.6-26) with the maximum in-plane amplitude again corresponding to Fig. 6.5-2.

Consequently, the dynamic response of the tube is again displaying characteristics similar to that of a string with a harmonic excitation applied only in one plane. In other words, there are critical values of the excitation frequency for which the planar motion becomes unstable and the tube exhibits a whirling motion [2.84, 6.9]. On the other hand, fluid effects can also become important. Figure 6.6-27 shows the midspan displacement histories for $\bar{t}_{imp} = 5.0$ when the Coriolis acceleration term has been included ($\bar{a} = 1.0$). It can be seen that the whirling motion shown in Figs. 6.6-23 and 6.6-24 for the same excitation frequency has now been reduced to a planar oscillation only. In other words, the presence of a relatively low fluid velocity can cause shifts in the amplitude-frequency response.

With the number of variables involved, determining an entire set of parametric design plots (as in Section 6.4) to cover a range of values would not be practical. However, investigating a set of parameters for a specific system would be a necessity in order to predict whirling motion. Amplitude-frequency plots for both in-plane and out-of-plane motions could be determined numerically as was done for the nonlinear planar analysis. In order to obtain the entire jump phenomena for the system, it would again be necessary to numerically simulate experimental procedure by slowly increasing and decreasing $\bar{t}_{imp}$.

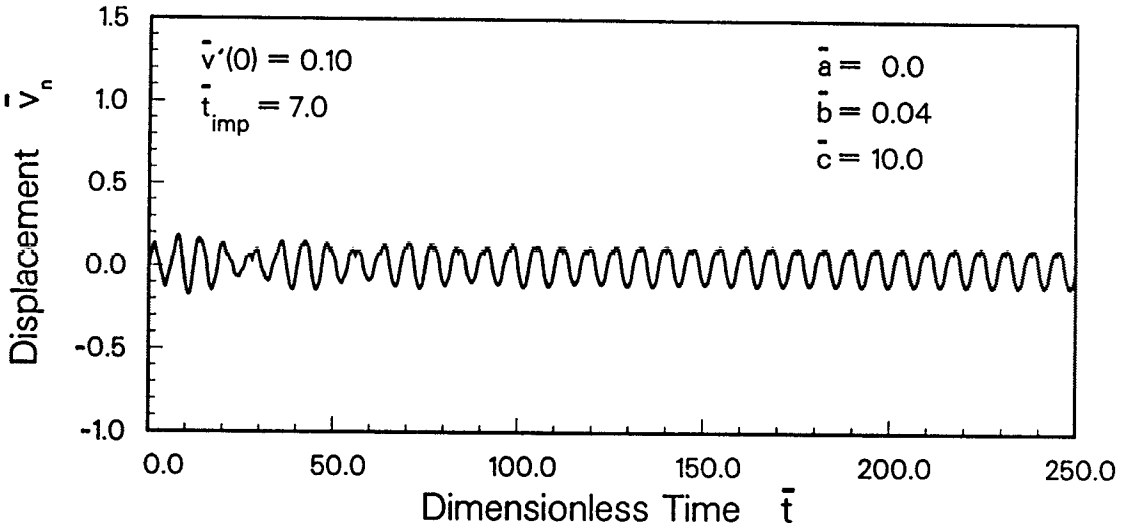

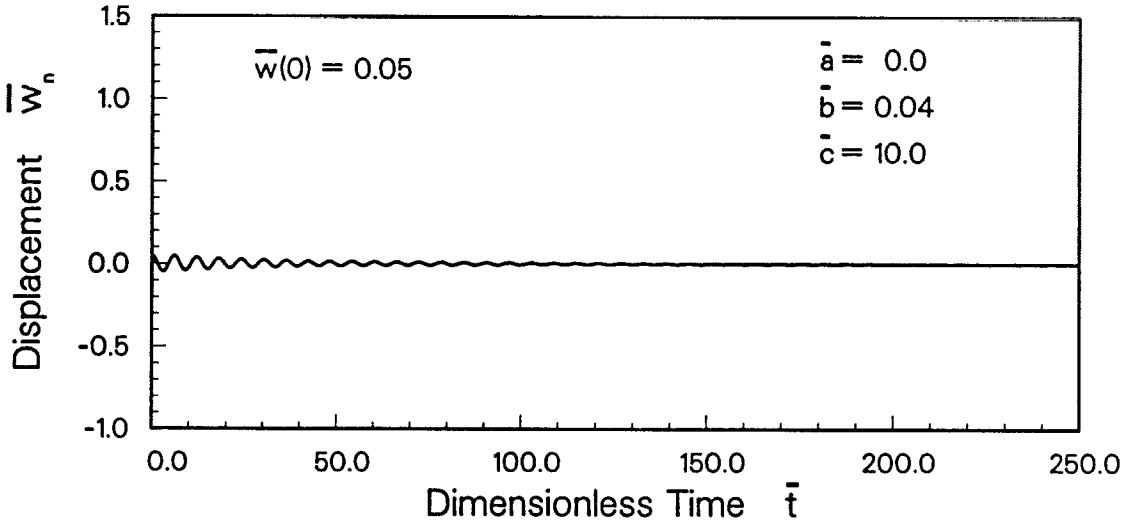

Fig. 6.6-27. Nonplanar Midspan Displacement Histories for Multiple Shot Analysis. ($\bar{a}$ = 1.0, $\bar{c}$ = 10.0, $\bar{t}_{imp}$ = 5.0, Damping = 2%)

6.7 REFERENCES

[6.1] Duderstadt, J.J. and Moses, G.A., *Inertial Confinement Fusion*, John Wiley & Sons, Inc., New York, 1982.

[6.2] Badger, B. et al., "HIBALL, A Conceptual Heavy Ion Beam Driven Fusion Reactor Study," University of Wisconsin Fusion Technology Institute Report UWFDM-450/KfK-3202, June 1981.

[6.3] Badger, B. et al., "HIBALL-II - An Improved Conceptual Heavy Ion Beam Driven Reactor Study," University of Wisconsin Fusion Technology Institute Report UWFDM-625/KfK-3840, December 1984.

[6.4] Badger, B. et al., "Annual Report of Research Performed on the LIBRA Project Between 1 January and 31 December 1982 by Fusion Power Associates," Fusion Power Associates Report FPA-82-7, December 1982.

[6.5] Kulcinski, G.L. et al., "The INPORT Concept - An Improved Method to Protect ICF Reactor First Walls," *Journal of Nuclear Materials*, Vols. 103-104, 1981, pp. 103-108.

[6.6] B. Badger et al., "Progress Report for the LIBRA Light Ion Beam Fusion Reactor Project for the Period January-June 1983," Fusion Power Associates Report FPA-82-7, July 1983.

[6.7] R.R. Peterson, "CONRAD - A Coupled Radiation Hydrodynamics - Condensation Computer Code," University of Wisconsin Fusion Technology Institute Report UWFDM-670, January 1986.

[6.8] Wen, Y.-K., "Dynamic Response of Transmission Line System to Wind Load," Engineering Science Research Report BLWT-9-68, University of Western Ontario, London, Ontario, April 1968.

[6.9] Nayfeh, A.H. and Mook, D.T., *Nonlinear Oscillations*, John Wiley & Sons, Inc., New York, 1979.

CHAPTER 7

FLOW-INDUCED VIBRATIONS

7.1 PARAMETRIC EXCITATION

One of the more common problems found in the piping of fluids is the instability generated by flow-induced vibrations. For example, the oscillatory response of a pipe to pumping pulsations can become unstable. In the previous chapter, the investigations were concerned with tubes conveying fluid flowing at a constant velocity, with an externally applied excitation. However, it is also necessary to consider the case of pulsating fluid. In Chapter 3, the equations of motion were derived allowing the flow velocity to have a harmonic fluctuation about a mean value, i.e., $c = c_o\ (1 + \mu \cos \Omega t)$. A realistic characterization of the fluid velocity may require components other than a purely harmonic one. However, this is still regarded as the fundamental representation of periodic flow (Refs. [2.53,2.54] and [2.56-2.58]). When this harmonic component is included in the equations of motion the result is parametric excitation of the system. Equations (5.3-7) and (5.3-8) are the complete nondimensional equations of motion. Various simplifications of these are considered in order to analyze different categories of the problem and identify parametric instabilities.

7.2 COPLANAR PARAMETRIC RESONANCE

One important case to consider is when the nonlinear coefficient $\bar{c}$ is small enough to neglect. This would then decouple the

v and w equations and the resulting motion would be essentially coplanar. Therefore, only Eq. (5.3-7) is used and is reproduced here with $\bar{c} = 0$.

$$\bar{v}_r'' + \bar{a}\,(1 - \mu \cos \bar{\Omega}\,\bar{t}) \sum_{n=1}^{\infty} \frac{rn}{(r^2 - n^2)}\,\bar{v}_n'$$

$$+ \bar{b}\,r\,\bar{v}_r' + r^2\,\bar{v}_r + \bar{d}\,\mu\,\bar{\Omega}\,(\sin \bar{\Omega}\,\bar{t}) \sum_{n=1}^{\infty} \frac{(rn)^3}{(n^2 - r^2)}\,\bar{v}_n$$

$$- \bar{e}\,r^2\,(2\,\mu \cos \bar{\Omega}\,\bar{t} + \mu^2 \cos^2 \bar{\Omega}\,\bar{t})\,\bar{v}_r = 0$$

$$r = 1,2,3 \ldots \qquad (r \pm n) = \text{odd} \qquad (7.2\text{-}1)$$

This can be written in matrix form as

$$\{\bar{v}''\} + \bar{a}\,(1 - \mu \cos \bar{\Omega}\,\bar{t})\,[A]\,\{\bar{v}'\} + \bar{b}\,[B]\,\{\bar{v}'\}$$

$$+ [R]\,\{\bar{v}\} + \bar{d}\,\mu\,\bar{\Omega}\,(\sin \bar{\Omega}\,\bar{t})\,[D]\,\{\bar{v}\}$$

$$- \bar{e}\,(2\,\mu \cos \bar{\Omega}\,\bar{t} + \mu^2 \cos^2 \bar{\Omega}\,\bar{t})\,[E]\,\{\bar{v}\} = 0 \qquad (7.2\text{-}2)$$

where $\{\bar{v}\}$ is the vector $\{\bar{v}_1, \bar{v}_2, \ldots\}^T$; [B], [R] and [E] are diagonal matrices determined from index coefficients, and [A] and [D] are antisymmetric matrices determined from the summations on n which also couple the system of equations.

One procedure that can be used to compute the boundaries of regions of parametric resonance for Eq. (7.2-2) is Bolotin's method [7.1]. His stability criterion is based on the observation that periodic solutions with periods P and 2P ($P = 2\pi/\bar{\Omega}$) separate regions of unboundedly increasing solutions from regions of stability.

For the primary instability boundaries (with period of 2P), a solution to the system of equations is sought in the form

$$\{\bar{v}\} = \sum_{k = 1,3,5,\ldots} \left(\{\alpha_k\} \sin \frac{k\,\bar{\Omega}\,\bar{t}}{2} + \{\beta_k\} \cos \frac{k\,\bar{\Omega}\,\bar{t}}{2}\right) . \qquad (7.2\text{-}3)$$

Equation (7.2-3) is then substituted into (7.2-2) and expanded. Consequently, the coefficients of $\cos \frac{k\,\bar{\Omega}\,\bar{t}}{2}$ and $\sin \frac{k\,\bar{\Omega}\,\bar{t}}{2}$ with the same index k, can be equated to zero. This yields an infinite set of algebraic equations which can be written in the form

$$\begin{bmatrix} \cdots & \cdots & \cdots & \cdots & \cdots & \cdots \\ \cdots & [G_{33}] & [G_{31}] & [G_{32}] & [G_{34}] & \cdots \\ \cdots & [G_{13}] & [G_{11}] & [G_{12}] & [G_{14}] & \cdots \\ \cdots & [G_{23}] & [G_{21}] & [G_{22}] & [G_{24}] & \cdots \\ \cdots & [G_{43}] & [G_{41}] & [G_{42}] & [G_{44}] & \cdots \\ \cdots & \cdots & \cdots & \cdots & \cdots & \cdots \end{bmatrix} \begin{Bmatrix} \vdots \\ \{\alpha_3\} \\ \{\alpha_1\} \\ \{\beta_1\} \\ \{\beta_3\} \\ \vdots \end{Bmatrix} = \{0\} \qquad (7.2\text{-}4)$$

The boundary equation for the instability regions can be determined by setting the determinant of the coefficients of $\{\alpha_k\}$ and $\{\beta_k\}$ to zero, i.e.,

$$\det [G_{jk}] = 0. \tag{7.2-5}$$

From Eq. (7.2-4) it can be seen that the $[G_{jk}]$ matrix is of infinite order, and thus the determinant is also. However, Bolotin showed that this determinant belonged to the class of normal determinants, which implies absolute convergence. For the k = 1 approximation, the boundaries of the principal region of instability can be located by

$$\begin{vmatrix} [G_{11}] & [G_{12}] \\ [G_{21}] & [G_{22}] \end{vmatrix} = 0 \tag{7.2-6}$$

where

$$[G_{11}] = -\frac{\bar{\Omega}^2}{4}[I] + [R] + \bar{e}\,\mu\,[E] - \frac{1}{2}\bar{e}\,\mu^2\,[E]$$

$$[G_{12}] = -\bar{a}\,\frac{\bar{\Omega}}{2}[A] - \bar{b}\,\frac{\bar{\Omega}}{2}[B] - \bar{a}\,\mu\,\frac{\bar{\Omega}}{4}[A] + \frac{1}{2}\bar{d}\,\mu\,\bar{\Omega}\,[D]$$

$$[G_{21}] = \bar{a}\,\frac{\bar{\Omega}}{2}[A] + \bar{b}\,\frac{\bar{\Omega}}{2}[B] - \bar{a}\,\mu\,\frac{\bar{\Omega}}{4}[A] + \frac{1}{2}\bar{d}\,\mu\,\bar{\Omega}\,[D]$$

$$[G_{22}] = -\frac{\bar{\Omega}^2}{4}[I] + [R] - \bar{e}\,\mu\,[E] - \frac{1}{2}\bar{e}\,\mu^2\,[E] \tag{7.2-7}$$

and [I] is the identity matrix. (To obtain better accuracy and higher regions of instability it would be necessary to consider the k = 3 approximation, which would include all of the terms shown in Eq. (7.2-4).) The order of the square matrices and the column matrices in Eq. (7.2-4) directly corresponds to the number of modes included in the solution. For this case a 5 mode solution was considered which yields a 10 x 10 determinant for Eq. (7.2-6). The nonzero components of this determinant are given in Appendix D.1.

To obtain secondary instabilities (boundaries of instability having period P), the solution of the system of equations is expressed as

$$\{\bar{v}\} = \sum_{k = 0,2,4\ldots} \left(\{\alpha_k\} \sin \frac{k\,\bar{\Omega}\,\bar{t}}{2} + \{\beta_k\} \cos \frac{k\,\bar{\Omega}\,\bar{t}}{2} \right) \qquad (7.2\text{-}8)$$

where the index k is now evaluated at 0,2,4,... . Equation (7.2-8) is again substituted into (7.2-2) and expanded. As was done for primary instabilities, coefficients with the same index k are collected yielding another set of equations as in (7.2-4), but with a vector $\{\ldots, \alpha_4, \alpha_2, \alpha_0, \beta_0, \beta_2, \beta_4, \ldots\}^T$. Hence, to determine secondary instability regions the determinant of the coefficients of $\{\alpha_k\}$ and $\{\beta_k\}$ is again set to zero. For the k=2 approximation, all the submatrices shown in Eq. (7.2-4) are included in the calculations, i.e.,

$$\begin{vmatrix} [G_{33}] & [G_{31}] & [G_{32}] & [G_{34}] \\ [G_{13}] & [G_{11}] & [G_{12}] & [G_{14}] \\ [G_{23}] & [G_{21}] & [G_{22}] & [G_{24}] \\ [G_{43}] & [G_{41}] & [G_{42}] & [G_{44}] \end{vmatrix} = 0 \qquad (7.2\text{-}9)$$

where

$$[G_{33}] = -\bar{\Omega}^2 [I] + [R] - \frac{1}{4} \bar{e} \mu^2 [E]$$

$$[G_{31}] = [0]$$

$$[G_{32}] = \bar{d} \mu \bar{\Omega} [D]$$

$$[G_{34}] = -\bar{a} \bar{\Omega} [A] - \bar{b} \bar{\Omega} [B]$$

$$[G_{13}] = \bar{e} \mu [E]$$

$$[G_{11}] = [R] - \frac{1}{2} \bar{e} \mu^2 [E]$$

$$[G_{12}] = [0]$$

$$[G_{14}] = -\frac{1}{2} \bar{a} \mu \bar{\Omega} [A] + \frac{1}{2} \bar{d} \mu \bar{\Omega} [D]$$

$$[G_{23}] = -\frac{1}{2}\,\bar{a}\,\mu\,\bar{\Omega}\,[A] + \frac{1}{2}\,\bar{d}\,\mu\,\bar{\Omega}\,[D]$$

$$[G_{21}] = [0]$$

$$[G_{22}] = [R] - \frac{1}{2}\,\bar{e}\,\mu^2\,[E]$$

$$[G_{24}] = -\,\bar{e}\,\mu\,[E]$$

$$[G_{43}] = \bar{a}\,\bar{\Omega}\,[A] + \bar{b}\,\bar{\Omega}\,[B]$$

$$[G_{41}] = [0]$$

$$[G_{42}] = -\,2\,\bar{e}\,\mu\,[E]$$

$$[G_{44}] = -\,\bar{\Omega}^2\,[I] + [R] - \frac{3}{4}\,\bar{e}\,\mu^2\,[E] \qquad (7.2\text{-}10)$$

and [0] represents the zero matrix. For a 5 mode solution the determinant in Eq. (7.2-9) is 20 x 20. The nonzero components of this determinant are given in Appendix D.2.

7.3 NUMERICAL CALCULATIONS

A computer code was developed to solve Eqs. (7.2-6) and (7.2-9) in the μ-$\bar{\Omega}$ parameter space. With the large number of variables involved in this system it is not possible to show the effect of all parameters on stability. For this reason the tube and fluid

parameters used in the ICF examples in Chapter 6 have also been considered here. Specifically,

Tube Diameter = 3.0 cm

Tube Length = 6.0 m

Tube Thickness = 3.0 mm

Mean Tension = 1500 N

LiPb Density = 9.44 g/cm^3

SiC Density = 2.60 g/cm^3

With these parameters fixed, the effect of the fluid velocity and damping on the system is obtained. For the case of zero damping, Fig. 7.3-1 shows the regions of principal and secondary instability for flow velocities of 6, 8 and 10 m/s, respectively. Boundaries were determined by numerically solving for the zeros of the determinants, i.e., scanning $\bar{\Omega}$ at a specific value of μ and refining the solution by the method of bisection. Figure 7.3-1 shows that the principal regions of instability are substantially wider than the secondary regions. Also, as the fluid velocity increases, the width of the instability regions also increases. It should be noted that for ICF applications there should be little or no problem with parametric resonance if the flow velocities are kept at 6 m/s or less and the pumping amplification factors are kept low. Figure 7.3-2 shows the effect of dissipation on the same system as Fig. 7.3-1 (with a flow velocity of 10 m/s). Damping reduces the size of the regions of instability such that for small values of μ, parametric resonance is not possible. Moreover, there is a more pronounced effect on the

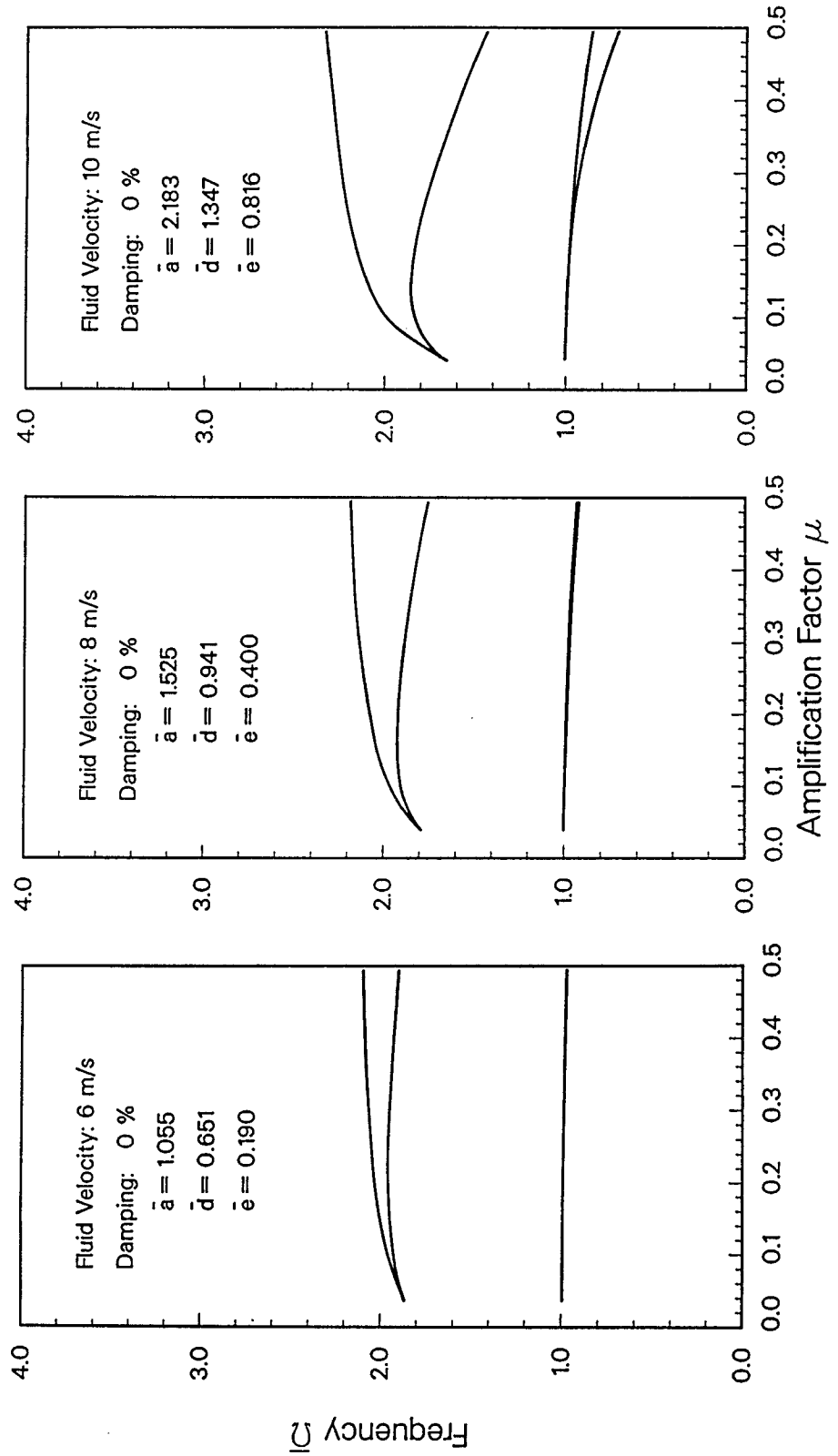

Fig. 7.3-1. The Effect of Fluid Velocity on Primary and Secondary Instability Regions.

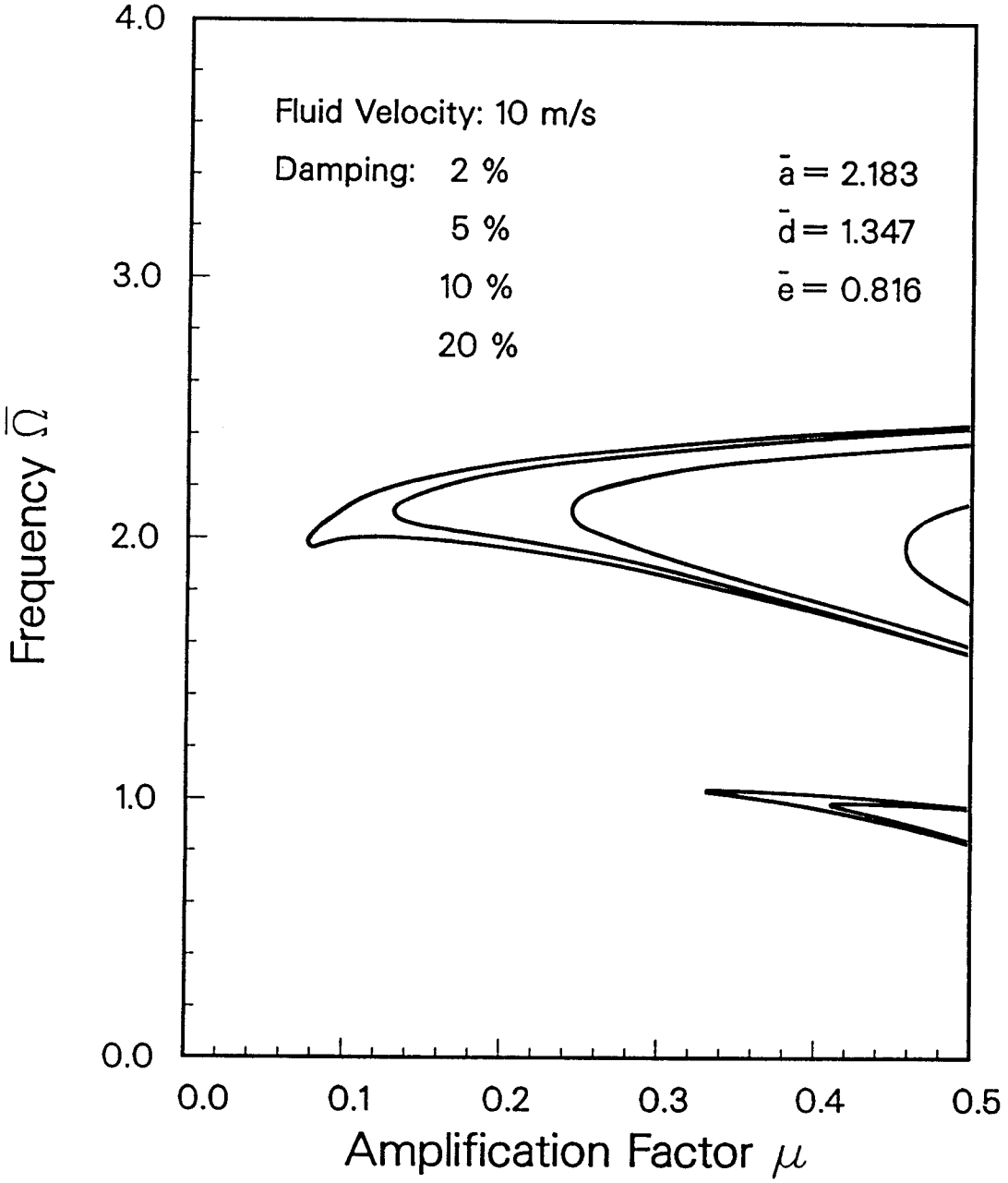

Fig. 7.3-2. The Effect of Damping on Primary and Secondary Instability Regions.

secondary regions, i.e., for damping $\geq$ 10% secondary parametric resonance will never occur for μ less than 0.5.

To illustrate the parametric instabilities of the tube for the different regions, displacement histories have been determined by using the Runge-Kutta method to numerically integrate the equation of motion, Eq. (7.2-1). Using the specific system parameters given in Fig. 7.3-2 (with damping at 2%), a five mode solution was again considered. Figure 7.3-3 shows the response of the tube when the excitation frequency $\bar{\Omega}$ falls within the primary instability region (μ = 0.3, $\bar{\Omega}$ = 1.9). If the frequency $\bar{\Omega}$ is dropped to 0.8 with μ remaining the same, the system is now within the stabile region and the response is shown in Fig. 7.3-4. The initial perturbation in this figure is due to a very small impulse given to start the tube in motion. For 2% damping this initial energy is eventually dissipated. Finally with $\bar{\Omega}$ = 0.8, the amplification factor μ is increased to 0.5 and the system's parameter point falls within the secondary instability boundaries. Figure 7.3-5 shows the corresponding tube response with the same initial velocity as the preceding case. It should be noted that the response for the secondary zones grows much slower than for the primary zones. (The displacement amplitude scale in Fig. 7.3-5 is an order of magnitude less than that used in Fig. 7.3-3 and the time scale has been increased by a factor of 3.)

7.4 REFERENCES

[7.1] Bolotin, V.V., *Dynamic Stability of Elastic Systems*, Holden-Day, Inc., San Francisco, 1964.

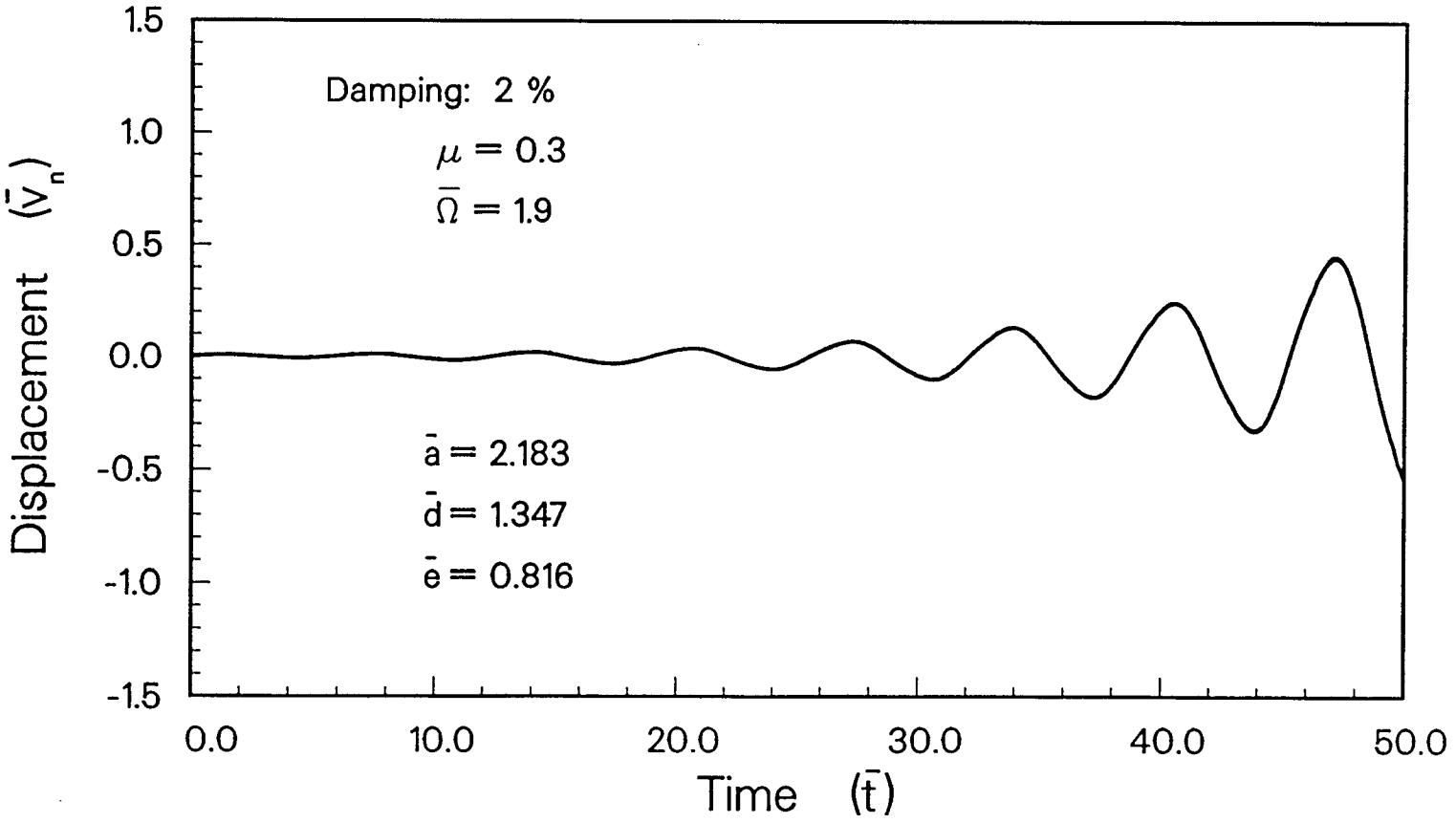

Fig. 7.3-3. Tube Displacement History in Primary Instability Zone.

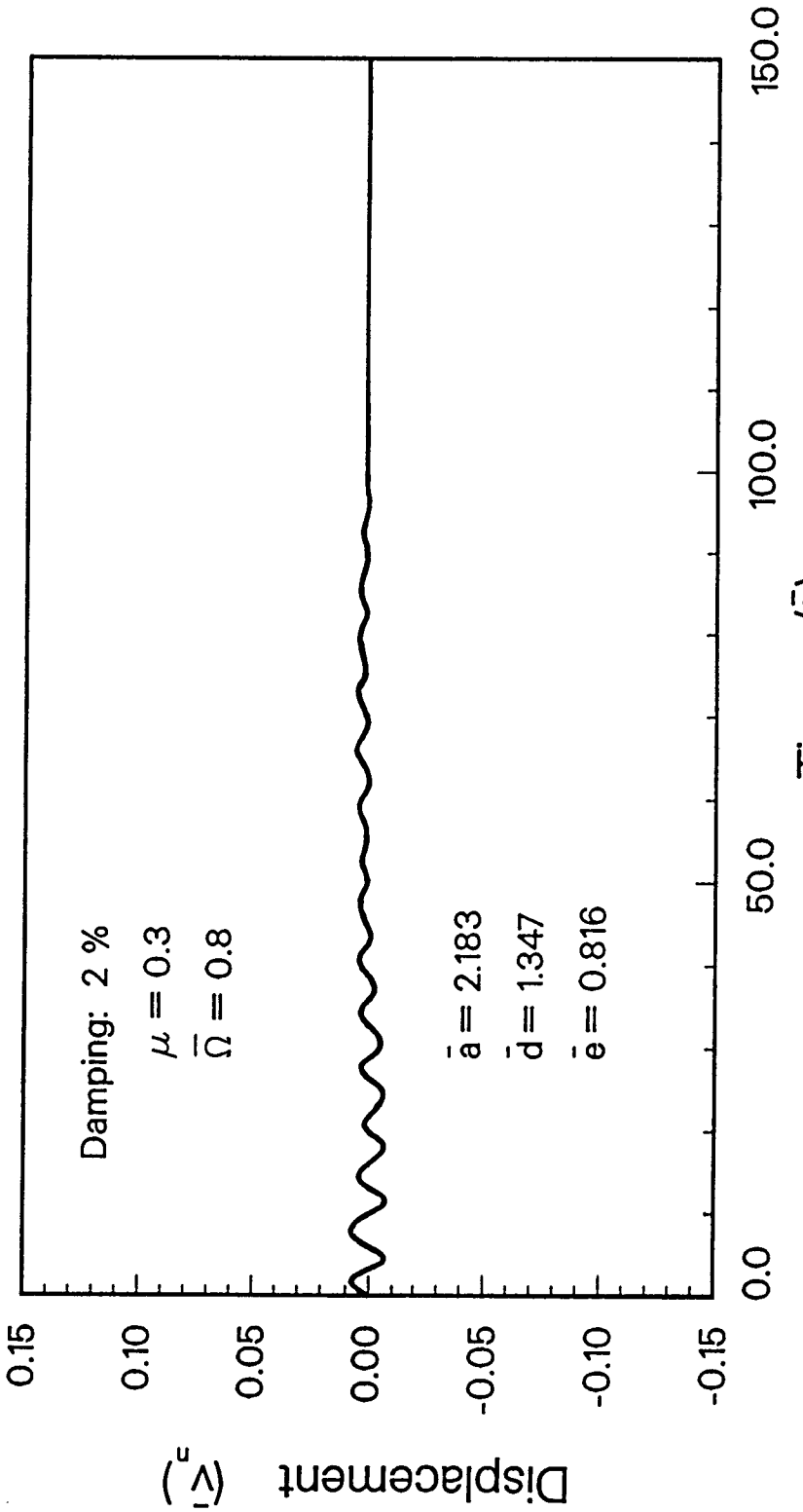

Fig. 7.3-4. Tube Displacement History within Stability Region.

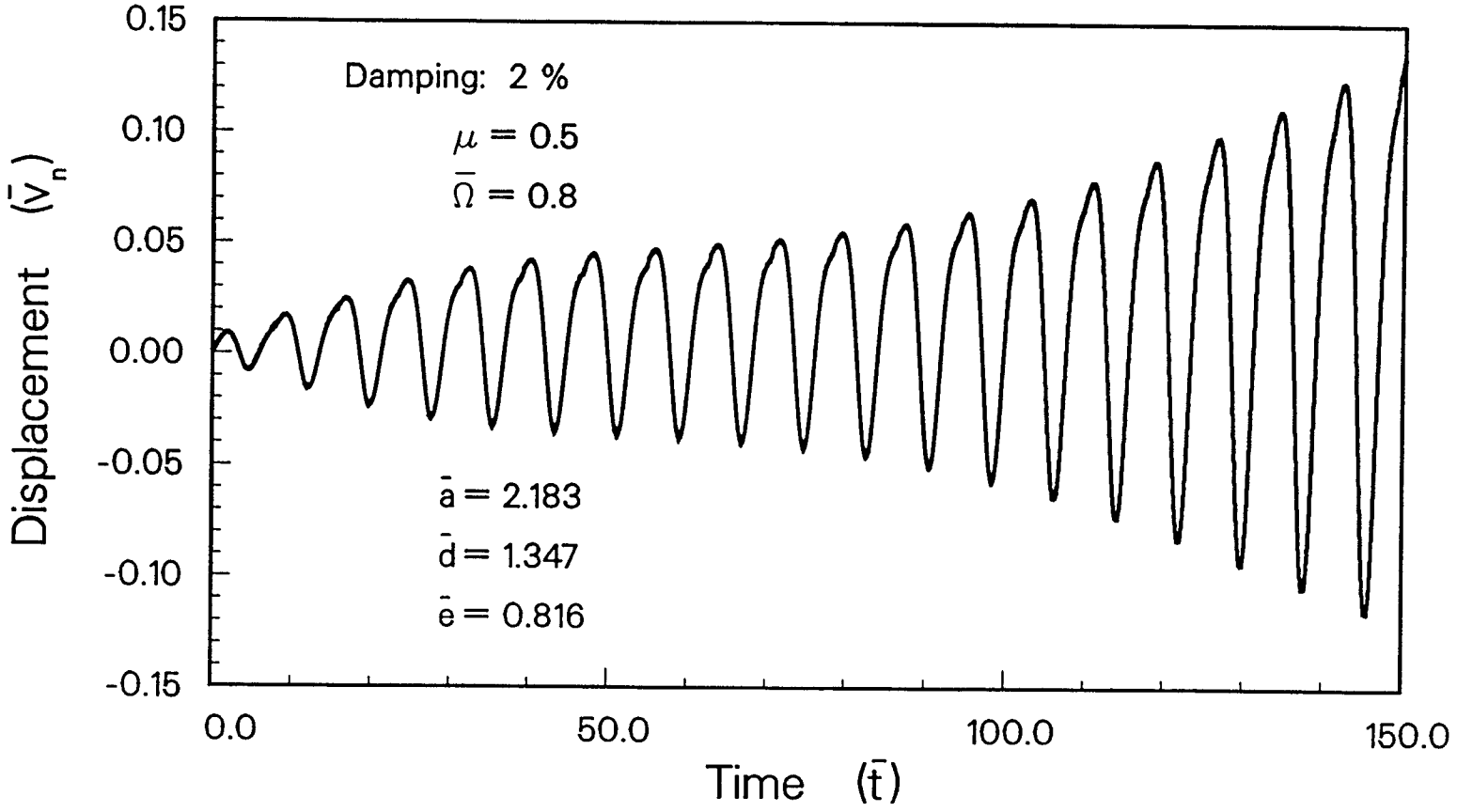

Fig. 7.3-5. Tube Displacement History in Secondary Instability Zone.

CHAPTER 8

SUMMARY AND CONCLUSIONS

The vibration and dynamic stability of completely flexible tubes conveying fluid has been investigated to aid in the development of proposed inertia confinement reactor designs. The primary external loading condition included a mechanical impulsive pressure applied sequentially at the repetition rate of the reactor. Parametric excitation due to a pulsating component associated with the internal flow velocity was also considered.

In order to avoid resonance problems due to synchronization with the repetition rate of the driver, natural frequencies were determined for tubes with both variable and constant tension. It was found that tension gradients could produce strong asymmetries in the mode shapes and shifts in the numerical values of the natural frequencies. However, the results from a perturbation analysis showed that for an effective tension substantially larger than the weight, the tension gradient could be replaced by a mean value equal to the effective tension plus half the weight.

The dynamic response of the tube to planar impulsive pressures displayed characteristics similar to that of a classic string with a planar harmonic forcing function. For the planar analysis, amplitude-frequency relationships were determined for a range of parameters including the effects of damping and the Coriolis acceleration of the fluid. Discontinuities in the amplitude response curves

were identified for nonlinear oscillations. Actual experimental procedures were numerically simulated to illustrate the entire range of jump phenomena. The conditions under which whirling motion began were also identified. The orbital and precessional response of the tube for free vibrations was investigated again emphasizing fluid effects. An analysis of the sequentially applied planar impulses showed that nonplanar oscillations of the tube were possible. However, three-dimensional motion was definitely dependent upon the frequency of the forcing function and fluid interaction. Parametric design curves outlining in-plane and out-of-plane amplitude-frequency responses were left for future research.

Finally, in the case of a harmonically varying flow velocity, stability maps were computed by Bolotin's method. It was found that increasing the flow velocity also increased the regions of instability, whereas damping reduced them. For the relatively low fluid velocity used in ICF applications, parametric excitation of the tube is not expected. However, it should be pointed out that the flow-induced vibration analysis presented here, also provides a tool for examining the stability of any flexible tubular component conveying liquid, i.e., propellant lines. In fact, the most recent application of this method involves space tethers used for fluid transport.

APPENDIX A

STRENGTH AND FATIGUE ANALYSIS OF SILICON CARBIDE

A.1 FIBER CHARACTERISTICS

Since silicon carbide fiber has been proposed as the primary material for the INPORT units, it is important to identify static and dynamic mechanical strength characteristics. The fiber used is "NICALON®", manufactured by a polymer pyrolysis process by Nippon Carbon Co., Japan, and distributed by Dow Corning Co. It is composed of ultrafine β-SiC crystals with excess carbon and is able to retain its strength at high temperatures. Typical properties of a single filament, as published by Dow [A.1], are shown in Table A.1-1.

Table A.1-1

NICALON® SiC Fiber Properties

Filament Diameter	10 ~ 15 μm
Cross Section	Round
Filaments/Yarn	500
Density	2.55 g/cm^3
Tensile Strength	2480 ~ 3240 MPa
Tensile Modulus	179 ~ 200 GPa
Strain to Failure	1.5% Average

Since fiber bundle or yarn data was not available tensile and fatigue tests were carried out on a MTS T5002 universal testing machine equipped with a 100 N load cell. Special load grips designed for fibrous and stranded materials were used and are shown in Fig. A.1-1. Cords are wound around stationary cylinders and the ends are clamped at the top and bottom.

Tensile tests were run on ten specimens with the overall failure characterized by a "brooming" effect. Figure A.1-2 shows half of a specimen photographed on a 20 x 20/inch grid background. Such a result might lead one to expect predominately sequential fiber failure and a definite knee on the stress-strain diagrams. However, this is not the case; the dominant failure mode is simultaneous fracture of the majority of fibers. Quantitative results of the tension tests are given in Table A.1-2. The average tensile strength and modulus were approximately 50% of those reported for single filaments, a result attributable to nonuniform load sharing by individual filaments in the yarn.

A scanning electron microscope (SEM) was used to photograph fracture surfaces and also verify the uniformity of the fibers. In Fig. A.1-3 a yarn which has failed in tension is shown at a magnification factor of 130. In Fig. A.1-4 the magnification has been increased to 3600 to measure the diameter of untested filaments. A mean diameter of 12.6 μm was obtained by scanning along a number of filaments. Fracture surfaces were found to be clean breaks on planes normal to the filament axes as shown in Figs. A.1-5 and A.1-6. The

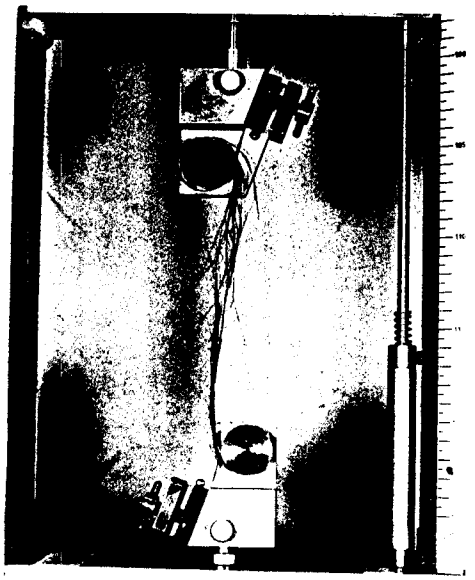

Fig. A.1-1. Tensile failure of SiC fibers.

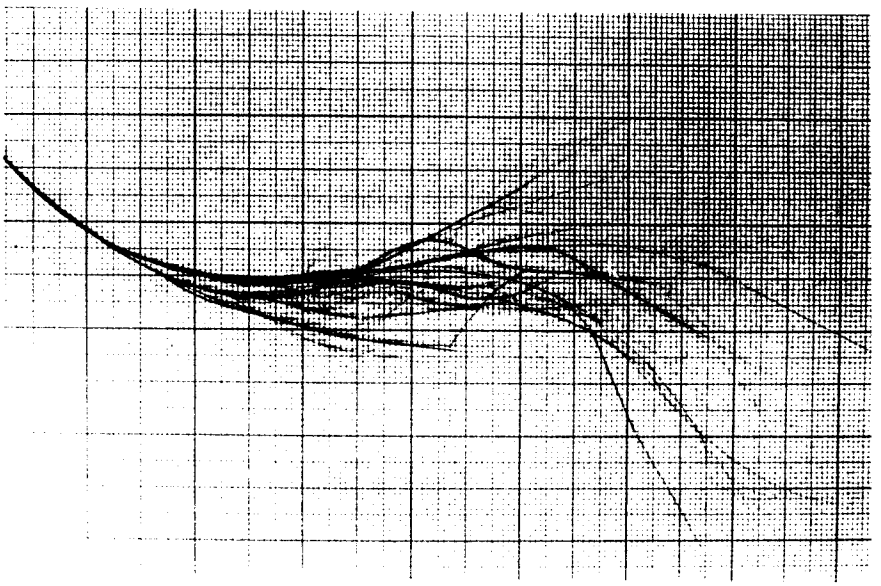

Fig. A.1-2. Specimen after testing, on 20x20/inch grid.

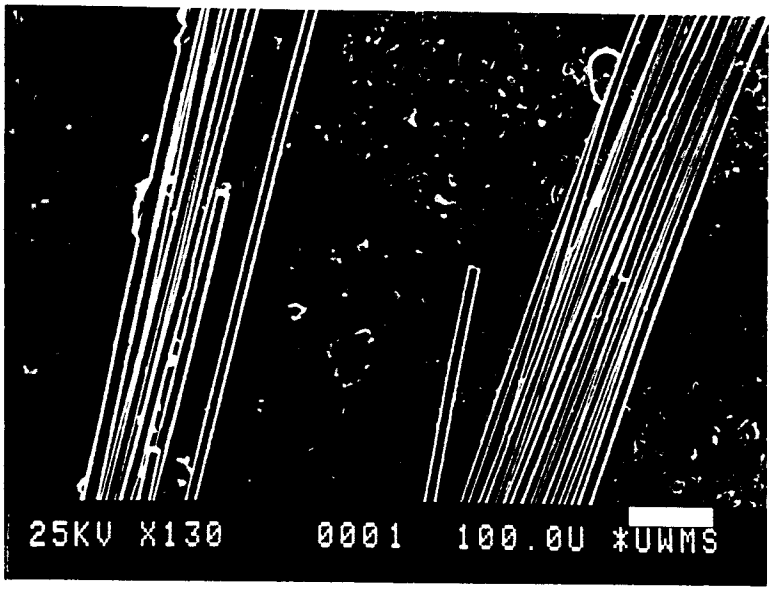

Fig. A.1-3. Static tensile fracture of SiC fibers (Bar scale = 100 μm).

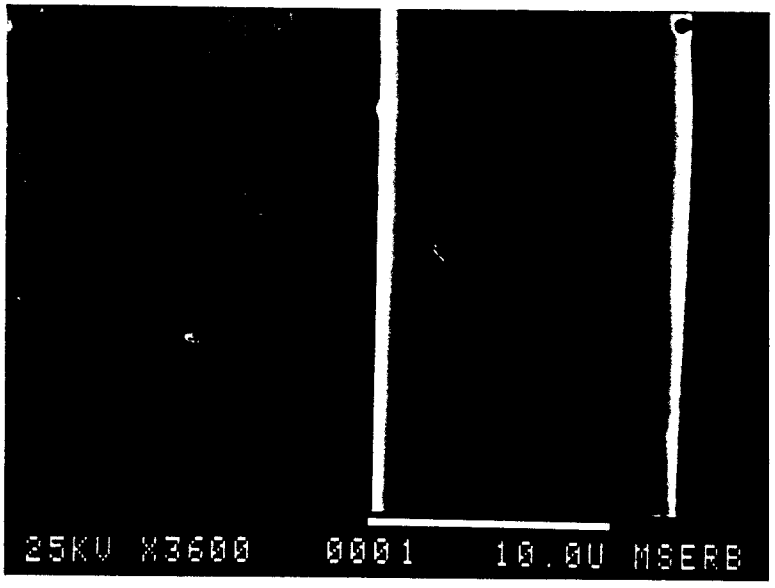

Fig. A.1-4. SEM photograph of single fiber (Bar scale = 10 μm).

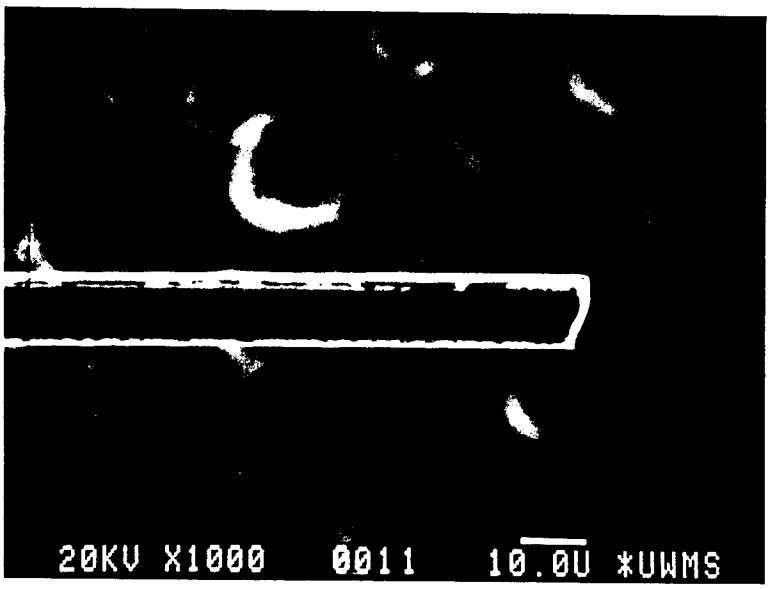

Fig. A.1-5. Sem micrograph of filament tensile failure.

Fig. A.1-6. SEM micrograph of filament tensile failure.

Table A.1-2

SiC Fiber Tension Test Data

Filament Diameter	12.6 μm
Filaments/Yarn	500
Cross Sectional Area	6.23×10^{-8} m^2
Specimen Gage Length	0.15 m
Strain Rate	1.67×10^{-4} m/s
Maximum Load (average)	84.4 N
Failure Stress (average)	1346 MPa
Elastic Modulus (average)	90.04 GPa

dark central circular area in Fig. A.1-6 may be the result of a penny crack which originated and subsequently propagated across the filament.

The same apparatus was used for cyclic testing of the fibers with the maximum load frequency at 0.25 Hz and the gage length remaining at 0.15 m. The load state consisted of a tensile mean stress (σ_m) and a cyclic alternating stress (σ_a). The various combinations were such as to produce a maximum value less than the fracture stress (σ_f) and a minimum greater than zero. In Fig. A.1-7, alternating stress as a fraction of fracture stress is plotted as a function of the number of cycles to failure. It should be noted that the curve for σ_m/σ_f equal to 40% terminates at a value of σ_a/σ_f equal to 40%. Curves for mean stresses of 50% and 60% have been extended

to the simple tension data corresponding to N_F = 0.5. Similarly maximum tensile stress can be plotted as a function of the number of cycles to failure as shown in Fig. A.1-8. The results indicate the possibility of an endurance limit but additional high cycle tests are needed. The development of graphs such as Fig. A.1-9 are useful for design purposes. Rays are shown for different ratios of σ_a/σ_m, the largest acceptable value being 1.0. In using such curves, for example, a point stressed to state "A" could sustain 10^2 cycles but not 10^3.

SEM micrographs were also taken of fatigued fibers. Figure A.1-10 is typical, characterized by a more complex or rougher fracture surface than static tension. A small percentage of fibers failed on inclined surfaces in more complex patterns. Figure A.1-11 shows a scalloped curved surface usually associated with progressive cyclic failure.

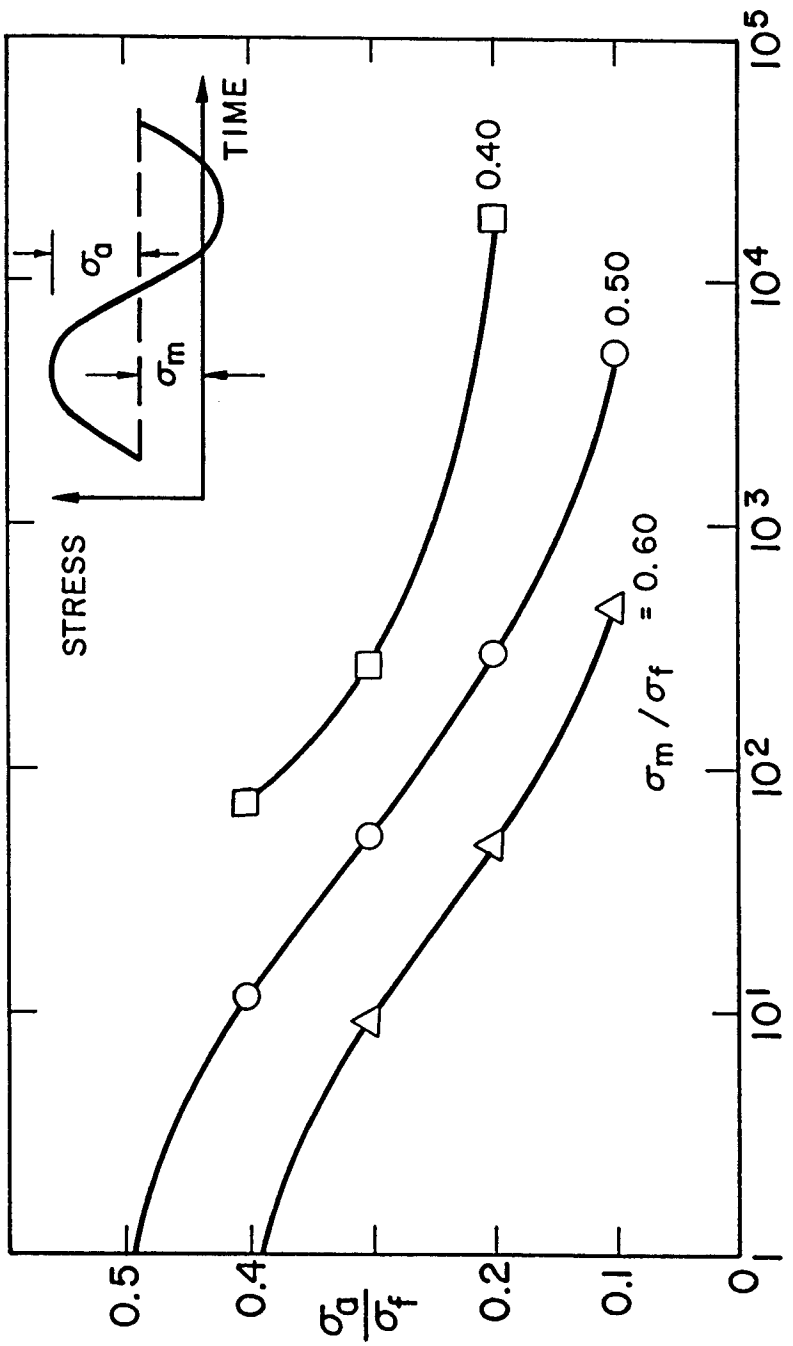

Fig. A.1-7. Alternating stress amplitude vs. number of cycles to failure.

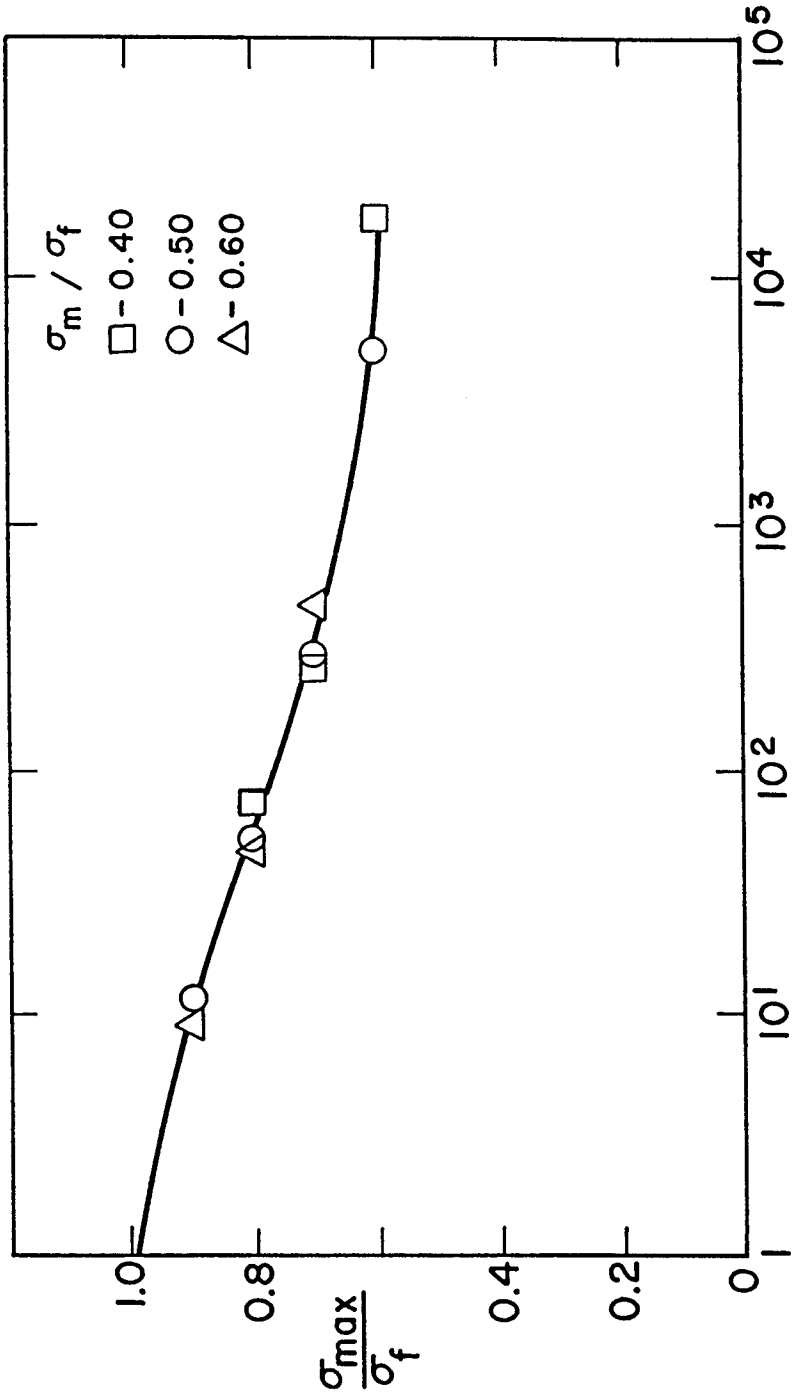

Fig. A.1-8. Maximum tensile stress vs. number of cycles to failure.

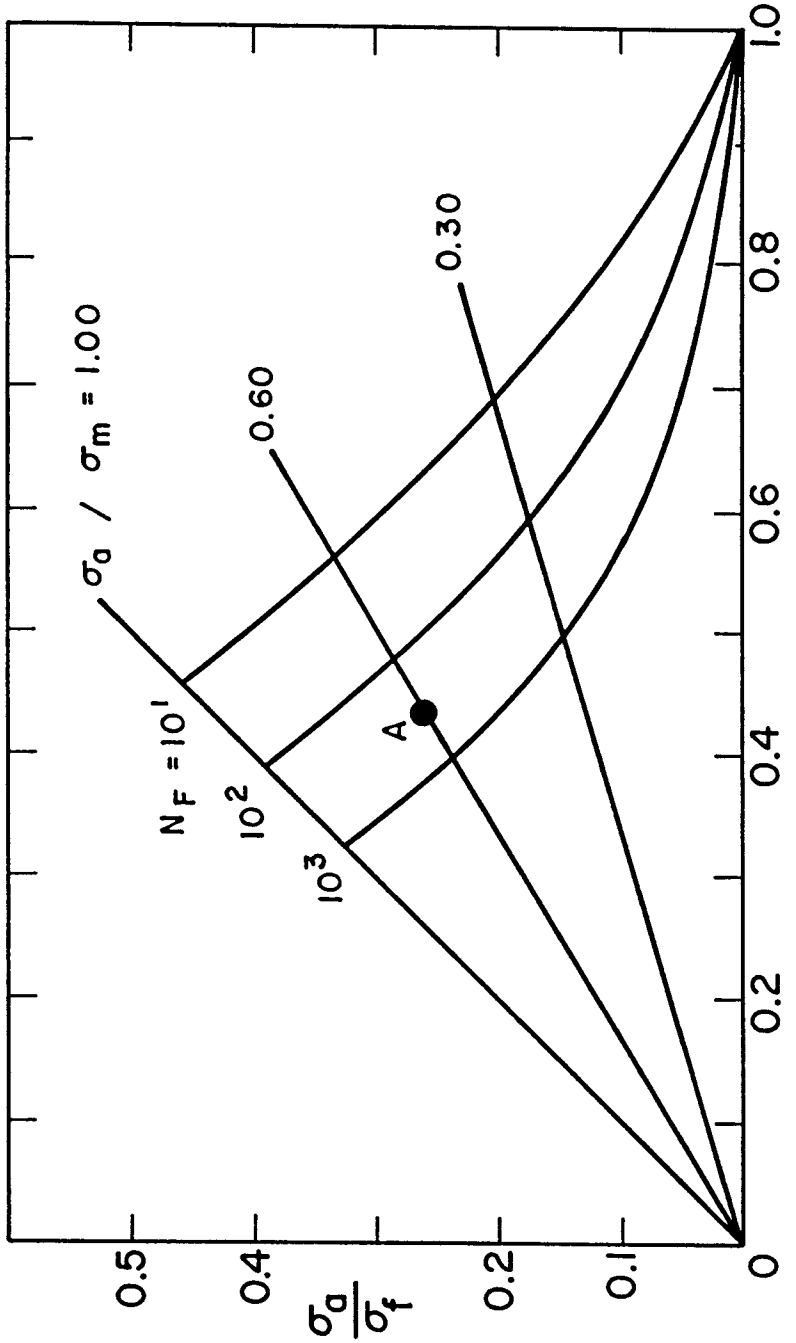

Fig. A.1-9. Alternating stress vs. mean stress for various cycles to failure.

Fig. A.1-10. Fatigue fiber fracture at 18,600 cycles for σ_m/σ_f = 40%, σ_a/σ_f = 20%.

Fig. A.1-11. Fatigue fiber fracture at 13,700 cycles for σ_m/σ_f = 40%, σ_a/σ_f = 20%.

A.2 INPORT TESTING

McDonnell Douglas Corp., St. Louis, MO, fabricated seven braided SiC tubes and tested six to failure in static tension. Tubes were made with and without axial tows and, in addition, some INPORTs received a SiC chemical vapor deposition (CVD) treatment. Tests were carried out at two temperatures, 350 and 550°C, with the results summarized in Table A.2-1 [A.2]. It can be seen that the CVD process substantially increased the tensile strength. This improved the load sharing capability of the fibers but produced a brittle tube. The axial cords in untreated tubes failed prematurely since they carried the total tensile load.

Results of the INPORT tests show that second generation designs need to incorporate a greater number of axial cords with provisions to insure load sharing. Also, for all applications a larger number of filaments per tow is necessary. (It should be noted that from a manufacturing standpoint it is technically possible to produce fiber yarns with thousands of filaments, as is the case with THORNEL® carbon fibers [A.3].) For example, if an INPORT unit (untreated) was fabricated with approximately 50 axial tows and 1000 filaments per tow, a failure load of 2000 N could be possible. This estimate is based upon the load sharing efficiency of 22% shown by the McDonnell Douglas tests.

Table A.2-1

INPORT Tension Data

Braided Tube Thickness	0.38 mm
SiC/CVD Tube Thickness	0.69 mm
Mandrel Diameter	2.86 cm
Braiding Angle	30°
No. of Braiding Tows	48
No. of Filaments/Tow	500
No. of Axial Tows	0 and 9

		Failure Load (N)	
Test Temperature	Axial Tows	Untreated INPORTs	CVD INPORTs
350°C	0	------	690
350°C	9	------	1108
550°C	0	334	578
550°C	9	165	1103

A.3 REFERENCES

[A.1] "New Product Information," Dow Corning Corporation, Midland, Michigan, 1986.

[A.2] Sapp, J., "An Investigation Into the Use of Graphite and Silicon Carbide in Heavy Ion Beam Reactors," McDonnell Douglas Technical Report 7F-05-E016-5507, 1982.

[A.3] "THORNEL® Product Information," AMOCO Performance Products, Inc., Ridgefield, CT, 1987.

APPENDIX B

PERTURBATION ANALYSIS

A perturbation analysis is developed for the equation of motion of a completely flexible tube which has small gradients in axial tension and density. The purpose of the work is to provide a limited verification of the eigenvalue problem results previously obtained in exact form for the planar case with a linear tension gradient.

The relevant equation of motion (4.1-1) has been presented and is simply reproduced here in undamped form:

$$\frac{\partial}{\partial x}\left\{\left[T_o - pA_f(1 - 2\nu) + (m_f + m_t)g(\ell - x) - m_f c^2\right]\frac{\partial v}{\partial x}\right\} - (m_f + m_t)\frac{\partial^2 v}{\partial t^2} = 0 \ . \tag{B-1}$$

For small axial gradients, the following replacements are made for the effective tension and total mass per unit length

$$\left(T_o - pA_f(1 - 2\nu) + (m_f + m_t)g(\ell - x) - m_f c^2\right) \to T_e[1 + \delta(x)] \tag{B-2}$$

$$(m_f + m_t) \to M[1 + \varepsilon(x)] \ . \tag{B-3}$$

This problem is generalized slightly with $\delta(x)$ and $\varepsilon(x)$, but restricted by requiring both functions to have very small amplitudes.

The form of the solution used for a typical modal component can be expressed as

$$v_n(x,t) = [V_n(x) + \sum_{m \neq n} a_m V_m(x)] \exp(i\omega_n t) \tag{B-4}$$

$$\omega_n^2 = \omega_n^{*2}(1 + b_n) \ . \tag{B-5}$$

Here $V_n(x)$ and ω_n^* represent solutions to the gradient-free problem. The coefficients a_m and b_n are small order terms and facilitate the development of the perturbation solution. These equations can be substituted directly into (B-1) giving

$$\begin{aligned} &\frac{\partial}{\partial x} \{[T_e(1 + \delta(x)][V_n' + \sum a_m V_m']\} \\ &\quad + \omega_n^2 M[1 + \varepsilon(x)][V_n + \sum a_m V_m] = 0 \end{aligned} \tag{B-6}$$

where $(\ )' = \partial/\partial x$. This is now expanded

$$\begin{aligned} &(T_e V_n'' + M\omega_n^{*2} V_n) + T_e \sum a_m V_m'' + T_e[\delta(x)V_n']' \\ &+ M\omega_n^{*2} \sum a_m V_m + M\omega_n^{*2}[\varepsilon(x) + b_n]\, V_n = -T_e[\sum \delta(x)\, a_m V_m']' \\ &- M\omega_n^{*2}[(1 + b_n)\varepsilon(x)] \sum a_m V_m \ . \end{aligned} \tag{B-7}$$

If only first order perturbation terms are to be retained, quantities on the right side of (B-7) are neglected; the first pair of terms on the left side is identically zero. Thus,

$$T_e[\delta(x)V_n']' + M\omega_n^{*2}[\varepsilon(x) + b_n]V_n \qquad \text{(B-8)}$$

$$+ \sum_{m\neq n} a_m[T_eV_m'' + M\omega_n^{*2}V_m] = 0.$$

The expression for determining the series coefficients, a_m, is obtained from (B-8) by taking the product with $V_p(x)$, $(p \neq n)$, and integrating over the length

$$a_m = \{T_e \int_0^{\ell} [\delta(x)V_n']'V_m \, dx \qquad \text{(B-9)}$$

$$+ M\omega_n^{*2} \int_0^{\ell} \varepsilon(x)V_nV_m \, dx\}/k_mM(\omega_m^{*2} - \omega_n^{*2})$$

where $V_m''(x) = -\omega_m^{*2}V_m(x)M/T_e$ and $k_m = \int_0^{\ell} [V_m(x)]^2 \, dx$.

Using the same procedure, an expression for b_n can be developed by multiplying (B-8) by $V_n(x)$

$$b_n = -(T_e/Mk_n\omega_n^{*2}) \int_0^{\ell} [\delta(x)V_n']'V_n \, dx - (1/k_n) \int_0^{\ell} \varepsilon(x)V_n^2 \, dx \, . \qquad \text{(B-10)}$$

When $\varepsilon(x)$ and $\delta(x)$ are specified, a_m and b_n can be calculated from (B-9) and (B-10).

The preceding analysis is now specialized for the problem in which the mass per unit length is constant and the tension varies linearly. The axial coordinate, x, originates at the top with the positive direction downward, coincident with gravity as in Fig. 3.1-1:

$$M[1 + \varepsilon(x)] = M; \quad \varepsilon(x) = 0 \tag{B-11}$$

$$T_e[1 + \delta(x)] = T_e + W(1 - x/\ell) \ . \tag{B-12}$$

Here W denotes the total tube weight, assumed to be considerably less than the pretension T_e. The zero gradient mode shapes and frequencies are

$$V_n(x) = \sin n\pi x/\ell \qquad \omega_n^{*2} = n^2\pi^2 T_e/M\ell^2 \ . \tag{B-13}$$

The modified frequencies from the perturbation solution are obtained by using (B-12) in (B-5)

$$b_n = W/2T_e \tag{B-14}$$

$$\omega_n^2 = (T_e + W/2)n^2\pi^2/M\ell^2 \ . \tag{B-15}$$

Although the formula for calculating b_n is lengthy, the result is rather straightforward. It should be noted that b_n is independent

of n and the effect upon the frequencies is equivalent to replacing the non-uniform tension distribution by its mean value.

The perturbation coefficients for the mode shapes are now determined from (B-9) with $\delta(x)$ given by (B-12) and $\varepsilon(x)$ equal to zero

$$a_m = - \frac{2\ mnW}{\pi^2(m^2 - n^2)T_e} \left[\frac{1}{(n - m)^2} + \frac{1}{(n + m)^2}\right] \qquad \text{(B-16)}$$

where $m \neq n$ and $m \pm n$ = odd. With this, the modified mode shapes can be expressed as

$$V_n(x) + \sum_{m \neq n} a_m V_m(x) \qquad \text{(B-17)}$$

$$= \sin \frac{n\pi x}{\ell} - \frac{2W}{\pi^2 T_e} \sum_{m \neq n} \frac{mn}{(m^2 - n^2)} \left[\frac{1}{(n - m)^2} + \frac{1}{(n + m)^2}\right] \sin \frac{m\pi x}{\ell} \ .$$

For example, the shape for the fundamental mode is

$$\sin \frac{\pi x}{\ell} - \frac{W}{T_e} \left(0.1501 \sin \frac{2\pi x}{\ell}\right. \qquad \text{(B-18)}$$

$$\left. + 0.0082 \sin \frac{4\pi x}{\ell} + 0.0021 \sin \frac{6\pi x}{\ell} + \ldots\right) \ .$$

The exact gravity-gradient solutions for vibration frequencies and mode shapes previously obtained and the results from the perturbation analysis are, to a limited degree, complementary. A comparison of the fundamental frequencies for both solutions is made and the

results are shown in Fig. 4.3-1. In summary, it has been shown that for an error of less than 5%, the tension gradient can be replaced by a constant tension of $T_e + W/2$ up to $W = 2\ T_e$.

APPENDIX C

JUMP PHENOMENA IN NONLINEAR SYSTEMS

One of the classic equations in the theory of nonlinear systems is Duffing's equation

$$\frac{d^2x}{dt^2} + k\frac{dx}{dt} + \omega_o^2 x + hx^3 = F_o \cos \omega t \ . \qquad \text{(C-1)}$$

A phenomenon that appears in systems such as this is the discontinuous jumps in the response amplitude as the frequency ω is varied smoothly. For example, Fig. C-1 shows the form of the response curves as h changes from positive to negative. The value $|A_o|$ represents the absolute value of the amplitude. Therefore, it can be seen from the figure that $|A_o|$ is single-valued for h=0, but for $h < 0$ or $h > 0$ there are frequencies for which $|A_o|$ has three possible values.

Figure C-2 explains in detail the jump phenomenon associated with the nonlinear resonance response for $h > 0$. An initial value of ω is chosen to correspond to the point A on the figure. Then the amplitude F_o of the forcing function is held constant while ω is slowly increased. The value of $|A_o|$ will follow the curve past point B to peak C. However, if ω is further increased $|A_o|$ will jump discontinuously to point D and continue along the curve to E. Now as ω is slowly decreased from point E the amplitude $|A_o|$ will again jump discontinuously at F to B, after which it continues on the upper branch to point A. The portion of the curve between F and C, denoted

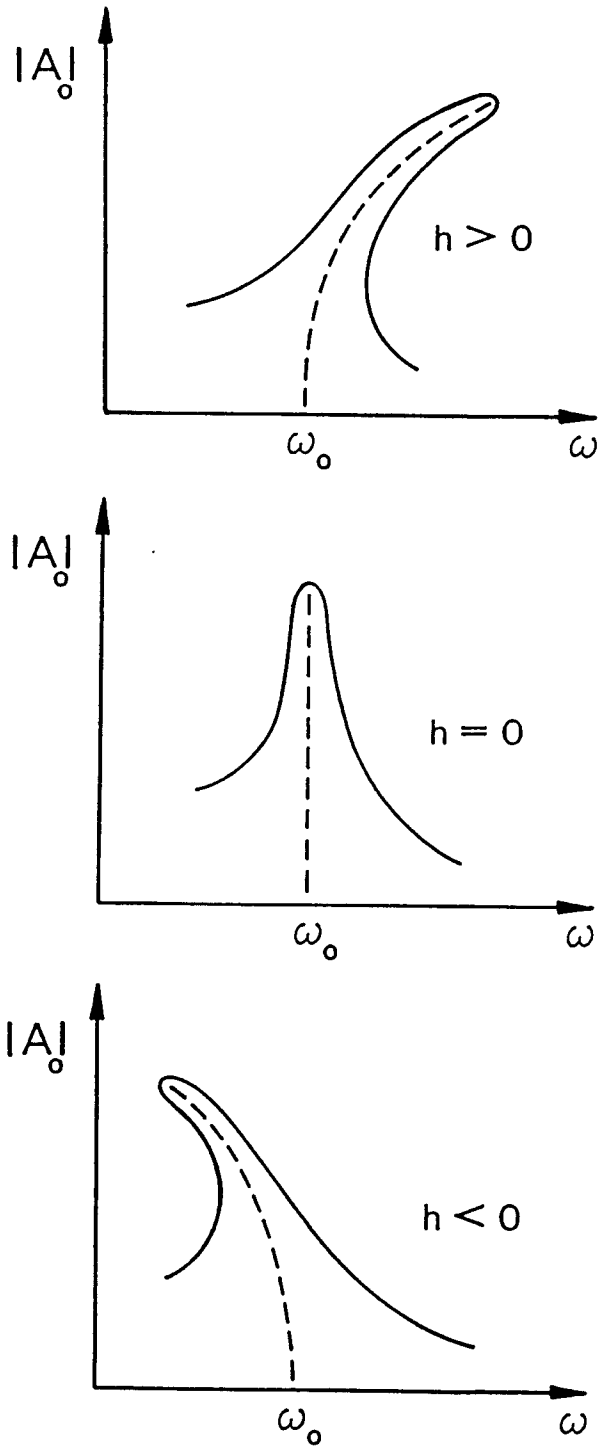

Fig. C-1. Amplitude-Frequency Response for Duffing's Equation.

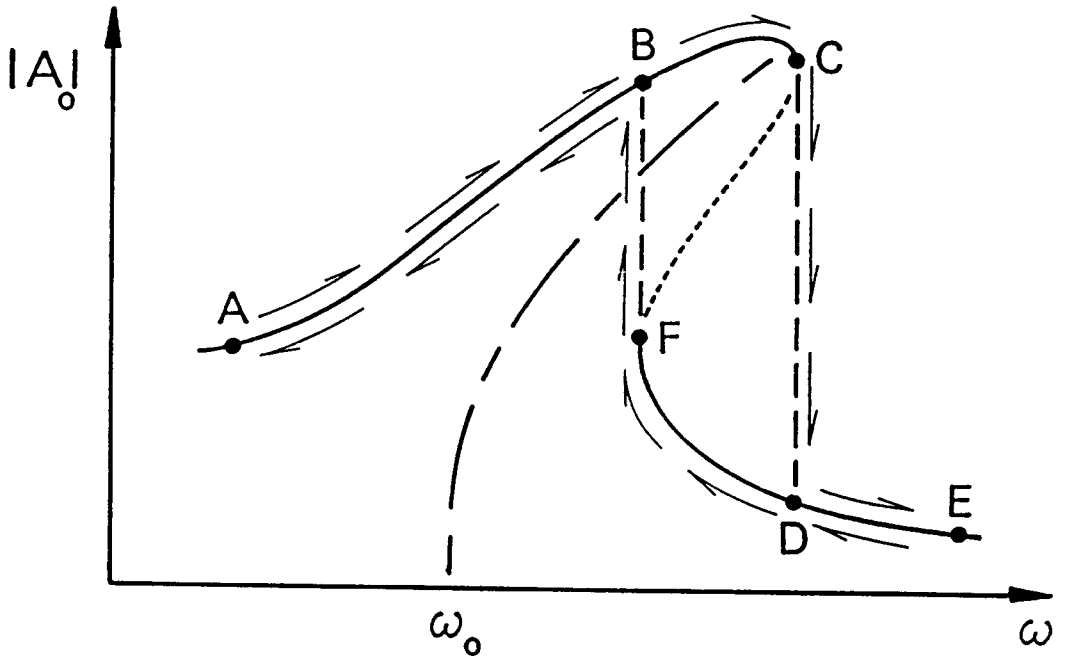

Fig. C-2. The Jump Phenomenon for h > 0.

by the dotted line, is never traversed and is considered to be unstable. Therefore, there is a range of frequencies, between the two jumps for which $|A_0|$ is stable on either the upper or lower branch. The value that $|A_0|$ actually takes depends upon the previous history of the system.

This phenomenon has been observed experimentally by a number of investigators. For example, Lee and Oplinger, Refs. [2.82] and [2.83], were the first to study the nonlinear characteristics of a string excited near resonance. By gradually increasing and decreasing the frequency of the driving force, they identified discontinuities in amplitude response curves similar to Fig. C-2.

APPENDIX D

DETERMINANTS FOR LOCATING INSTABILITY BOUNDARIES

D.1 PRIMARY INSTABILITY REGIONS

The k = 1 approximation for obtaining the primary regions of parametric instability results in Eq. (7.2-6). For a 5 mode solution the determinant is of order 10. Nonzero components of that determinant from the computer program listing are given below. (Bars have been omitted from the constants a, b, d and e and Greek letters have been typed out.)

```
gmat(1,1)=(-omega**2-2.*mu**2*e+4.*mu*e+4.)/4.
gmat(1,6)=(-omega*b)/2.
gmat(1,7)=(omega*(421.*mu*a+5460.*mu*d+842.*a))/2526.
gmat(1,9)=(omega*(8.*mu*a+415.*mu*d+16.*a))/120.
gmat(2,2)=(-omega**2-8.*mu**2*e+16.*mu*e+16.)/4.
gmat(2,6)=(omega*(-421.*mu*a-5460.*mu*d-842.*a))/2526.
gmat(2,7)=-omega*b
gmat(2,8)=(omega*(18.*mu*a+2101.*mu*d+36.*a))/60.
gmat(2,10)=(omega*(355.*mu*a+115101.*mu*d+710.*a))/2982.
gmat(3,3)=(-omega**2-18.*mu**2*e+36.*mu*e+36.)/4.
gmat(3,7)=(omega*(-18.*mu*a-2101.*mu*d-36.*a))/60.
gmat(3,8)=(-3.*omega*b)/2.
gmat(3,9)=(omega*(9.*mu*a+4202.*mu*d+18.*a))/21.
gmat(4,4)=(-omega**2-32.*mu**2*e+64.*mu*e+64.)/4.
gmat(4,6)=(omega*(-8.*mu*a-415.*mu*d-16.*a))/120.
gmat(4,8)=(omega*(-9.*mu*a-4202.*mu*d-18.*a))/21.
gmat(4,9)=-2.*omega*b
gmat(4,10)=(omega*(10.*mu*a+12969.*mu*d+20.*a))/18.
gmat(5,5)=(-omega**2-50.*mu**2*e+100.*mu*e+100.)/4.
gmat(5,7)=(omega*(-355.*mu*a-115101.*mu*d-710.*a))/2982.
gmat(5,9)=(omega*(-10.*mu*a-12969.*mu*d-20.*a))/18.
gmat(5,10)=(-5.*omega*b)/2.
gmat(6,1)=(omega*b)/2.
gmat(6,2)=(omega*(421.*mu*a+5460.*mu*d-842.*a))/2526.
gmat(6,4)=(omega*(8.*mu*a+415.*mu*d-16.*a))/120.
gmat(6,6)=(-omega**2-2.*mu**2*e-4.*mu*e+4.)/4.
gmat(7,1)=(omega*(-421.*mu*a-5460.*mu*d+842.*a))/2526.
```

```
gmat(7,2)=omega*b
gmat(7,3)=(omega*(18.*mu*a+2101.*mu*d-36.*a))/60.
gmat(7,5)=(omega*(355.*mu*a+115101.*mu*d-710.*a))/2982.
gmat(7,7)=(-omega**2-8.*mu**2*e-16.*mu*e+16.)/4.
gmat(8,2)=(omega*(-18.*mu*a-2101.*mu*d+36.*a))/60.
gmat(8,3)=(3.*omega*b)/2.
gmat(8,4)=(omega*(9.*mu*a+4202.*mu*d-18.*a))/21.
gmat(8,8)=(-omega**2-18.*mu**2*e-36.*mu*e+36.)/4.
gmat(9,1)=(omega*(-8.*mu*a-415.*mu*d+16.*a))/120.
gmat(9,3)=(omega*(-9.*mu*a-4202.*mu*d+18.*a))/21.
gmat(9,4)=2.*omega*b
gmat(9,5)=(omega*(10.*mu*a+12969.*mu*d-20.*a))/18.
gmat(9,9)=(-omega**2-32.*mu**2*e-64.*mu*e+64.)/4.
gmat(10,2)=(omega*(-355.*mu*a-115101.*mu*d+710.*a))/2982.
gmat(10,4)=(omega*(-10.*mu*a-12969.*mu*d+20.*a))/18.
gmat(10,5)=(5.*omega*b)/2.
gmat(10,10)=(-omega**2-50.*mu**2*e-100.*mu*e+100.)/4.
```

D.2 SECONDARY INSTABILITY REGIONS

The k=2 approximation for obtaining the secondary regions of parametric instability results in Eq. (7.2-9). For a 5 mode solution the determinant is of order 20. Nonzero components of that determinant from the computer program listing are given below. (Bars have been omitted from the constants a, b, d and e and Greek letters have been typed out.)

```
gmat(1,1)=(-4.*omega**2-e*mu**2+4.)/4.
gmat(1,12)=(1820.*omega*mu*d)/421.
gmat(1,14)=(83.*omega*mu*d)/12.
gmat(1,16)=-omega*b
gmat(1,17)=(2.*omega*a)/3.
gmat(1,19)=(4.*omega*a)/15.
gmat(2,2)=-omega**2-e*mu**2+4.
gmat(2,11)=(-1820.*omega*mu*d)/421.
gmat(2,13)=(2101.*omega*mu*d)/30.
gmat(2,15)=(5481.*omega*mu*d)/71.
gmat(2,16)=(-2.*omega*a)/3.
gmat(2,17)=-2.*omega*b
gmat(2,18)=(6.*omega*a)/5.
```

```
gmat(2,20)=(10.*omega*a)/21.
gmat(3,3)=(-4.*omega**2-9.*e*mu**2+36.)/4.
gmat(3,12)=(-2101.*omega*mu*d)/30.
gmat(3,14)=(8404.*omega*mu*d)/21.
gmat(3,17)=(-6.*omega*a)/5.
gmat(3,18)=-3.*omega*b
gmat(3,19)=(12.*omega*a)/7.
gmat(4,4)=-omega**2-4.*e*mu**2+16.
gmat(4,11)=(-83.*omega*mu*d)/12.
gmat(4,13)=(-8404.*omega*mu*d)/21.
gmat(4,15)=1441.*omega*mu*d
gmat(4,16)=(-4.*omega*a)/15.
gmat(4,18)=(-12.*omega*a)/7.
gmat(4,19)=-4.*omega*b
gmat(4,20)=(20.*omega*a)/9.
gmat(5,5)=(-4.*omega**2-25.*e*mu**2+100.)/4.
gmat(5,12)=(-5481.*omega*mu*d)/71.
gmat(5,14)=-1441.*omega*mu*d
gmat(5,17)=(-10.*omega*a)/21.
gmat(5,19)=(-20.*omega*a)/9.
gmat(5,20)=-5.*omega*b
gmat(6,1)=e*mu
gmat(6,6)=(-e*mu**2+2.)/2.
gmat(6,17)=(421.*omega*mu*a+2730.*omega*mu*d)/1263.
gmat(6,19)=(16.*omega*mu*a+415.*omega*mu*d)/120.
gmat(7,2)=4.*e*mu
gmat(7,7)=2.*(-e*mu**2+2.)
gmat(7,16)=(-421.*omega*mu*a-2730.*omega*mu*d)/1263.
gmat(7,18)=(36.*omega*mu*a+2101.*omega*mu*d)/60.
gmat(7,20)=(710.*omega*mu*a+115101.*omega*mu*d)/2982.
gmat(8,3)=9.*e*mu
gmat(8,8)=(9.*(-e*mu**2+2.))/2.
gmat(8,17)=(-36.*omega*mu*a-2101.*omega*mu*d)/60.
gmat(8,19)=(2.*(9.*omega*mu*a+2101.*omega*mu*d))/21.
gmat(9,4)=16.*e*mu
gmat(9,9)=8.*(-e*mu**2+2.)
gmat(9,16)=(-16.*omega*mu*a-415.*omega*mu*d)/120.
gmat(9,18)=(2.*(-9.*omega*mu*a-2101.*omega*mu*d))/21.
gmat(9,20)=(20.*omega*mu*a+12969.*omega*mu*d)/18.
gmat(10,5)=25.*e*mu
gmat(10,10)=(25.*(-e*mu**2+2.))/2.
gmat(10,17)=(-710.*omega*mu*a-115101.*omega*mu*d)/2982.
gmat(10,19)=(-20.*omega*mu*a-12969.*omega*mu*d)/18.
gmat(11,2)=(421.*omega*mu*a+2730.*omega*mu*d)/1263.
gmat(11,4)=(16.*omega*mu*a+415.*omega*mu*d)/120.
gmat(11,11)=(-e*mu**2+2.)/2.
gmat(11,16)=-e*mu
gmat(12,1)=(-421.*omega*mu*a-2730.*omega*mu*d)/1263.
gmat(12,3)=(36.*omega*mu*a+2101.*omega*mu*d)/60.
```

```
gmat(12,5)=(710.*omega*mu*a+115101.*omega*mu*d)/2982.
gmat(12,12)=2.*(-e*mu**2+2.)
gmat(12,17)=-4.*e*mu
gmat(13,2)=(-36.*omega*mu*a-2101.*omega*mu*d)/60.
gmat(13,4)=(2.*(9.*omega*mu*a+2101.*omega*mu*d))/21.
gmat(13,13)=(9.*(-e*mu**2+2.))/2.
gmat(13,18)=-9.*e*mu
gmat(14,1)=(-16.*omega*mu*a-415.*omega*mu*d)/120.
gmat(14,3)=(2.*(-9.*omega*mu*a-2101.*omega*mu*d))/21.
gmat(14,5)=(20.*omega*mu*a+12969.*omega*mu*d)/18.
gmat(14,14)=8.*(-e*mu**2+2.)
gmat(14,19)=-16.*e*mu
gmat(15,2)=(-710.*omega*mu*a-115101.*omega*mu*d)/2982.
gmat(15,4)=(-20.*omega*mu*a-12969.*omega*mu*d)/18.
gmat(15,15)=(25.*(-e*mu**2+2.))/2.
gmat(15,20)=-25.*e*mu
gmat(16,1)=mu*b
gmat(16,2)=(-2.*mu*a)/3.
gmat(16,4)=(-4.*mu*a)/15.
gmat(16,11)=-2.*e*mu
gmat(16,16)=(-4.*omega**2-3.*e*mu**2+4.)/4.
gmat(17,1)=(2.*mu*a)/3.
gmat(17,2)=2.*mu*b
gmat(17,3)=(-6.*mu*a)/5.
gmat(17,5)=(-10.*mu*a)/21.
gmat(17,12)=-8.*e*mu
gmat(17,17)=-omega**2-3.*e*mu**2+4.
gmat(18,2)=(6.*mu*a)/5.
gmat(18,3)=3.*mu*b
gmat(18,4)=(-12.*mu*a)/7.
gmat(18,13)=-18.*e*mu
gmat(18,18)=(-4.*omega**2-27.*e*mu**2+36.)/4.
gmat(19,1)=(4.*mu*a)/15.
gmat(19,3)=(12.*mu*a)/7.
gmat(19,4)=4.*mu*b
gmat(19,5)=(-20.*mu*a)/9.
gmat(19,14)=-32.*e*mu
gmat(19,19)=-omega**2-12.*e*mu**2+16.
gmat(20,2)=(10.*mu*a)/21.
gmat(20,4)=(20.*mu*a)/9.
gmat(20,5)=5.*mu*b
gmat(20,15)=-50.*e*mu
gmat(20,20)=(-4.*omega**2-75.*e*mu**2+100.)/4.
```